Characterization of the Intermediates of Heme Bound Peptides and Synthetic Analogues Associated with Amyloidogenic Diseases

Dissertation Submitted to Jadavpur University

for the Degree of

Doctor of Philosophy (Science) in Chemistry

by

Ishita Pal

School of Chemical Sciences

Indian Association for the Cultivation of Science

2A & 2B Raja S. C. Mullick Road, Kolkata- 700032

West Bengal, India.

Indian Association for the Cultivation of Science
2A and 2B Raja S. C. Mullick Road, Kolkata, INDIA-700032
Somdatta Ghosh Dey, Ph.D.
Professor, School of Chemical Sciences
Phone: +913324734971 (Ext 1376)
Email: ***icsgd@iacs.res.in***

CERTIFICATE FROM THE SUPERVISOR

This is to certify that the thesis entitled **"Characterization of the Intermediates of Heme Bound Peptides and Synthetic Analogues Associated with Amyloidogenic Diseases"** submitted by **Ms. *Ishita Pal*** who got her name registered on 16/02/2018 for the award of Ph. D. (Science) degree of Jadavpur University, is absolutely based upon her own work under the supervision of **Professor Somdatta Ghosh Dey** and that neither this thesis nor any part of it has been submitted for either any degree / diploma or any other academic award anywhere before.

Somdatta Ghosh Dey
20.01.2022

Signature of the Supervisor
date with official seal

Dr. Somdatta Ghosh Dey
Professor
School of Chemical Sciences
Indian Association for the Cultivation of Science
Jadavpur, Kolkata - 700032

DECLARATION

I hereby declare that the research work presented in this thesis entitled **"Characterization of the Intermediates of Heme Bound Peptides and Synthetic Analogues Associated with Amyloidogenic Diseases"** is the result of the studies carried out by me under the supervision of ***Professor Somdatta Ghosh Dey*** at the School of Chemical Sciences, Indian Association for the Cultivation of Science, Kolkata, and the same has not been submitted elsewhere for any other degree or diploma.

Ishita Pal

.....

Date: 20/01/2022 **Ishita Pal**

"What I am looking for is not out there, it is in me."

-Helen Keller

Dedicated to

Ma, Baba, Bon

and Soumyajit

Acknowledgement

I feel overwhelmed that I even am writing a THESIS! I don't know if I have been successful or not in this academic journey but the thing I know for certain is that, I have grown a lot. Maybe, I have learnt the most in my life during this significant five years compared to what I had learnt in my pre-Ph.D. life and this is not only in terms of educational extent. In that sense, this can be called a true "doctorate of philosophy", I guess. During this process of getting the highest academic degree of our genre, I have faced quite a few challenges like everyone else, be it personal, or professional and dangling constantly in between success and failure, somehow I have managed to survive till now. But it would be very unfair if I don't mention the names of the people at the end here, who helped me anchor my ship to the shore. My journey started with holding the hands of prof. Somdatta Ghosh Dey, my Ph.D. supervisor. She is, in a genuine sense, the 'Guide' because she has not only provided the guidance in my research, but also has got my back in the vulnerable stages of my personal crisis. I could not think of completing these works without the tremendous support given by her and unfortunately, saying only a thank you for all these would be the tiniest acknowledgement. Apart from being an intellectual academician, madam is a humble human being from whom I have cultured enormously, and if I manage to preserve a fraction of it, I believe, I will be set for a long run. I am also very much grateful to sir, prof. Abhishek Dey who has always motivated me and has always been there when I needed any kind of help. His never-ending enthusiasm towards his passion for science has inspired me from day one. I therefore sincerely thank sir for the valuable insights that makes my research worthy at the end. I indeed consider myself privileged to have these two wonderful mentors in my career.

Coming to my second home, the SoMAD lab in IACS, where I joined in the month of June, 2016 to start my excursion. I became stunned as I didn't actually expect the number of lab members to be as large as this lab had at that time. Being an introvert person, I had never met this much variety of people at once but I was heartily welcomed by all of them. My first encounter was with Manas da who eventually became my direct mentor afterwards. He had taught me the basics from the beginning including spectroscopic techniques (UV-VIS, CD, EPR), data analysis, experimental setup and what not. I am fortunate that I got to learn from such a talented person. It was always a learning experience with him and I must say that you are certainly a wise, honest and humorous person. In this same line, I would also like to thank Chandra da, whom I was a little afraid of in our first interactions, although in the later time, I had acquired a copious amount of knowledge regarding kinetics analysis, EPR, data presentation, many software programs and so on. We shared a creative side as well and I had a great learning time assisting him during the organisation of SABIC, 2017. I realised that he has the great combination of intellectuality, creativity and courage at the same time. Thank you Chandra da for your wise and resourceful inputs which turns my thesis for the better. Soumya da, the senior from my alma-mater, IIT Kharagpur; was another helpful mentor of mine. His thoughtful suggestions made some of the experimental results really easier. I am lucky to have you all guiding me in this stressful journey. Arnab (Anath) and Madhuparna both have been the perfect co-workers and friends of mine in this lab. We three joined this lab almost in the same time span, and built quite a strong bonding through these five years. Working with them is always a fun and enlightening experience for me. Madhuparna deserves a special mention here since I would not be able to acquire the degree without the constant backing of her. I am thankful for her huge mental

support and advices that made this journey possible for me in spite of all the hitches. The 'neighbours' from AD lab, Kushal da, Lombu da, Biswa da, Bijan da, Auto da, Samir da, Aman da, Estak da, Sarmistha di, Pritha di, Aishik, Arnab Ghatak, Arnab Mondal, Puru, Dibya, Paramita, Abhijit, Sudipta da, Suvam da; each one of them contributed in many ways whether in lab or outside the profession for which I can't express my obligations enough. The newly joined juniors, Chinmay, Souvik, Soumya, Suman, Soumili and Sudip; all are really helpful as well as talented. I hope their success in every way. I always want to tell to Durba di, Asmita di, Manjistha di, and Ankita di; that I found the real empowerment, enormous strength, steady scientific minds and a vibrant inspiration within you all. Asmita di had literally taught me the Raman spectroscopy by hand and without her, the 6th chapter would not exist in my thesis. Each of these people had not only helped me in the workplace but more than that they created a family outside my home. I consider myself fortunate to be around you all and to have the chance of learning so much in every aspects of life that make it possible for me to fight the odds.

Apart from this huge family, I must acknowledge my school teachers, my college professors, and tutors including Gobinda Rakhshit sir, Sutanu sir, Debdulal Rath sir, Tridib Tripathi sir, Anup Das Mahapatra sir, Jayashree Laha madam, Prafulla Dule sir, Nirmal Hazra sir, prof. Manish Bhattacharya, prof. prof. Sabyasachi Mishra, prof. Dibakar Dhara sir who laid the initial stones on the path of my future educations. I had the first research experience during my M.Sc. project in Dr. Madhab C. Das's lab and I am thankful to Santanu da, Arun da and Sir for teaching me the initial research. I am also thankful to prof. Sudip Malik, prof. T.K. Paine, Prof. Pradyut Ghosh, Dr. Mintu Mondal, Dr. Subhadeep Datta, prof. S. k. Bhattacharya for their help.

The most devoted gratitude of course goes to my parents, my sister, nomasi and to dadu who always stand beside me to keep me going. My parents are undeniably the people for whom I can be what I am today. I can't repay those sleepless nights, those hard works and all the sacrifices they have done for me and my success, if any, are the fruits of their endurance. My sister, knowing all my ups and downs, and tolerating those on a daily basis, deserves a massive endorsement from my end. She braces each and every step I have taken till date. Even if I failed to achieve this degree now, I know these people will still be on my side of the earth! I can't miss this opportunity to express my hearty gratitude to Soumyajit with whom I probably shared the inmost connection. He is the ultimate 'Friend, Philosopher and Guide' of mine. He always pushed me one step forward when I was going to quit altogether, he encouraged me when I felt lost, and he actually knew my capabilities better than I ever knew. Thank you for being my best friend, for tolerating me at my worst and for being the mirror to reflect my worth that I can't see often. You all are the co-authors of my story and I hope that I can fulfil the dreams you have dreamt together with me. I am also grateful to Soumya's parents, to Noma and other family members for providing mental strength in our toughest times.

I am blessed to have friends and well-wishers like Surojit, Upama, Archita, Mistu, Gopu, Debu, Puspendu, Manzil da, Debmalya da, Gourab, Ratul, Avik, Abhishek, Shilpi, Swapno, Subhra, Ranjana (I seek apology for my fragile memory if I missed anyone!). I could always count on them when I needed help.

I take this opportunity to thank the funding institution; University Grant Commission (UGC) for providing me with the fellowship; IACS and Jadavpur University for academic support; the non-academic staffs including Tamal da, Ujjwala di, Chanchal da, Sujit da, Goutam da, who had smoothened the path by

their cooperation and the vendors without whom our primary requirements of reagents would not have been fulfilled to start with.

Last but not the least, I would surely want to acknowledge myself for standing still so far to see the end of this journey. The epitome of this extensive voyage, what I have realised is that, life would never be fair to most of us but anyhow you have to keep walking the path you have chosen to create a purposeful and happy life. And now I have the faith in me that these long years have made me strong enough to sustain my values and to run my own race in the upcoming life.

Ishita Pal

PREFACE

The work embodied in the thesis entitled ***"Characterization of the intermediates of heme bound peptides and synthetic analogues associated with amyloidogenic diseases"*** *focusses broadly in the four areas;* ***(1)*** *investigating the role of heme in amyloidogenic diseases like Alzheimer's diseases, Diabetes mellitus* ***(2)*** *trapping and characterisation of the plausible heme based reactive intermediates which are toxic in nature as they can interfere with the essential biomolecules, proteins etc., hampering their normal biological functions* ***(3)*** *probing the role of second sphere in tuning the reaction pathway and the related intermediates which they generate in between and lastly* ***(4)*** *the probable in-vitro way of sequestering heme to get rid of heme-based cytotoxicity in physiological conditions. Various spectroscopic techniques including UV-Vis, Resonance Raman, EPR, Stopped flow, Rapid freeze quench, Fluorescence etc. and Gel electrophoresis have been used to understand the electronic active site environment of heme bound peptides and their reactivities in different experimental conditions. A few techniques and assays like centrifugation, apoglobin preparation by Teal's method, Peroxidase assay, Xylenol orange assay etc. have been used throughout these works. All of these works have been performed at Indian Association for the Cultivation of Science, Kolkata.*

The dissertation begins with a brief general introduction, ***Chapter 1****, which serves as a background for this thesis and as a basis for the works that are presented in the following chapters.*

In ***Chapter 2****, a summary of the experimental techniques and procedures used at multiple times have been discussed with a hope that it will help the readers to understand the works and experiment designs performed in this thesis.*

Chapter 3 *deals with the characterisation of a high valent intermediate, Compound I, using spectroscopy, rapid kinetics and freeze quenching technique. This is a commonly formed intermediate, known in the peroxidase pathway of natural enzyme and by characterising this intermediate in heme-Aβ complex, we provide a basis for elucidating the oxidative degradation of neurotransmitters, resulting in abnormal neurotransmission, which is a key pathological feature of AD.*

Previous literature suggest the involvement of heme in the T2Dm etiology. In this context, the interaction between two vital components; heme and insulin has been studied spectroscopically in ***Chapter 4****. Under different conditions like in presence of excess peptide as well as increasing pH of the medium, a shift of equilibrium between two components of heme-insulin complexes can be observed. One component is a mono histidine bind species which can serve as a peroxidase and another one is a bis-Histidine type active site similar to cytochrome b.*

After knowing the overall active site structure of heme-insulin complexes the research obviously was navigated to find their significant role in T2Dm. So, a detailed study of reactivity of heme bound insulin has been discussed in ***Chapter 5.*** *The quantification of PROS, peroxidase activity and the high valent oxidant species, the dityrosine formation in presence of heme-insulin and finally, the protective role of insulin in heme-amylin complexes have been dealt with in this chapter.*

The effect of second sphere on the reactivity of porphyrins with peracid, comprises the ***Chapter 6.*** *Different synthetic heme porphyrins with attached pendant groups like quinol and phenol are synthesised and are reacted with peroxides where different final products are observed. Thus, modification of second sphere residues can tune the reaction pathways by going through different types of intermediates.*

*In **Chapter 7**, the interaction of Heme bound amylin/hIAPP, with apomyoglobin (ApoMb) has been investigated using a combination of spectroscopic and electrophoresis techniques and the results confirm that ApoMb can uptake heme from Heme-hIAPP and constitute a six-coordinate high-spin ferric heme active site identical to that of myoglobin (Mb). The amount of PROS diminishes significantly after the sequestration. This not only potentially diminishes heme-induced toxicity in the pancreatic β-cells but also produces Mb which has well-documented functions throughout the respiratory system and can thereby likely reduce the risks associated with T2Dm.*

School of Chemical Sciences (SCS)

Indian Association for the Cultivation of Science (IACS)

Kolkata-700 032

Ishita Pal

CONTENTS

Chapter 1

General Introduction

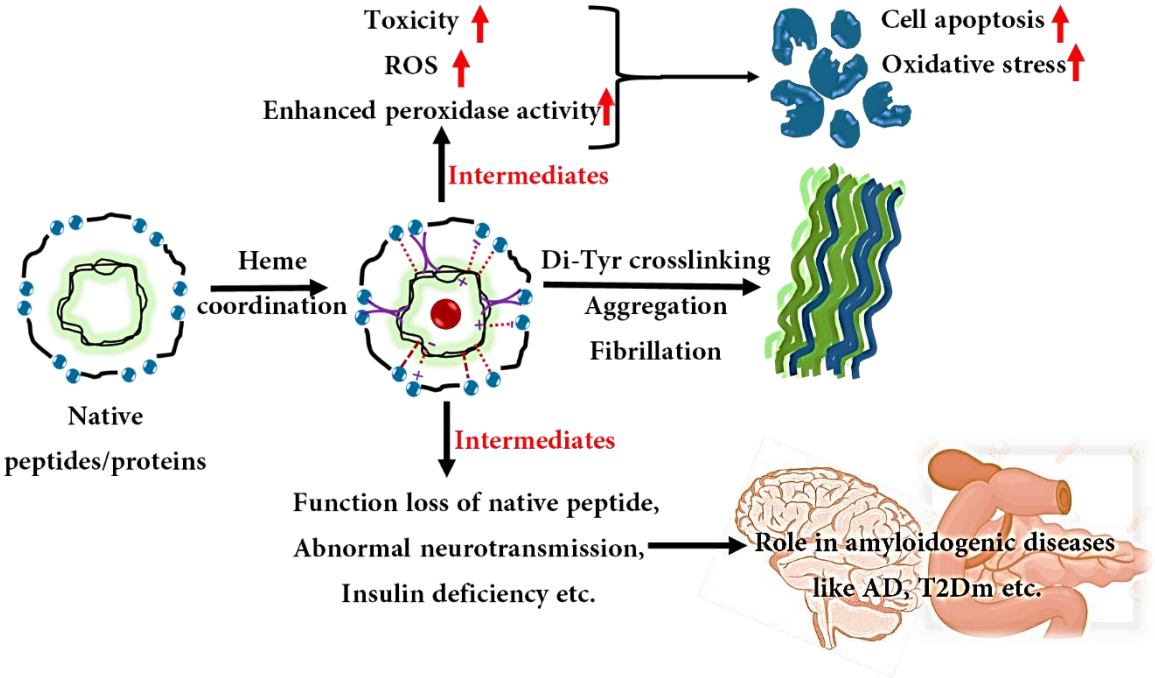

A copious amount of studies over more than a decade leads to establish an alternative hypothesis of the involvment of heme in different amyloidogenic diseases, which is succesful in explaining some of the critical observations in the disease pathogenesis and prognosis. Our lab has been discovering this relatively new perspective and has shown the possible covalent interactions between heme and peptides (e.g. Aβ, amylin, and insulin) spectroscopically using different site directed mutants in diverse experimental conditions. Knowing the overall active site environment of such heme-peptide complexes, we have navigated towards the investigation of their reactivity and possible role in diseases pathology. This thesis significantly contributes to this ongoing exploration by trapping and characterising the intermediates which might be responsible for abnormalities in diseased conditions. It also explains a new perspective of heme association in T2Dm by coordinating to insulin peptide and enhancing the cytotoxicity exerted by high valent reactive intermediates. Role of second sphere residues has also been examined using some modified synthetic porphyrins. Finally, an in vitro approach has been discussed to mitigate the ill effect of heme by sequestering it from heme-peptide complex using a biomolecule.

1.1. Amyloidogenic diseases and protein aggregation

Amyloids are protein aggregates bearing a highly ordered cross β structural motif, which are mostly pathogenic. Their formation, deposition in tissues and consequent organ dysfunction is the central event in many amyloidogenic diseases. Human disorders like Alzheimer's disease (AD), type 2 diabetes mellitus (T2Dm), dialysis related amyloidosis (DRA), frontotemporal dementia (FTD), Huntington's disease (HD), multiple system atrophy (MSA), familial amyloid polyneuropathy (FAP) etc., share this common histopathological feature of the formation and deposition of amyloids leading to organ dysfunction.[1–4] Hence, these apparently dissimilar pathogenic conditions having a range of different clinical presentations, can be unified by one specific benchmark and are grouped under the category of amyloidogenic diseases or amyloidosis. Some of these diseases are entirely hereditary, while some are mostly sporadic, with a minor percentage of cases arising due to genetic factors and a few are transmissible (e.g., human prion diseases). Amyloid formation may also result from long term medical treatment, for example in DRA, linked to hemodialysis, injection-localized amyloidosis associated with treatment for type I diabetes and iatrogenic Creutzfeldt Jakob disease (iCJD).[5]

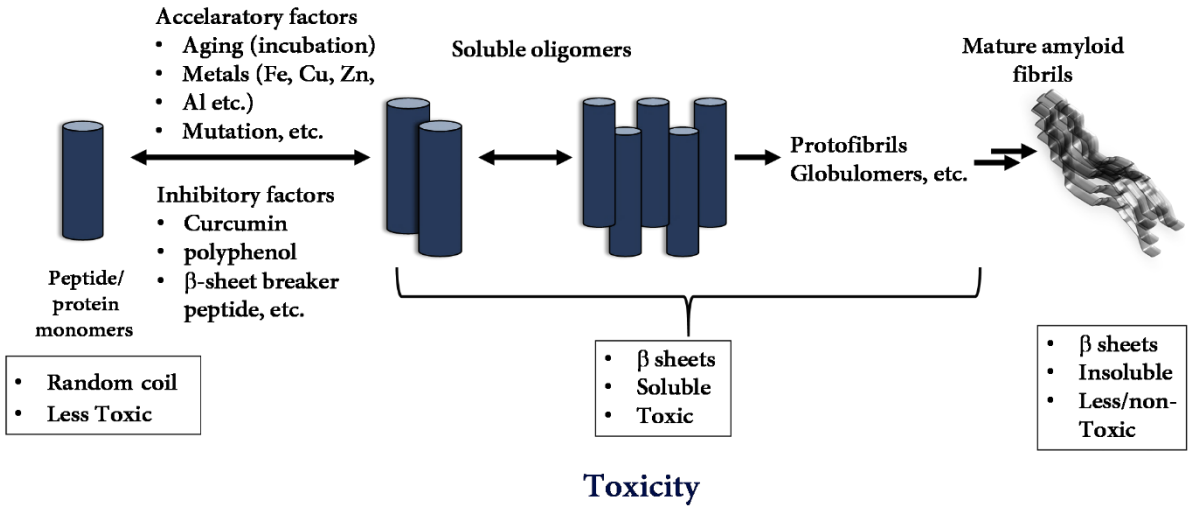

Scheme 1. Proposed mechanism of amyloidosis. The monomeric peptide or natively folded protein slowly undergo oligomerization when native protein folding gets disturbed. The oligomeric nuclei promote protofibril formation and protofibrils eventually aggregate creating cross β-sheet fibrils and mature amyloid plaques.

The amyloids are typically proteinase resistant, insoluble, unbranched protein fibrils of 7-10 nm diameter and indefinite length.[6,9] Although, protein is the major constituent of these

fibrils; sulphated glycosaminoglycans and the normal plasma glycoprotein serum amyloid P component (SAP) are invariably present in the amyloid deposits as well, possibly to promote their aggregation, stabilization and persistence.[11] In case of all amyloidogenic diseases, the key event thought to be responsible for the pathological consequences is the misfolding and self-assembly of native proteins or peptides (Scheme 1). Usually, the soluble monomeric precursors, which are either intrinsically unstructured or partially folded, aggregate into insoluble fibrils via a nucleated polymerization mechanism.[17] When these amyloid aggregates cannot be eliminated effectively they can cause toxicity which lead to diseased conditions.

It should be noted here that most amyloids are in fact pathogenic with approximately 50 different proteins/peptides being known till date to form such aggregates under disease conditions.[6] With greater understanding of its underlying structure and years of extensive investigations, the definition of the term amyloid has undergone much evolution. This leads us to the modern biophysical definition of amyloids which considers them to be non-branching long protein filaments wherein the repeating substructure consists of anti-parallel β-strands arranged orthogonally to the fibre long axis forming what is called cross β sheet.[14] Irrespective of the diversity in structure and function of the numerous precursor proteins or peptides from which the amyloids are derived or whether they are functional or pathogenic, the cross-β structural motif is exclusive to the amyloid fold.[16] Despite such uniformity in the core fibril structure, polymorphism can result in the formation of multiple structural states.[5,15] Better understanding of the mechanisms which drive these protein downhill to the path of amyloidosis should unravel new drug targets and therapeutic.

1.2. Amyloid β (Aβ) in Alzheimer's disease (AD)

Alzheimer's disease (AD), first described in 1906 by the German psychiatrist Alois Alzheimer, is a terminal neurodegenerative disorder of cognitive abnormalities which is projected to affect around 115.4 million people worldwide by 2050.[18] It manifests itself as advanced dementia, particularly in the elderly and since most of the symptoms, such as confusion, rapid mood swings, long term memory loss, disorientation, behavioral alterations etc. are age related, early diagnosis is quite difficult.[19,20] Neuronal damage arises due to the presence of excess misfolded proteins, which in case of AD is the amyloid β (Aβ) peptide.[5] In fact, the characteristic histopathological feature of AD is the presence of neuritic senile plaques

(SP, highly insoluble and proteolysis resistant fibrils), primarily in the frontal cortex and hippocampus region of the brain and intracellular tau-containing neurofibrillary tangles (NFT) with Aβ as the major constituent leading up to a high degree of synaptic breakdown, loss of neurons and decrease in neurotransmitter levels.[6] Additionally, the level of Aβ in the AD brain is ~15 times greater (~31 μg/g) than that in the age-matched non-AD brain.[10,11] This peptide is derived from the cleavage of trans-membrane amyloid precursor protein (APP) from the C-terminal region (Scheme 2, 3).[11] In amyloidogenic pathway three different proteolytic enzymes α-, β- and γ-secretases cleave APP at different sites to produce various Aβ chain lengths.[20] The most abundant and widely investigated peptide variants are Aβ(1-40) and Aβ(1-42).[14] Aβ(1-42) is the major Aβ variant in non-demented elderly controls while Aβ(1-40) is predominant in sporadic AD, forms fibril deposits which damage the cerebral vessel walls (Scheme 2,3).[7, 15, 16] It is relatively soluble in aqueous media, whereas the Aβ(1-42) rapidly forms fibril-like, insoluble structures. The first 16 amino acid residues from the N-terminus constitute the hydrophilic fragment of these peptides.[17] The rest of the 17-40/42 amino acids form the hydrophobic part of Aβ which is responsible for aggregation and fibrillation (Scheme 3).[18] The abnormal accumulation of Aβ peptide in the AD brain resulting in the formation of plaques and tangles led to the proposition of the amyloid cascade hypothesis in the early 90s which gets its major support from genetic studies (Scheme 2).[19] Recent studies using cryo-electron microscopy show that the Aβ amyloid fibrils in the AD brain are polymorphic but consist of similarly structured protofilaments and also that they are right-hand twisted with peptide fold differing sharply from previously analysed Aβ fibrils that were formed *in vitro*.[20] These results may help explain the structural basis of the disease.

Unfortunately among the drugs purported to prevent or treat AD by inhibiting Aβ aggregation, such as synthetic glycosaminoglycan 3-amino-1-propaneosulfonic acid (3APS, tramiprosate), colostrinin, scyllo-inositol etc., have been discontinued at phase III of clinical trials while some were unable to sustain beneficial effects over prolonged period.[21-24] Similarly, drugs targeting Aβ production have mostly yielded negative results with the exception of β-secretase/BACE1 inhibitors which have shown promising results at phase I clinical trials.[22, 23]

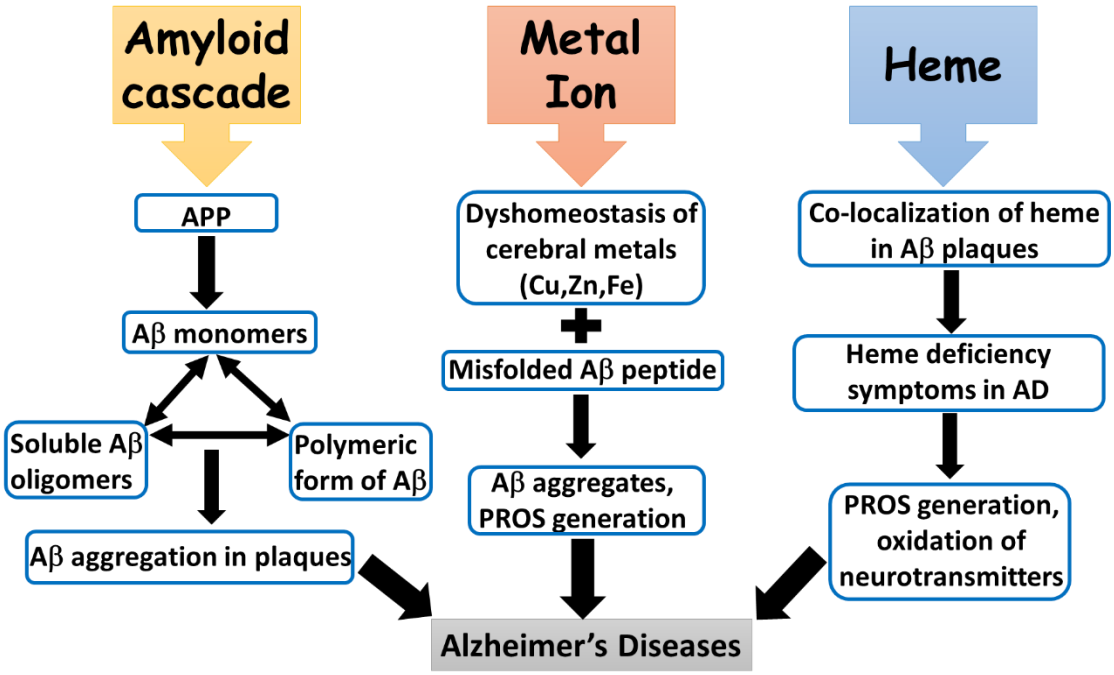

Scheme 2. Schematic representation of the different hypothesis regarding the origin of Alzheimer's disease.

Apart from Aβ, several metal ions having a natural distribution in the brain have been implicated to have a possible role in AD and have evoked the 'Metal ion' hypothesis (Scheme 2).[25] Analysis of autopsy of AD brain has demonstrated the presence of abnormally high levels of some metal ions, mainly Zn (69 µg/g, ~1055 µM), Cu (25µg/g, ~393 µM) and Fe (52µg/g, ~980 µM) in the senile plaques.[26] Although there is no consensus regarding the fate of zinc concentration in the AD brain, it is well established that Zn binds Aβ promoting its aggregation to form neurotoxic species.[27-30] However, it is still unclear if zinc binds to free A*β* peptides which then subsequently aggregate or whether zinc binds to A*β* in preformed plaques. Such a disruption in zinc homeostasis may result in synaptic and memory deficits which in turn may help in the progression of AD.[31] On the other hand, the redox active metals Cu and Fe, which regulate various essential processes of the central nervous system (CNS), like neurotransmitter synthesis, oxygen transportation, myelin production and synaptic signalling, are a source of reactive oxygen species (ROS).[32,33] ROS generation can lead to neurodegeneration via oxidation, misfolding and aggregation of essential proteins, lipid peroxidation etc. ultimately causing death of the neurons.[34] In case of AD there is a pronounced imbalance in Cu and Fe levels in the brain with these metals being accumulated in the core and rims of the senile plaques where they co-localise with Aβ.[35-37] Cu(II) ion binds Aβ with high affinity where the metal-peptide complex displays some peroxidase activity and in the reduced state generates

ROS by reacting with molecular oxygen.[38-41] In fact, both Aβ and APP have Cu binding sites. Also, the interaction between Cu(II) and Aβ may favour the peptide's aggregation by increasing the proportion of β-sheet and α-helix structures.[42] A recent study shows the presence of two different forms of Cu(II)-Aβ, termed as component I and component II, depending on the pH of the solution having a pKa of 8.1.[43]

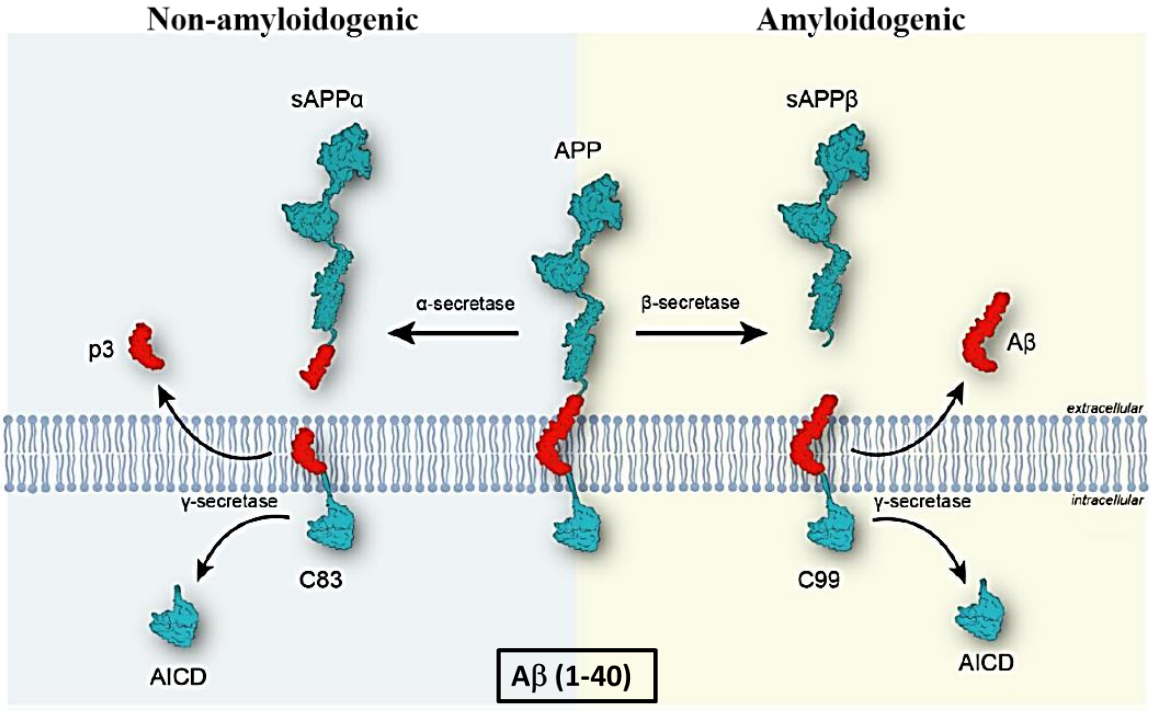

Scheme 3. Schematic representation of non-amyloidogenic and amyloidogenic APP processing pathways by secretases leading to the formation of Aβ peptides of different chain lengths (above) and amyloid precursor protein intracellular domain (ACID). Amino acid sequence in blue represents the hydrophilic part (1-16) and black represents the hydrophobic part (17-40) of the Aβ peptide as processed from APP (below).

On the other hand, histochemical studies suggest Fe can bind Aβ but its complex with Fe(III) is not very stable and quickly precipitates.[43,44] The ability of Fe to generate ROS via Fenton chemistry may contribute towards the oxidative stress seen in AD (Scheme 2).[43] Other than Zn, Cu and Fe, another metal that has been associated with AD is Al despite difference in opinion as to the exact role of this neurotoxin in the disease. Al was found to be co-localised

with amyloid in the senile plaques.[44] In vitro studies show that Al(III) can bind Aβ which is said to inhibit fibril formation but the annular oligomers co-exist in the aggregation pathway.[45] It is interesting to note that for all the metal-Aβ complexes mentioned above, the proposed metal coordinating amino acid residues lie within the hydrophilic Aβ(1-16) segment of the peptide (Scheme 3).[46-50] Several metal chelators or ionophores like clioquionol, a bioavailable anti-parasitic agent, PBT2, a second-generation 8-OH quinoline, etc. have been put forward as potential AD therapeutic because of their ability to restore metal homeostasis in the brain.[51-55] However, their limited success in improving cognition or motor dysfunction has necessitated further investigation as to the possible origin and mechanism of AD.[30]

1.2. Amylin (hIAPP) and Insulin in type 2 diabetes mellitus (T2Dm)

Type-2 diabetes mellitus (T2Dm) is the most common chronic metabolic disorder characterized by dysfunction in both insulin action and insulin secretion from the β-cells of pancreatic islets of Langerhans, resulting in hyperglycemia.[51] According to the International Diabetes Federation more than 368 million people worldwide have T2Dm, with 80 % of diabetes occurring in developing countries like India. The invariant histopathological feature of 90% of the patients suffering from T2Dm is the presence of extracellular amyloid deposits around the β-cells of pancreas.[52,53]

The principal constituent of these amyloid deposits is a polypeptide hormone called amylin or Islet Amyloid Polypeptide Protein (IAPP) comprising of 37 amino-acid residues.[54,55] IAPP is co-produced and co-secreted with insulin by the pancreatic β-cells and have complementary hormonal activities.[56,57] IAPP controls metabolic functions in concert with insulin by controlling glucose levels and gastric emptying and inhibits glucagon secretion. After being expressed as pro-amylin in response to increased glucose concentrations, amylin undergoes post-translational modification inducing removal of 13 residues from the N-terminus and 19 residues from the C-terminus (Scheme 4).[58] Subsequently the C-terminus is enzymatically amidated and a disulfide bond between Cys2 and Cys7 is formed. These post-translational modifications are necessary for the physiological activity of amylin. The amyloidogenic propensity of amylin also increases as it undergoes post-translational modifications. Human IAPP (hIAPP) is a highly amyloidogenic peptide, with residues 20-29 forming the part of its amyloidogenic core (Scheme 5).[59] Several reports indicate that

aggregation of hIAPP(1-37) is responsible for the death of the pancreatic β-cells.[22] However it is increasingly becoming apparent that it is the smaller oligomers that have the ability to induce membrane instability and β-cell apoptosis.[32]

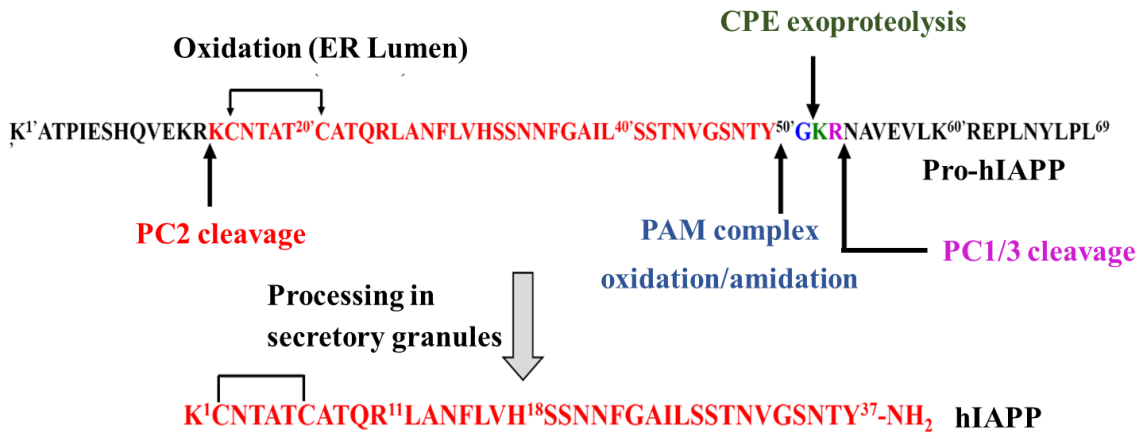

Scheme 4. Schematic representation of the processing of pro-hIAPP by endroproteases to yield the final (1-37) residue, amidated peptide hIAPP with a disulfide bond between Cys2 and Cys7. The proteases involved are prohormone convertase (PC2 and PC1/3), carboxypeptidase (CPE) and peptidyl amidating monooxygenase (PAM) complexes.

The mechanism by which hIAPP contributes to the amyloid deposition in and around the β-cells remains still unclear. HIAPP contains an abnormally larger number of Asn (6) and Ser/Thr (10) residues compared to its specific length (Scheme 5). Asn, being both an H-bond donor and acceptor residue, is capable of forming ladder-like networks of inter-polypeptide hydrogen bonds, which are envisaged to play an important role in amyloid fibril stabilization. Similarly, Ser can form extended H-bonding network within peptide chains, contributing in fibrils formation.[60] Another profoundly significant residue that has been found to change the course of amyloid formation in rats is Pro (at 25, 28 and 29th position). Pro being energetically unfavourable in the β-sheet form, is considered as a familiar disrupter of the secondary structure of amyloids. Lack of this residue in hIAPP makes a huge difference in the disease onset and progression compared to murine (Scheme 5).[25]

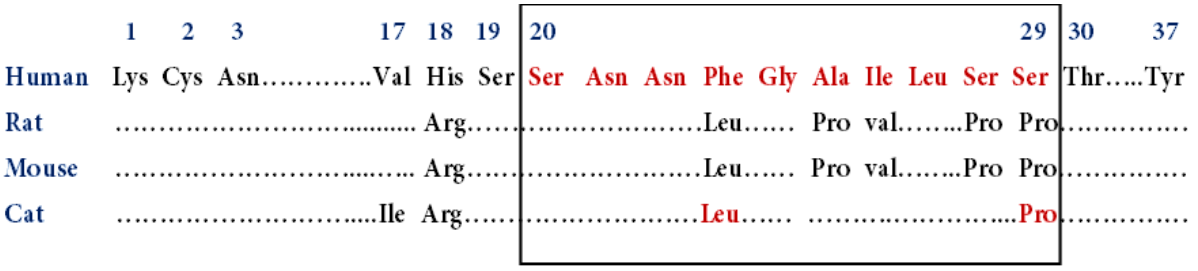

Scheme 5. Schematic representation of the arrangement of IAPP amino acid sequences in different species having slight differences between human, rat, mouse, and cat sequences. Red letters denote the amyloidogenic regions.

The another diabetes related peptide is insulin because an impaired glucose metabolism can arise from acquired and/or genetic defects in both insulin activity of the peripheral insulin sensitive tissues and insulin secretion from islet β-cells.[12] It is a small peptide hormone secreted in pulses by the β cells of the pancreatic islets of Langerhans and is synthesized in the β-cells in the form of proinsulin which then undergoes PTMs to form the mature insulin. Structurally, insulin is a dipeptide, comprising of 51 amino acids distributed in two chains (A and B chain), with a molecular weight of 5.8 kDa. The B chain has a central helical section while the A chain has an N-terminal helix connected to an anti-parallel C-terminal helix. The two chains are joined by two disulfide bridges between cysteine residues, which join the N- and C-terminal helices of the A chain to the central helix of the B chain. An additional disulfide bridge exists in the A-chain itself (Scheme 6).

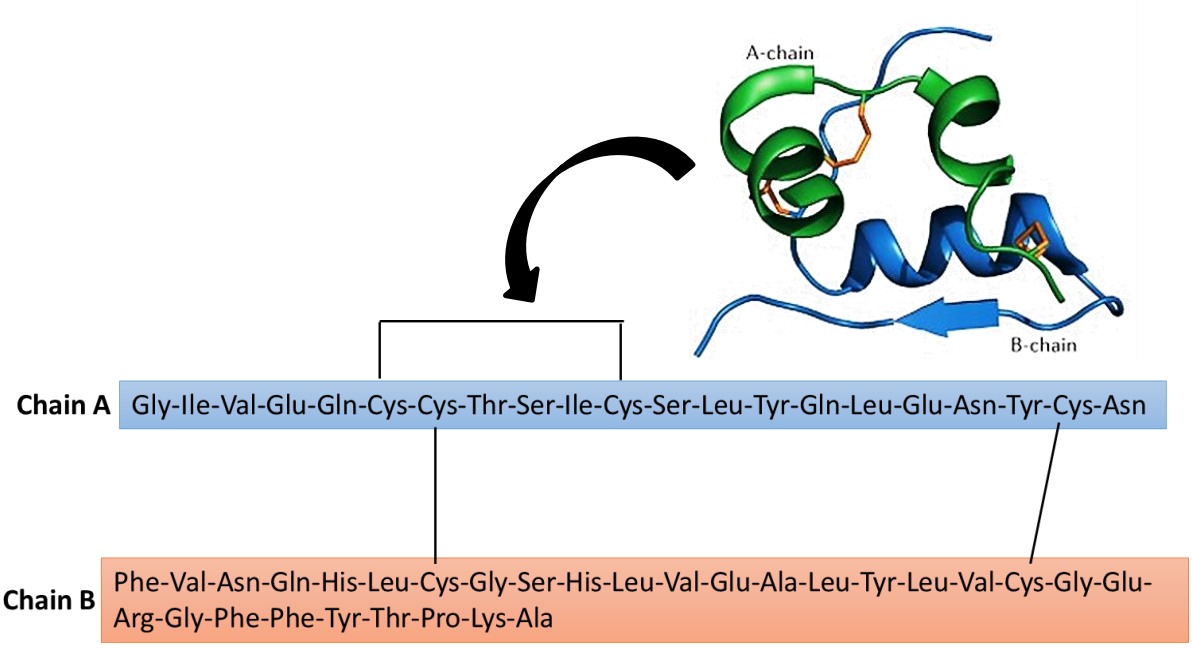

Scheme 6. The amino acid sequence of human insulin, a dipeptide linked via disulphide bridges between chain A and chain B.

As the vital regulator of glucose homeostasis, insulin has to be secreted in an adequate quantity in our body. Thus, insulin resistance, abnormal/reduced insulin secretion, declined glucose utilization, and simultaneous increase in glucose production lead to one of the defining characteristics of T2Dm, *i.e.* hyperglycemia.[28] Insulin resistance/insulin deficiency can be broadly originated due to 1) reduced insulin secretion by β-cells i.e., β-cells dysfunction; 2) counter-regulatory hormones of insulin or non-hormonal bodies that compete and supress the function of insulin receptors; 3) malfunctioned insulin response in target tissues in pancreas; 4) faulty action of insulin in the extra-pancreatic insulin-sensitive organs; skeletal muscle, adipose tissue and liver that play major roles in regulatory processes.[62]

Apart from amylin (hIAPP) and insulin, various metals like Cu, Zn, Fe etc. are said to be involved in T2Dm. In relation with T2Dm, Fe overload, elevated serum ferritin level (the index of body iron stores), lower ratio of transferrin and Fe deposition in tissues are significant etiology found from recent studies.[50] In fact, Fe accumulation in body increases linearly with the duration of the disease. Such elevated level of iron in the β cells leads to reactive oxygen species (ROS) like H_2O_2, $HO_2^{\cdot -}$, $\cdot OH$ via Fenton's mechanism, causing β cell death and in turn insulin deficiency.[25] Insulin resistance can also be induced by excess Fe storage, as it inhibits the glucose uptake by skeletal muscles and adipose tissues along with reduction in insulin extraction capacity of liver. Disturbances in copper levels in various bio-fluids and cell tissues

are found to be associated with the irregularities in metabolic pathways of diabetic complications. High levels of Cu have been found in the blood serum of diabetic patients which in excess can generate oxidative stress.[55] Cu can increase IAPP-induced cell apoptosis from 45% to 70% in the cultured β cells. Lately, it has been shown that Cu ions also bind monomeric insulin with a higher affinity. Some recent studies show Cu binding to monomeric amylin hinders β sheet fibril formation while favouring the generation of oligomers, which are known for their potentially more toxic nature towards the β cells of the pancreas than the corresponding fibrillar form.[39] Zn plays a key role in the storage and secretion of insulin, which subsequently increases the glucose uptake. As a result of the increased urinary depletion, a less than optimal Zn level in blood is found in T2Dm patients. Consequently, hypozincemia and hyperzincuria are common to them and this decreased plasma level of Zn adversely affects the ability of islet cells to make and secrete insulin. Also, mutation of Zn transporter, ZnT8 that is a key protein for the regulation of insulin secretion from the pancreatic β-cells has been associated with T2Dm.[51-53,66]

1.3. Role of heme in amyloidogenic diseases

Pathological link like increased oxidative stress, compromised mitochondrial activity etc. between AD and T2Dm has been long established now in such an extent that AD is sometimes called as Type 3 diabetes or inversely, T2Dm as the Alzheimer's of the pancreas.[47,48,64] Consistent with this, the epidemiological researches have shown that the incidence of AD is almost 2-5 times higher in T2Dm affected individuals.[49] In AD, an excessive Fe accumulation, especially in the form of heme *b* is found in the Aβ deposited region of the brain. Such anomalous increase of heme concentration in AD brain has been associated with the complexation of heme with Aβ monomers which consecutively leads to heme depletion and results in elevated Fe intake, amplified stress-related enzymes or proteins like heme oxygenase-1 and transferrin, increased bilirubin concentration, abnormal Fe homeostasis, degradation of Fe regulatory proteins, dysfunction of mitochondrial complex IV, enhancement of oxidative stress, and so forth.[50–52] Incidentally many of these symptoms of AD are also common pathological features of T2Dm.[53] Contemporary prospective studies and systematic meta-analysis have positively associated high heme Fe ingestion, the major dietetic resource of body Fe stores, with high threat of developing T2Dm in future.[53] All these lead to the proposition of

fairly recent 'Heme hypothesis' to investigate the role of heme in amyloidosis (Scheme 2). A decade of experiments have accumulated evidences in support of the heme coordination to Aβ and hIAPP monomers (Scheme 7).[61,62]

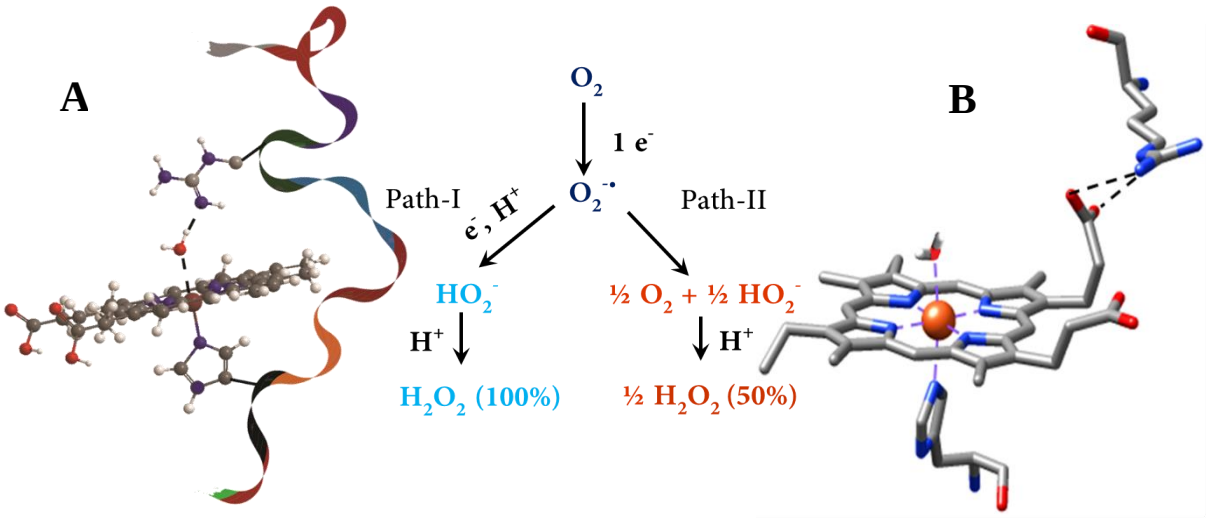

Scheme 7. Schematic representation of the active site environment of **(A)** heme-Aβ **(B)** heme-hIAPP and the PROS formation pathway (middle). Path-I for PROS from heme-Aβ (100%) and Path-II for heme-hIAPP (50%).

The active site environment of these heme bound peptides have been electronically characterised by far and the ligating amino acid residues have been identified using different site directed mutants. Apart from the primary coordination sphere, the environment of second sphere and their role in maintaining the active site structure as well as their reactivities have also been observed in details.[63] It has been found that these peptides share many similar reactivities in presence of heme. They can produce ROS like H_2O_2 and toxic hydroxyl radicals ($OH^{\cdot}$), they can enhance the oxidative stress, can stimulate the peroxidase activity which eventually generate higher population of reactive intermediates and altered chemical reaction with other small molecules which supress the native functionalities of these biomolecules. These are all more or less common features for both the diseases.[52,54] The similar etiology and pathogenic features in both AD and T2Dm indicate a common underlying mechanism, with heme playing as a protagonist.

Thus, understanding the role of the heme in binding the amyloid peptides and severe detrimental effects imposed by these heme-peptide complexes that sabotage the normal biological functions can elucidate the cause and effect of these fatal diseases. On this note, this

thesis discusses the spectroscopic characterization of the active site environment of heme bound to insulin and its reactivity generating highly oxidising ferryl oxo type intermediates which is found to generate dityrosine linkages in insulin, hampering its normal function in relevance to T2Dm. The enhanced peroxidase activity and the high valent Fe-oxo intermediates in this pathway of previously known heme-Aβ complexes has been studied using spectroscopy and the interaction of this intermediates with different biomolecules and neurotransmitter that plays vital role in signalling, has been discussed simultaneously. The role of second sphere has been investigated using synthetic porphyrins which have different pendant groups attached to them, tuning the reaction pathways. Finally, an *in-vitro* approach has been deliberated to eliminate the cytotoxicity of heme from heme bound peptide complexes relevant in amyloidosis paradigm.

1.4. References

(1) Prasansuklab, A.; Tencomnao, T. Amyloidosis in Alzheimer's Disease: The Toxicity of Amyloid Beta (A β), Mechanisms of Its Accumulation and Implications of Medicinal Plants for Therapy. *Evid. Based. Complement. Alternat. Med.* **2013**, *2013*, 413808. https://doi.org/10.1155/2013/413808.

(2) Höppener, J. W.; Ahrén, B.; Lips, C. J. Islet Amyloid and Type 2 Diabetes Mellitus. *N. Engl. J. Med.* **2000**, *343* (6), 411–419. https://doi.org/10.1056/NEJM200008103430607.

(3) Li, L.; Hölscher, C. Common Pathological Processes in Alzheimer Disease and Type 2 Diabetes: A Review. *Brain Res. Rev.* **2007**, *56* (2), 384–402. https://doi.org/10.1016/j.brainresrev.2007.09.001.

(4) Morozova-Roche, L. A.; Zurdo, J.; Spencer, A.; Noppe, W.; Receveur, V.; Archer, D. B.; Joniau, M.; Dobson, C. M. Amyloid Fibril Formation and Seeding by Wild-Type Human Lysozyme and Its Disease-Related Mutational Variants. *J. Struct. Biol.* **2000**, *130* (2–3), 339–351. https://doi.org/10.1006/jsbi.2000.4264.

(5) Iadanza, M. G.; Jackson, M. P.; Hewitt, E. W.; Ranson, N. A.; Radford, S. E. A New Era for Understanding Amyloid Structures and Disease. *Nat. Rev. Mol. Cell Biol.* **2018**, *19* (12), 755–773. https://doi.org/10.1038/s41580-018-0060-8.

(6) Chiti, F.; Dobson, C. M. Protein Misfolding, Amyloid Formation, and Human Disease: A Summary of Progress over the Last Decade. *Annu. Rev. Biochem.* **2017**, *86* (May), 27–68. https://doi.org/10.1146/annurev-biochem-061516-045115.

(7) Scarpioni, R.; Ricardi, M.; Albertazzi, V.; De Amicis, S.; Rastelli, F.; Zerbini, L. Dialysis-Related Amyloidosis: Challenges and Solutions. *Int. J. Nephrol. Renovasc. Dis.* **2016**, *9*, 319–328. https://doi.org/10.2147/IJNRD.S84784.

(8) Collinge, J.; Palmer, M. S.; Dryden, A. J. Genetic Predisposition to Iatrogenic Creutzfeldt-Jakob Disease. *Lancet* **1991**, *337* (8755), 1441–1442. https://doi.org/https://doi.org/10.1016/0140-6736(91)93128-V.

(9) Paravastu, A. K.; Leapman, R. D.; Yau, W.-M.; Tycko, R. Molecular Structural Basis for Polymorphism in Alzheimer's Beta-Amyloid Fibrils. *Proc. Natl. Acad. Sci. U. S. A.*

2008, *105* (47), 18349–18354. https://doi.org/10.1073/pnas.0806270105.

(10) Nilsson, M. R. Techniques to Study Amyloid Fibril Formation in Vitro. *Methods* **2004**, *34* (1), 151–160. https://doi.org/10.1016/j.ymeth.2004.03.012.

(11) Sunde, M.; Blake, C. The Structure of Amyloid Fibrils by Electron Microscopy and X-Ray Diffraction. *Adv. Protein Chem.* **1997**, *50*, 123–159. https://doi.org/10.1016/s0065-3233(08)60320-4.

(12) Greenwald, J.; Riek, R. Biology of Amyloid: Structure, Function, and Regulation. *Structure* **2010**, *18* (10), 1244–1260. https://doi.org/https://doi.org/10.1016/j.str.2010.08.009.

(13) Riek, R. The Three-Dimensional Structures of Amyloids. *Cold Spring Harb. Perspect. Biol.* **2017**, *9* (2). https://doi.org/10.1101/cshperspect.a023572.

(14) Chen, G.; Xu, T.; Yan, Y.; Zhou, Y.; Jiang, Y.; Melcher, K.; Xu, H. E. Amyloid Beta: Structure, Biology and Structure-Based Therapeutic Development. *Acta Pharmacol. Sin.* **2017**, *38* (9), 1205–1235. https://doi.org/10.1038/aps.2017.28.

(15) Pellarin, R.; Guarnera, E.; Caflisch, A. Pathways and Intermediates of Amyloid Fibril Formation. *J. Mol. Biol.* **2007**, *374* (4), 917–924. https://doi.org/https://doi.org/10.1016/j.jmb.2007.09.090.

(16) Chatani, E.; Yamamoto, N. Recent Progress on Understanding the Mechanisms of Amyloid Nucleation. *Biophys. Rev.* **2018**, *10* (2), 527–534. https://doi.org/10.1007/s12551-017-0353-8.

(17) Viles, J. H. Metal Ions and Amyloid Fiber Formation in Neurodegenerative Diseases . Copper , Zinc and Iron in Alzheimer ' s , Parkinson ' s and Prion Diseases. **2012**, *256* (May), 2271–2284.

(18) Calabrese, M. F.; Miranker, A. D. Metal Binding Sheds Light on Mechanisms of Amyloid Assembly. *Prion* **2009**, *3* (March), 1–4.

(19) Alghrably, M.; Czaban, I.; Jaremko, Ł.; Jaremko, M. Interaction of Amylin Species with Transition Metals and Membranes. *J. Inorg. Biochem.* **2019**, *191* (November 2018), 69–76. https://doi.org/10.1016/j.jinorgbio.2018.11.004.

(20) Gupta, V. B.; Suram, A.; Hegde, M. L. Cellular and Molecular Life Sciences Aluminium in Alzheimer ' s Disease : Are We Still at a Crossroad. *C. Cell. Mol. Life Sci.* **2005**, *62* (February), 143–158. https://doi.org/10.1007/s00018-004-4317-3.

(21) Xu, L.; Shan, S.; Chen, Y.; Wang, X.; Nussinov, R.; Ma*, B. Coupling of Zinc-Binding and Secondary Structure in Non-Fibrillar Aβ40 Peptide Oligomerization. *J Chem Inf Model.* **2019**, *55* (6), 1218–1230. https://doi.org/10.1021/acs.jcim.5b00063.Coupling.

(22) Smith, D. P.; Ciccotosto, G. D.; Tew, D. J.; Fodero-Tavoletti, M. T.; Johanssen, T.; Masters, C. L.; Barnham, K. J.; Cappai, R. Concentration Dependent Cu2+ Induced Aggregation and Dityrosine Formation of the Alzheimer's Disease Amyloid-β Peptide. *Biochemistry* **2007**, *46* (10), 2881–2891. https://doi.org/10.1021/bi0620961.

(23) Nadal, R. C.; Rigby, S. E. J.; Viles, J. H. Amyloid B−Cu2+ Complexes in Both Monomeric and Fibrillar Forms Do Not Generate H2O2 Catalytically but Quench Hydroxyl Radicals. *Biochemistry* **2008**, *47* (44), 11653–11664. https://doi.org/10.1021/bi8011093.

(24) Ghosh, C.; Dey, S. G. Ligand-Field and Ligand-Binding Analysis of the Active Site of Copper-Bound Aβ Associated with Alzheimer's Disease. *Inorg. Chem.* **2013**, *52* (3), 1318–1327. https://doi.org/10.1021/ic301865n.

(25) Faller, P.; Hureau, C. Bioinorganic Chemistry of Copper and Zinc Ions Coordinated to Amyloid-β Peptide. *Dalt. Trans.* **2009**, No. 7, 1080–1094. https://doi.org/10.1039/B813398K.

(26) Pramanik, D.; Ghosh, C.; Mukherjee, S.; Ghosh, S. *Interaction of Amyloid β Peptides with Redox Active Heme Cofactor: Relevance to Alzheimer's Disease*; 2013; Vol. 257. https://doi.org/10.1016/j.ccr.2012.02.025.

(27) Ghosh, C.; Seal, M.; Mukherjee, S.; Ghosh Dey, S. Alzheimer's Disease: A Heme–Aβ Perspective. *Acc. Chem. Res.* **2015**, *48* (9), 2556–2564. https://doi.org/10.1021/acs.accounts.5b00102.

(28) Roy, M.; Pal, I.; Nath, A. K.; Dey, S. G. Peroxidase Activity of Heme Bound Amyloid β Peptides Associated with Alzheimer's Disease. *Chem. Commun.* **2020**, *56* (33), 4505–4518. https://doi.org/10.1039/C9CC09758A.

(29) Yang, G.; Liu, H.; Ma, D.-L.; Leung, C.-H. Rebalancing Metal Dyshomeostasis for Alzheimer's Disease Therapy. *JBIC J. Biol. Inorg. Chem.* **2019**. https://doi.org/10.1007/s00775-019-01712-y.

(30) Mancuso, C.; Santangelo, R.; Calabrese, V. The Heme Oxygenase/Biliverdin Reductase System: A Potential Drug Target in Alzheimers Disease. *J. Biol. Regul. Homeost. Agents* **2013**, *27* (2 Suppl), 75–87.

(31) Wu, Y.; Ding, Y.; Tanaka, Y.; Zhang, W. Risk Factors Contributing to Type 2 Diabetes and Recent Advances in the Treatment and Prevention. *Int. J. Med. Sci.* **2014**, *11* (11), 1185–1200. https://doi.org/10.7150/ijms.10001.

(32) Nagarathna, R.; Bali, P.; Anand, A.; Srivastava, V.; Patil, S.; Sharma, G.; Manasa, K.; Pannu, V.; Singh, A.; Nagendra, H. R. Prevalence of Diabetes and Its Determinants in the Young Adults Indian Population-Call for Yoga Intervention. *Front. Endocrinol. (Lausanne).* **2020**, *11* (December), 1–9. https://doi.org/10.3389/fendo.2020.507064.

(33) Reaven, G. M. Insulin-Independent Diabetes Mellitus: Metabolic Characteristics. *Metabolism* **1980**, *29* (5), 445–454. https://doi.org/https://doi.org/10.1016/0026-0495(80)90170-5.

(34) Kahn, B. B. Type 2 Diabetes: When Insulin Secretion Fails to Compensate for Insulin Resistance. *Cell* **1998**, *92* (5), 593–596. https://doi.org/10.1016/s0092-8674(00)81125-3.

(35) Maedler, K.; Donath, M. Y. β-Cells in Type 2 Diabetes: A Loss of Function and Mass. *Horm. Res. Paediatr.* **2004**, *62(suppl 3* (Suppl. 3), 67–73. https://doi.org/10.1159/000080503.

(36) Kajimoto, Y.; Kaneto, H. Role of Oxidative Stress in Pancreatic Beta-Cell Dysfunction. *Ann. N. Y. Acad. Sci.* **2004**, *1011*, 168–176. https://doi.org/10.1007/978-3-662-41088-2_17.

(37) Jeong-a Kim, Yongzhong Wei, and J. R. S. Role of Mitochondrial Dysfunction in Insulin Resistance. *Circ. Res.* **2008**, *102* (4), 401–414.

(38) Reaven, G. M.; Hollenbeck, C. B.; Chen, Y. D. I. Relationship between Glucose Tolerance, Insulin Secretion, and Insulin Action in Non-Obese Individuals with Varying

Degrees of Glucose Tolerance. *Diabetologia* **1989**, *32* (1), 52–55. https://doi.org/10.1007/BF00265404.

(39) Weyer, C.; Bogardus, C.; Mott, D. M.; Pratley, R. E. The Natural History of Insulin Secretory Dysfunction and Insulin Resistance in the Pathogenesis of Type 2 Diabetes Mellitus. *J. Clin. Invest.* **1999**, *104* (6), 787–794. https://doi.org/10.1172/JCI7231.

(40) Mitrakou, A.; Kelley, D.; Mokan, M.; Veneman, T.; Pangburn, T.; Reilly, J.; Gerich, J. Role of Reduced Suppression of Glucose Production and Diminished Early Insulin Release in Impaired Glucose Tolerance. *N. Engl. J. Med.* **1992**, *326* (1), 22–29. https://doi.org/10.1056/NEJM199201023260104.

(41) Mitrakou, A.; Vuorinen-Markkola, H.; Raptis, G.; Toft, I.; Mokan, M.; Strumph, P.; Pimenta, W.; Veneman, T.; Jenssen, T.; Bolli, G. Simultaneous Assessment of Insulin Secretion and Insulin Sensitivity Using a Hyperglycemia Clamp. *J. Clin. Endocrinol. Metab.* **1992**, *75* (2), 379–382. https://doi.org/10.1210/jcem.75.2.1639939.

(42) Viles, J. H. Metal Ions and Amyloid Fiber Formation in Neurodegenerative Diseases . Copper, Zinc and Iron in Alzheimer ’s , Parkinson ’ s and Prion Diseases. *Coord. Chem. Rev.* **2012**, *256* (May), 2271–2284.

(43) Rosas, H. D.; Chen, Y. I.; Doros, G.; Salat, D. H.; Chen, N.; Kwong, K. K.; Bush, A.; Fox, J.; Hersch, S. M. Alterations in Brain Transition Metals in Huntington Disease: An Evolving and Intricate Story. *Arch. Neurol.* **2012**, *69* (7), 887–893. https://doi.org/10.1001/archneurol.2011.2945.

(44) Atari-hajipirloo, S.; Valizadeh, N.; Rasmi, Y.; Kheradmand, F. Altered Concentrations of Copper , Zinc , and Iron Are Associated With Increased Levels of Glycated Hemoglobin in Patients With Type 2 Diabetes Mellitus and Their First-Degree Relatives. *Int J Endocrinol Metab.* **2016**, *14* (2), 10–16. https://doi.org/10.5812/ijem.33273.Research.

(45) Taylor, C. G. Zinc, the Pancreas, and Diabetes: Insights from Rodent Studies and Future Directions. *Biometals an Int. J. role Met. ions Biol. Biochem. Med.* **2005**, *18* (4), 305–312. https://doi.org/10.1007/s10534-005-3686-x.

(46) Thomas, M. C.; MacIsaac, R. J.; Tsalamandris, C.; Jerums, G. Elevated Iron Indices in

Patients with Diabetes. *Diabet. Med.* **2004**, *21* (7), 798–802. https://doi.org/https://doi.org/10.1111/j.1464-5491.2004.01196.x.

(47) Yu, Y.-P.; Lei, P.; Hu, J.; Wu, W.-H.; Zhao, Y.-F.; Li, Y.-M. Copper-Induced Cytotoxicity: Reactive Oxygen Species or Islet Amyloid Polypeptide Oligomer Formation. *Chem. Commun.* **2010**, *46* (37), 6909–6911. https://doi.org/10.1039/C0CC02141E.

(48) Lee, S. J. C.; Choi, T. S.; Lee, J. W.; Lee, H. J.; Mun, D.-G.; Akashi, S.; Lee, S.-W.; Lim, M. H.; Kim, H. I. Structure and Assembly Mechanisms of Toxic Human Islet Amyloid Polypeptide Oligomers Associated with Copper. *Chem. Sci.* **2016**, *7* (8), 5398–5406. https://doi.org/10.1039/C6SC00153J.

(49) Gavrilova, J.; Tõugu, V.; Palumaa, P. Affinity of Zinc and Copper Ions for Insulin Monomers. *Metallomics* **2014**, *6* (7), 1296–1300. https://doi.org/10.1039/c4mt00059e.

(50) Xu, Y.; Yan, Y.; Seeman, D.; Sun, L.; Dubin, P. L. Multimerization and Aggregation of Native-State Insulin: Effect of Zinc. *Langmuir* **2012**, *28* (1), 579–586. https://doi.org/10.1021/la202902a.

(51) Chausmer, A. B. Zinc, Insulin and Diabetes. *J. Am. Coll. Nutr.* **1998**, *17* (2), 109–115. https://doi.org/10.1080/07315724.1998.10718735.

(52) Khan, A. R.; Awan, F. R. Metals in the Pathogenesis of Type 2 Diabetes. *J. Diabetes Metab. Disord.* **2014**, *13* (1), 16. https://doi.org/10.1186/2251-6581-13-16.

(53) Poudel, R.; Bhusal, Y.; Tharu, B.; Kafle, N. Role of Zinc in Insulin Regulation and Diabetes. *J. Soc. Heal. Diabetes* **2017**, *5*, 83.

(54) Li, L.; Hölscher, C. Common Pathological Processes in Alzheimer Disease and Type 2 Diabetes: A Review. *Brain Res. Rev.* **2007**, *56* (2), 384–402. https://doi.org/10.1016/j.brainresrev.2007.09.001.

(55) Ott, A.; Stolk, R. P.; Hofman, A.; van Harskamp, F.; Grobbee, D. E.; Breteler, M. M. Association of Diabetes Mellitus and Dementia: The Rotterdam Study. *Diabetologia* **1996**, *39* (11), 1392–1397. https://doi.org/10.1007/s001250050588.

(56) Janson, J.; Laedtke, T.; Parisi, J. E.; O'Brien, P.; Petersen, R. C.; Butler, P. C. Increased

Risk of Type 2 Diabetes in Alzheimer Disease. *Diabetes* **2004**, *53* (2), 474.

(60) Smith, M. A.; Harris, P. L.; Sayre, L. M.; Perry, G. Iron Accumulation in Alzheimer Disease Is a Source of Redox-Generated Free Radicals. *Proc. Natl. Acad. Sci. U. S. A.* **1997**, *94* (18), 9866–9868. https://doi.org/10.1073/pnas.94.18.9866.

(61) Ghosh, C.; Seal, M.; Mukherjee, S.; Dey, S. G. Alzheimer ' s Disease : A Heme − Aβ Perspective. *J. Alzheimer's Dis*. **2015**, *48*, 2556–2564. https://doi.org/10.1021/acs.accounts.5b00102.

(62) Pramanik, D.; Dey, S. G. Active Site Environment of Heme-Bound Amyloid Associated with Alzheimer ' s Disease. *J. AM. CHEM. SOC.* **2011**, *133* (15), 81–87.

(63) Roy, M.; Pal, I.; Nath, A. K.; Dey, S. G. Peroxidase Activity of Heme Bound Amyloid b Peptides Associated with Alzheimer ' s Disease. *Chem. Comm.* **2020**, *56*, 4505–4518. https://doi.org/10.1039/c9cc09758a.

(64) Desai, G.; Zheng, C.; Geetha, T.; Mathews, S. T.; White, B. D.; Huggins, K. W.; Zizza, C. A.; Broderick, T. L.; Babu, J. R. The Pancreas-Brain Axis : Insight into Disrupted Mechanisms Associating Type 2 Diabetes and Alzheimer's Disease. *J. Alzheimer's Dis.* **2014**. https://doi.org/10.3233/JAD-140018.

(65) Madhuparna Roy†, Ishita Pal†, Chinmay Dey, A. D.; Dey*, and S. G. Electronic Structure and Reactivity of Heme Bound Insulin. *J. Porphyrins Phthalocyanines* **2021**, *1088424621* (Scheme 1), A-K. https://doi.org/10.1142/S1088424621500346.

(66) Huang, Y.; Yang, Z.; Xu, H.; Zhang, P.; Gao, Z.; Li, H. Insulin Enhances the Peroxidase Activity of Heme by Forming Heme-Insulin Complex : Relevance to Type 2 Diabetes Mellitus. *Int. J. Biol. Macromol.* **2017**, *102*, 1009–1015.

Chapter 2

Experimental details: Methods & Methodology

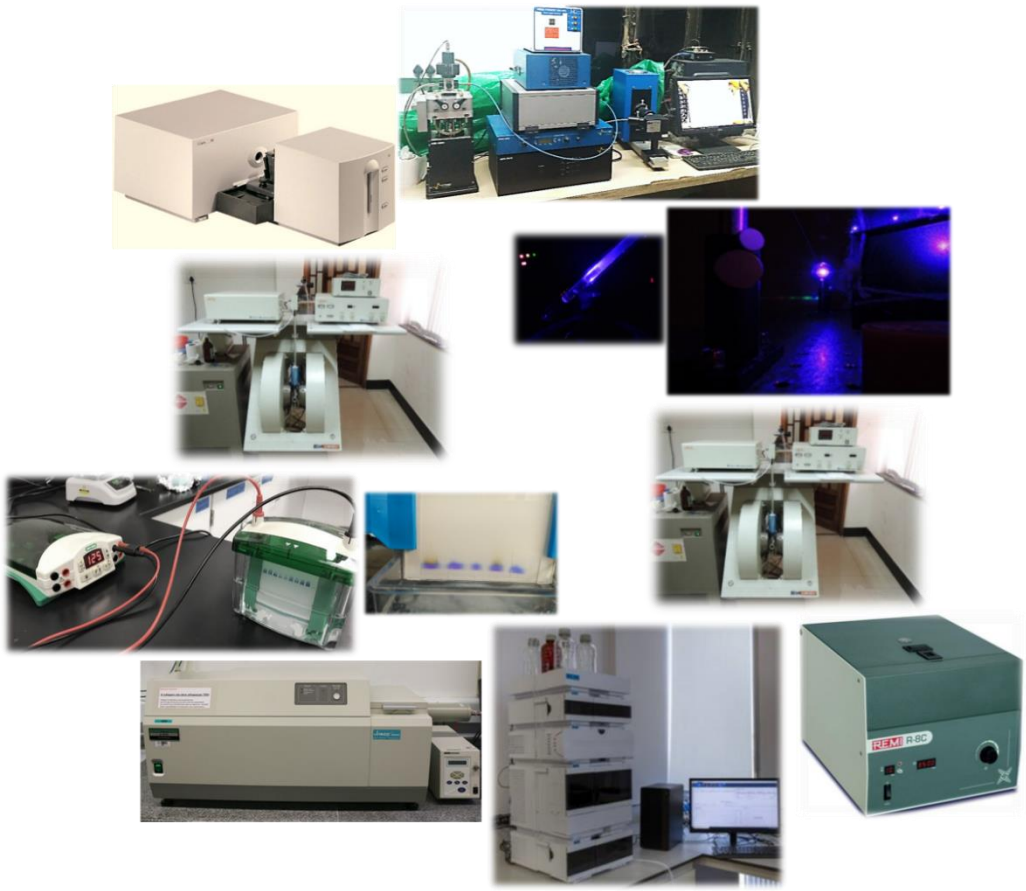

2.1 Instrumentation

An UV-Vis diode array spectrophotometer (Agilent 8453) were used for collecting the absorption spectra. For measuring the slower kinetics the same instrument was used while to follow the rapid kinetics and to characterize the short-lived intermediate species the stopped flow kinetics instrument (Biologic SFM 4000) was used. Along with this the intermediates were trapped in rapid freeze quenching (RFQ) technique at low temperature. Electron paramagnetic resonance (EPR) data were collected at 77 K in a liquid nitrogen finger dewar and obtained by a X-band Jeol (JES FA200) spectrophotometer. Some of the EPR solution samples were frozen in a low temperature bath and were run at 11K and 13K in liquid Helium setup (JANIS cryostat). EPR settings were as follows: Freq. ≈ 9.13GHz, Power ≈ 1mW, Mod. Width = 16 gauss, Amplitude = 50.00, Time Constant = 0.03 sec, Sweep time = 30 sec. Resonance Raman (rR) spectroscopy data were obtained using a Trivista 555 spectrograph (Princeton Instruments) and 413.1 nm excitation from a Kr^+ laser (Coherent, Sabre Innova SBRC-DBW-K). The optics (plano-convex lens, mirror etc.), used for the collection of rR data were purchased from Sigma-Koki Japan. The Raman shifts were calibrated against naphthalene frequencies. The wavenumber accuracy was ±1 cm^{-1} for well defined peaks. The laser power was varied between 10 and 15 mW on the samples. All reagents used in experiments were of the highest grade commercially available and were used without further purification. Native peptides and their site directed mutants were purchased from Ontores, China with >95% purity. Hemin, the buffers, Serotonin and m-CPBA were purchased from Sigma. The synthetic iron porphyrin complexes were prepared as per the early reports and are also mentioned in relevant chapter.

2.2. PROS quantitation

For PROS calculation, the following xylenol orange assay was applied. A total of 4.9 mg of Mohr's salt and 3.9 mg of xylenol orange were dissolved in 5 mL, 250 mM H_2SO_4 and stirred for 10 min. 200 µL of this solution was taken in 1.8 mL of nanopure water and a calibration curve for the quantitative estimation of H_2O_2 was obtained for 0.05, 0.1, 0.5, 1, 2.5, 5, and 10 µM concentrations of H_2O_2 by recording their absorbance at 560 nm. The calibration curve was expressed as absorbance at a fixed wavelength of 560 nm versus concentration of H_2O_2 in micromolar units for a 2 mL volume. For the detection of PROS of the heme-peptide

complexes, a blank was obtained in the UV-visible spectrophotometer with 1.8 mL nanopure water in a cuvette. A total of 50 µL 0.5 mM heme-hIAPP complex and 200 µL xylenol orange solution was added to the above cuvette and absorbance was measured. This served as the control. The complexes and all the buffer and reagent solutions were degassed first and then were purged with argon in anaerobic vials for~30 min. Then they were reduced using minimal amount of dithionite under anaerobic condition, followed by their reoxidation by O_2 (monitored by absorption). A total of 200 µL of 0.025 mM reoxidized solution was added to the cuvette containing the control and absorbance of this solution was recorded. The value of absorbance of the above solution (after deducting the control) at 560 nm when plotted on the calibration curve yielded the corresponding H_2O_2 concentration.

2.3. SDS-PAGE Gel electrophoresis

In the SDS-PAGE, 10 % - 15 % gradient polyacrylamide gel was used as the resolving gel. The samples were prepared by mixing 20 µL of each sample (containing 20 µg samples) with equal volume of Laemmli buffer. Laemmli buffer was prepared following the standard protocol.(ref: Laemmli, U. K. Cleavage of Structural Proteins during the Assembly of the Head of Bacteriophage T4. Nature 1970, 227, 680-685.) 4% stacking gel was prepared on top of the resolving gel, and the comb was inserted carefully. After formation of the defined wells the gel was loaded in the electrophoresis setup. It was then filled with 1x tank buffer (conc. SDS etc), and the samples were loaded into the wells. It was then allowed to run for 1 h at 150 V. After the run time was over, the gel was removed carefully from the setup. Finally it was stained overnight with Coomassie blue (G-250) dye to obtain the protein bands, and after complete staining, it was de-stained several times with a solution of 25% methanol, 7% acetic acid, and water.

2.4. Preparation of Apoglobins

ApoMyoglobin (ApoMb) was prepared from Myoglobin (Mb) using Teale's method.(ref: Teale, F. W. J. Cleavage of the haem-protein link by acid methylethylketone. Biochimica et Biophysica Acta 1959, 35, 543.) In brief, pH of the sample protein was lowered to 2.0 using ice-chilled 0.1 M HCl followed by mixing with equal volume of cold butanone to separate the phases. The colourless aqueous layer containing ApoMb was separated carefully

from the heme containing red organic layer and dialyzed against 20 mM phosphate buffer, pH 7.0. The apoprotein was then centrifuged at 4^0C to a concentrated solution. The concentration of the Mb and ApoMb solutions were determined using the molar extinction coefficients (ϵ =179 mM^{-1} cm^{-1} at 408 nm for Mb and ϵ =13.5 mM^{-1} cm^{-1} at 280 nm for ApoMb).

2.5. High-performance liquid chromatography (HPLC)

Oxidation products of serotonin by heme–peptide complexes were separated by reversed-phase HPLC (RP-HPLC) using a Waters 1525 Separation Module coupled to a diode-array detector (Waters 2487). A Symmetry^R C18 reversed-phase column (250 mm 9 4.6 mm, 5 lm particle size) (Phenomenex) was used to separate unreacted species from its oxidation products using the linear gradient method. The mobile phase consisted of eluant A (1 % acetic acid and 1 mM ammonium acetate in water) and eluant B (100 % acetonitrile). The gradients applied were 0–10 min, 98–85 % eluant A; 10–12 min, 85–50 % eluant A; 12–14 min, 50 % eluant A. The flow rate was 0.8 mL/min. At specific time intervals, the oxidation products were analyzed by injecting 25 µL of the reaction mixture into the column. Serotonin and its oxidation products were analyzed with a UV-online detector set at 260 nm.

2.6. Peroxidase activity

3,3′,5,5′-Tetramethylbenzidine (TMB) was used as the substrate for peroxidase activity measurement. A 0.5 mg portion of TMB was dissolved in 50uL of glacial AcOH. Kinetics experiment was performed by adding 25 µl heme-peptide solutions (0.1 mM) and 15 µl peroxide/peracid (1 M) to 15 µL TMB (83 mM), taken in 1.2 ml 50 mM pH 8 phosphate buffer. The concentration ratio of catalyst, oxidant and substrate was varied accordingly. Kinetic traces were obtained by monitoring the increase of the 652 nm absorption band with time and then compared with respect to the peroxidase activity of free hemin.

2.7. Fluorescence measurement

0.5 mmol peptide were dissolved in 200 ml 0.1 M sodium phosphate buffer, pH 8, 0.3 mmol of peroxidase solution and 10 eqv of hydrogen peroxide in 1 ml of the above buffer were added

and the solution was oxidised at a constant temperature of 37 °C for 1 h in aerobic condition. Excess hydrogen peroxide was destroyed by the addition of sodium metabisulfite and the solution neutralised with concentrated hydrochloric acid. Fluorescence experiments were carried out in 0.1 M sodium phosphate buffer solutions at pH 8 with a Fluoromax-3 instrument (Horiva JovinYvon). samples were continuously excited at 280 and 325 nm during 1 h, 1.5 h of incubation. Emission spectra were acquired with 310 nm and 400 nm, 440nm excitation to monitor the di and tri-tyrosine formation. The quartz cell of 1 cm path length has been used for this experiment and the samples were excited at 265 and 325 nm. Emission scans were documented by using a slit width of 2 nm.

Chapter 3

Formation of Compound I in Heme Bound Aβ Peptides Relevant to Alzheimer's Disease

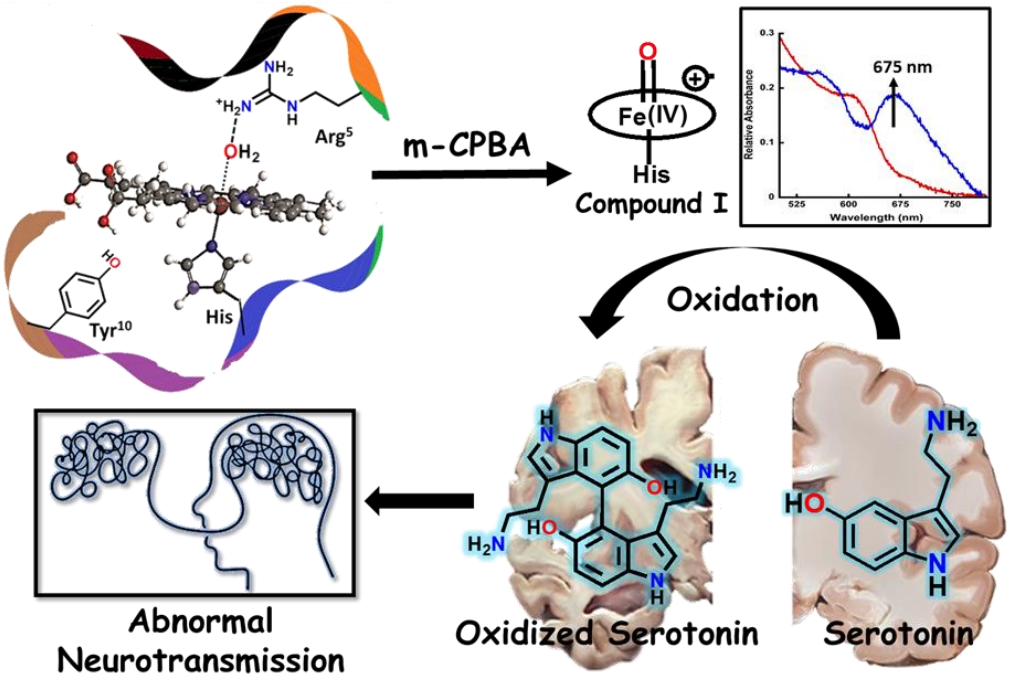

Recently the failure of therapeutic agents in prohibiting the Aβ aggregation and metal (Cu/Zn) in providing symptomatic relief to AD patients has questioned the proposed amyloid and metal ion hypothesis. Alternatively, abnormal heme homeostasis and reduced levels of neurotransmitters in the brain are hallmark features of AD. Heme has been shown to bind Aβ, forming a peroxidase like active site which can oxidatively degrade neurotransmitters like serotonin. In this chapter, using rapid kinetics and freeze quenching, we show that heme bound Aβ forms a highly reactive intermediate, compound I which provides a basis for elucidating the oxidative degradation of neurotransmitters like serotonin, resulting in abnormal neurotransmission, and a key pathological feature of AD. Site directed mutants indicate that the Arg5 and Tyr10 residues, unique to human Aβ, affect the rates of formation and decay of compound I providing insight into their roles in the oxidative degradation of neurotransmitters. Moreover, Tyr10 residue can potentially play a natural protective role against compound I.

3.1. Introduction

Alzheimer's disease (AD) is a terminal neurodegenerative disease that is likely to affect around 115.4 million people by 2050.[1] Generally, amyloidogenic plaques formed by the aggregation of small amyloid β (Aβ) peptides resulting from the hydrolysis of amyloid precursor protein (APP) by the action of secretases, are observed in the hippocampus cortex of the brain of an AD affected patient.[2–4] Co-localization of Zn and Cu metals in these Aβ plaques have led the community to invoke a potential role of these metals in aggregation.[5] Specifically for Cu, neurotoxicity can be derived from oxidative stress owing to the generation of reactive oxygen species by the reaction of Aβ peptide/aggregate bound cuprous ion with oxygen.[6] Over the last few decades several small molecule inhibitors of aggregation and Cu/Zn chelators have been tested as potential drug candidates.[7] Unfortunately, till date, molecules that show dissolution of such aggregates and/or chelation of Cu/Zn have failed to provide credible symptomatic relief during clinical trials.[7–9] This has prompted investigation of other likely origins of the disease. Heme, the chromophore present in proteins like haemoglobin and myoglobin, is ubiquitous in mammalian body (~ 60 g of heme in a grown adult) and has been detected in the Aβ plaques.[10,11] While the takers of the heme hypothesis are few, the role of heme in the important cytopathologies of AD is difficult to ignore.[12,13] AD pathology includes disruption in heme homeostasis, enhanced heme oxygenase activity, reduced levels of heme proteins like NO synthase, increase in iron uptake, dysfunction in mitochondrial complex IV, etc., all indicating a potential association of heme with AD.[14,15] Heme has been established to bind Aβ peptide via a histidine residue in the hydrophilic segment (1-16) of Aβ peptide.[15–18] The three residues deemed relevant to the reactivity of heme-Aβ complexes, namely the His13, Arg5 and Tyr10, are unique to human Aβ peptides and are absent in rodents who do not show AD.[19] The heme-Aβ complexes show peroxidase activity owing to the presence of a distal Arg5 residue and can catalyze the oxidation of the neurotransmitter, serotonin (5-HT).[19,20] Serotonin, an essential neurotransmitter, for cognitive functions and formation of new memories, is catalytically oxidized by heme-Aβ and H_2O_2 primarily to its dimer dihydroxybitryptamine.[21,22] Significant reduction of serotonin level and their oxidation leading to neurotoxicity are common phenomena in the pathology of AD.[23,24] Since the peroxidase activity of heme-Aβ is unregulated, such reactivity of heme-Aβ can account for the abnormal neurotransmission observed in AD (Scheme 1).[20,25] In the absence of substrate heme-Aβ can oxidize the Tyr10 residue to cause dityrosine linkage between Aβ peptides leading to their

aggregation.[12,26] Apart from its peroxidase activity with H_2O_2, reduced heme-Aβ is known to generate H_2O_2 following a 2-electron reduction of molecular O_2, in which one of the electron is donated by the Tyr residue at the 10th position in the peptide which acts as a redox non-innocent residue similar to the redox active Tyr residues in other heme and non-heme enzymes in nature.[27]

Scheme 1. **Schematic representation of oxidation of neurotransmitters catalyzed by heme-Aβ complex in presence of H_2O_2.**

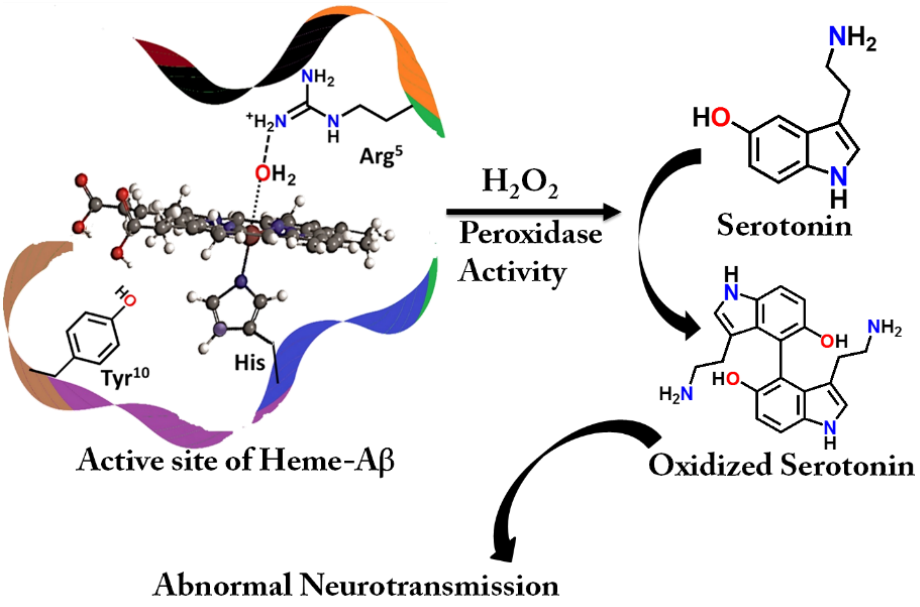

Although the peroxidase activity of heme-Aβ complexes are known, till date there is no report on the reactive intermediates involved in the reaction. Peroxidases are known to contain a highly conserved Arg residue in the distal pocket which assists in the O-O bond heterolysis by protonation of the distal oxygen atom of a Fe(III)-OOH intermediate species (also known as Compound 0).[28] This role of the Arg residue is also described as the "pull effect".[29] The protonation assisted O-O bond cleavage of Compound 0 results in the formation of the reactive oxidant Compound I, formally described as a Fe(IV)=O porphyrin π cation radical species, which is the active oxidant in peroxidases.[30,31] However, the intermediate involved in the peroxidase activity of heme-Aβ has not been trapped and characterized and remains to be established.

This chapter demonstrates that heme-Aβ complexes rapidly react with m-CPBA (meta-chloro perbenzoic acid), a surrogate for H_2O_2, to generate Compound I by the heterolytic cleavage of O-O bond.[20] The Compound I species, having half-life of 0.6 s, can oxidize

neurotransmitters like serotonin. The distal Arg5 and Tyr10 residues control the rate of formation and decay of Compound I.

3.2. Methods and Materials

3.2.1. General Methods

All reagents were of the highest grade commercially available and were used without further purification. Aβ peptides of chain lengths 1-40 and 1-16 have been used for this study. The site directed mutants of Aβ(1-16) used were Arg5Asn and Tyr10Phe. All peptides were purchased from Ontores, China with >95% purity. Hemin, the buffers, Serotonin and m-CPBA were purchased from Sigma. All the experiments were done at pH 8 and Aβ(1-40), Aβ(1-16) and all the mutants were made in 50 mM phosphate buffer, while hemin solution was made in 1 M NaOH solution.

Peptide stock solutions were 0.5 mM for absorption, EPR and resonance Raman studies. Heme-Aβ complexes were prepared by incubating 1 equivalent of Aβ solution with 0.8 equivalent of heme solutions for ~1 h. Serotonin (5-HT) was prepared in Millipore water and was of 5 mM strength. Meta-chloro perbenzoic acid (m-CPBA) was prepared by dissolving it in 20% (v/v) Acetonitrile-water mixture.

3.2.2. Physical Methods

Absorption

Absorption spectra were recorded by adding ~100 μL of the heme-Aβ complex solution in a cuvette of 1 mm path length. Absorption spectra were obtained by a UV-Vis diode array spectrophotometer (Agilent 8453).

Stopped Flow

Stopped-flow analysis of the reaction of heme-Aβ complexes and it's mutants with m-CPBA were performed on SFM 4000 stopped-flow absorption spectrophotometer (light source Xe lamp). The reactions were performed by mixing 0.3 mM of heme-Aβ complexes (wild type and mutants) with 2 mM m-CPBA in 1:10 concentration ratio.

The formation and decay time of Compound I was calculated from the kinetic trace followed at 675 nm. The time where kinetic trace at 675 nm shows maximum was considered to be the

absorption spectrum of Compound I (e.g. 27 msec for heme-Aβ(1-16)). In order to observe the absorption bands of Compound I clearly, the initial spectrum of heme-Aβ (* a factor) was subtracted from that spectra to remove contribution of some unreacted heme-Aβ. The difference spectrum is commonly used to clearly observe the formation of new bands of low intensities.

Fitting of Kinetics Data

$y = y0 + A0 \exp(-kt)$

The above monophasic equation was used to fit the kinetics data and thus obtain the formation and decay rate constants. A positive pre-exponential factor 'A0' was used to fit the decay kinetics while a negative value of the same was used to fit the formation kinetics. Here 'k' is the rate constant and 'y0' is a constant.

Serotonin Oxidation

Absorption spectra and kinetics of serotonin oxidation was monitored in a UV-vis diode array spectrophotometer (Agilent 8453). The concentration of serotonin solution was 5 mM. Strength of heme- Aβ solution and m-CPBA were 0.3 mM and 500 mM respectively. Kinetics experiment was performed by adding 5 µl heme- Aβ solution and 8.5 µl m-CPBA to 70 µl serotonin taken in 1.2 ml 50 mM pH 8 phosphate buffer. The concentration ratio of Heme-Aβ, m-CPBA and serotonin was 1: 2360:176.

Peroxidase Activity

3,3′,5,5′-Tetramethylbenzidine (TMB) was used as the substrate for peroxidase activity measurement. A 0.5 mg portion of TMB was dissolved in 50uL of glacial AcOH. Kinetics experiment was performed by adding 25 µl heme- Aβ solution (0.1 mM) and 15 µl m-CPBA (1 M) to 15 µL TMB (83 mM), taken in 1.2 ml 50 mM pH 8 phosphate buffer. The concentration ratio of Heme-Aβ, m-CPBA and TMB was 1: 6000: 498. Kinetic traces were obtained by monitoring the increase of the 652 nm absorption band with time.

EPR

EPR spectra were obtained with a JEOL FA200 spectrometer. The EPR samples were 0.35 mM in concentration and were prepared by adding 5 equivalents of m-CPBA to heme-Aβ (Tyr mutant) solution frozen in a low temperature n-Pentane bath (kept at -20^0C) and were run at

11K and 13K in liquid He setup(JANIS cryostat). The 77 K data of these samples were acquired in a liquid nitrogen finger dewar. EPR settings were as follows: Freq. ≈ 9.13GHz, Power ≈ 1mW, Mod. Width = 16 gauss, Amplitude = 50.00, Time Constant = 0.03 sec, Sweep time = 30 sec.

Resonance Raman

RR data were obtained using a Trivista 555 spectrograph (Princeton Instruments) using 415 nm excitation from a diode laser (MDL-E-415-50mW). The optics (plano-convex lens, mirror etc.), used for the collection of rR data were purchased from Sigma-Koki Japan. The power on the samples was ~5 mW. The rR samples were 0.35 mM in concentration and were prepared by adding 5 equivalents of m-CPBA to Tyr10Phe mutant, frozen in a low temperature n-Pentane bath (kept at -20^0C). For the preparation of compound I of the native peptide with m-CPBA , SFM-400 Rapid Freeze Quench (RFQ) technique was used and samples were frozen in a low temperature n-Pentane bath (kept at -60^0C).

HPLC

Oxidation products of 5-HT by heme–Ab complexes were separated by reversed-phase HPLC (RP-HPLC) using a Waters 1525 Separation Module coupled to a diode-array detector (Waters 2487). A SymmetryR C18 reversed-phase column (250 mm 9 4.6 mm, 5 lm particle size) (Phenomenex) was used to separate 5-HT from its oxidation products using the linear gradient method. The mobile phase consisted of eluant A (1 % acetic acid and 1 mM ammonium acetate in water) and eluant B (100% acetonitrile). The gradients applied were 0–10 min, 98–85 % eluant A; 10–12 min, 85–50 % eluant A; 12–14 min, 50 % eluant A. The flow rate was 0.8 mL/min. For the HPLC assay, 5 mM 5-HT was incubated with 335 mM H2O2/ m-CPBA and 0.3 mM heme–Ab in 100 mM Hepes, pH 8 with a conc. ratio of Heme-Aβ, m-CPBA and serotonin to be 1: 2360: 176. At specific time intervals, the oxidation products were analyzed by injecting 25 μL of the reaction mixture into the column. Serotonin and its oxidation products were analyzed with a UV-online detector set at 260 nm.

3.3. Results and Analysis

3.3.1. Formation of reactive intermediates in the reaction of heme-Aβ with m-CPBA

Heme-Aβ complex reacts with m-CPBA with an observed rapid decrease in the absorbance of the Soret band and a concomitant blue shift of the Soret band from 392 nm to 365 nm (Figure 1A). The Q-band at 606 nm corresponding to heme bound Aβ red shifts to ~ 675 nm, in ~ 27 ms (Figure 1B and S1A). Reaction of heme with peroxide/peracid can lead to a ferric peroxide which can either cleave the O-O bond homolytically to form compound II or heterolytically to form compound I. Heme peroxides are characterized by absorption at 526-540 nm and 556-575 nm while compound II is characterized by absorption at 525-551 and 556-586 nm.[32–37] Alternatively, compound I is characterized by an absorption at 645-690 nm.[36–45] An absorbance in this region results in a green colour and is characteristic of a ferryl porphyrin cation radical (FeIV=O Por .+) or Compound I (Table S1).[39,40,46] The absorbance at ~ 675 nm is found to diminish within 4 sec indicating the decay of Compound I (Figure 2A). As the reaction progresses, a new species is formed which is characterized by a red shift of the Soret band to 403 nm and new bands at ~565 nm and 595 nm indicating the decay of Compound I to another intermediate species, likely, ferryl heme (FeIV=O porphyrin) or Compound II (Figure 1 and S1A).[34,35,38] Note that we have not been able to accumulate high enough population of Compound I with H_2O_2 because the rate of formation of Compound I in H_2O_2 is slower than in m-CPBA as is well documented in peroxidases.[39] On the contrary, the decay of Compound I to Compound II is independent of the source of peroxide. This is why Compound I is barely observed in the reaction of heme-Aβ with H_2O_2; rather Compound II is observed (Figure S1B).

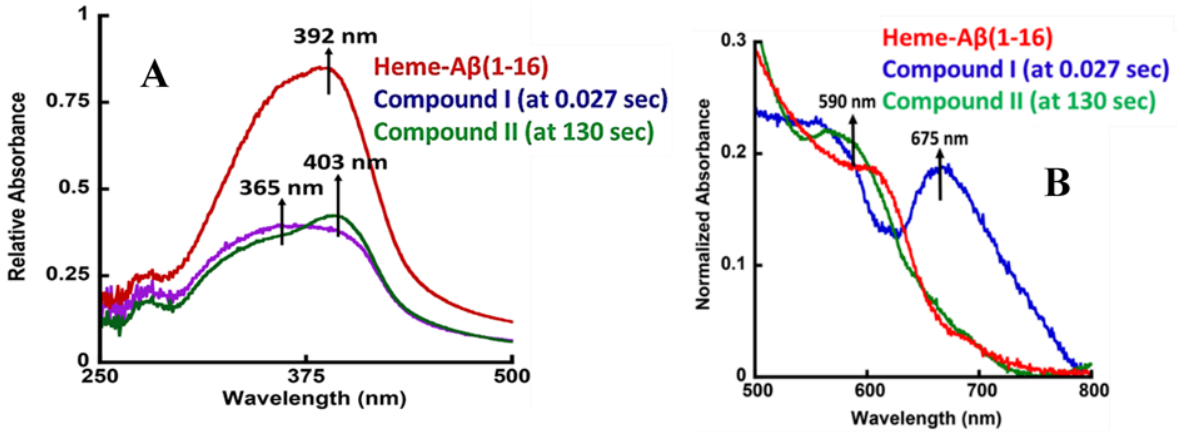

Figure 1. **(A)** Absorption spectrum of heme-Aβ(1-16), red ; for the reaction of heme-Aβ(1-16) with m-CPBA, in 50 mM PO43- buffer at pH 8 in the soret region **(B)** the same spectra along

with the difference spectrum at 0.027 sec (Compound I), blue ; and difference spectrum at 130 sec (Compound II), green in the Q-band region. The difference spectrum is the difference between the spectrum at a given time and the spectrum of initial heme-Aβ complex. The arrows indicate the direction of the spectral change.

3.3.2. Kinetic assays

The kinetic trace of the reaction between heme-Aβ and m-CPBA at 675 nm shows an exponential increase followed by a decay indicating the formation and decay of Compound I, respectively (Figure 2A). The rate constants for the formation and decay have been estimated to be 115 s^{-1} and 1.2 s^{-1} for heme-Aβ(1-16). In the presence of serotonin, the decay of Compound I is accelerated as the Compound I formed oxidizes it to its dimer dihydroxybitryptamine (Figure 2B, and S2), at a rate which is faster than its auto decay in the absence of substrate (Table 1 and Scheme 2). Note that heme-Aβ can oxidize serotonin to its dimer dihydroxybitryptamine (peak 1) in the presence of both m-CPBA as well as H_2O_2, confirmed by HPLC experiment (Figure 3).

Heme-Aβ(1-40) also shows formation of both Compound I and Compound II (Figure S3). It has a slower rate of formation and a faster rate of decay of Compound I relative to heme-Aβ(1-16) (Figure 2A and Table 1), suggesting that the presence of the hydrophobic region retards the formation of Compound I and marginally accelerates its decay. The decay of Compound I is faster, in the presence of serotonin, (Figure 2B and S4), similar to heme-Aβ(1-16).

The reactions of heme-Aβ(1-40) and heme-Aβ(1-16) with m-CPBA have been monitored at 675 nm in D_2O (Figure 4, Table 2). Both complexes exhibit a slower rate of formation of Compound I in D_2O relative to H_2O suggesting protonation is involved in the rate determining step (r.d.s). The K_H/K_D was found to be ~ 2 (Table 1) which compares very well with the K_H/K_D reported for the O-O bond heterolysis in peroxidases.[47] However, no isotope effect was observed in case of decay of Compound I (Figure S5) consistent with reports on peroxidases as Compound I decays by outer sphere electron transfer. These data are consistent with a protonation assisted O-O bond heterolysis as the rate determining step in the formation of Compound I.[48,49]

Table 1. The rate constants of formation and decay of Compound I on reaction of heme-Aβ(1-16), and heme-Aβ(1-40) with m-CPBA in H_2O and in D_2O, in presence and in absence of substrate (serotonin) as well as for the reaction of the heme-Aβ complexes of the site directed mutants with m-CPBA.

Heme-Aβ complexes	Formation rate (S^{-1})	Decay rate (S^{-1})
Heme-Aβ(1-16)	115 ± 5	1.20 ± 0.10
Heme-Aβ(1-16) in D_2O	45 ± 2	1.10 ± 0.10
Heme-Aβ(1-40)	47 ± 1	2.40 ± 0.20
Heme-Aβ(1-16)+Serotonin	180 ± 5	2.05 ± 0.20
Heme-Aβ(1-40)+Serotonin	70 ± 2	3.00 ± 0.15
Heme-Aβ(1-16,Arg5Asn)	40 ± 2	1.32 ± 0.20
Heme-Aβ(1-16,Tyr10Phe)	55 ± 3	0.40 ± 0.05

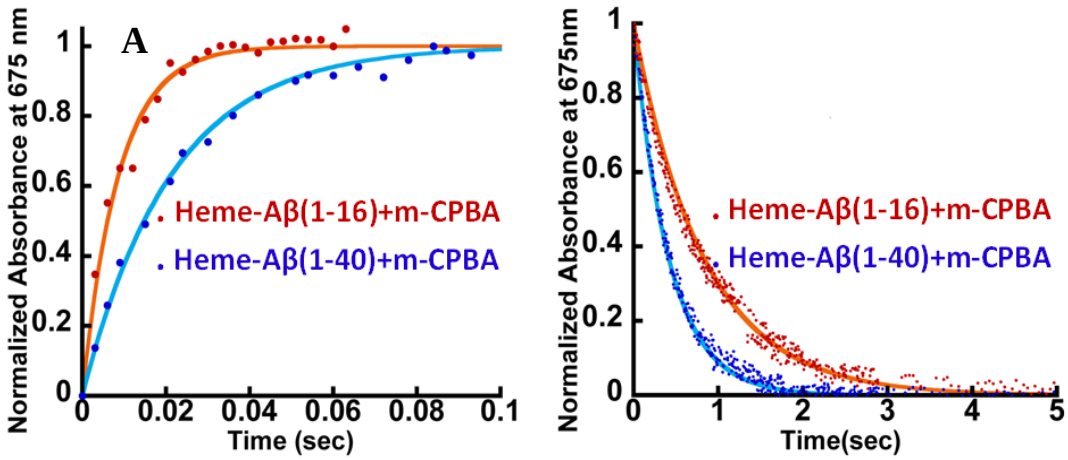

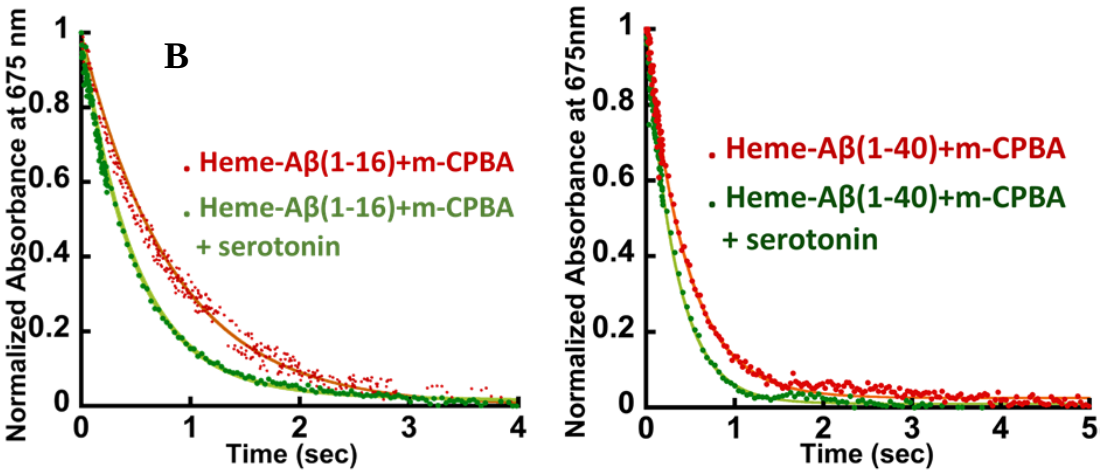

Figure 2 **(A)** Comparison of formation and decay of Compound I during reaction of heme-Aβ(1-16) with m-CPBA, red and heme-Aβ(1-40) with m-CPBA, blue. **(B)** Comparison of decay of Compound I during reaction of heme-Aβ(1-16) with m-CPBA, in absence of substrate, red; and in presence of substrate, green and heme-Aβ(1-40) with m-CPBA, in absence of substrate, red; and in presence of substrate, green; in 50 mM PO_4^{3-} buffer at pH 8.

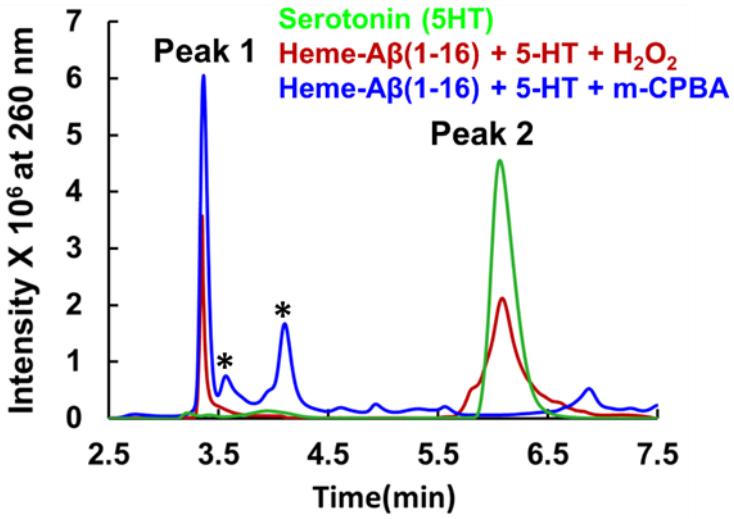

Figure 3. Separation of the 5-HT and its products by RP-HPLC after its incubation with heme–Aβ(1–16) + H_2O_2 and .heme–Aβ(1–16) + m-CPBA; 5-HT without reaction mixture (peak 2), green, separated reaction mixture injected 3.25 min after incubation resulting in major product (peak 1) for heme–Aβ(1–16) + H_2O_2, red and heme–Aβ(1–16) + m-CPBA, blue in 50 mM PO_4^{3-} buffer at pH 8. These peaks (*) are minor products which are likely the oxidized products of serotonin, 3,5-dihydroxy-3-ethyl amino-2-oxindole (3,5-DHEO) and 5,6-dihydroxytryptamine (5,6-DHT).[50]

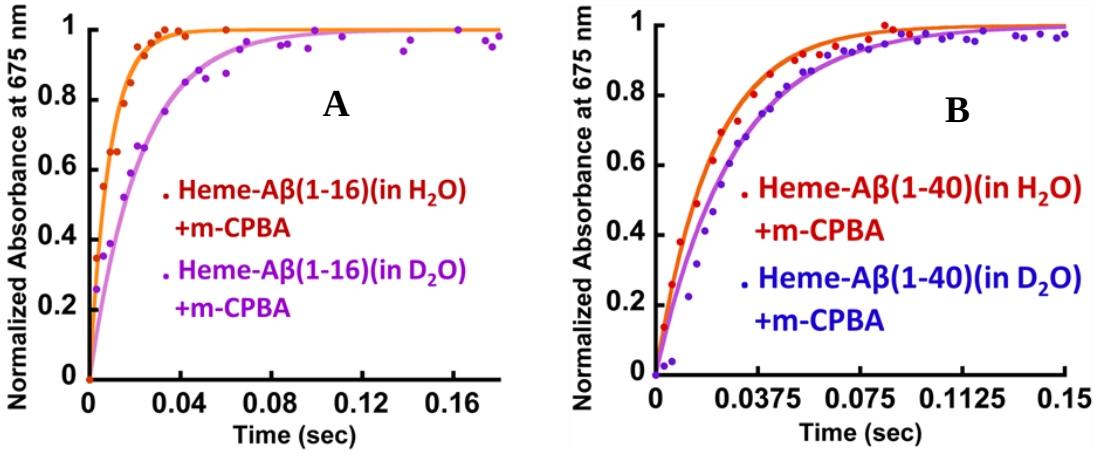

Figure 4. Formation of Compound I for heme-Aβ in H2O, red and in D_2O, purple in 50 mM PO_4^{3-} buffer at pH/D 8. All kinetics were followed at 675 nm. **(A)** for Aβ(1-16) **(B)** for Aβ(1-40).

Table 2. Rate constants of formation and decay of Compound I in D_2O, in 50 mM PO_4^{3-} buffer at pD 8 and in H_2O, in 50 mM PO_4^{3-} buffer at pH 8.

Heme-Aβ(1-40) complex	Formation rate constant	Decay rate constant
D_2O	35 ± 2	2.4 ± 0.1
H_2O	47 ± 1	2.4 ± 0.2

3.3.3. Role of second sphere residues in controlling the rate of formation and decay of Compound I

The Arg5 and Tyr10 residues are involved in peroxidase activity and reactive oxygen species generation, respectively by heme-Aβ complexes.18 In naturally occurring heme peroxidases a distal Arg residue plays a key role in the heterolytic cleavage of the O-O bond as well as stabilizing the FeIV=O intermediate.[30] The Arg5Asn mutant of heme-Aβ(1-16), i.e. heme-Aβ(1-16, Arg5Asn) reacts with m-CPBA and shows a slower rate of formation and a comparable rate of decay of the band at 675 nm suggesting the Arg5 residue assists the formation of Compound I (Table 1, Figure 5A) akin to natural peroxidases. Thus, the role of the Arg5 residue, which was proposed to induce a pull effect assisting in O-O bond heterolysis,

and helping heme-Aβ complex function as peroxidase, stands vindicated. Similar results are obtained with the Arg5Asn mutant of heme-Aβ(1-40) (Figure S6A). The Tyr10Phe mutant of heme-Aβ(1-16), i.e. heme-Aβ(1-16, Tyr10Phe) complex shows a slower rate of formation of Compound I followed by a slower rate of decay relative to the native heme-Aβ(1-16) complex (Scheme 2, Figure 5B). In fact the decay of the Compound I for heme-Aβ(1-16, Tyr10Phe) is almost three times slower compared to native Aβ(1-16) suggesting that, Tyr10 is likely associated with the decay of Compound I. Similar results are obtained with the Tyr10Phe mutant of heme-Aβ(1-40) (Figure S6B). It can thereby possibly exhibit a protective role by mitigating the highly reactive oxidant, Compound I.[51] Attempts to trap a tyrosine radical that would be produced upon its oxidation were not successful implying that the lifetime of such a radical is short. Note that the slower rate of decay of Compound I in the Tyr10 mutant is consistent with faster peroxidase activity exhibited by this mutant (Figure S7), since a slower self-decay rate allows the Compound I to oxidise more of the substrate.

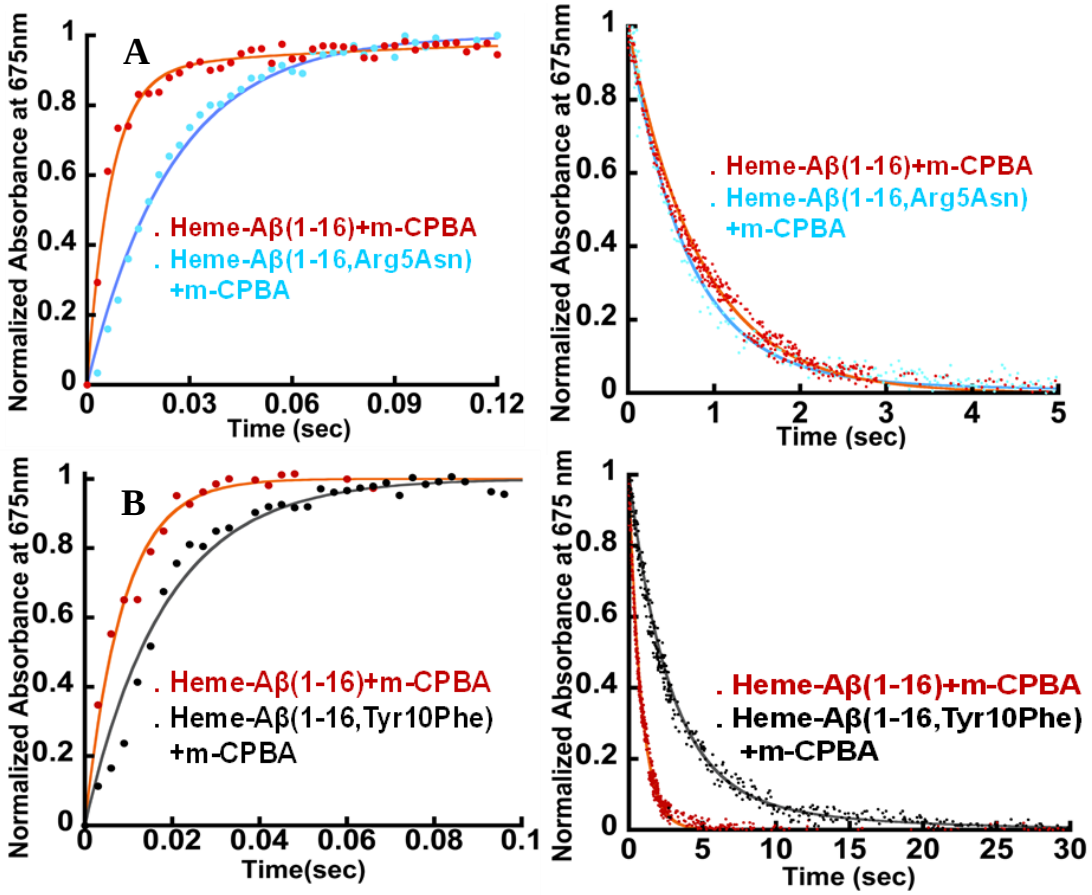

Figure 5 **(A)** Formation and decay of Compound I during reaction between heme-Aβ(1-16) and m-CPBA, red; and between heme-Aβ(1-16, Arg5Asn) and m-CPBA, cyan. (**B)** Formation

and decay of Compound I during reaction between heme-Aβ(1-16) and m-CPBA, red; and between heme-Aβ(1-16, Tyr10Phe) and m-CPBA, black followed at 675 nm, in 50 mM PO_4^{3-} buffer at pH 8.

***Scheme 2*. Schematic representation of the fate of Compound I.**

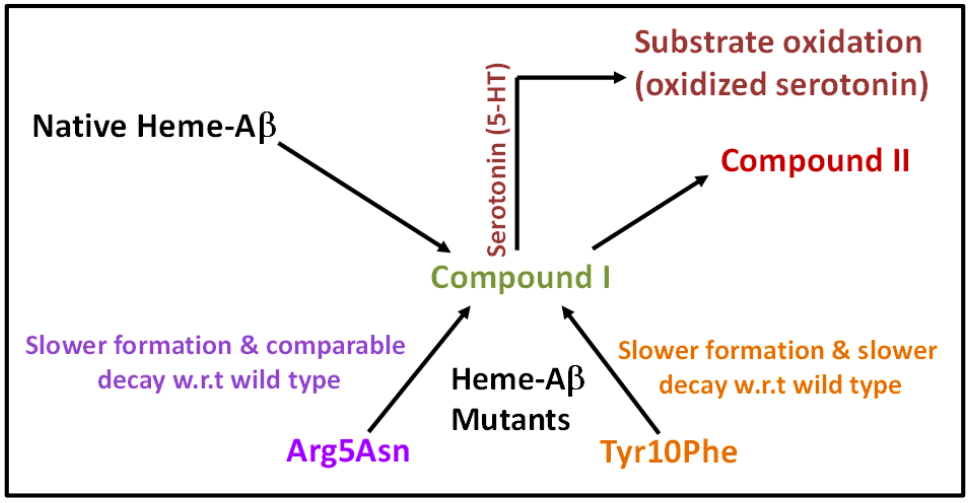

3.3.4. Characterization of Compound I by temperature dependent EPR

Compound I [Fe(IV)=O Por.+] in heme proteins are characterized by an asymmetric signal ~ 15 Gauss wide with g ~1.995, which results from the weak coupling between the S = 1 ferryl centre and S = ½ porphyrin radical.[29,42,52] The broad EPR signal is temperature sensitive and almost disappears at temperature ≥ 30 K, due to the spin relaxation, inflicted by the interaction between porphyrin radical and heme centre.[53] Since the Tyr10Phe and Arg5Asn mutants of Aβ exhibit slower kinetics relative to native heme-Aβ (Table 1), these mutants are used for the spectroscopic characterisation of Compound I. EPR data of the green species formed by the reaction of heme-Aβ(1-16, Tyr10Phe) and heme-Aβ(1-16, Arg5Asn) with m-CPBA frozen within their decay times, show an axial signal with a broad estimated $g_{\perp} = 2.05$ and $g_{\parallel} = 1.97$ at 11 K and 5 K respectively. The data are similar to that reported for Compound I of turnip peroxidase by Ivancich et al. and thereby consistent with the formation of Compound I.[54] The intensity of the broad signal was found to diminish with increasing temperature and at 77 K there was hardly any signal, attributing the spin relaxation phenomena (Figure 6, Figure S8).[54,55]

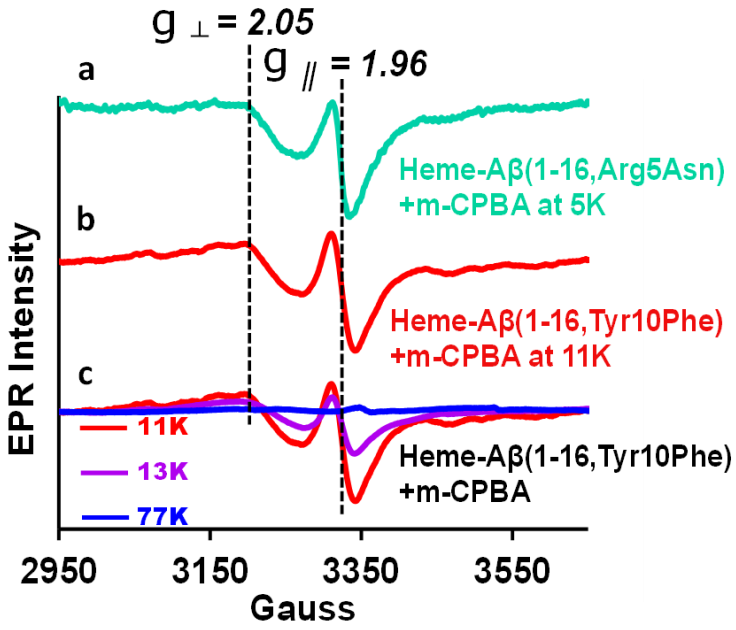

Figure 6. **(a)** EPR spectrum of heme-Aβ(1-16, Arg5Asn) complex on reaction with m-CPBA (mixing time 5 sec), at 5 K, green **(b)** heme-Aβ(1-16, Tyr10Phe) complex on reaction with m-CPBA (mixing time 10 sec), at 11 K, red **(c)**Temperature dependent EPR spectra of heme-Aβ(1-16, Tyr10Phe) complex on reaction with m-CPBA (mixing time 10 sec), at 11 K, red; at 13 K, purple and at 77 K, blue; in 50 mM PO_4^{3-} buffer at pH 8.

3.3.5. Characterization of Compound I by resonance Raman Spectroscopy

Resonance Raman (rR) spectroscopy provides a unique technique for the characterization of structures of heme proteins.[56,57] The rR spectra obtained from heme-Aβ complexes reacted with 5 times excess of m-CPBA clearly indicate a broadening of the oxidation state marker ν4 band region due to the presence of Compound I at 1368 cm^{-1} (Figure 7B, blue) along with compound II at 1382 cm^{-1}(Figure. 7B, orange) in addition to the ν4 band of resting ferric species at 1375 cm^{-1} (Figure 7A, B, green).[58,59] All these signals could be deconvoluted by fitting the ν4 region of the spectrum. More importantly, in the low frequency region (600-900cm^{-1}) of rR spectra, we observe a weak feature at 843 cm^{-1} which shifted to 803 cm^{-1} when isotope labelled solvent (H_2O^{18}) was employed. This corresponds to the ν(Fe-0) of the oxyferryl fragment of Compound I.[60,61] Another less intense band at 817 cm^{-1} was observed corresponding to ν(Fe-0) of Compound II (Figure 7C). We were unable to see convincing isotopic shifts of this band likely because of its weak intensity relative to the strong

heme vibrations and due to low yields of these high valent intermediates, as expected due to the high reactivities of these species.

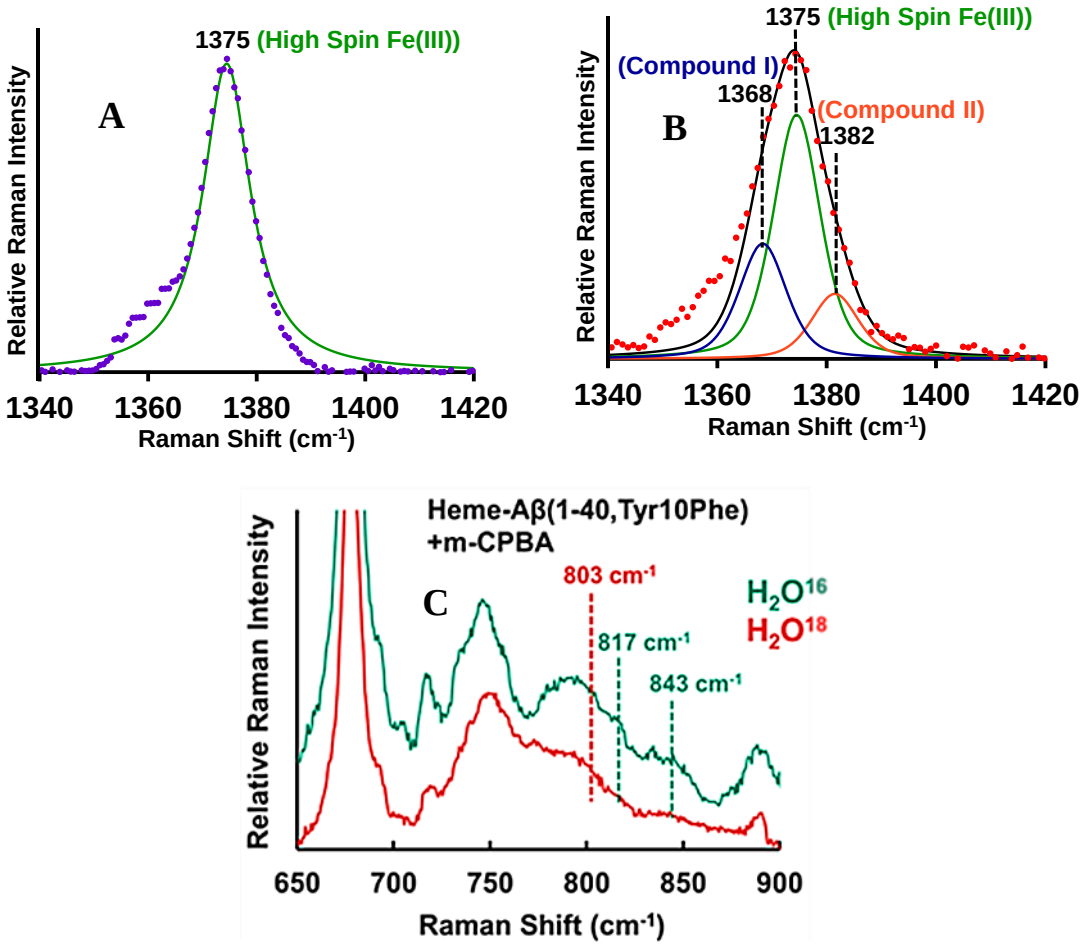

Figure 7. **(A)** High frequency region of resonance Raman- experimental spectrum of heme−Aβ(1-16,Tyr16Phe), purple; simulation spectrum, green **(B)** experimental spectrum of heme−Aβ(1-16,Tyr16Phe) + m-CPBA, red; simulation spectrum, black; .Components of the rR spectrum were determined by simulating the spectra at ν4 region. Data were obtained with an excitation wavelength of 413.1 nm (5 mW) at 77 K. **(C)** low frequency region of resonance Raman spectra of heme−Aβ(1-40, Tyr10Phe) + m-CPBA in H_2O^{16},green; H_2O^{18}

3.4. Discussion

Heme-Aβ complexes show a peroxidase type active site. It reacts with m-CPBA to form a high valent iron-oxo species, which shows a characteristic absorption band at 675 nm and a broad axial EPR signal with effective $g_{\perp} = 2.05$ and $g_{\parallel} = 1.97$ at liquid helium temperatures,

which disappeared almost completely at 77 K. In the rR spectra, the mixture of heme-Aβ and m-CPBA also shows appearance of new oxidation state marker (ν4) bands at 1368 cm^{-1} in the high frequency region and 843 cm^{-1} in the low frequency region respectively. The low frequency band at 843 cm^{-1} shifts to about 803 cm^{-1} on isotope incorporation (40 cm^{-1} shift). These features are characteristic of a reactive Compound I type intermediate which can oxidize neurotransmitters like serotonin. This can potentially lead to abnormal neurotransmission, which is a key pathological feature of AD (Scheme 3). A slower rate of formation of Compound I in D_2O than in H_2O, but a comparable decay is consistent with a protonation assisted O-O bond heterolysis as the rate determining step for Compound I formation. The effect of the second sphere residues Arg5 and Tyr10 on the formation and decay of this intermediate were probed using mutated Aβ peptides. In the absence of Arg5 residue, the rate of formation of the 675 nm band was found to be slower while the decay was comparable to native heme-Aβ, indicating the role of Arg5 in assisting the Compound I formation by inducing a pull effect helping in the O-O bond heterolysis and consequently in the peroxidase activity of heme-Aβ complex. The Tyr10 mutant of the heme-Aβ complex shows a slower rate of formation of Compound I and a slower decay of the same, relative to native heme-Aβ complex suggesting a likely association of Tyr10 in the decay of Compound I. Thus Tyr10 residue might act as a natural defence against oxidation by Compound I. Isolation and characterization of Compound I in the oxidative degradation of neurotransmitters like serotonin provides a possible explanation and mechanism for the abnormal neurotransmission that is observed in AD. It must be noted that AD is a very slow progressing disease. The catalytic oxidation of neurotransmitters like serotonin by heme-Aβ is expected to be slow, so that the deleterious effects of it would occur over a prolong period of time, which also correlated with the relatively late onset of this disease. The relatively slow rate of serotonin oxidation is thus well in accordance with the established facts of AD.[10,18,20,62]

Scheme 3. **Schematic representation of the possible mechanism of peroxidase activity of heme-Aβ in its reaction with m-CPBA.**

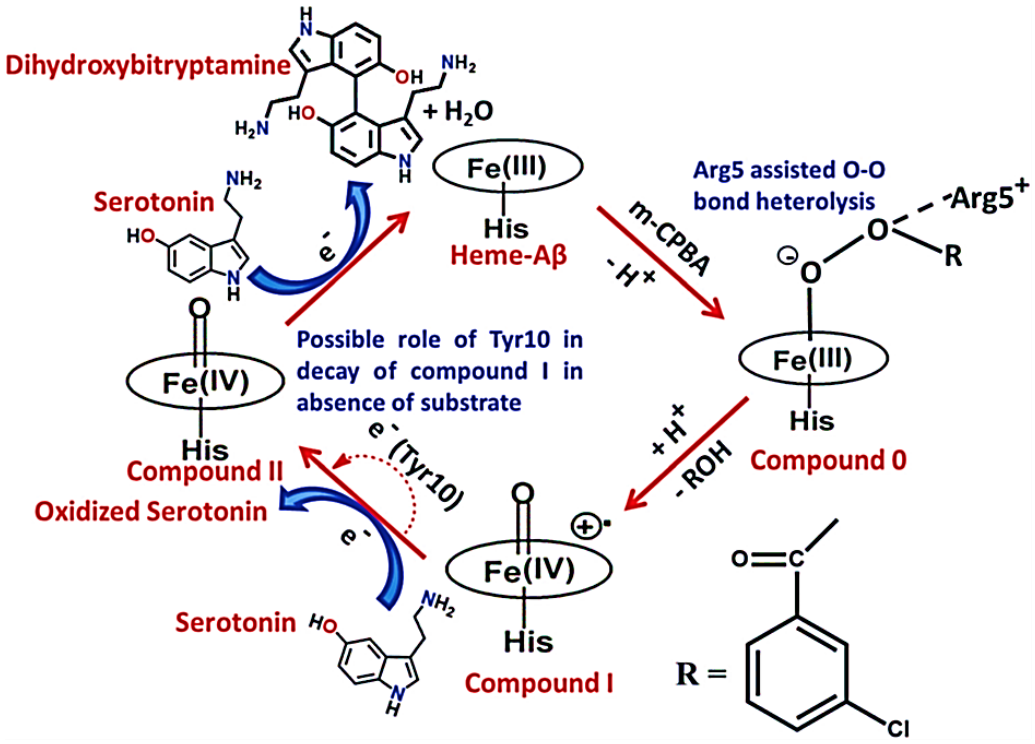

3.5. Conclusions

Heme binds Aβ via a histidine residue (His13/14) within the hydrophilic (1-16) segment and functions as a peroxidase. This heme bound peptide is known to oxidize the neurotransmitter serotonin (5-HT) to its dimer dihydroxybitryptamine (DHT) in presence of H_2O_2/m-CPBA which somewhat explains the decrease in serotonin levels and the abnormal neurotransmission seen in AD patients. The active oxidant in this case is the highly reactive intermediate compound I i.e., Fe^{IV}=O porphyrin π cation radical. Using m-CPBA instead of H_2O_2, this intermediate could be detected using absorption (stopped-flow), EPR (liquid helium temperatures) and resonance Raman spectroscopy. The proton assisted O-O bond cleavage is the rate determining step for compound I formation as is evident from a slower rate of formation in D_2O than in H_2O with the decay being comparable in the two media. The distal Arg5 residue is responsible for the peroxidase behaviour of heme-Aβ and also controls the stability of compound I as it helps in the the O-O bond heterolysis by inducing pull effect. This explains

the slower formation but comparable decay of compound I in absence if Arg5. Tyr10 is found to have a possible association with the decay of compound I for in its absence, the decay of the intermediate is around three times slower than when the native peptide is used. Thus Tyr10 may play a protective role against oxidation by compound I. It should be noted here that the observed catalytic oxidation of the neurotransmitter serotonin by heme-Aβ complexes is relatively slow which tallies well with the slow progressing nature of AD and may also be correlated with the late onset of the disease. Another point of interest here is that there are three amino acid residues which are important with regards to the formation and reactivity of heme-Aβ complexes, namely His13, Arg5 and Tyr10, which are present in human Aβ but absent in rodents who do not suffer from AD. Thus all three amino acids may play a more significant role in the AD pathology than previously thought of. However, all these studies have been done in vitro and as such they need to be substantiated by doing more conclusive studies in vivo. Overall, the trapping and characterization of compound I derived from heme-Aβ, and its ability to oxidatively degrade neurotransmitters like serotonin may provide some insights into a possible mechanism for the abnormal neurotransmission typical to AD.

3.6. References

(1) Alberdi, A.; Aztiria, A.; Basarab, A. On the Early Diagnosis of Alzheimer's Disease from Multimodal Signals: A Survey. *Artif. Intell. Med.* **2016**, *71*, 1–29. https://doi.org/https://doi.org/10.1016/j.artmed.2016.06.003.

(2) Lührs, T.; Ritter, C.; Adrian, M.; Riek-Loher, D.; Bohrmann, B.; Döbeli, H.; Schubert, D.; Riek, R. 3D Structure of Alzheimer's Amyloid-Beta(1-42) Fibrils. *Proc. Natl. Acad. Sci. U. S. A.* **2005**, *102* (48), 17342–17347. https://doi.org/10.1073/pnas.0506723102.

(3) O'Brien, R. J.; Wong, P. C. Amyloid Precursor Protein Processing and Alzheimer's Disease. *Annu. Rev. Neurosci.* **2011**, *34* (1), 185–204. https://doi.org/10.1146/annurev-neuro-061010-113613.

(4) Storey, E.; Cappai, R. The Amyloid Precursor Protein of Alzheimer's Disease and the Abeta Peptide. *Neuropathol. Appl. Neurobiol.* **1999**, *25* (2), 81–97. https://doi.org/10.1046/j.1365-2990.1999.00164.x.

(5) Cornett, C. R.; Markesbery, W. R.; Ehmann, W. D. Imbalances of Trace Elements Related to Oxidative Damage in Alzheimer's Disease Brain. *Neurotoxicology* **1998**, *19* (3), 339–345.

(6) Bush, A. I.; Masters, C. L.; Tanzi, R. E. Copper, β-Amyloid, and Alzheimer's Disease: Tapping a Sensitive Connection. *Proc. Natl. Acad. Sci.* **2003**, *100* (20), 11193 LP – 11194. https://doi.org/10.1073/pnas.2135061100.

(7) Bush, A. I. Drug Development Based on the Metals Hypothesis of Alzheimer's Disease. *J. Alzheimers. Dis.* **2008**, *15* (2), 223–240. https://doi.org/10.3233/jad-2008-15208.

(8) Drew, S. C. The Case for Abandoning Therapeutic Chelation of Copper Ions in Alzheimer's Disease. *Frontiers in Neuroscience*. 2017. https://doi.org/10.3389/fnins.2017.00317.

(9) Karran, E.; Mercken, M.; De Strooper, B. The Amyloid Cascade Hypothesis for Alzheimer's Disease: An Appraisal for the Development of Therapeutics. *Nat. Rev. Drug Discov.* **2011**, *10* (9), 698–712. https://doi.org/10.1038/nrd3505.

(10) Rauk, A. The Chemistry of Alzheimer's Disease. *Chem. Soc. Rev.* **2009**, *38* (9), 2698–

2715. https://doi.org/10.1039/B807980N.

(11) Masters, C. L.; Simms, G.; Weinman, N. A.; Multhaup, G.; McDonald, B. L.; Beyreuther, K. Amyloid Plaque Core Protein in Alzheimer Disease and Down Syndrome. *Proc. Natl. Acad. Sci. U. S. A.* **1985**, *82* (12), 4245–4249. https://doi.org/10.1073/pnas.82.12.4245.

(12) Chiziane, E.; Telemann, H.; Krueger, M.; Adler, J.; Arnhold, J.; Alia, A.; Flemmig, J. Free Heme and Amyloid-Beta: A Fatal Liaison in Alzheimer's Disease. *J. Alzheimers. Dis.* **2018**, *61* (3), 963–984. https://doi.org/10.3233/JAD-170711.

(13) Flemmig, J.; Zámocký, M.; Alia, A. Amyloid β and Free Heme: Bloody New Insights into the Pathogenesis of Alzheimer's Disease. *Neural Regen. Res.* **2018**, *13* (7), 1170–1174. https://doi.org/10.4103/1673-5374.235021.

(14) Valla, J.; Schneider, L.; Niedzielko, T.; Coon, K. D.; Caselli, R.; Sabbagh, M. N.; Ahern, G. L.; Baxter, L.; Alexander, G.; Walker, D. G.; Reiman, E. M. Impaired Platelet Mitochondrial Activity in Alzheimer's Disease and Mild Cognitive Impairment. *Mitochondrion* **2006**, *6* (6), 323–330. https://doi.org/10.1016/j.mito.2006.10.004.

(15) Atamna, H.; Frey, W. H. 2nd. A Role for Heme in Alzheimer's Disease: Heme Binds Amyloid Beta and Has Altered Metabolism. *Proc. Natl. Acad. Sci. U. S. A.* **2004**, *101* (30), 11153–11158. https://doi.org/10.1073/pnas.0404349101.

(16) Pramanik, D.; Ghosh, C.; Dey, S. G. Heme–Cu Bound Aβ Peptides: Spectroscopic Characterization, Reactivity, and Relevance to Alzheimer's Disease. *J. Am. Chem. Soc.* **2011**, *133* (39), 15545–15552. https://doi.org/10.1021/ja204628b.

(17) Atamna, H.; Boyle, K. Amyloid-β Peptide Binds with Heme to Form a Peroxidase: Relationship to the Cytopathologies of Alzheimer's Disease. *Proc. Natl. Acad. Sci. U. S. A.* **2006**, *103* (9), 3381 LP – 3386. https://doi.org/10.1073/pnas.0600134103.

(18) Ghosh, C.; Seal, M.; Mukherjee, S.; Ghosh Dey, S. Alzheimer's Disease: A Heme–Aβ Perspective. *Acc. Chem. Res.* **2015**, *48* (9), 2556–2564. https://doi.org/10.1021/acs.accounts.5b00102.

(19) Pramanik, D.; Dey, S. G. Active Site Environment of Heme-Bound Amyloid Associated with Alzheimer ' s Disease. *J. AM. CHEM. SOC.* **2011**, *133* (15), 81–87.

(20) Mukherjee, S.; Seal, M.; Dey, S. G. Kinetics of Serotonin Oxidation by Heme–Aβ Relevant to Alzheimer's Disease. *JBIC J. Biol. Inorg. Chem.* **2014**, *19* (8), 1355–1365. https://doi.org/10.1007/s00775-014-1193-7.

(21) Berumen, L. C.; Rodríguez, A.; Miledi, R.; García-Alcocer, G. Serotonin Receptors in Hippocampus. *ScientificWorldJournal.* **2012**, *2012*, 823493. https://doi.org/10.1100/2012/823493.

(22) Wrona, M. Z.; Dryhurst, G. Oxidation of Serotonin by Superoxide Radical: Implications to Neurodegenerative Brain Disorders. *Chem. Res. Toxicol.* **1998**, *11* (6), 639–650. https://doi.org/10.1021/tx970185w.

(23) Crino, P. B.; Vogt, B. A.; Chen, J. C.; Volicer, L. Neurotoxic Effects of Partially Oxidized Serotonin: Tryptamine-4,5-Dione. *Brain Res.* **1989**, *504* (2), 247–257. https://doi.org/10.1016/0006-8993(89)91364-4.

(24) Rodríguez, J. J.; Noristani, H. N.; Verkhratsky, A. The Serotonergic System in Ageing and Alzheimer's Disease. *Prog. Neurobiol.* **2012**, *99* (1), 15–41. https://doi.org/10.1016/j.pneurobio.2012.06.010.

(25) Mutisya, E. M.; Bowling, A. C.; Beal, M. F. Cortical Cytochrome Oxidase Activity Is Reduced in Alzheimer's Disease. *J. Neurochem.* **1994**, *63* (6), 2179–2184. https://doi.org/10.1046/j.1471-4159.1994.63062179.x.

(26) Mukherjee, S.; Kapp, E. A.; Lothian, A.; Roberts, A. M.; Vasil'ev, Y. V; Boughton, B. A.; Barnham, K. J.; Kok, W. M.; Hutton, C. A.; Masters, C. L.; Bush, A. I.; Beckman, J. S.; Dey, S. G.; Roberts, B. R. Characterization and Identification of Dityrosine Cross-Linked Peptides Using Tandem Mass Spectrometry. *Anal. Chem.* **2017**, *89* (11), 6136–6145. https://doi.org/10.1021/acs.analchem.7b00941.

(27) Pramanik, D.; Ghosh, C.; Mukherjee, S.; Ghosh, S. *Interaction of Amyloid β Peptides with Redox Active Heme Cofactor: Relevance to Alzheimer's Disease*; 2013; Vol. 257. https://doi.org/10.1016/j.ccr.2012.02.025.

(28) Derat, E.; Shaik, S. The Poulos−Kraut Mechanism of Compound I Formation in Horseradish Peroxidase: A QM/MM Study. *J. Phys. Chem. B* **2006**, *110* (21), 10526–10533. https://doi.org/10.1021/jp055412e.

(29) Poulos, T. L. Heme Enzyme Structure and Function. *Chem. Rev.* **2014**, *114* (7), 3919–3962. https://doi.org/10.1021/cr400415k.

(30) Poulos, T. L. Thirty Years of Heme Peroxidase Structural Biology. *Arch. Biochem. Biophys.* **2010**, *500* (1), 3–12. https://doi.org/10.1016/j.abb.2010.02.008.

(31) Huang, X.; Groves, J. T. Oxygen Activation and Radical Transformations in Heme Proteins and Metalloporphyrins. *Chem. Rev.* **2018**, *118* (5), 2491–2553. https://doi.org/10.1021/acs.chemrev.7b00373.

(32) Rodriguez-Lopez, J. N.; Smith, A. T.; Thorneley, R. N. Effect of Distal Cavity Mutations on the Binding and Activation of Oxygen by Ferrous Horseradish Peroxidase. *J. Biol. Chem.* **1997**, *272* (1), 389–395. https://doi.org/10.1074/jbc.272.1.389.

(33) Denisov, I. G.; Makris, T. M.; Sligar, S. G. Formation and Decay of Hydroperoxo-Ferric Heme Complex in Horseradish Peroxidase Studied by Cryoradiolysis. *J. Biol. Chem.* **2002**, *277* (45), 42706–42710. https://doi.org/10.1074/jbc.M207949200.

(34) Egawa, T.; Shimada, H.; Ishimura, Y. Formation of Compound I in the Reaction of Native Myoglobins with Hydrogen Peroxide. *J. Biol. Chem.* **2000**, *275* (45), 34858–34866. https://doi.org/10.1074/jbc.M004026200.

(35) Fielding, A. J.; Singh, R.; Boscolo, B.; Loewen, P. C.; Ghibaudi, E. M.; Ivancich, A. Intramolecular Electron Transfer versus Substrate Oxidation in Lactoperoxidase: Investigation of Radical Intermediates by Stopped-Flow Absorption Spectrophotometry and (9−285 GHz) Electron Paramagnetic Resonance Spectroscopy. *Biochemistry* **2008**, *47* (37), 9781–9792. https://doi.org/10.1021/bi801032k.

(36) Coulter, E. D.; Cheek, J.; Ledbetter, A. P.; Chang, C. K.; Dawson, J. H. Preparation and Initial Characterization of the Compound I, II, and III States of Iron Methylchlorin-Reconstituted Horseradish Peroxidase and Myoglobin: Models for Key Intermediates in Iron Chlorin Enzymes. *Biochem. Biophys. Res. Commun.* **2000**, *279* (3), 1011–1015. https://doi.org/10.1006/bbrc.2000.4077.

(37) Watanabe, Y.; Nakajima, H.; Ueno, T. Reactivities of Oxo and Peroxo Intermediates Studied by Hemoprotein Mutants. *Acc. Chem. Res.* **2007**, *40* (7), 554–562. https://doi.org/10.1021/ar600046a.

(38) Hewson, W. D.; Hager, L. P. Oxidation of Horseradish Peroxidase Compound II to Compound I. *J. Biol. Chem.* **1979**, *254* (9), 3182–3186.

(39) Yokota, S.; Fujii, H. Critical Factors in Determining the Heterolytic versus Homolytic Bond Cleavage of Terminal Oxidants by Iron(III) Porphyrin Complexes. *J. Am. Chem. Soc.* **2018**, *140* (15), 5127–5137. https://doi.org/10.1021/jacs.7b13037.

(40) Fujii, H.; Ichikawa, K. Preparation and Characterization of an A1u (Oxo) Iron(IV) Porphyrin .Pi.-Cation-Radical Complex. *Inorg. Chem.* **1992**, *31* (6), 1110–1112. https://doi.org/10.1021/ic00032a039.

(41) Schulz, C. E.; Rutter, R.; Sage, J. T.; Debrunner, P. G.; Hager, L. P. Moessbauer and Electron Paramagnetic Resonance Studies of Horseradish Peroxidase and Its Catalytic Intermediates. *Biochemistry* **1984**, *23* (20), 4743–4754. https://doi.org/10.1021/bi00315a033.

(42) Rutter, R.; Hager, L. P.; Dhonau, H.; Hendrich, M.; Valentine, M.; Debrunner, P. Chloroperoxidase Compound I: Electron Paramagnetic Resonance and Moessbauer Studies. *Biochemistry* **1984**, *23* (26), 6809–6816. https://doi.org/10.1021/bi00321a082.

(43) Rittle, J.; Green, M. T. Cytochrome P450 Compound I: Capture, Characterization, and C-H Bond Activation Kinetics. *Science (80-.).* **2010**, *330* (6006), 933 LP – 937. https://doi.org/10.1126/science.1193478.

(44) Maupin, C. M.; Voth, G. A. Preferred Orientations of His64 in Human Carbonic Anhydrase II. *Biochemistry* **2007**, *46* (11), 2938–2947. https://doi.org/10.1021/bi062170f.

(45) Fujii, H.; Yoshimura, T.; Kamada, H. Imidazole and P-Nitrophenolate Complexes of Oxoiron(IV) Porphyrin π-Cation Radicals as Models for Compounds I of Peroxidase and Catalase. *Inorg. Chem.* **1997**, *36* (27), 6142–6143. https://doi.org/10.1021/ic970271j.

(46) Hewson, W. D.; Hager, L. P. Oxidation of Horseradish Peroxidase Compound II to Compound I. *J. Biol. Chem.* **1979**, *254* (9), 3182–3186.

(47) Dunford, H. B.; Hewson, W. D.; Steiner, H. Horseradish Peroxidase. XXIX. Reactions in Water and Deuterium Oxide: Cyanide Binding, Compound I Formation, and

Reactions of Compounds I and II with Ferrocyanide. *Can. J. Chem.* **1978**, *56* (22), 2844–2852. https://doi.org/10.1139/v78-468.

(48) Vidakovic, M.; Sligar, S. G.; Li, H.; Poulos, T. L. Understanding the Role of the Essential Asp251 in Cytochrome P450cam Using Site-Directed Mutagenesis, Crystallography, and Kinetic Solvent Isotope Effect. *Biochemistry* **1998**, *37* (26), 9211–9219. https://doi.org/10.1021/bi980189f.

(49) Chreifi, G.; Baxter, E. L.; Doukov, T.; Cohen, A. E.; McPhillips, S. E.; Song, J.; Meharenna, Y. T.; Soltis, S. M.; Poulos, T. L. Crystal Structure of the Pristine Peroxidase Ferryl Center and Its Relevance to Proton-Coupled Electron Transfer. *Proc. Natl. Acad. Sci.* **2016**, *113* (5), 1226 LP – 1231. https://doi.org/10.1073/pnas.1521664113.

(50) Wrona, M. Z.; Yang, Z.; McAdams, M.; O'Connor-Coates, S.; Dryhurst, G. Hydroxyl Radical-Mediated Oxidation of Serotonin: Potential Insights into the Neurotoxicity of Methamphetamine. *J. Neurochem.* **1995**, *64* (3), 1390–1400. https://doi.org/10.1046/j.1471-4159.1995.64031390.x.

(51) Liu, J. J.; Diaz, D. E.; Quist, D. A.; Karlin, K. D. Copper(I)-Dioxygen Adducts and Copper Enzyme Mechanisms. *Isr. J. Chem.* **2016**, *56*, 9–10. https://doi.org/10.1002/ijch.201600025.

(52) Aasa, R.; Vänngård, T.; Dunford, H. B. EPR Studies on Compound I of Horseradish Peroxidase. *Biochim. Biophys. Acta - Enzymol.* **1975**, *391* (2), 259–264. https://doi.org/https://doi.org/10.1016/0005-2744(75)90249-1.

(53) Colvin, J. T.; Rutter, R.; Stapleton, H. J.; Hager, L. P. Zero-Field Splitting of Fe3+ in Horseradish Peroxidase and of Fe4+ in Horseradish Peroxidase Compound I from Electron Spin Relaxation Data. *Biophys. J.* **1983**, *41* (2), 105–108. https://doi.org/10.1016/S0006-3495(83)84412-9.

(54) Ivancich, A.; Mazza, G.; Desbois, A. Comparative Electron Paramagnetic Resonance Study of Radical Intermediates in Turnip Peroxidase Isozymes. *Biochemistry* **2001**, *40* (23), 6860–6866. https://doi.org/10.1021/bi002826j.

(55) Smith, A. T.; Doyle, W. A.; Dorlet, P.; Ivancich, A. Spectroscopic Evidence for an

Engineered, Catalytically Active Trp Radical That Creates the Unique Reactivity of Lignin Peroxidase. *Proc. Natl. Acad. Sci. U. S. A.* **2009**, *106* (38), 16084–16089. https://doi.org/10.1073/pnas.0904535106.

(56) Hu, S.; Smith, K. M.; Spiro, T. G. Assignment of Protoheme Resonance Raman Spectrum by Heme Labeling in Myoglobin. *J. Am. Chem. Soc.* **1996**, *118* (50), 12638–12646. https://doi.org/10.1021/ja962239e.

(57) Spiro, T. G.; Strekas, T. C. Resonance Raman Spectra of Heme Proteins. Effects of Oxidation and Spin State. *J. Am. Chem. Soc.* **1974**, *96* (2), 338–345. https://doi.org/10.1021/ja00809a004.

(58) Paeng, K. J.; Kincaid, J. R. The Resonance Raman Spectrum of Horseradish Peroxidase Compound I. *J. Am. Chem. Soc.* **1988**, *110* (23), 7913–7915. https://doi.org/10.1021/ja00231a073.

(59) Reczek, C. M.; Sitter, A. J.; Terner, J. Resonance Raman Characterization of Heme Fe(IV)=O Groups of Intermediates of Yeast Cytochrome C Peroxidase and Lactoperoxidase. *J. Mol. Struct.* **1989**, *214*, 27–41. https://doi.org/https://doi.org/10.1016/0022-2860(89)80004-3.

(60) Kincaid, J. R.; Zheng, Y.; Al-Mustafa, J.; Czarnecki, K. Resonance Raman Spectra of Native and Mesoheme-Reconstituted Horseradish Peroxidase and Their Catalytic Intermediates. *J. Biol. Chem.* **1996**, *271* (46), 28805–28811.

(61) Oertling, W. A.; Babcock, G. T. Time-Resolved and Static Resonance Raman Spectroscopy of Horseradish Peroxidase Intermediates. *Biochemistry* **1988**, *27* (9), 3331–3338. https://doi.org/10.1021/bi00409a032.

(62) Atamna, H.; Boyle, K. Amyloid-Beta Peptide Binds with Heme to Form a Peroxidase: Relationship to the Cytopathologies of Alzheimer's Disease. *Proc. Natl. Acad. Sci. U. S. A.* **2006**, *103* (9), 3381–3386. https://doi.org/10.1073/pnas.0600134103.

3.7. Supporting information

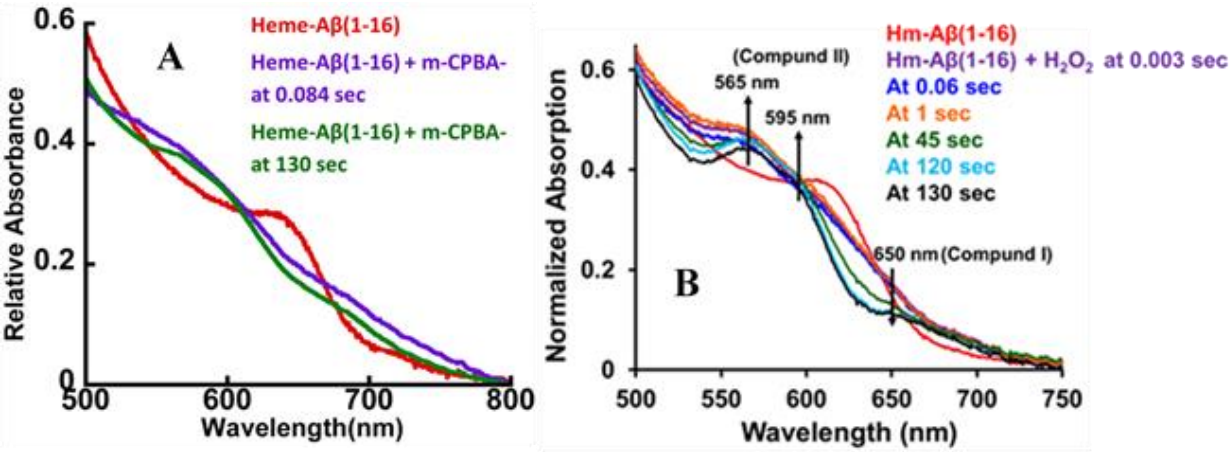

Figure S1. Absorption spectrum of heme-Aβ(1-16), red ; A) for the reaction of heme-Aβ(1-16) with m-CPBA, in 50 mM PO_4^{3-} buffer at pH 8 at 0.027 sec, purple ; and at 130 sec, green in the Q-band region B) for the reaction of heme-Aβ(1-16) with H_2O_2, the difference spectrum at 0.003 sec, purple ; at 0.06 sec, blue; at 1 sec, orange; at 45 sec, green; at 120 sec, cyan and at 130 sec, black; in 50 mM PO_4^{3-} buffer at pH 8. The *arrows* indicate the direction of the spectral changes for compound I and compound II.

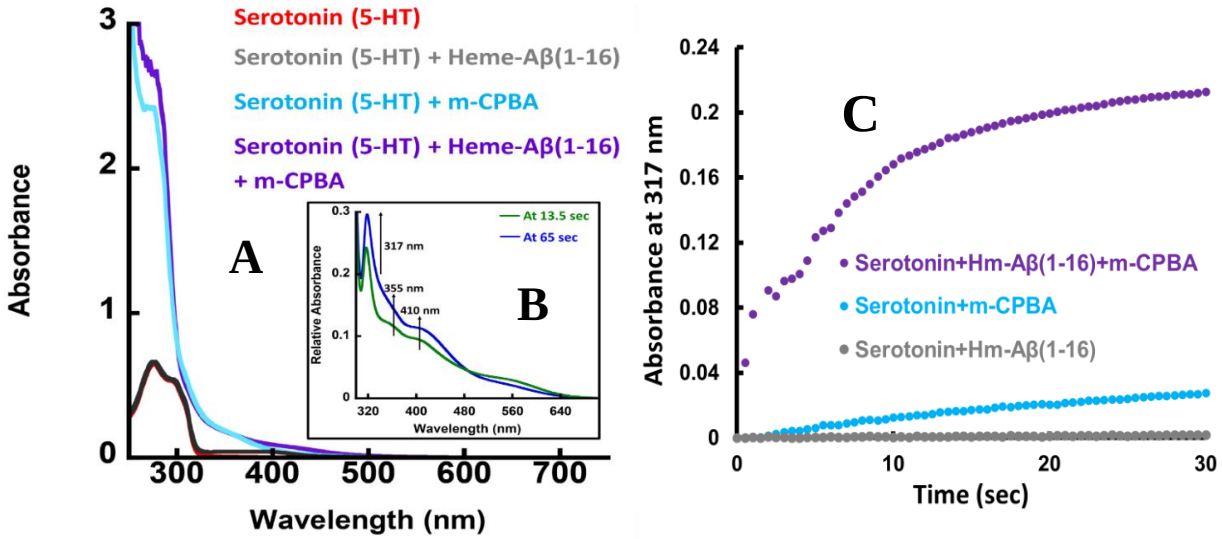

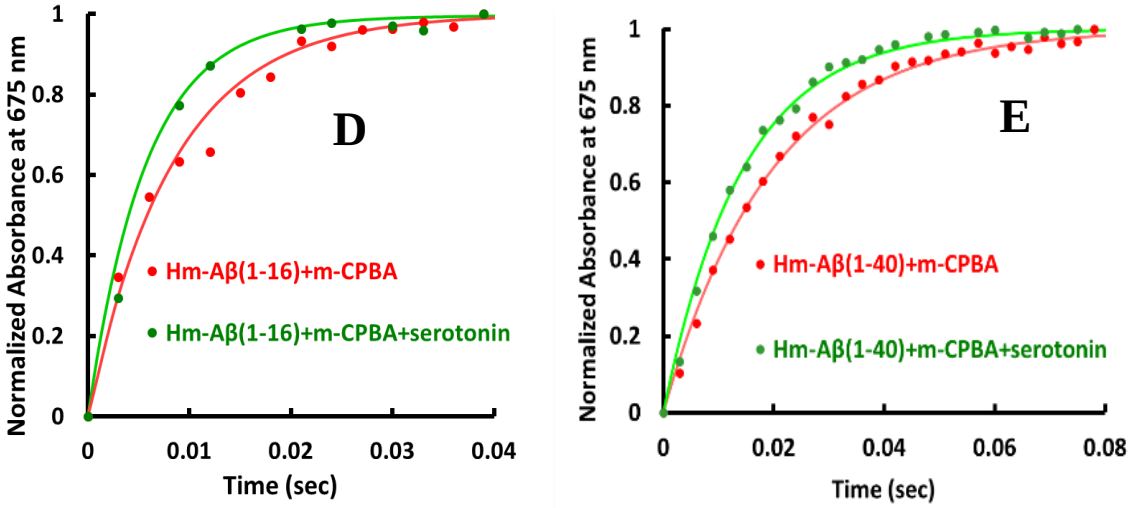

Figure S2. A) Absorption spectrum of serotonin (5-HT), red ; reaction of serotonin with heme-Aβ(1-16), grey ; serotonin with m-CPBA, cyan **;** serotonin with heme-Aβ(1-16) and m-CPBA, violet ; B) Difference Spectra of oxidized compared with unoxidized serotonin (5-HT) at 13.5 sec, green and 65 sec, blue respectively. C) Kinetic trace for the reaction of serotonin with heme-Aβ(1-16) and m-CPBA, purple ; serotonin with m-CPBA, cyan **;** serotonin with heme-Aβ(1-16), grey D**)** Comparison of formation of compound I during reaction of heme-Aβ(1-16) with m-CPBA, in absence of substrate, red; and in presence of substrate, green. E) Comparison of formation of compound I during reaction of heme-Aβ(1-40) with m-CPBA, in absence of substrate, red; and in presence of substrate, green.

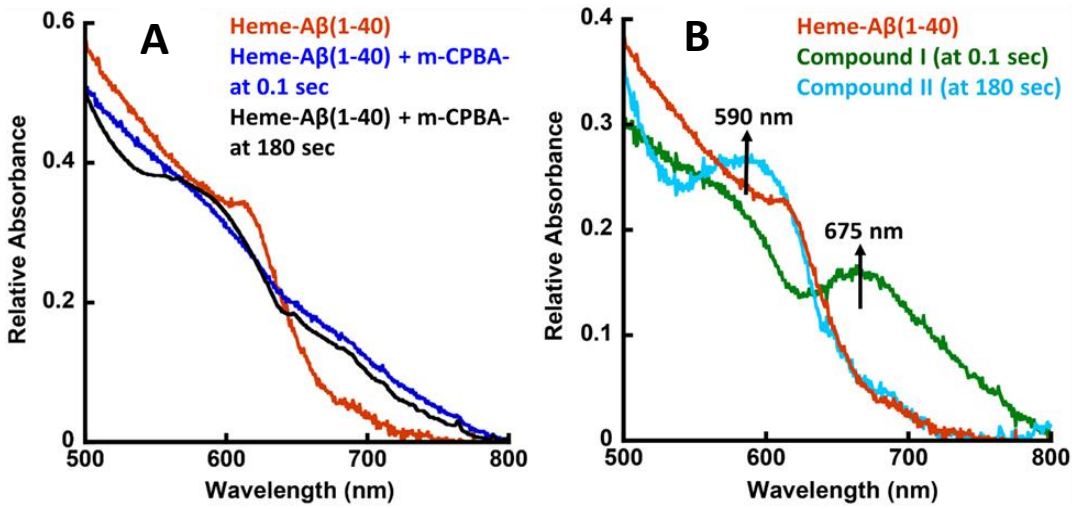

Figure S3. A) Absorption spectra of heme-Aβ(1-40), orange ; heme-Aβ(1-40) with m-CPBA, at 0.1 sec, blue ; and at 180 sec, black. B) Absorption spectra of heme-Aβ(1-40), orange ; difference spectrum of heme-Aβ(1-40) with m-CPBA, at 0.1 sec (Compound I), green and at

180 sec (Compound II), cyan. The *arrows* indicate the direction of the spectral changes. Data acquired in 50 mM PO_4^{3-} buffer at pH 8.

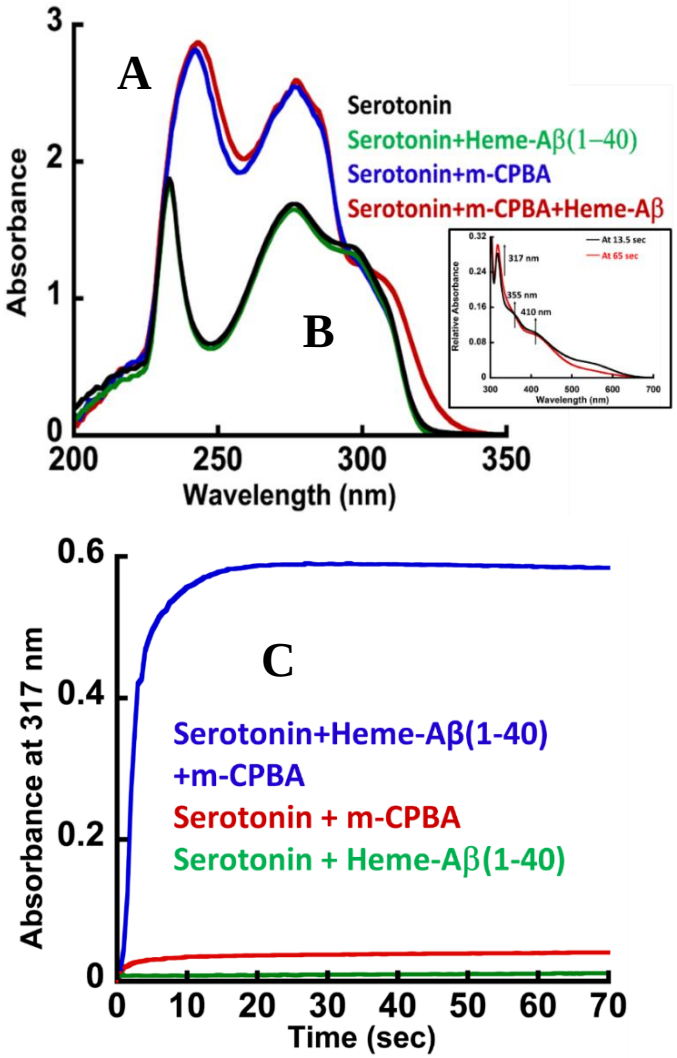

Figure S4. A) Absorption spectrum of serotonin (5-HT), black ; reaction of serotonin with heme-Aβ(1-40), greeen ; serotonin with m-CPBA, blue **;** serotonin with heme-Aβ(1-16) and m-CPBA, red ; B) Difference Spectra of oxidized compared with unoxidized serotonin (5-HT) at 13.5 sec, black and 65 sec, red respectively. C) Kinetic trace for the reaction of serotonin with heme-Aβ(1-40) and m-CPBA, blue ; serotonin with m-CPBA, red **;** serotonin with heme-Aβ(1-16), green.

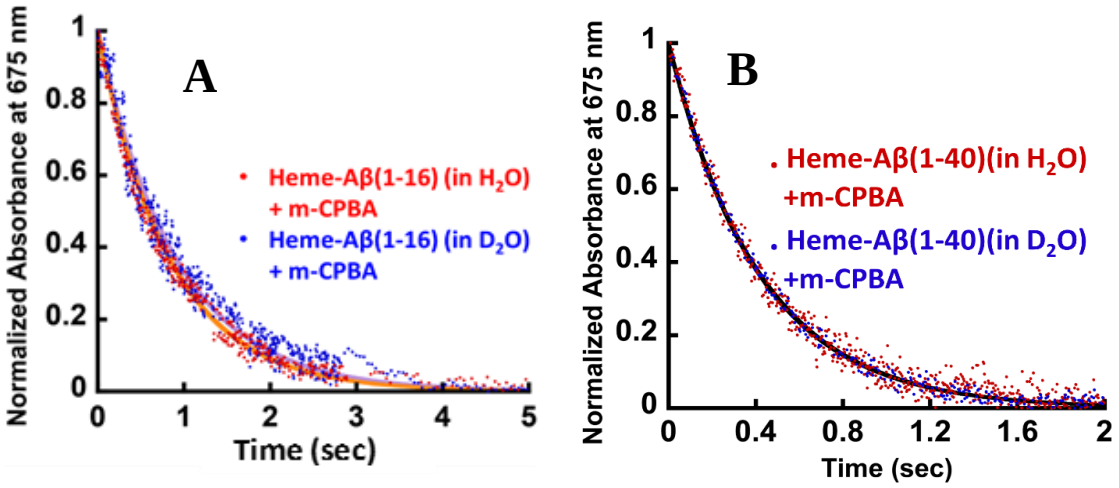

Figure S5. Kinetic trace for A) decay of Compound I of heme-Aβ(1-16) in H_2O (pH 8), red; and in D_2O (pD 8), blue ;.B) decay of Compound I of heme-Aβ(1-40) in H_2O (pH 8), red; and in D_2O (pD 8), blue ; followed at 675 nm.

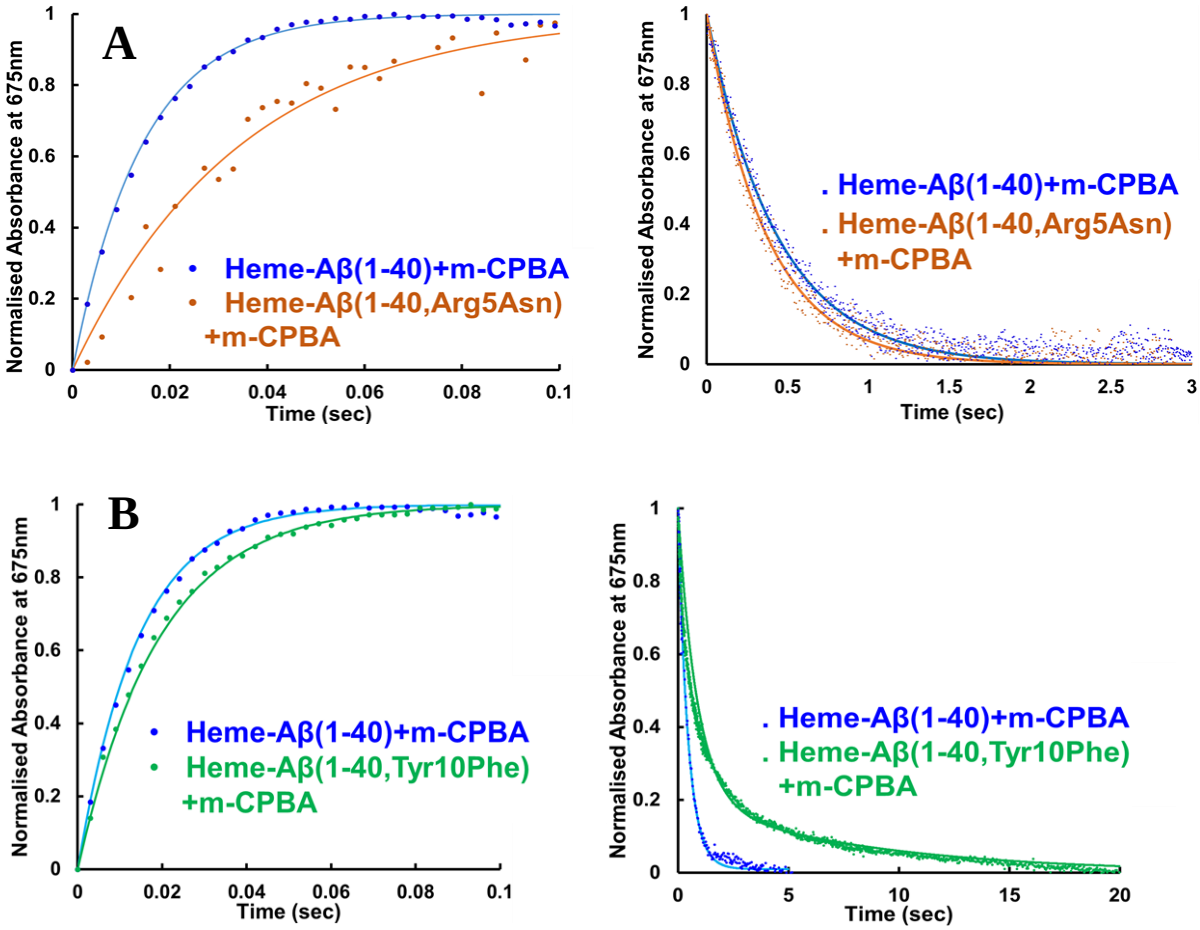

Figure S6. A) Formation and decay of Compound I during reaction between heme-Aβ(1-40) and m-CPBA, blue; and between heme-Aβ(1-40, Arg5Asn) and m-CPBA, orange. B)

Formation and decay of Compound I during reaction between heme-Aβ(1-40) and m-CPBA, blue; and between heme-Aβ(1-40, Tyr10Phe) and m-CPBA, green followed at 675 nm, in 50 mM PO_4^{3-} buffer at pH 8.

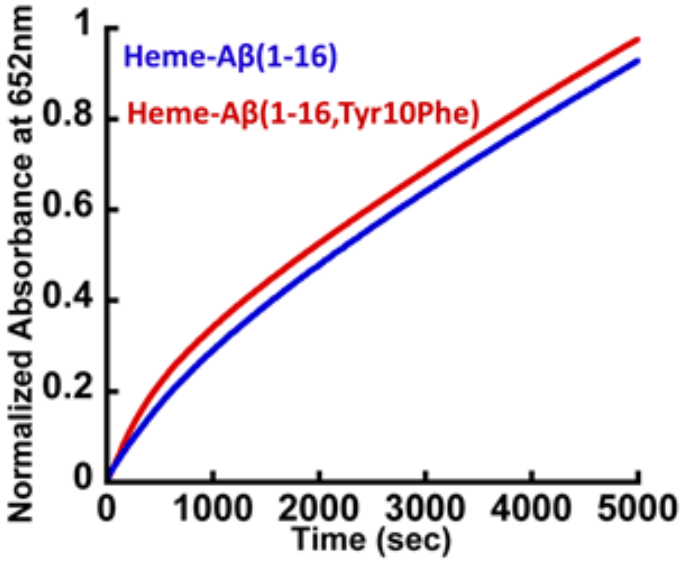

Figure S7. Kinetic trace of peroxidase activity of Heme-Aβ(1-16), blue and Heme-Aβ(1-16,Tyr10Phe), red; followed at 652 nm for the oxidation of TMB at pH 8 in 50 mM PO_4^{3-} buffer.

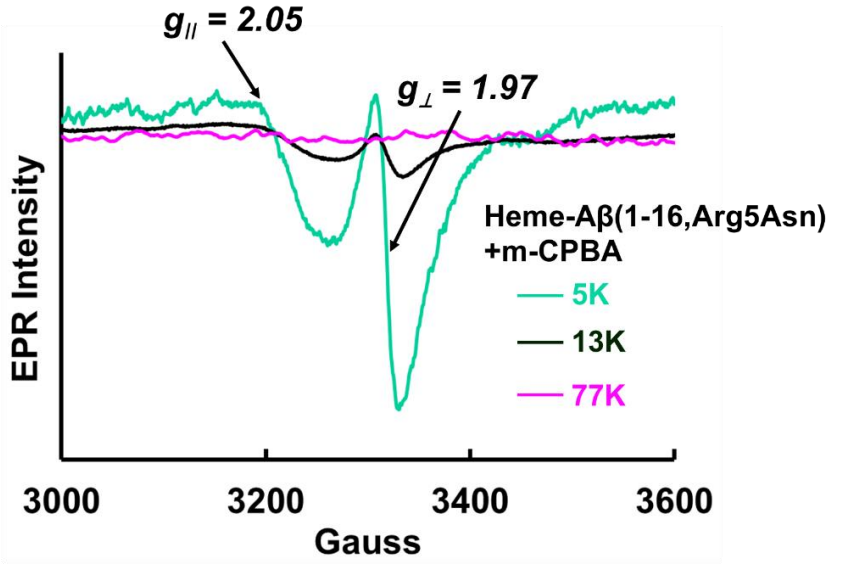

Figure S8. Temperature dependent EPR spectra of heme-Aβ(1-16, Arg5Asn) complex on reaction with m-CPBA (mixing time 5 sec), at 5 K, green; at 13 K, black and at 77 K, pink; in 50 mM PO_4^{3-} buffer at pH 8.

Table S1. **Absorption bands of Compound I above 600 nm**

	Heme Proteins / Porphyrins	Axial Ligand	Absorption Band of Compound I	References
1	HRP	Histidine	650	*Biochemistry* 1984, *23*, 4743
2	CPO	Cysteine	688	*Biochemistry* 1984, *23*, 6809
3	P450 (CYP119)	Cysteine	690	*Science* 2010, 330, 933
4	Catalase	Tyrosine	657	*Biochemistry* 2007, *46*, 11
5	TMP	Imidazole	667	*Inorg. Chem.* 1997, *36*, 6142

Chapter 4

Electronic Structure of the Active Site of Heme Bound Insulin

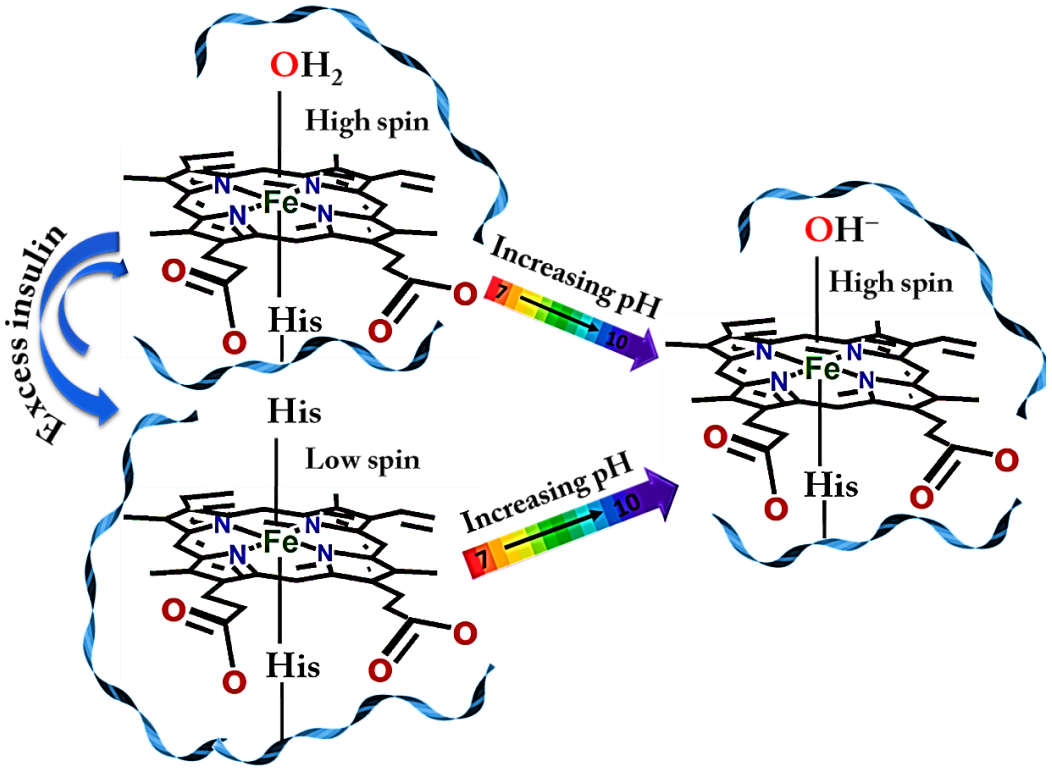

Insulin resistance as well as insulin deficiency are said to be one of the characteristic sign in the development of type 2 diabetes mellitus (T2Dm). Heme has also been suggested to play an important role in the disease etiology since many of the heme deficiency symptoms constitute the common pathological features of T2Dm. Besides, iron overload, higher heme iron intake and transfusion requiring diseases are associated with a higher risk of T2Dm development. Considering all these relevant facts, in this study the interaction between these two key components i.e. heme and insulin has been studied spectroscopically. Under different conditions like in presence of excess peptide as well as increasing pH of the medium, a shift of equilibrium between two components of heme-insulin complexes can be observed. One component is a mono histidine bind species which can serve as a peroxidase and another one is a bis-His type active site similar to cytochrome b. These components are present in different ratio during varying conditions.

4.1. Introduction

Diabetes mellitus is a chronic and widespread public health problem throughout the world and unfortunately, the total number of people affected with diabetes is projected to rise alarmingly from 171 million in 2000 to 366 million in 2030 by WHO.[1,2] Of the diagnosed cases of diabetes, ~90–95% are those of type 2 diabetes mellitus (T2Dm).[3] This particular pathogenic state is triggered by the defects in insulin secretion (impaired β-cell function) as well as in insulin action (insulin inhibition by the liver and muscle tissues).[4] T2Dm ultimately makes a significant contribution towards substantial morbidity in the form of metabolic complications, neuropathy, vision disorders, kidney disease, ulcers and amputations, cardiac diseases, infection *etc*.[5,6] Indeed, the associated mortality rate has been estimated to be ~18.9% annually, with a reduction in life expectancy by almost 5–10 years.[7]

As mentioned above, insulin plays an important part in T2Dm etiology.[8] It is a small peptide hormone secreted in pulses by the β cells of the pancreatic islets of Langerhans. It is synthesized in the β-cells in the form of its precursor, proinsulin which undergoes post translational modification to form the mature insulin. Structurally, insulin is a dipeptide, comprising of 51 amino acids distributed in two chains (A and B chain), with a molecular weight of 5.8 kDa. The B chain has a central helical section while the A chain has an N-terminal helix connected to an anti-parallel C-terminal helix. The two chains are joined by two disulfide bridges between cysteine residues, which join the N- and C-terminal helices of the A chain to the central helix of the B chain. An additional disulfide bridge exists in the A-chain itself (Scheme 1).[9,10] Insulin helps in maintaining the normal blood glucose level by enabling the cellular glucose uptake. It also regulates the metabolism of carbohydrate, lipid and protein. All these actions are mediated through the binding of insulin to the insulin receptors which are members of the class II (cysteine) family of tyrosine kinase receptors.[11,12]

Scheme 1. **The amino acid sequence of human insulin.**

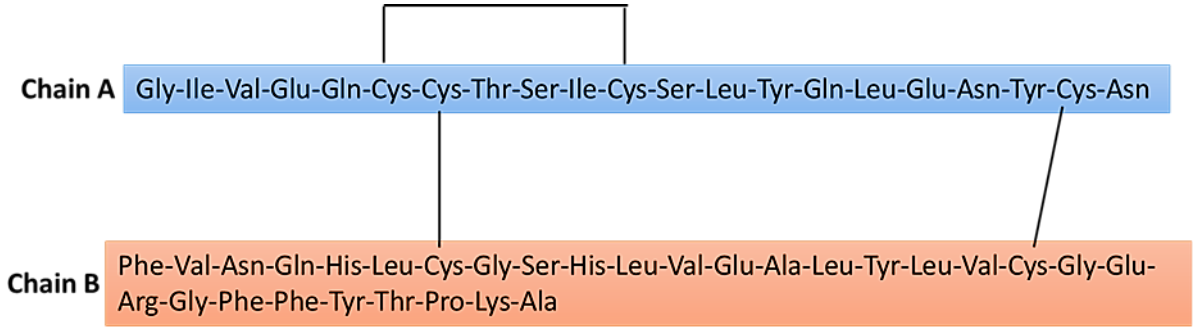

Being the most important regulator of glucose homeostasis, insulin must be secreted in an adequate quantity in the human body. Thus, insulin resistance, abnormal/reduced insulin secretion, declined glucose utilization, and simultaneous increase in glucose production lead to one of the defining characteristics of T2Dm, *i.e.* hyperglycemia.[13–15] In fact, prospective studies show that patients with T2Dm secrete ~70% less insulin than control subjects during the hyperglycemic clamp.[13,16] However, T2Dm has traditionally been associated with insulin resistance while type 1 diabetes mellitus (T1Dm) has been linked to deficiency in insulin production. In recent times though, evidences are emerging in support of loss of β-cell mass in the early stages of T2Dm which declines further with the progression of the disease and eventually leads to impaired insulin secretion.[17,18] Thus not only insulin resistance, but also inability of the β-cells to produce enough insulin is an underlying cause of T2Dm. The resultant cascade of events include higher glucose levels, further β-cell deterioration, diminished glucose sensitivity and elevated hypergycaemia.[19]

Apart from insulin, various metals are said to be involved in T2Dm.[20,21] Being one of the most essential transition metals, Fe plays an important role in heme synthesis and thus maintaining the basic life functions. In relation with T2Dm, Fe overload, elevated serum ferritin level which is the index of body iron stores, lower ratio of transferrin to ferritin and Fe deposition in tissues are significant etiology found from recent studies.[22–24] In fact, Fe accumulation in body increases linearly with the duration of the disease. Such elevated level of iron in the β cells leads to reactive oxygen species (ROS) like H2O2, HO2 ▪ ⁻, OH *via* Fenton's mechanism, causing β cell death and in turn insulin deficiency.[25] Insulin resistance can also be induced by excess Fe storage, as it inhibits the glucose uptake by skeletal muscles and adipose tissues along with reduction in insulin extraction capacity of liver.[26]

Disturbances in copper levels in various bio-fluids and cell tissues are found to be associated with the irregularities in metabolic pathways of diabetic complications.[27–29] Cu can act as a protector of body tissues from oxidative damage.[30] Albeit, high levels of Cu have been found in the blood serum of diabetic patients, probably indicating a natural preventive pathway, but in the long run, Cu in excess can generate oxidative stress, which is a factor in the onset and the advancement of T2Dm.[31,32] Lately it has been shown that Cu ions also bind monomeric insulin with a higher affinity.[33]

Probably, the most important trace element related to T2Dm is Zn as it plays a key role in the storage and secretion of insulin, which subsequently increases the glucose uptake.[34–36] As a result of the increased urinary depletion, a less than optimal Zn level in blood is found in T2Dm patients.[20] Consequently, hypozincemia and hyperzincuria are common to them and this decreased plasma level of Zn adversely affects the ability of islet cells to make and secrete insulin.[37] Also, mutation of Zn transporter, ZnT8 that is a key protein for the regulation of insulin secretion from the pancreatic β-cells has been associated with T2Dm.[38]

Overall, normal levels of essential metals like Ni, Mg, Cr, Mn are disbalanced in T2D patients.[39] It is also suggested that toxic metals like Pb, Ni and Cd may have a role in causing renal tubular dysfunction in diabetes.[40]

The heme moiety is found abundantly in nature as the cofactor of various enzymes having diverse functions.[41] Apart from that, it has also been implicated in diseases such as Alzheimer's disease (AD) and T2Dm which are said to have a similar underlying mechanism.[42–45] The fact that a number of pathological features common to these two diseases such as mitochondrial complex IV dysfunction, altered heme homeostasis, high iron intake, increased levels of heme oxygenase I and transferrin, elevated bilirubin concentration, oxidative stress *etc*. are also the consequences of heme deficiency, help to establish a correlation between heme and the said diseases.[46–48] Specifically for T2Dm, many studies have linked increased heme iron intake to an elevated risk of developing this disease.[24,49,50] Besides, higher incidence of diabetes have been seen in patients undergoing blood transfusions such as those with thalassemia and bone-marrow transplant or patients with hereditary hemochromatosis where iron overload takes place.[51–53] Also, in some of these pathological conditions lysis of erythrocytes occur releasing heme into the plasma whose concentration can become as high as 20–50 uM under severe conditions.[54–56] Such extracellular heme can act as pro-oxidant and thus can give rise to anti-inflammatory response which includes higher expression of heme oxygenase I as seen in T2Dm.[57,58] This enzyme is also involved in insulin signalling as well as in countering the oxidative stress induced insulin resistance which is typical to T2Dm.[59,60] Hence, considering all these factors, a connection between heme and insulin relevant to the disease pathology may exist and as such the interaction between the two has been studied here using absorption and resonance Raman (rR) spectroscopy. Additionally the effect of insulin on heme-amylin complex has also been reported here. This is significant since amylin, a small peptide hormone secreted along with insulin from the pancreatic β-cells,

is also a part of the T2Dm paradigm.[61] Its aggregation and deposition in the β-cells is considered a central event in the development of the disease.[62] More importantly, the heme-amylin complex, whose active site environment has been spectroscopically determined to consist of heme coordinated by a His residue at the 18th position in the peptide and a loosely bound water molecule trans axial to the His, is known to generate a considerable amount of partially reduced oxygen species (PROS) on reaction with oxygen. This may be responsible in part for the oxidative stress observed in T2Dm patients.[63] The present study shows that insulin can take up heme from heme-amylin forming heme-insulin which is experimentally found to generate a negligible amount of PROS.

4.2. Materials and methods

4.2.1. Materials

All reagents were of the highest grade commercially available and were used without further purification. Hemin, human recombinant insulin and buffer were purchased from Sigma.

4.2.2. Sample preparation

Insulin peptide stock solutions was prepared in 100 mM phosphate buffer at pH 8. Hemin solution was prepared by dissolving hemin chloride in 1 M NaOH and the concentration of the heme solution was determined spectrophotometrically ($\varepsilon 385 = 58.44\ mM^{-1}\ cm^{-1}$). Peptide stock solutions were 0.5 mM, and heme stock solution was 5 mM. Heme-insulin complexes were prepared by incubating 1 equivalent of peptide with 0.8 equivalent of heme solution for ~1 h. The pH of the heme-peptide complexes were calibrated accordingly using 1 M H_3PO_4 and 1M NaOH.

4.2.3. Absorption spectroscopy

All the spectral data were obtained by an UV-vis diode array spectrophotometer (Agilent 8453). For all absorption spectroscopy experiments, final concentration of 1:1 heme-insulin complexes were 0.5 mM while that of 1:5 heme-insulin was 0.1 mM with respect to heme.

4.2.4. Resonance Raman spectroscopy

Resonance Raman data were obtained at room temperature using a Trivista 555 spectrograph (Princeton Instruments) using 413.1 nm excitation from a Kr^+ laser (Coherent, Sabre Innova SBRC-DBW-K). The optics (plano-convex lens, mirror *etc*.), used for the collection of rR data were purchased from Sigma-Koki Japan. The power on the samples was ~5 mW. rR samples were 0.2 mM in concentration.

4.2.5. PROS calculation

Xylenol orange assay was applied for PROS calculation. A total of 4.9 mg of Mohr's salt and 3.9 mg of xylenol orange were dissolved in 5 mL of 250 mM H_2SO_4 and stirred for 10 min. A 200 µL portion of this solution was taken in 1.8 mL of nanopure water, and a calibration curve for the quantitative estimation of H_2O_2 was obtained for 0.05, 0.1, 0.5, 1, 2.5, 5, and 10 µM concentrations of H_2O_2 by recording their absorbance at 560 nm as a function of H_2O_2 concentrations in micromolar units for a 2 mL volume. A blank was obtained in the UVvis spectrophotometer with 1.8 mL nanopure water in a cuvette. A total of 200 µL xylenol orange solution was added to the above cuvette and absorbance was measured. This served as the control. The heme-insulin complexes and all the buffer and reagent solutions were degassed first and then were purged with argon in anaerobic vials for ~30 min. Thereafter, the samples were reduced using a minimal amount of dithionite under anaerobic conditions, followed by their reoxidation by O_2 (monitored by absorption). A total of 200 µL of 0.025 mM of reoxidized solutions were separately added to the cuvette containing the control, and their absorbance were recorded. The value of absorbance of the above solutions (after deducting the control) at 560 nm when plotted on the calibration curve yielded the corresponding H_2O_2 concentration.

4.3. Results and Analysis

4.3.1. Heme binding to insulin

Absorption spectroscopy

When one equivalent heme is incubated with one equivalent insulin for ~1 h at pH 7.4, a decrease in intensity of the 365 nm band with a simultaneous formation of the 399 nm band in the Soret band region is observed in the absorption spectrum (Figure 1A). Additionally, the characteristic charge transfer band of heme at ~618 nm is shifted to 630 nm, and new bands appear at 535 nm and 565 nm in the Q-band region (Figure 1B). This suggests the formation of a 1:1 heme-insulin complex.

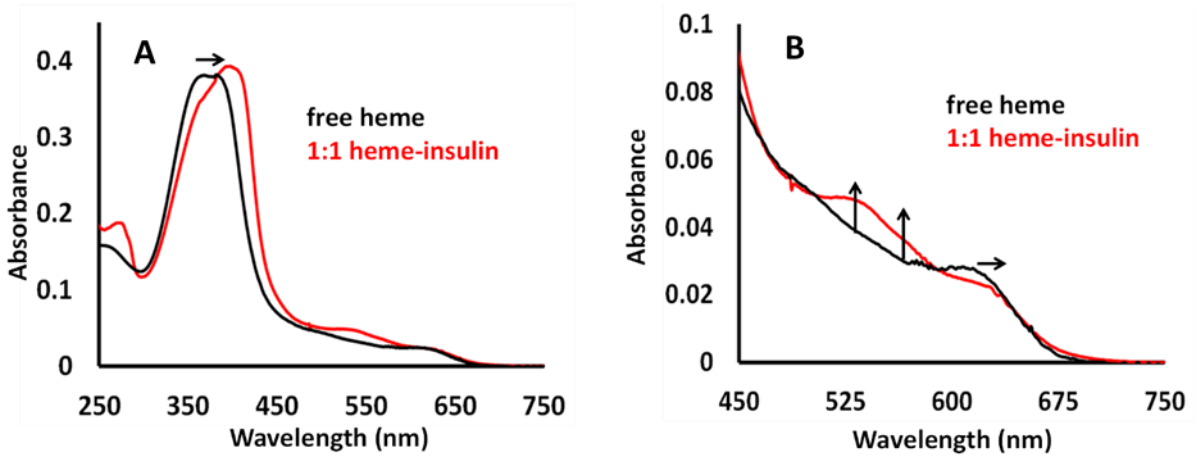

Figure 1. **(A)** Absorption spectra of free heme and 1:1 heme-insulin complex at pH 7.4 in 100 mM phosphate buffer (**B)** enlarged Q-band region showing changes as indicated by arrows relative to heme.

On increasing the concentration of insulin with respect to heme, distinct changes in the absorption spectrum of the heme-insulin complex can be observed. The Soret band of the 1:1 complex at 399 nm shows a red shift to 410 nm concomitant with a gradual increase in its intensity when the heme:insulin ratio is increased from 1:1 to 1:5 (Figure 2A). Excess insulin addition results in an increase in the intensities of the Q bands at 565 and 535 nm (Figure 2B). This spectral feature matches well with the characteristic absorption features of bis-Histidine

type coordination observed in proteins like Cytochrome *b*.[64] Such changes implicates the predominance of a low-spin species at higher equivalents of insulin relative to heme.

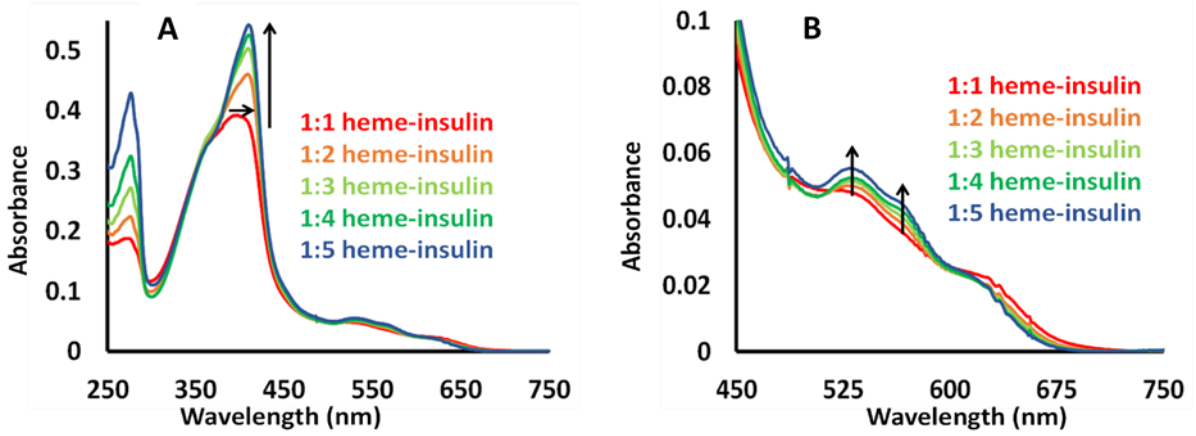

Figure 2. **(A)** Absorption spectra of heme-insulin complexes with different heme:insulin ratios where insulin equivalence is increased at pH 7.4 in 100 mM phosphate buffer. **(B)** enlarged Q-band region showing changes as indicated by arrows relative to 1:1 heme-insulin complex.

Resonance Raman spectroscopy

The resonance Raman (rR) spectrum of the 1:1 heme-insulin species shows an oxidation state marker band (ν4) at 1374 cm−1, indicating the presence of a ferric heme centre.[65] The ν2, ν3, and ν10 vibrational frequencies are sensitive to the core size of the porphyrin ring and denote the coordination and spin-state marker bands.[66] Experimentally, it has been found that the 1:1 complex at pH 7.4 shows mixed features in the ν3, ν2 and ν10 region. The bands at 1492 cm^{-1} (ν3) 1572 cm^{-1} (ν2) and 1630 cm^{-1} (ν10) indicate the presence of a six-coordinate high spin species with a weakly bound exchangeable sixth ligand while the slightly less intense bands at 1505 cm^{-1} (ν3), 1580 cm^{-1} (ν2) and 1641 cm^{-1} (ν10) point towards the occurrence of a six coordinate low spin component. The 1580 cm-1 band denotes the ν37 of six-coordinate high spin heme.[67] These features are quite different compared to those of free heme which has its ν4 at 1373 cm^{-1}, ν2 at 1490 cm^{-1}, ν3 at 1570 cm^{-1} and ν10 at 1627 cm^{-1}, further confirming the heme-insulin complex formation (Figure 3). Thus when heme and insulin are present in equimolar ratio, it is a mixture of a six-coordinate high spin (with a poorly bound distal ligand) and a six coordinate low spin species.

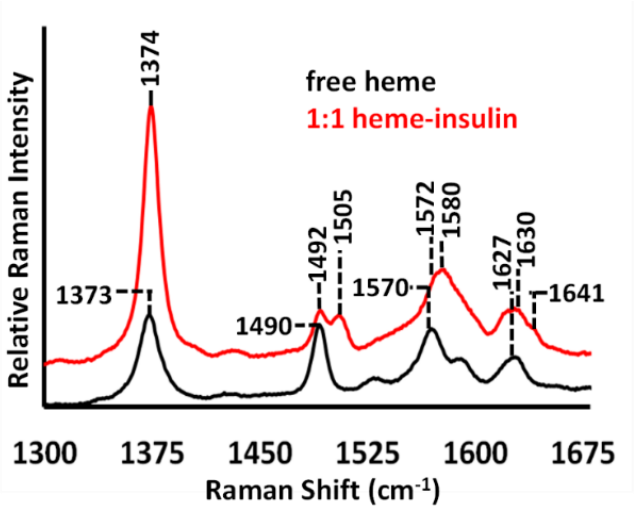

Figure 3. High-frequency rR spectra (excitation 413.1 nm) of free heme and 1:1 heme-insulin complex at pH 7.4 in 100 mM phosphate buffer.

On gradual increment of insulin equivalence relative to heme, an enhancement in the ν2, ν3, and ν10 bands at 1505 cm^{-1}, 1580 cm^{-1} and 1641 cm^{-1} respectively are observed. These changes along with the growth of the ν38 band at 1546 cm^{-1} suggest that a six-coordinate low-spin species is the major component at higher peptide concentration. There is presence of a six-coordinate high spin species as the minor component (Figure 4).

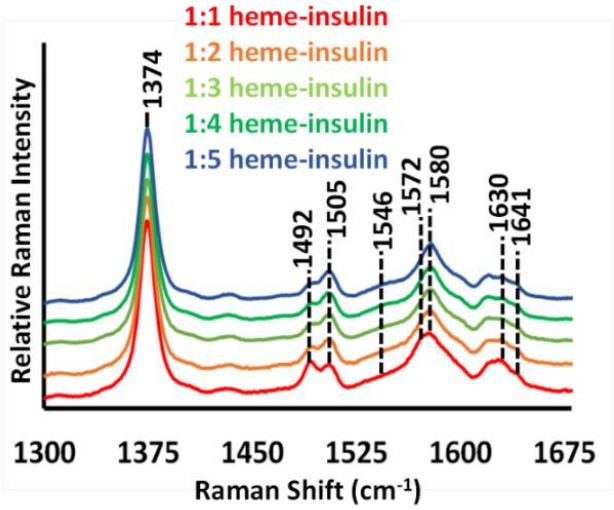

Figure 4. High-frequency rR spectra (excitation 413.1 nm) of heme-insulin complexes with different heme-to-insulin ratios at pH 7.4 in 100 mM phosphate buffer.

4.3.2. Effect of pH on heme–insulin complexes

A pH perturbation study can help probe the nature of the exchangeable ligand in the six-coordinate high spin component present in the heme-insulin complexes. Additionally, changing the pH of the medium can alter the protonation state of charged amino acid residues which in turn can affect the coordination environment. Hence, the effect of pH variation on the heme-insulin complexes were monitored using absorption and resonance Raman spectroscopy. On increasing the pH of the 1:1 heme-insulin complex, the Soret band at 399 nm at pH 7.4 blue shifts and decreases in intensity (Figure 5A). This is accompanied by a simultaneous decrease in intensities of the Q bands at 535 nm and 565 nm and a blue shift of the charge-transfer band at 630 nm (Figure 5B).

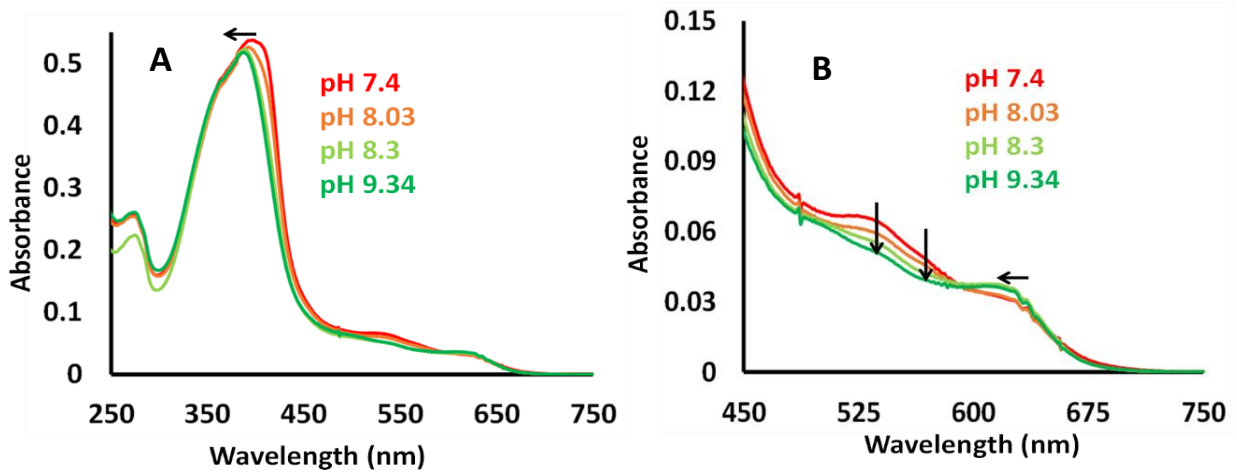

Figure 5. **(A)** Absorption spectra of 1:1 heme-insulin complexes at different pH (**B)** enlarged Q-band region showing changes as indicated by arrows relative to 1:1 heme-insulin complex at pH 7.4 in 100 mM phosphate buffer.

The associated pKa is found to be 8.5 ± 0.2 (Figure 6) which corresponds well to the $H_2O \leftrightarrow OH^-$ equilibrium similar to heme proteins like myoglobin having a water derived ligand distal to the heme centre.[68]

With increase in pH, the rR spectra also exhibit a sharp increase of the ν2, ν3 and ν10 bands at 1492 cm^{-1}, 1572 cm^{-1} and 1630 cm^{-1} respectively, while the bands at 1505 cm^{-1}, 1580 cm^{-1} and 1641 cm^{-1} respectively, do not completely disappear (Figure 7). This implies a gradual increase in the population of a hexa-coordinate high spin species with increase in pH.

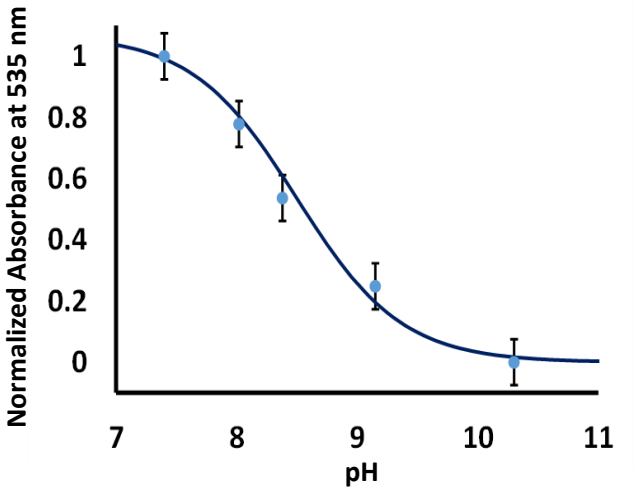

Figure 6. pKa plot of 1:1 heme-insulin complex.

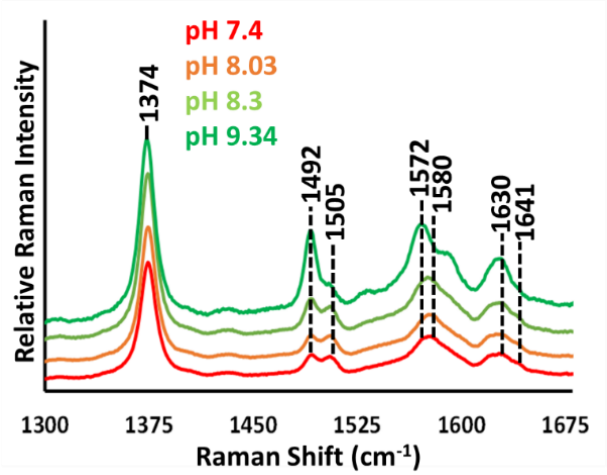

Figure 7. High-frequency rR spectra (excitation 413.1 nm) of 1:1 heme-insulin complexes at different pH in 100 mM phosphate buffer.

On increasing the pH of the 1:3 heme-insulin complex, the blue shift of the Soret band at 410 nm at pH 7.4 along with a decrease in intensities of the Q-bands at 535 nm and 565 nm and blue shift of the charge transfer band from 630 nm are observed (Figure 8). The pKa is found to be ~ 8.5 ± 0.2 (Figure 9).

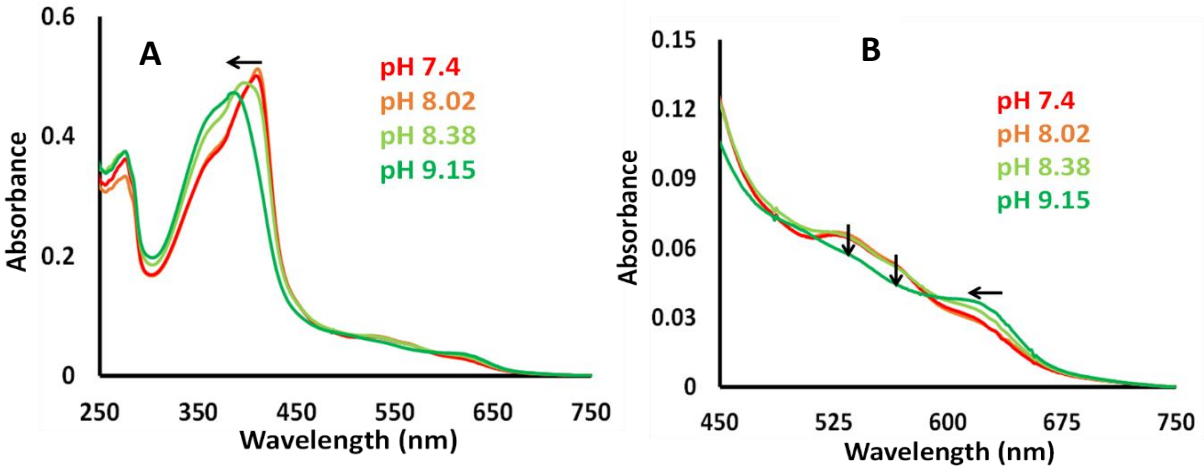

Figure 8. **(A)** Absorption spectra of 1:3 heme-insulin complexes at different pH **(B)** Enlarged Q-band region showing changes as indicated by arrows relative to 1:3 heme-insulin complex at pH 7.4 in 100 mM phosphate buffer.

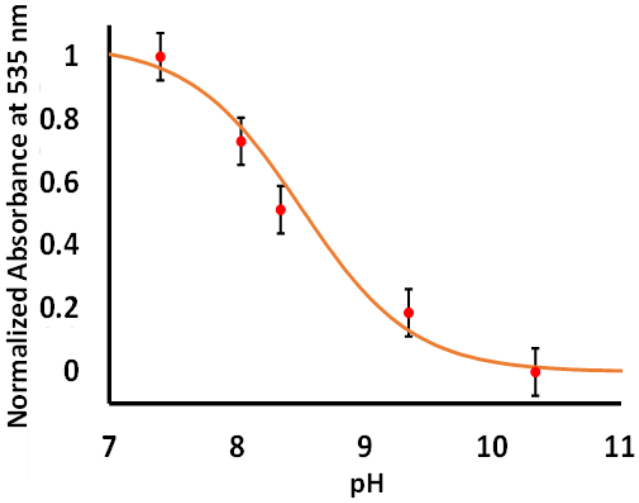

Figure 9. pKa plot of 1:3 heme-insulin complex.

In the high frequency rR spectra, a sharp increase in intensities of bands at 1492 cm^{-1} (ν3), 1572 cm^{-1} (ν2) and 1630 cm^{-1} (ν10) are observed along with residual bands at 1505 cm^{-1} (ν3), 1580 cm^{-1} (ν2) and 1641 cm^{-1} (ν10) (Figure 10). These changes likely indicate the predominance of a high spin component at higher pH with a weakly bound hydroxide ligand.

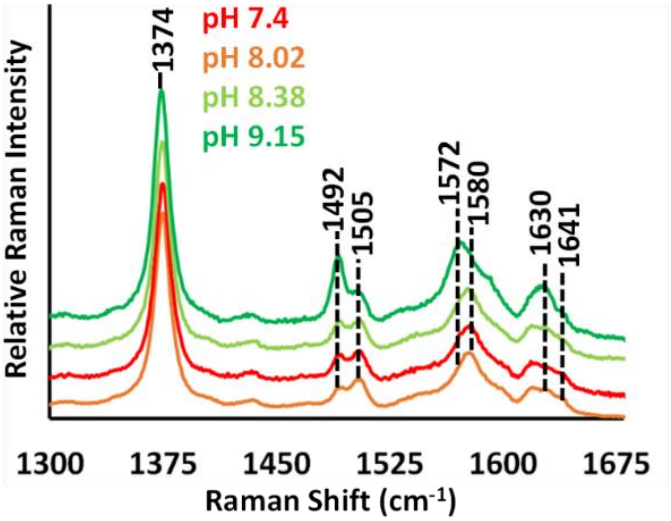

Figure 10. High-frequency rR spectra (excitation 413.1 nm) of 1:3 heme-insulin complexes at different pH in 100 mM phosphate buffer.

4.4. Discussion

When heme binds insulin in equimolar ratio, the absorption spectrum displays a Soret band at 399 nm and a charge transfer band at 630 nm akin to class III plant peroxidases (Figure 1).[70] This is reminiscent of 1:1 heme-amyloid β (Aβ) and heme-amylin complexes associated with AD and T2Dm respectively where the active site consists of a mono-histidine bound high spin heme along with a trans axial weakly bound water derived ligand.[71] On the other hand, the absorption spectrum of 1:1 heme-insulin complex also shows Q bands at 565 nm and 535 nm, which are characteristic of low spin ferric heme species with bis-His type coordination as seen in case of cytochrome *b* and low spin heme-Aβ complex (Figure 1B).[72,73] Thus, the 1:1 heme-insulin complex consists of a mixture of a high spin mono-His and a low spin bis-His species. Considering the amino acid sequence of insulin (Scheme 1), the possible heme coordinating residues are the two His at the 5th and the 10th position in the insulin B chain with the low spin species likely being formed in an intermolecular fashion. The conclusion from the absorption data is corroborated by the rR spectrum of the said heme-insulin complex as it shows a mixture of bands in the ν3, ν2 and ν10 region (Figure 3). The bands at 1492 cm^{-1} (ν3), 1572 cm^{-1} (ν2) and 1630 cm^{-1} (ν10) resemble those observed for the afore mentioned AD and T2Dm relevant

heme-peptide complexes and thus signify the presence of a hexa-coordinate high spin species with a loosely bound sixth ligand while the bands at 1505 cm^{-1} (ν3), 1580 cm^{-1} (ν2) and 1641 cm^{-1} (ν10) point towards the presence of a hexa-coordinate low spin species (comparable to those observed for 1:5 heme-Aβ complex). In addition to that, 1580 cm^{-1} is the ν37 of the six-coordinate high spin species.[67] The relative intensities of these marker bands imply a slightly greater proportion of the high spin component relative to the low spin one.

Excess insulin with respect to heme is found to shift the equilibrium more towards the bis-His low spin complex compared to the mono-His high spin one (Scheme 2). The sharpening and red shift of the Soret to 410 nm and the intensification of the 535 nm and 565 nm Q-bands in the absorption spectra (Figure 2) as well as growth of the hexa-coordinate low spin marker bands (ν3 at 1505 cm^{-1}, ν2 at 1580 cm^{-1} and ν10 at 1641 cm^{-1}) in the rR spectra (Figure 4) on increasing the ratio of insulin to heme from 1:1 to 5:1 provide the supporting evidence.

Scheme 2. **Mixture of high spin and low spin species in heme-insulin complexes. At 1:1 heme : insulin ratio high Spin component is major, and at 1:5 heme : insulin ratio low spin species is major.**

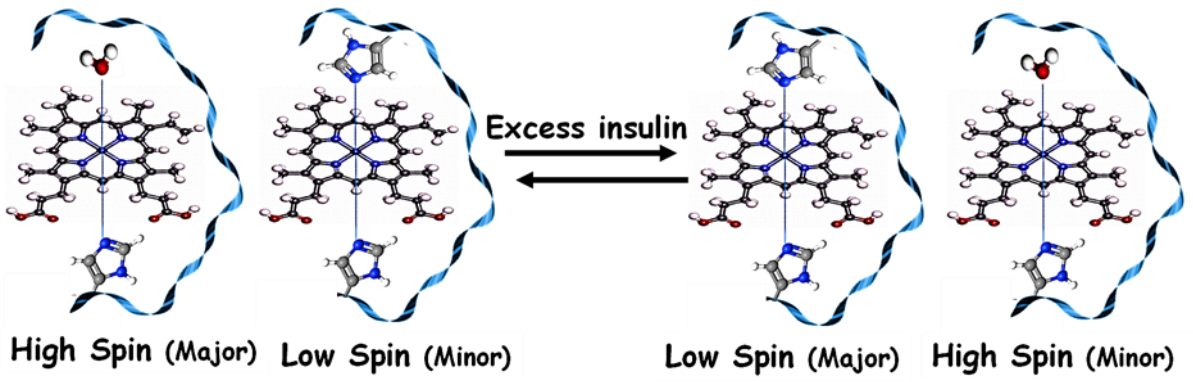

The 1:1 heme-insulin complex shows pH dependence. As pH is increased, notable changes are observed in the Soret and Q-band regions of the absorption spectra (Figure 5) which lead to a pKa of ~ 8.5, similar to that of myoglobin, a heme bound protein with water as the sixth ligand and devoid of any strongly basic hydrogen bonding residue in the distal pocket (Figure 6). Resonance Raman spectroscopy further indicates an increase in the population of a high spin species while some of the low spin component of the 1:1 heme-insulin complex remains intact (Figure 7). These features thus together suggests that at high pH a weakly bound water molecule is likely converted to hydroxide in the mono-His species. In case of the 1:3

heme-insulin complex, changes in the absorption and high frequency rR spectra with gradually increasing alkalinity resemble those observed for the 1:1 heme-insulin complex with a similar pKa (Figures 8–10). These results thus imply that at high pH the axial ligand in the sixth coordination site is essentially a hydroxide in all 1:1 to 1:5 heme-insulin complexes (Scheme 3). However, a small fraction of the bis-His component remains unchanged even at high pH. It is hence important to note here that the relative population of these species is governed by the heme to insulin stoichiometry as well as by the pH of the medium.

Scheme 3. **High spin and low spin heme-insulin generate a hydroxide bound high spin complex at alkaline pH.**

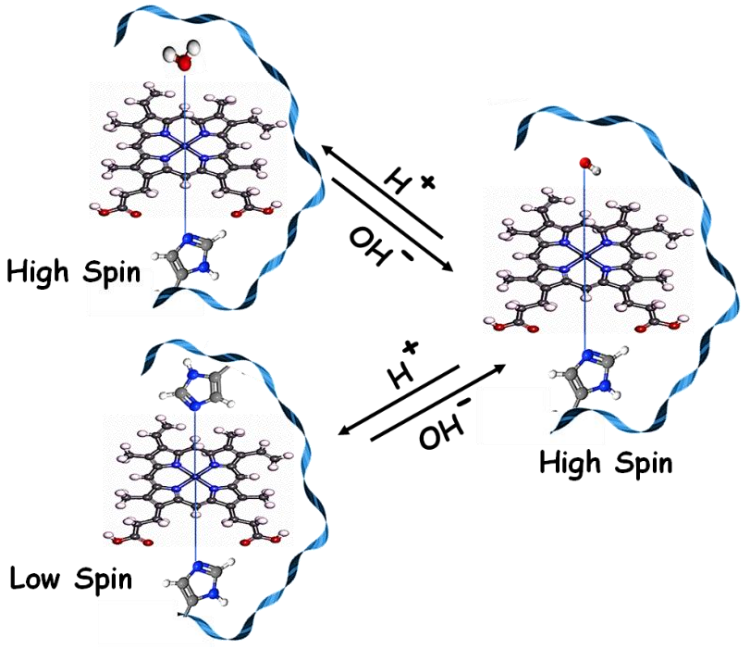

Thus, spectroscopic techniques indicates that heme can bindi to insulin in equimolecular ratio in *in vitro* physiological conditions. This binding is offered via the His residue (either 5th or 10th position in the B chain) of insulin peptide.[62,63] A molecular docking experiment provided evidence that His5 of insulin is the axial binding ligand to heme-Fe(III). They have also suggested that there are contributions from second sphere amino acid residues like Phe1 and Tyr26 which can promote hydrophobic/electrostatic interaction and Val2 which forms H-bond to the heme centre, thus assist in heme-insulin active site formation.[64]

4.5. Conclusion

Type 2 diabetes mellitus, the prolonged metabolic disease, which is characterized by hyperglycemia and is instigated via hampered insulin secretion, making it unable to maintain glucose homeostasis over the progression of the disease. We have found a vital role of heme in the pathogenesis of this disease as heme can form peptide bound complexes and simultaneously alter the reactivities. Along with the interaction of heme with amylin peptide, which is involved in the amyloid deposits around the β-cells, heme is also found to bind another diabetes related peptide, insulin. Spectroscopy demonstrate that when heme is incubated with insulin in 1:1 stoichiometric ratio, heme binds insulin to form a mixture of six-coordinate high spin species as the major component with a possible mono-His coordination and a weakly bound water derived ligand in the distal site similar to a peroxidase type active site. In presence of excess insulin, the six-coordinate low spin species, with a probable bis-His coordination, as seen in case of cytochrome *b* and low spin heme-Aβ complex, predominates. The low spin species is likely formed in an intermolecular fashion, connecting two His residues from two nearby insulin peptides to the heme centre. At higher pH, both high spin and low spin complexes show that the weakly bound water molecule, present at the axial 6^{th} position of active site, is converted to a hydroxide bound high spin species. Overall, here we get a probable electronic structure of the active site of heme bound insulin peptide which is a mixture of both mono-His and bis-His bound components. This will further help in investigating the physiological functions and role of these complexes in T2Dm pathology.

4.6. References

(1) Kaveeshwar, S. A.; Cornwall, J. The Current State of Diabetes Mellitus in India. *Australas. Med. J.* **2014**, *7* (1), 45–48. https://doi.org/10.4066/AMJ.2014.1979.

(2) Risk, N. C. D.; Collaboration, F. Worldwide Trends in Diabetes since 1980: A Pooled Analysis of 751 Population-Based Studies with 4.4 Million Participants. *Lancet (London, England)* **2016**, *387* (10027), 1513–1530. https://doi.org/10.1016/S0140-6736(16)00618-8.

(3) Deshpande, A. D.; Harris-Hayes, M.; Schootman, M. Epidemiology of Diabetes and Diabetes-Related Complications. *Phys. Ther.* **2008**, *88* (11), 1254–1264. https://doi.org/10.2522/ptj.20080020.

(4) Cerf, M. E. Beta Cell Dysfunction and Insulin Resistance. *Front. Endocrinol. (Lausanne).* **2013**, *4*, 37. https://doi.org/10.3389/fendo.2013.00037.

(5) Papatheodorou, K.; Banach, M.; Bekiari, E.; Rizzo, M.; Edmonds, M. Complications of Diabetes 2017. *J. Diabetes Res.* **2018**, *2018*, 10–13. https://doi.org/10.1155/2018/3086167.

(6) Jame Caro, J.; Alexandra, J.; O'Brien, J. A. Lifetime Costs of Complications Resulting. *Diabetes Care* **2002**, *25* (3), 476–481.

(7) Cusick, M.; Meleth, A. D.; Agrón, E.; Fisher, M. R.; Reed, G. F.; Knatterud, G. L.; Barton, F. B.; Davis, M. D.; Ferris, F. L.; Chew, E. Y. Associations of Mortality and Diabetes Complications in Patients With Type 1 and Type 2 Diabetes. *Diabetes Care* **2005**, *28* (3), 617 LP – 625. https://doi.org/10.2337/diacare.28.3.617.

(8) Martin, B. C.; Warram, J. H.; Krolewski, A. S.; Soeldner, J. S.; Kahn, C. R.; Martin, B. C.; Bergman, R. N. Role of Glucose and Insulin Resistance in Development of Type 2 Diabetes Mellitus: Results of a 25-Year Follow-up Study. *Lancet* **1992**, *340* (8825), 925–929. https://doi.org/https://doi.org/10.1016/0140-6736(92)92814-V.

(9) Brange, J.; Langkjœr, L. Insulin Structure and Stability BT - Stability and Characterization of Protein and Peptide Drugs: Case Histories; Wang, Y. J., Pearlman, R., Eds.; Springer US: Boston, MA, 1993; pp 315–350. https://doi.org/10.1007/978-1-

4899-1236-7_11.

(10) Blundell, T.; Dodson, G.; Hodgkin, D.; Mercola, D. Insulin: The Structure in the Crystal and Its Reflection in Chemistry and Biology By; Anfinsen, C. B., Edsall, J. T., Richards, in P. C., Eds.; Academic Press, 1972; Vol. 26, pp 279–402. https://doi.org/https://doi.org/10.1016/S0065-3233(08)60143-6.

(11) De Meyts, P. Insulin and Its Receptor: Structure, Function and Evolution. *BioEssays* **2004**, *26* (12), 1351–1362. https://doi.org/https://doi.org/10.1002/bies.20151.

(12) Tokarz, V. L.; MacDonald, P. E.; Klip, A. The Cell Biology of Systemic Insulin Function. *J. Cell Biol.* **2018**, *217* (7), 2273–2289. https://doi.org/10.1083/jcb.201802095.

(13) Reaven, G. M.; Hollenbeck, C. B.; Chen, Y. D. I. Relationship between Glucose Tolerance, Insulin Secretion, and Insulin Action in Non-Obese Individuals with Varying Degrees of Glucose Tolerance. *Diabetologia* **1989**, *32* (1), 52–55. https://doi.org/10.1007/BF00265404.

(14) Guillausseau, P.-J.; Meas, T.; Virally, M.; Laloi-Michelin, M.; Médeau, V.; Kevorkian, J.-P. Abnormalities in Insulin Secretion in Type 2 Diabetes Mellitus. *Diabetes Metab.* **2008**, *34*, S43–S48. https://doi.org/https://doi.org/10.1016/S1262-3636(08)73394-9.

(15) Weyer, C.; Bogardus, C.; Mott, D. M.; Pratley, R. E. The Natural History of Insulin Secretory Dysfunction and Insulin Resistance in the Pathogenesis of Type 2 Diabetes Mellitus. *J. Clin. Invest.* **1999**, *104* (6), 787–794. https://doi.org/10.1172/JCI7231.

(16) Mitrakou, A.; Kelley, D.; Mokan, M.; Veneman, T.; Pangburn, T.; Reilly, J.; Gerich, J. Role of Reduced Suppression of Glucose Production and Diminished Early Insulin Release in Impaired Glucose Tolerance. *N. Engl. J. Med.* **1992**, *326* (1), 22–29. https://doi.org/10.1056/NEJM199201023260104.

(17) Fukushima, M.; Suzuki, H.; Seino, Y. Insulin Secretion Capacity in the Development from Normal Glucose Tolerance to Type 2 Diabetes. *Diabetes Res. Clin. Pract.* **2004**, *66*, S37–S43. https://doi.org/https://doi.org/10.1016/j.diabres.2003.11.024.

(18) Yabe, D.; Seino, Y.; Fukushima, M.; Seino, S. β Cell Dysfunction Versus Insulin Resistance in the Pathogenesis of Type 2 Diabetes in East Asians. *Curr. Diab. Rep.*

2015, *15* (6). https://doi.org/10.1007/s11892-015-0602-9.

(19) Mitrakou, A.; Vuorinen-Markkola, H.; Raptis, G.; Toft, I.; Mokan, M.; Strumph, P.; Pimenta, W.; Veneman, T.; Jenssen, T.; Bolli, G. Simultaneous Assessment of Insulin Secretion and Insulin Sensitivity Using a Hyperglycemia Clamp. *J. Clin. Endocrinol. Metab.* **1992**, *75* (2), 379–382. https://doi.org/10.1210/jcem.75.2.1639939.

(20) Khan, A. R.; Awan, F. R. Metals in the Pathogenesis of Type 2 Diabetes. *J. Diabetes Metab. Disord.* **2014**, *13* (1), 16. https://doi.org/10.1186/2251-6581-13-16.

(21) Zheng, Y.; Li, X.-K.; Wang, Y.; Cai, L. The Role of Zinc, Copper and Iron in the Pathogenesis of Diabetes and Diabetic Complications: Therapeutic Effects by Chelators. *Hemoglobin* **2008**, *32* (1–2), 135–145. https://doi.org/10.1080/03630260701727077.

(22) Rajpathak, S. N.; Crandall, J. P.; Wylie-Rosett, J.; Kabat, G. C.; Rohan, T. E.; Hu, F. B. The Role of Iron in Type 2 Diabetes in Humans. *Biochim. Biophys. Acta - Gen. Subj.* **2009**, *1790* (7), 671–681. https://doi.org/https://doi.org/10.1016/j.bbagen.2008.04.005.

(23) Swaminathan, S.; Fonseca, V. A.; Alam, M. G.; Shah, S. V. The Role of Iron in Diabetes and Its Complications. *Diabetes Care* **2007**, *30* (7), 1926 LP – 1933. https://doi.org/10.2337/dc06-2625.

(24) Bao, W.; Rong, Y.; Rong, S.; Liu, L. Dietary Iron Intake, Body Iron Stores, and the Risk of Type 2 Diabetes: A Systematic Review and Meta-Analysis. *BMC Med.* **2012**, *10* (1), 119. https://doi.org/10.1186/1741-7015-10-119.

(25) Rehman, K.; Akash, M. S. H. Mechanism of Generation of Oxidative Stress and Pathophysiology of Type 2 Diabetes Mellitus: How Are They Interlinked? *J. Cell. Biochem.* **2017**, *118* (11), 3577–3585. https://doi.org/https://doi.org/10.1002/jcb.26097.

(26) Arija, V.; Fernández-Cao, J. C.; Basora, J.; Bulló, M.; Aranda, N.; Estruch, R.; Martínez-González, M. A.; Salas-Salvadó, J. Excess Body Iron and the Risk of Type 2 Diabetes Mellitus: A Nested Case–Control in the PREDIMED (PREvention with MEDiterranean Diet) Study. *Br. J. Nutr.* **2014**, *112* (11), 1896–1904. https://doi.org/DOI: 10.1017/S0007114514002852.

(27) Naka, T.; Kaneto, H.; Katakami, N.; Matsuoka, T. A.; Harada, A.; Yamasaki, Y.; Matsuhisa, M.; Shimomura, I. Association of Serum Copper Levels and Glycemic

Control in Patients with Type 2 Diabetes. *Endocr. J.* **2013**, *60* (3), 393–396. https://doi.org/10.1507/endocrj.EJ12-0342.

(28) Bjørklund, G.; Dadar, M.; Pivina, L.; Doşa, M. D.; Semenova, Y.; Aaseth, J. The Role of Zinc and Copper in Insulin Resistance and Diabetes Mellitus. *Current Medicinal Chemistry*. pp 6643–6657.

(29) Eshak, E. S.; Iso, H.; Maruyama, K.; Muraki, I.; Tamakoshi, A. Associations between Dietary Intakes of Iron, Copper and Zinc with Risk of Type 2 Diabetes Mellitus: A Large Population-Based Prospective Cohort Study. *Clin. Nutr.* **2018**, *37* (2), 667–674. https://doi.org/https://doi.org/10.1016/j.clnu.2017.02.010.

(30) Zheng, H.; Blat, D.; Youdim, M. B. H.; Weiner, L. M.; Dangoor, D.; Gozes, I.; Fridkin, M. Novel Neuroprotective Neurotrophic NAP Analogs Targeting Iron Toxicity and Oxidative Stress in Neurodegenerative Diseases BT - Understanding Biology Using Peptides; Blondelle, S. E., Ed.; Springer New York: New York, NY, 2006; pp 443–444.

(31) TANAKA, A.; KANETO, H.; MIYATSUKA, T.; YAMAMOTO, K.; YOSHIUCHI, K.; YAMASAKI, Y.; SHIMOMURA, I.; MATSUOKA, T.; MATSUHISA, M. Role of Copper Ion in the Pathogenesis of Type 2 Diabetes. *Endocr. J.* **2009**, *56* (5), 699–706. https://doi.org/10.1507/endocrj.K09E-051.

(32) Masad, A.; Hayes, L.; Tabner, B. J.; Turnbull, S.; Cooper, L. J.; Fullwood, N. J.; German, M. J.; Kametani, F.; El-Agnaf, O. M. A.; Allsop, D. Copper-Mediated Formation of Hydrogen Peroxide from the Amylin Peptide: A Novel Mechanism for Degeneration of Islet Cells in Type-2 Diabetes Mellitus? *FEBS Lett.* **2007**, *581* (18), 3489–3493. https://doi.org/https://doi.org/10.1016/j.febslet.2007.06.061.

(33) Gavrilova, J.; Tõugu, V.; Palumaa, P. Affinity of Zinc and Copper Ions for Insulin Monomers. *Metallomics* **2014**, *6* (7), 1296–1300. https://doi.org/10.1039/c4mt00059e.

(34) Xu, Y.; Yan, Y.; Seeman, D.; Sun, L.; Dubin, P. L. Multimerization and Aggregation of Native-State Insulin: Effect of Zinc. *Langmuir* **2012**, *28* (1), 579–586. https://doi.org/10.1021/la202902a.

(35) Chausmer, A. B. Zinc, Insulin and Diabetes. *J. Am. Coll. Nutr.* **1998**, *17* (2), 109–115. https://doi.org/10.1080/07315724.1998.10718735.

(36) Dunn, M. F. Zinc–Ligand Interactions Modulate Assembly and Stability of the Insulin Hexamer – A Review. *Biometals* **2005**, *18* (4), 295–303. https://doi.org/10.1007/s10534-005-3685-y.

(37) Poudel, R.; Bhusal, Y.; Tharu, B.; Kafle, N. Role of Zinc in Insulin Regulation and Diabetes. *J. Soc. Heal. Diabetes* **2017**, *5*, 83.

(38) Huang, Q.; Du, J.; Merriman, C.; Gong, Z. Genetic, Functional, and Immunological Study of ZnT8 in Diabetes. *Int. J. Endocrinol.* **2019**, *2019*, 1524905. https://doi.org/10.1155/2019/1524905.

(39) Badran, M.; Morsy, R.; Soliman, H.; Elnimr, T. Assessment of Trace Elements Levels in Patients with Type 2 Diabetes Using Multivariate Statistical Analysis. *J. Trace Elem. Med. Biol.* **2016**, *33*, 114–119. https://doi.org/https://doi.org/10.1016/j.jtemb.2015.10.006.

(40) Wang, Y.; Zhang, P.; Chen, X.; Wu, W.; Feng, Y.; Yang, H.; Li, M.; Xie, B.; Guo, P.; Warren, J. L.; Shi, X.; Wang, S.; Zhang, Y. Multiple Metal Concentrations and Gestational Diabetes Mellitus in Taiyuan, China. *Chemosphere* **2019**, *237*, 124412. https://doi.org/https://doi.org/10.1016/j.chemosphere.2019.124412.

(41) Dawson, J. H. Probing Structure-Function Relations in Heme-Containing Oxygenases and Peroxidases. *Science* **1988**, *240* (4851), 433–439. https://doi.org/10.1126/science.3358128.

(42) Atamna, H.; Frey, W. H. 2nd. A Role for Heme in Alzheimer's Disease: Heme Binds Amyloid Beta and Has Altered Metabolism. *Proc. Natl. Acad. Sci. U. S. A.* **2004**, *101* (30), 11153–11158. https://doi.org/10.1073/pnas.0404349101.

(43) Atamna, H.; Boyle, K. Amyloid-Beta Peptide Binds with Heme to Form a Peroxidase: Relationship to the Cytopathologies of Alzheimer's Disease. *Proc. Natl. Acad. Sci. U. S. A.* **2006**, *103* (9), 3381–3386. https://doi.org/10.1073/pnas.0600134103.

(44) Pramanik, D.; Ghosh, C.; Mukherjee, S.; Ghosh, S. *Interaction of Amyloid β Peptides with Redox Active Heme Cofactor: Relevance to Alzheimer's Disease*; 2013; Vol. 257. https://doi.org/10.1016/j.ccr.2012.02.025.

(45) Mukherjee, S.; Dey, S. G. Heme Bound Amylin : Spectroscopic Characterization ,

Reactivity , and Relevance to Type 2 Diabetes. *Inorg. Chem.* **2013**, *52*, 5226−5235.

(46) Grünblatt, E.; Bartl, J.; Riederer, P. The Link between Iron, Metabolic Syndrome, and Alzheimer's Disease. *J. Neural Transm.* **2011**, *118* (3), 371–379. https://doi.org/10.1007/s00702-010-0426-3.

(47) Lim, Y.-A.; Rhein, V.; Baysang, G.; Meier, F.; Poljak, A.; Raftery, M. J.; Guilhaus, M.; Ittner, L. M.; Eckert, A.; Götz, J. Abeta and Human Amylin Share a Common Toxicity Pathway via Mitochondrial Dysfunction. *Proteomics* **2010**, *10* (8), 1621–1633. https://doi.org/10.1002/pmic.200900651.

(48) de la Monte, S. M.; Wands, J. R. Alzheimer's Disease Is Type 3 Diabetes—Evidence Reviewed. *J. Diabetes Sci. Technol.* **2008**, *2* (6), 1101–1113. https://doi.org/10.1177/193229680800200619.

(49) Rajpathak, S.; Ma, J.; Manson, J.; Willett, W. C.; Hu, F. B. Iron Intake and the Risk of Type 2 Diabetes in Women: A Prospective Cohort Study. *Diabetes Care* **2006**, *29* (6), 1370–1376. https://doi.org/10.2337/dc06-0119.

(50) Zhao, Z.; Li, S.; Liu, G.; Yan, F.; Ma, X.; Huang, Z.; Tian, H. Body Iron Stores and Heme-Iron Intake in Relation to Risk of Type 2 Diabetes: A Systematic Review and Meta-Analysis. *PLoS One* **2012**, *7* (7), e41641. https://doi.org/10.1371/journal.pone.0041641.

(51) Simcox, J. A.; McClain, D. A. Iron and Diabetes Risk. *Cell Metab.* **2013**, *17* (3), 329–341. https://doi.org/10.1016/j.cmet.2013.02.007.

(52) De Sanctis, V.; Soliman, A.; Yassin, M. Iron Overload and Glucose Metabolism in Subjects with β-Thalassaemia Major: An Overview. *Curr. Diabetes Rev.* **2013**, *9* (4), 332–341. https://doi.org/10.2174/1573399811309040005.

(53) Borgna-Pignatti, C.; Gamberini, M. R. Complications of Thalassemia Major and Their Treatment. *Expert Rev. Hematol.* **2011**, *4* (3), 353–366. https://doi.org/10.1586/ehm.11.29.

(54) Belcher, J. D.; Beckman, J. D.; Balla, G.; Balla, J.; Vercellotti, G. Heme Degradation and Vascular Injury. *Antioxid. Redox Signal.* **2010**, *12* (2), 233–248. https://doi.org/10.1089/ars.2009.2822.

(55) Kato, G. J.; Taylor 6th, J. G. Pleiotropic Effects of Intravascular Haemolysis on Vascular Homeostasis. *Br. J. Haematol.* **2010**, *148* (5), 690–701. https://doi.org/10.1111/j.1365-2141.2009.08004.x.

(56) Roumenina, L. T.; Rayes, J.; Lacroix-Desmazes, S.; Dimitrov, J. D. Heme: Modulator of Plasma Systems in Hemolytic Diseases. *Trends Mol. Med.* **2016**, *22* (3), 200–213. https://doi.org/10.1016/j.molmed.2016.01.004.

(57) Kumar, S.; Bandyopadhyay, U. Free Heme Toxicity and Its Detoxification Systems in Human. *Toxicol. Lett.* **2005**, *157* (3), 175–188. https://doi.org/10.1016/j.toxlet.2005.03.004.

(58) Karran, E.; Mercken, M.; De Strooper, B. The Amyloid Cascade Hypothesis for Alzheimer's Disease: An Appraisal for the Development of Therapeutics. *Nat. Rev. Drug Discov.* **2011**, *10* (9), 698–712. https://doi.org/10.1038/nrd3505.

(59) Ndisang, J. F.; Jadhav, A. Heme Oxygenase System Enhances Insulin Sensitivity and Glucose Metabolism in Streptozotocin-Induced Diabetes. *Am. J. Physiol. Endocrinol. Metab.* **2009**, *296* (4), E829-41. https://doi.org/10.1152/ajpendo.90783.2008.

(60) Ndisang, J. F.; Jadhav, A. Up-Regulating the Hemeoxygenase System Enhances Insulin Sensitivity and Improves Glucose Metabolism in Insulin-Resistant Diabetes in Goto-Kakizaki Rats. *Endocrinology* **2009**, *150* (6), 2627–2636. https://doi.org/10.1210/en.2008-1370.

(61) Kahn, S. E.; D'Alessio, D. A.; Schwartz, M. W.; Fujimoto, W. Y.; Ensinck, J. W.; Taborsky, G. J. J.; Porte, D. J. Evidence of Cosecretion of Islet Amyloid Polypeptide and Insulin by Beta-Cells. *Diabetes* **1990**, *39* (5), 634–638. https://doi.org/10.2337/diab.39.5.634.

(62) Lorenzo, A.; Razzaboni, B.; Weir, G. C.; Yankner, B. A. Pancreatic Islet Cell Toxicity of Amylin Associated with Type-2 Diabetes Mellitus. *Nature* **1994**, *368* (6473), 756–760. https://doi.org/10.1038/368756a0.

(63) Rittle, J.; Green, M. T. Cytochrome P450 Compound I: Capture, Characterization, and C-H Bond Activation Kinetics. *Science (80-.).* **2010**, *330* (6006), 933 LP – 937. https://doi.org/10.1126/science.1193478.

(64) Kitagawa, T.; Sugiyama, T.; Yamano, T. Differences in Stability against Thermal Unfolding between Trypsin- and Detergent-Solubilized Cytochromes B5 and Structural Changes in the Heme Vicinity upon the Transition: Resonance Raman and Absorption Study. *Biochemistry* **1982**, *21* (7), 1680–1686. https://doi.org/10.1021/bi00536a032.

(65) Spiro, T. G.; Burke, J. M. Protein Control of Porphyrin Conformation. Comparison of Resonance Raman Spectra of Heme Proteins with Mesoporphyrin IX Analogs. *J. Am. Chem. Soc.* **1976**, *98* (18), 5482–5489. https://doi.org/10.1021/ja00434a013.

(66) Callahan, P. M.; Babcock, G. T. Insights into Heme Structure from Soret Excitation Raman Spectroscopy. *Biochemistry* **1981**, *20* (4), 952–958. https://doi.org/10.1021/bi00507a048.

(67) Dasgupta, S.; Rousseau, D.; Anni, H.; Yonetani, T. Structural Characterization of Cytochrome c Peroxidase by Resonance Raman Scattering. *J. Biol. Chem.* **1989**, *264*, 654–662. https://doi.org/10.1016/S0021-9258(17)31311-X.

(68) Redaelli, C.; Monzani, E.; Santagostini, L.; Casella, L.; Sanangelantoni, A. M.; Pierattelli, R.; Banci, L. Characterization and Peroxidase Activity of a Myoglobin Mutant Containing a Distal Arginine. *ChemBioChem* **2002**, *3* (2–3), 226–233. https://doi.org/https://doi.org/10.1002/1439-7633(20020301)3:2/3<226::AID-CBIC226>3.0.CO;2-7.

(69) Pal, I.; Roy, M.; Dey, S. G. Interaction of ApoMyoglobin with Heme-HIAPP Complex. *J. Inorg. Biochem.* **2021**, *216* (December 2020), 111348. https://doi.org/10.1016/j.jinorgbio.2020.111348.

(70) Huang, Q.; Szigeti, K.; Fidy, J.; Schweitzer-Stenner, R. Structural Disorder of Native Horseradish Peroxidase C Probed by Resonance Raman and Low-Temperature Optical Absorption Spectroscopy. *J. Phys. Chem. B* **2003**, *107* (12), 2822–2830. https://doi.org/10.1021/jp026935e.

(71) Pramanik, D.; Ghosh, C.; Dey, S. G. Heme–Cu Bound Aβ Peptides: Spectroscopic Characterization, Reactivity, and Relevance to Alzheimer's Disease. *J. Am. Chem. Soc.* **2011**, *133* (39), 15545–15552. https://doi.org/10.1021/ja204628b.

(72) Ghosh, C.; Mukherjee, S.; Seal, M.; Ghosh, S. Peroxidase to Cytochrome b Type

Transition in the Active Site of Heme-Bound Amyloid β Peptides Relevant to Alzheimer's Disease. *Inorg. Chem.* **2016**, *55*. https://doi.org/10.1021/acs.inorgchem.5b02683.

(73) Huang, Y.; Yang, Z.; Xu, H.; Zhang, P.; Gao, Z.; Li, H. Insulin Enhances the Peroxidase Activity of Heme by Forming Heme-Insulin Complex : Relevance to Type 2 Diabetes Mellitus. *Int. J. Biol. Macromol.* **2017**, *102*, 1009–1015.

(74) Leighton, B.; Cooper, G. J. S. Pancreatic Amylin and Calcitonin Gene-Related Peptide Cause Resistance to Insulin in Skeletal Muscle in Vitro. *Nature* **1988**, *335* (6191), 632–635. https://doi.org/10.1038/335632a0.

Chapter 5

Reactivity of Heme Bound Insulin complexes

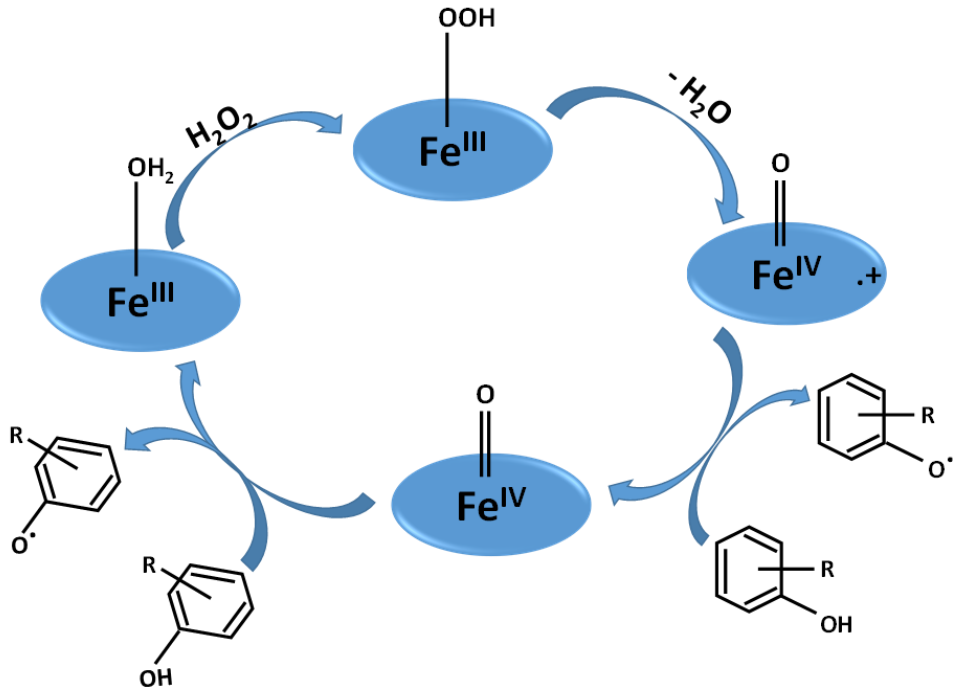

Previous studies show the interaction between heme and insulin spectroscopically under different experimental conditions which include the effect of excess peptide as well as increasing pH. Knowing the overall active site environment of this heme-insulin complexes navigate us towards the investigation of their reactivity and possible role in T2Dm pathology. In this study using various spectroscopic techniques we have reported some of the significant contributions of heme bound insulin complexes such as partially reduced oxygen species (PROS) generation, peroxidase activity and the high valent Fe-oxo intermediates that are known to oxidise the functional biomolecules. The resultant heme-insulin complexes in their reduced state are found to produce very little PROS on getting oxidized by molecular oxygen. Tyrosine crosslinking becomes a major event in presence of heme which in turn hampers the native functionality of insulin which is common in T2Dm. Additionally, the interaction between insulin and previously reported T2Dm relevant heme-amylin complex were also examined using absorption and resonance Raman spectroscopy. The corresponding data suggest that insulin sequesters heme from heme-amylin to form the much less harmful heme-insulin. Thus insulin might act as a natural defence against cytotoxic heme bound amylin complexes.

5.1. Introduction

Being an amyloidogenic disease, type 2 diabetes mellitus (T2Dm) too follows a common pathological mechanism of protein aggregation.[1–3] The key driving factors endorsing this epidemic are the sedentary lifestyles, genetic history, alarming upsurge in obesity, lack of physical activity, high caloric fast food-based diets and an increasing aged population, which have magnified the onset and prevalence of T2Dm worldwide.[4,5] According to the International Diabetes Federation (IDF), in 2019, ~ 463 million adults of 20 - 80 years old had been detected with diabetes while 1 in 3 people remain underdiagnosed and 2019 itself had seen the death of ~ 4.2 million individuals caused by T2dm only, which is likely to escalate up to 700 million by 2045.[4] India, the second largest country for diabetic patients expects an alarming growth up to 109.0 million by 2035.[6] The Type 2 diabetes mellitus is a prolonged metabolic disease, which is characterized by hyperglycemia and is instigated via hampered insulin secretion, making it unable to maintain glucose homeostasis over the progression of the disease, even unfortunately under fasting conditions.[7] It is frequently found to occur in aged beings and over the time can lead to damage heart, vascularity, eyes, kidneys and nerves etc.[8–11] An impaired glucose metabolism arising from acquired and/or genetic defects in both insulin activity of the peripheral insulin sensitive tissues and insulin secretion from islet β-cells contributes inextricably to this disease.[12] Insulin resistance/insulin deficiency can be broadly originated due to 1) reduced insulin secretion by β-cells i.e., β-cells dysfunction;[13] 2) counter-regulatory hormones of insulin or non-hormonal bodies in plasma that compete and hamper the function of insulin receptors and eventually the signaling pathway;[14] 3) malfunctioned insulin response in target tissues in pancreas;[15] 4) faulty action of insulin in the extra-pancreatic insulin-sensitive organs; skeletal muscle, adipose tissue and liver that play major roles in the glucose regulatory processes and regularly precedes the onset of systemic insulin resistance.[4,16] Although β-cell dysfunction is traditionally linked to β-cell death, recent research indicates a more complex network of interactions between molecular pathways of cell biology and the environmental effects on such cell apoptosis.[17–19] The hyper-nutritional conditions like obesity, hyperlipidemia, hyperglycemia emphatically favor insulin resistance and related inflammation in diabetic patients and under these circumstances, β-cells, having alterations in their genetic susceptibility, are subjected to multidirectional toxicity including inflammatory stress, endoplasmic reticulum (ER) stress, metabolic, amyloid and oxidative stress that ultimately lead to a loss of islet integrity.[18–20] Meanwhile, there is also an increasing indication that associates

mitochondrial dysfunction with the advance of T2Dm.[21] Under normal condition, mitochondria plays an important role in ROS clearance but the hyperglycaemic condition like T2Dm induces the generation of excess amount of ROS by mitochondria, which gives rise to insulin resistance, damage DNA and membrane lipids and intensifies other diabetes associated complication.[22] The ROS generated by mitochondria can oxidize the Cys and Met residues in proteins, thus blighting the protein structure and function which eventually leads to cell apoptosis.[4]

As discussed above, insulin shows an important role in T2Dm etiology.[23] It is a small peptide hormone secreted in pulses by the β cells of the pancreatic islets of Langerhans and is synthesized in the β-cells in the form of proinsulin which then undergoes post translational modifications to form the mature insulin. Structurally, insulin is a dipeptide, comprising of 51 amino acids distributed in two chains (A and B chain), with a molecular weight of 5.8 kDa. The B chain has a central helical section while the A chain has an N-terminal helix connected to an anti-parallel C-terminal helix. The two chains are joined by two disulfide bridges between cysteine residues, which join the N- and C-terminal helices of the A chain to the central helix of the B chain. An additional disulfide bridge exists in the A-chain itself (Scheme 1A).[24,25] Insulin helps in maintaining the normal blood glucose level by enabling the cellular glucose uptake and regulates the metabolism of carbohydrate, lipid and protein. As the vital regulator of glucose homeostasis, insulin has to be secreted in an adequate quantity in our body. Thus, insulin resistance, abnormal/reduced insulin secretion, declined glucose utilization, and simultaneous increase in glucose production lead to one of the defining characteristics of T2Dm, *i.e.* hyperglycemia.[26–28] In fact, prospective studies show that patients with T2Dm secrete ~70% less insulin than control subjects during the hyperglycemic clamp.[26,29] In recent times, evidences are emerging in support of the fact that not only insulin resistance, but also inability of the β-cells to produce enough insulin is an underlying cause of T2Dm. The resultant cascade of events include higher glucose levels, further β-cell deterioration, diminished glucose sensitivity and elevated hypergycaemia.[30]

Scheme 1. **The amino acid sequence of A) human insulin B) human hIAPP/amylin.**

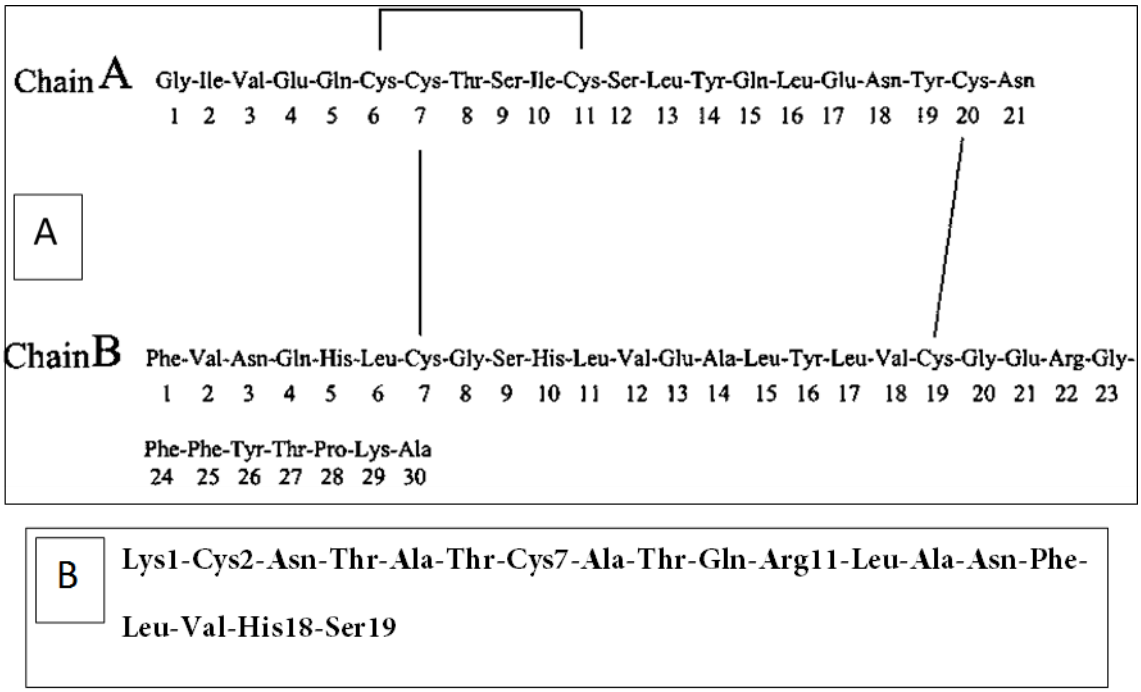

Metals are known to play vital roles in other amyloidogenic diseases including Alzheimer's, Parkinson's, Wilson, Prion, and Huntington.[31,32] similar metal interference is observed in the disease pathology of T2Dm as well.[33] Metals like Zn, Fe, and Cu have been found to be associated with T2Dm.[34] Zn concentration in pancreatic β cells increases and consequently Zn deficiency is observed in T2Dm.[35] An increased dietetic intake of Fe, particularly in the form of heme can enhance the risk of T2Dm.[36] A considerably higher level of Cu is found in the serum of diabetic patients, and Cu can increase IAPP-induced cell apoptosis from 45% to 70% in the cultured β cells.[37] Studies indicate that the interaction of Cu with hIAPP delays the peptide aggregation process, reducing the cellular toxicity of hIAPP.[38] Conversely, recent studies show Cu binding to monomeric amylin hinders β sheet fibril formation while favouring the generation of oligomers, which are known for their potentially more toxic nature towards the β cells of the pancreas than the corresponding fibrillar form.[39] Lately it has been shown that Cu ions also bind monomeric insulin with a higher affinity.[40] One of the important trace elements related to T2Dm, Zn plays a key role in the storage and secretion of insulin, which subsequently increases the glucose uptake.[41–43] As a result of the increased urinary depletion, a less than optimal Zn level in blood is found in T2Dm patients.[44] Consequently, hypozincemia and hyperzincuria are common to them and this decreased plasma level of Zn adversely affects the ability of islet cells to make and secrete insulin.[45] Also,

mutation of Zn transporter, ZnT8 that is a key protein for the regulation of insulin secretion from the pancreatic β-cells has been associated with T2Dm.[46]

Pathological link between AD and T2Dm has been long established now.[47,48] Consistent with this, the epidemiological researches have shown that the incidence of AD is almost 2-5 times higher in T2Dm affected individuals.[49] In AD, an excessive iron (Fe) accumulation, especially in the form of heme *b* is found in the Aβ deposited region of the brain. Such anomalous increase of heme concentration in AD brain has been associated with the complexation of heme with Aβ monomers which consecutively leads to heme depletion and results in elevated Fe intake, amplified stress-related enzymes or proteins like heme oxygenase-1 and transferrin, increased bilirubin concentration, abnormal Fe homeostasis, degradation of Fe regulatory proteins, dysfunction of mitochondrial complex IV, enhancement of oxidative stress, and so forth.[50–52] Incidentally many of these symptoms of AD are also common pathological features of T2Dm.[53] The serum concentration of Fe is also observed to be significantly higher (118.33±27.3 μg/dL), also in T2Dm compared to the control subjects.[34] Contemporary prospective studies and systematic meta-analysis have positively associated high heme Fe ingestion, the major dietetic resource of body Fe stores, with high threat of developing T2Dm in future.[53] Moreover, recent experiments have proved that heme can bind both Aβ and amylin and can produce ROS and related oxidative stress which is a common feature for both the diseases.[52,54] This is why AD is often called Type 3 diabetes or T2Dm as the Alzheimer's of the pancreas.[55]

Studies have suggested that heme can parallelly bind to insulin as well, which is the complementary peptide of hIAPP and plays essential role in T2Dm etiology. These heme-insulin complexes also contribute to the oxidative and nitrative stress related complications in disease pathogenesis. Spectroscopic techniques indicated that heme binding to insulin in equimolar ratio in *in vitro* physiological conditions. This binding is offered via the His residue (either 5^{th} or 10^{th} position in the B chain) of insulin peptide.[56,57] A molecular docking experiment support that His5 of insulin is the binding ligand with heme-Fe. In addition to that it has been also suggested that there are contributions of second sphere amino acids like Tyr26 and Phe1 residues which can promote hydrophobic/electrostatic interaction and Val2 which forms H-bond to the heme centre, thus assist in heme-insulin active site formation.[58] The 1:1 heme-insulin complex is found to consist of a mixture of species, a high spin mono-His bound compound as dominant species and a low spin hexa coordinated bis-His bound compound in a

minor amount. The low spin species is likely formed in an intermolecular fashion, connecting two His residues from two nearby peptides to the heme centre. In presence of excess insulin with respect to heme, the equilibrium is found to shift more towards the bis-His low spin complex compared to the mono-His high spin one. Moreover, at higher pH, both high spin and low spin complexes show that the weakly bound water molecule, present at the axial 6th position of active site, is converted to a hydroxide bound high spin species. Significantly, insulin can amplify the peroxidase activity of free heme which under oxidative and nitrative stressed conditions, is known to affect the disease pathogenesis via promoting Tyr radical and associated insulin cross-linking, leading to permanent loss of natural insulin functionality, and by enhancing the tyrosine nitration of insulin in the β-cells that may result in inactivation of proteins related to diabetes as well.[58,59] Till now, there is no experimental evidence of the mechanism and associated intermediates of the peroxidase activity of heme-insulin complexes and subsequent production of tyrosine cross-linking in presence of those high-valent intermediates.

The interaction between heme and insulin peptide results into the formation of heme-peptide complexes which has been studied here using absorption and resonance Raman (rR) spectroscopy earlier. In this chapter, the functions and reactivities of the resultant heme bound peptide complexes have been dealt with. We have measured the % of PROS that have been produced by the reduced heme(Fe) centre and the peroxidase activity which can go through a number of high valent Fe-oxo intermediates and the subsequent dityrosine formation. We have tried to trap and characterise those intermediates and investigated its further toxicity. Theses intermediates being highly reactive oxidant can oxidise proteins itself, hampering the biological functions which might be one of the reasons for insulin deficiency in T2Dm pathology. Additionally the effect of insulin on heme-amylin complex has also been examined here. This is significant since amylin, a small peptide hormone secreted along with insulin from the pancreatic β-cells, is also a part of the T2Dm paradigm (Scheme 1B).[60] Its aggregation and deposition in the β-cells is considered a central event in the development of the disease.[61] More importantly, the heme-amylin complex, whose active site environment has been spectroscopically determined to consist of heme coordinated by a His18 and a loosely bound water molecule trans axial to the His, is known to generate a considerable amount of partially reduced oxygen species (PROS) on reaction with oxygen. This may be responsible in part for the oxidative stress observed in T2Dm patients.[62] The present study shows that insulin can take

up heme from heme-amylin forming heme-insulin which is experimentally found to generate a negligible amount of PROS.

5.2. Materials and methods

5.2.1. Materials

All reagents were of the highest grade commercially available and were used without further purification. Hemin, TMB, human recombinant insulin and buffer were purchased from Sigma. Truncated amylin peptide containing the heme binding domain (sequence: Lys1-Cys2-Asn-Thr- Ala- Thr- Cys7- Ala- Thr- Gln- Arg11- Leu- Ala- Asn- Phe- Leu- Val- His18- Ser19) was purchased from Ontores (China) Ltd. with >95% purity.

5.2.2. Sample preparation

Insulin and amylin peptide stock solutions were prepared in 100 mM phosphate buffer at pH 8. Hemin solution was prepared by dissolving hemin chloride in 1 M NaOH and the concentration of the heme solution was determined spectrophotometrically (e385 = 58.44 mM-1 cm-1). Peptide stock solutions were 0.5 mM, and heme stock solution was 5 mM. Heme-insulin and heme–amylin complexes were prepared by incubating 1 equivalent of peptide with 0.8 equivalent of heme solution for ~1 h. The pH of the heme-peptide complexes were calibrated accordingly using 1 M H_3PO_4 and 1M NaOH.

5.2.3. Absorption spectroscopy

All the spectral data were obtained by an UV-vis diode array spectrophotometer (Agilent 8453). For all absorption spectroscopy experiments, final concentration of 1:1 heme-insulin and heme-amylin complexes were 0.5 mM while that of 1:5 heme-insulin was 0.1 mM with respect to heme. The heme-amylin sample was incubated with 2 equivalent of insulin for ~2 h.

5.2.4. Resonance Raman spectroscopy

Resonance Raman data were obtained at room temperature using a Trivista 555 spectrograph (Princeton Instruments) using 413.1 nm excitation from a Kr^+ laser (Coherent, Sabre Innova SBRC-DBW-K). The optics (plano-convex lens, mirror *etc*.), used for the collection of rR data were purchased from Sigma-Koki Japan. The power on the samples was ~5 mW. rR samples were 0.2 mM in concentration.

5.2.5. PROS calculation

Xylenol orange assay was applied for PROS calculation. A total of 4.9 mg of Mohr's salt and 3.9 mg of xylenol orange were dissolved in 5 mL of 250 mM H_2SO_4 and stirred for 10 min. A 200 µL portion of this solution was taken in 1.8 mL of nanopure water, and a calibration curve for the quantitative estimation of H_2O_2 was obtained for 0.05, 0.1, 0.5, 1, 2.5, 5, and 10 µM concentrations of H_2O_2 by recording their absorbance at 560 nm as a function of H_2O_2 concentrations in micromolar units for a 2 mL volume. A blank was obtained in the UVvis spectrophotometer with 1.8 mL nanopure water in a cuvette. A total of 200 µL xylenol orange solution was added to the above cuvette and absorbance was measured. This served as the control. The heme-insulin complexes and all the buffer and reagent solutions were degassed first and then were purged with argon in anaerobic vials for ~30 min. Thereafter, the samples were reduced using a minimal amount of dithionite under anaerobic conditions, followed by their reoxidation by O_2 (monitored by absorption). A total of 200 µL of 0.025 mM of reoxidized solutions were separately added to the cuvette containing the control, and their absorbance were recorded. The value of absorbance of the above solutions (after deducting the control) at 560 nm when plotted on the calibration curve yielded the corresponding H_2O_2 concentration.

5.2.6. Peroxidase activity measurement

3,3′,5,5′-Tetramethylbenzidine (TMB) was used as the substrate for peroxidase activity measurement. A 10 mg portion of TMB was dissolved in 0.5 mL of glacial AcOH and 10 mL of AcOH/NaOAc buffer (1 M, pH 4.5). The solution was diluted to 25 mL with water. This was followed by addition of 100 μL of 30 volume H_2O_2. A 10 μL volume of 0.05 mM protein sample was added to the above solution. Kinetic traces were obtained by monitoring the increase of the 652 nm absorption band with time.[63]

5.2.7. Preparation of dityrosine

0.5 mmol insulin peptide were dissolved in 200 ml 0.1 M sodium phosphate buffer, pH 8, 0.3 mmol of heme-insulin solution and 10 eqv of hydrogen peroxide in 1 ml of the above buffer were added and the solution was oxidised at a constant temperature of 37 °C for 1 h in aerobic condition. Excess hydrogenperoxide was destroyed by the addition of sodiummetabisulfite and the solution neutralised with concentrated hydrochloric acid. Finally the resultant dityrosine and trityrosine were observed under fluorescence spectroscopy which exhibited the typical ultraviolet and fluorescence spectrum of cross-linked tyrosine.

5.2.8. Fluorescence measurement

Fluorescence experiments were carried out in 0.1 M sodium phosphate buffer solutions at pH 8 with a Fluoromax-3 instrument (Horiva JovinYvon). Insulin incubated with peroxidase (heme-insulin) and H_2O_2 and control samples which contains insulin and H_2O_2 were continuously excited at 280 nm during 1 h, 1.5 h. Emission spectra were acquired with 310 nm and 400 nm, 440nm excitation to monitor the di and tri-tyrosine formation. The quartz cell of 1 cm path length has been used for this experiment and the samples were excited at 265 and 325 nm. Emission scans were documented by using a slit width of 2 nm.

5.3. Results and Analysis

5.3.1. PROS generation

Heme bound amylin reduces O_2 by one electron, derived from the reduced heme centre, producing 40 ± 2% H_2O_2.[64] The ferrous 1:1 heme-insulin complex on the other hand generates only 12 ± 2% H_2O_2 (Figure 1). With increase in insulin concentration, H_2O_2 generation further decreases to 8 ± 2% (Figure 1A). In general, all these heme-insulin complexes generate lesser amount of PROS compared to both heme-amylin and free heme (24 ± 2%). This indicates that the heme-insulin complexes are not involved in generating a significant amount of PROS or oxidative stress.

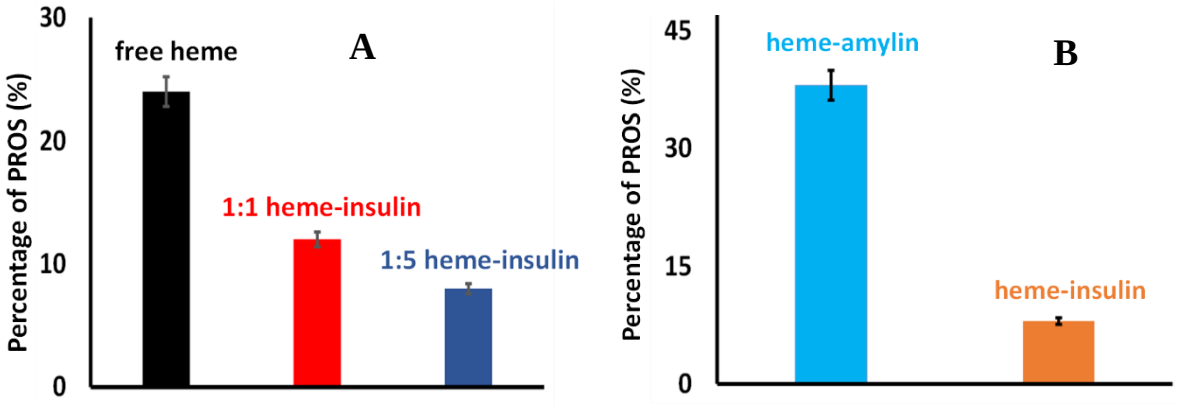

Figure 1. Percentage of PROS detected using xylenol orange assay for **(A)** free heme, 1:1 heme-insulin complex and 1:5 heme-insulin complex and **(B)** heme-amylin and heme-insulin complexes during heme transfer.

5.3.2. Effect of insulin on heme–amylin

Absorption spectroscopy

Amylin is known to bind heme in a 1:1 concentration ratio. The absorption spectrum of heme bound amylin is characterized by a split Soret band at 365 and 392 nm along with a Q-band at 605 nm. When 1:1 heme-amylin complex is incubated with 2 equivalents of insulin for ~1 h at pH 7.4, the final species shows a red shift in the Soret band region to 410 nm and Q-bands appear at 535 nm, 565 nm along with the charge transfer band at 630 nm, indicating the formation of heme-insulin (Figure 2). Thus, insulin can sequester heme from heme-amylin complex, which is clearly implicated by absorption spectroscopy.

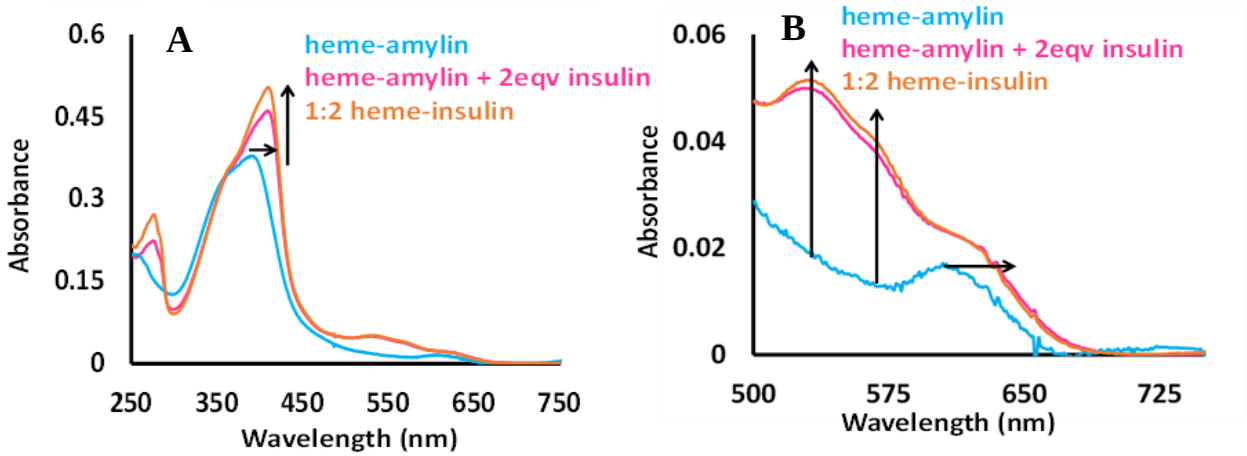

Figure 2. **(A)** Absorption spectra of heme-amylin, heme-amylin incubated with 2 equivalents of insulin and 1:2 heme-insulin complexes **(B)** Enlarged Q-band region showing changes as indicated by arrows relative to heme-amylin complex at pH 7.4 in 100 mM phosphate buffer.

Resonance Raman spectroscopy

The ν4, ν3, and ν2 marker bands of heme-amylin are observed at 1374, 1492, and 1572 (broad) cm^{-1} respectively, while, ν10, the depolarized spin state marker band arises at 1628 cm^{-1} indicating the presence of a six-coordinate high-spin Fe^{3+} centre. These marker bands distinctly differ for 1:2 heme-insulin complex which exhibits ν3 at 1492 cm^{-1} (weak) and 1505 cm^{-1}, ν2 at 1580 cm^{-1} and ν10 at 1630 cm^{-1} (weak) and 1641 cm^{-1} respectively. Figure 3 shows that when heme-amylin and insulin are incubated in 1:2 stoichiometric ratio, the resultant rR spectrum resembles that of the 1:2 heme-insulin, validating the heme transfer to insulin.

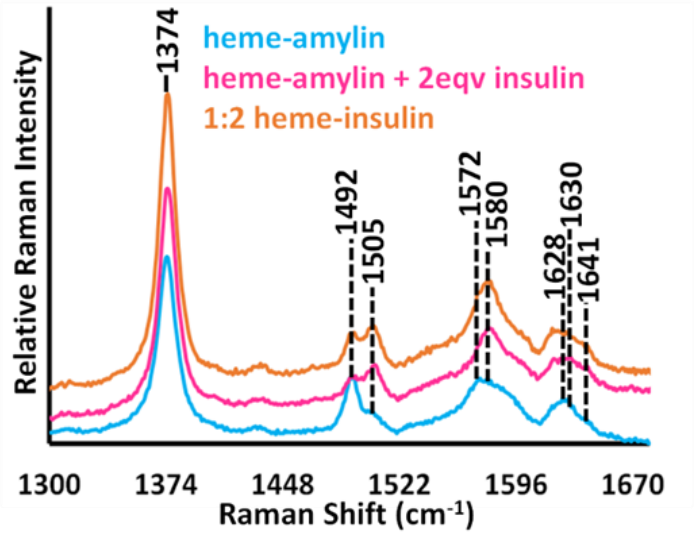

Figure 3. High frequency rR spectra of heme-amylin, heme-amylin incubated with insulin and 1:2 heme-insulin in 100 mM phosphate buffer at pH 7. Data were obtained with an excitation wavelength of 413.1 nm (~5 mW) at room temperature.

5.3.3. Peroxidase activity

The peroxidase activity of both mono and bis-histidine-coordinated heme insulin complexes and free heme are tested by following the catalytic oxidation of the substrate TMB by H_2O_2. At any particular pH, the 1:1 heme insulin complxes show ~ 2 times higher peroxidase activity than that of free heme, indicating that interaction of insulin can enhance the peroxidase activity of free heme in physiological condition (Figure 4.)

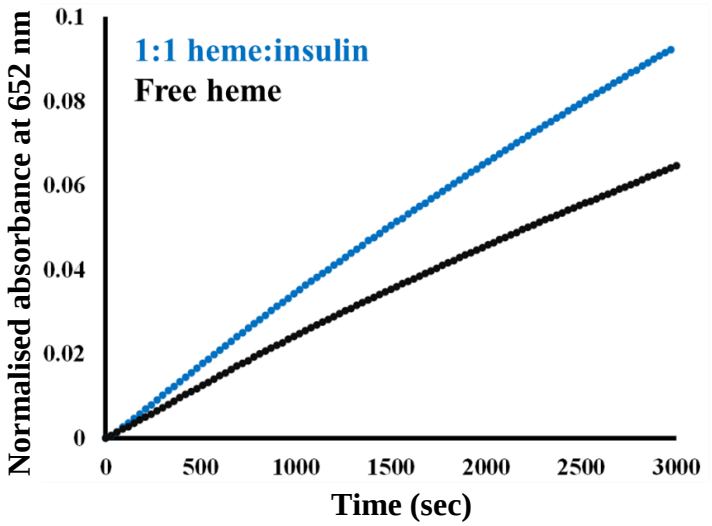

Figure 4. Kinetic traces for peroxidase activity, monitoring the increase of the 652 nm absorbance intensity, for 1:1 heme-insulin complex, blue; free heme, black in 100 mM phosphate buffer at pH 7.

Interestingly, when the concentration of insulin is increased, the peroxidase activity of heme bound insulin complexes remain almost same, implicating that the population of the oxidant, responsible for showing the peroxidase activity is similar in spite of increased insulin concentration, i.e., increased abundance of low spin bis-His component of heme bund insulin (Figure 5).

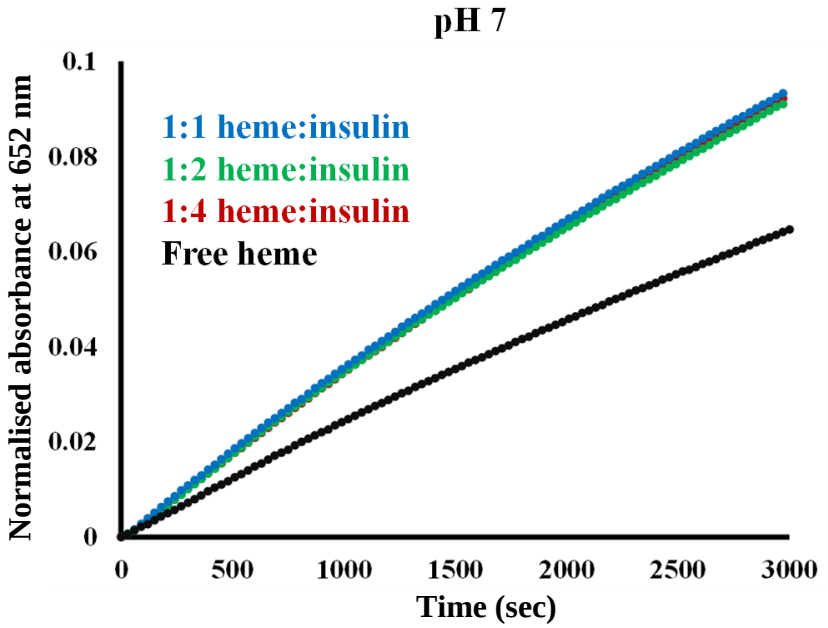

Figure 5. Kinetic traces for peroxidase activity, monitoring the increase of the 652 nm absorbance intensity, for different heme-insulin complexes, 1:1, blue; 1:2, green; 1:4, red; free heme, black in 100 mM phosphate buffer at pH 7.

With increase in the pH of buffer medium, the peroxidase activity of 1:1 heme-insulin complexes get increased (Figure 6). The probable reason might be either the ease of formation or the greater stability of the active oxidant at basic pH which in turn makes the oxidation of TMB greater at higher pH.

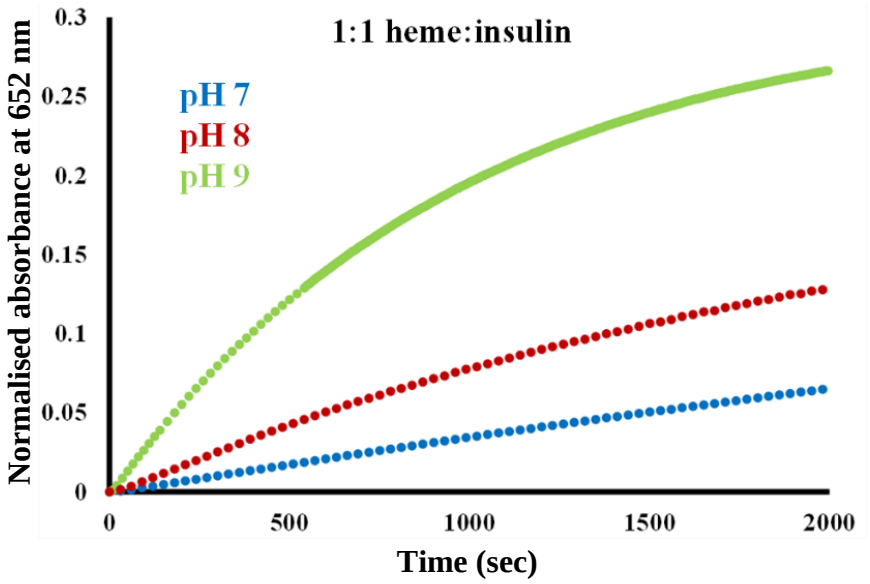

Figure 6. Kinetic traces for peroxidase activity, monitoring the increase of the 652 nm absorbance intensity, for different heme-insulin complexes, 1:1, blue; 1:2, green; 1:4, red; free heme, black in 100 mM phosphate buffer at pH 7.

5.3.4. Intermediate in the peroxidase pathway

The heme-insulin complexes show peroxidase activity greater than free heme. Peroxidases form two high valent oxoferryl intermediates, ferryl porphyrin π-cation radical ($FeIV{=}OPor^{\cdot+}$) or compound I and ferryl heme (FeIV=O porphyrin) or compound II (Scheme 2). For example, H_2O_2 addition to Fe(III) horseradish peroxidase (HRP) generates compound I (HRP-I). Reduction back to the ferric state with concomitant substrate oxidation occurs in two one electron steps via compound II (HRP-II) while, myoglobin (Mb) reacts with peroxides to form an oxoferryl compound II-like species (Mb-II), along with a transient tyrosine radical.[17-19] Due to the higher oxidation states, these intermediates are highly reactive and transient in nature.

Scheme 2. **The conventional peroxidase pathway for heme-based proteins/peptides.**

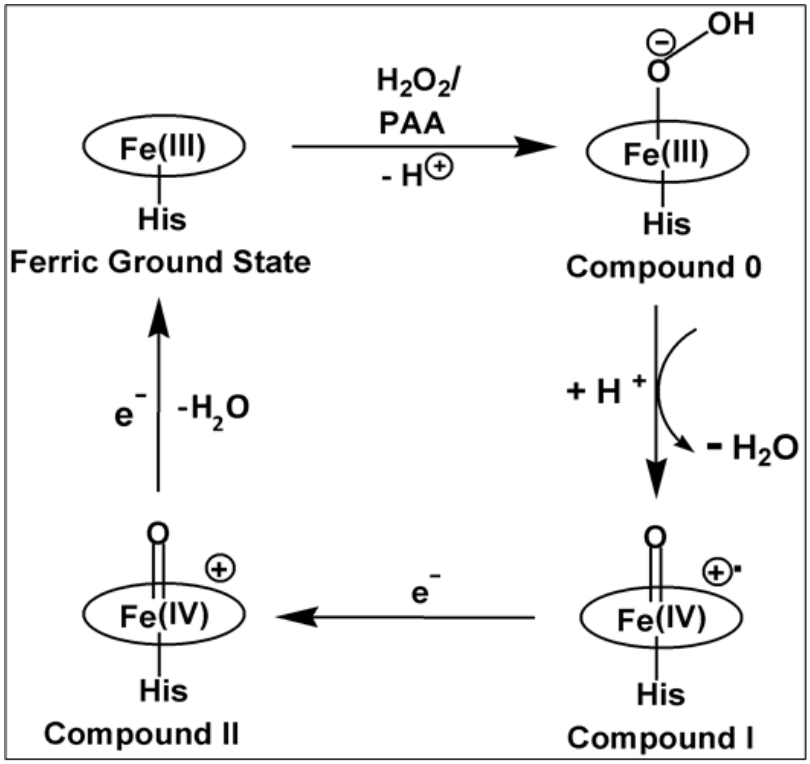

5.3.4.1. Formation of reactive intermediates in the reaction of heme-insulin with H_2O_2

The heme-insulin complexes (both 1:1 and 1:3) reacts with 10 equivalent of H_2O_2 with an observed rapid decrease in the absorbance of the Soret band of 410 nm (Figure 7A). The Q-band at 530 nm, 567 nm, 627 nm corresponding to heme bound insulin red shifs to ~600 nm in 40 sec (Figure 7B). At ~50 sec there is another broad band ~680 nm rising which maximises till ~15 min (Figure 7C) as the reaction progresses. previous literatures suggest that the reaction of heme based proteins with peroxide/peracid can lead to a ferric hydroperoxide (Fe^{III}-OOH) species; known as Compound 0 which can either cleave the O–O bond homolytically to form compound II or heterolytically to form compound I. Heme hydroperoxides are characterized by absorption at 556–575 nm and 600 nm while compound II is characterized by absorption at 525–551 and 556–586 nm.[65–67] Alternatively, compound I is characterized by absorption in the range of 645–690 nm.[68,69] Absorption in this region results in green colour and is characteristic of a ferryl porphyrin cation radical (FeIV=O Por $^{\cdot+}$) or compound I.[70,71] The absorbance at ~680 nm is therefore characteristic for compound I formation here.

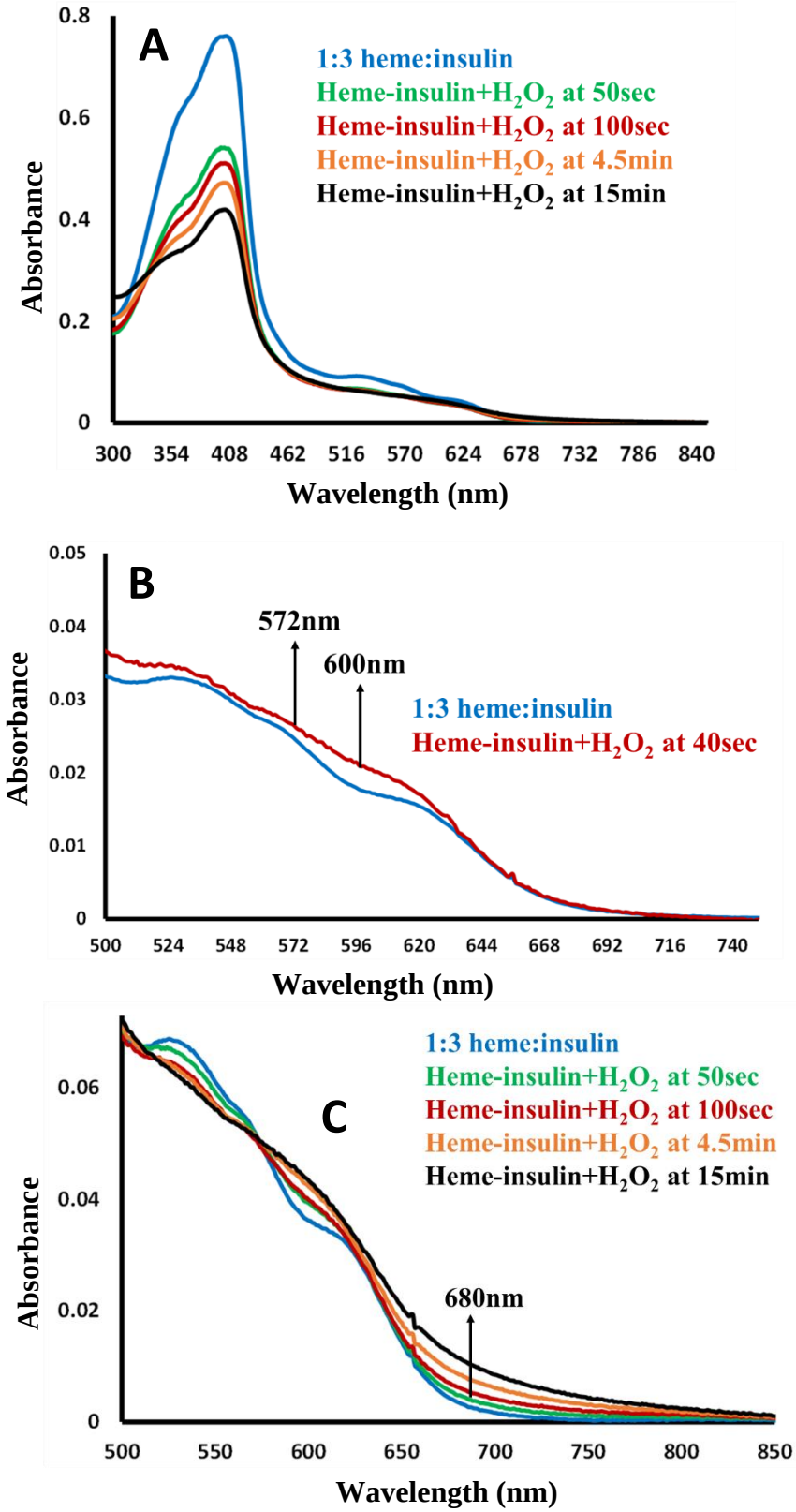

Figure 7. **(A)** Absorption spectra of 1:3 heme-insulin, blue ; heme-insulin incubated with 10 equivalent of H_2O_2 at different time interval **(B)** Enlarged Q-band region showing changes characteristic for Compound 0 at 40sec, red, as indicated by arrows relative to heme-insulin

complex **(C)** rise of 680nm band with time as indicated by arrow relative to heme-insulin at pH 8 in 100 mM phosphate buffer.

Note, we have not been able to detect the formation of other intermediate species, ferryl heme (FeIV=O porphyrin) or compound II by absorption spectroscopy, probably due to the masking of its characteristic bands by the broad region of 650-700nm.

5.3.4.2. Kinetic assays

The kinetic trace of the reaction between heme-insulin and H_2O_2 is followed by absoption with increasing time. The formation of Compound 0 is monitored by the rise of 600 nm band with time (Figure 8A). Additionally, the 680 nm shows an exponential increase indicating the formation of compound I (Figure 8B). The rate constants for the formation of Compound 0 and Compound I have been estimated to be and $6.5*10^{-3}$ s^{-1} and $6.0*10^{-3}$ s^{-1} respectively.

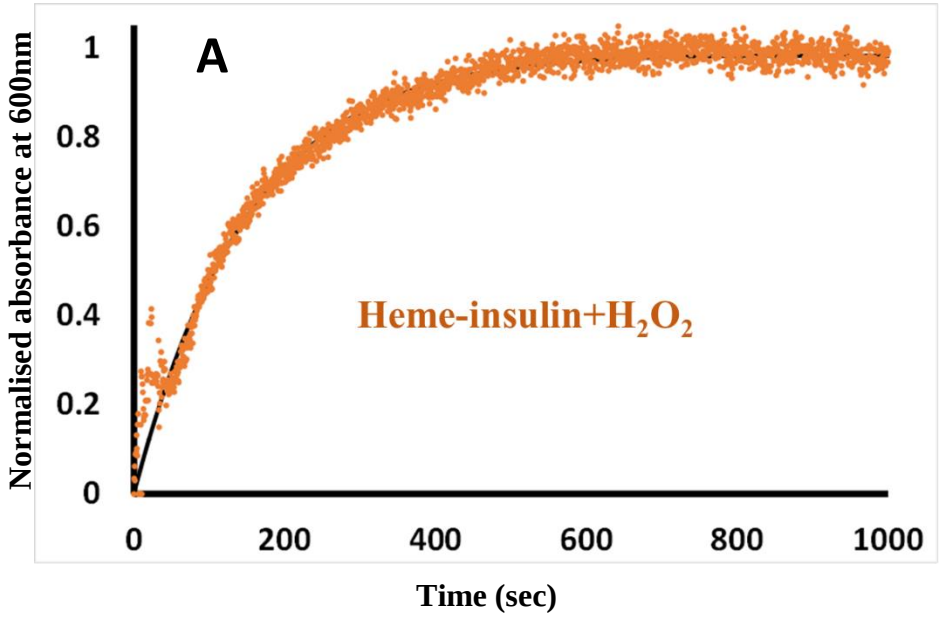

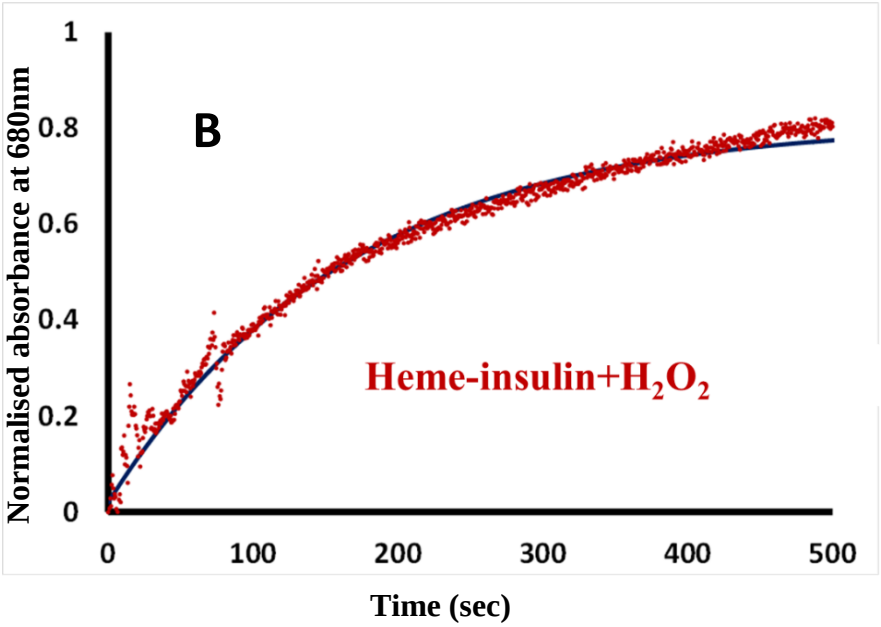

Figure 8. **(A)** Formation kinetics of Compound 0 during reaction of heme-insulin with H_2O_2, orange. **(B)** Formation kinetics of Compound I during reaction of heme-insulin with H_2O_2, red in 100 mM PO_4^{3-} buffer at pH 8.

5.3.4.3. Characterization of compound I by resonance Raman spectroscopy

Resonance Raman (rR) spectroscopy is a unique technique for the characterization of structures of heme proteins.[72,73] The rR spectra obtained from heme-insulin complexes reacted with 10 times excess of H_2O_2 clearly indicate a broadening of the oxidation state marker ν4 band region due to the presence of compound I at 1372 cm^{-1} (Figure 9). This increase can be seen from 5 sec spectrum (orange) and along with this another shoulder band for compound II at 1384 cm^{-1} (Figure 9) is observed at 15 sec. In addition to these bands, the ν4 band of resting ferric species at 1378 cm^{-1} is also present.[74] Note, there is no shift in ν4 for compound 0.[75] The ν2, ν3, and ν10 vibrational frequencies are sensitive to the core size of the porphyrin ring and denote the coordination and spin-state marker bands. The ν3 band at 1510 cm^{-1} gradually increases with time, indicating a six-coordinated species formation, mostly the intermediate species. These characteristic bands of compound I and II gradually get diminished with time and at ~ 1mint, the pure resting state of FeIII species can be seen only. The low frequency region (600–900 cm^{-1}) of rR spectra is the most important region for identifying the Fe-O and O-O stretching frequencies, which is yet to be observed along with their isotopic shifts.

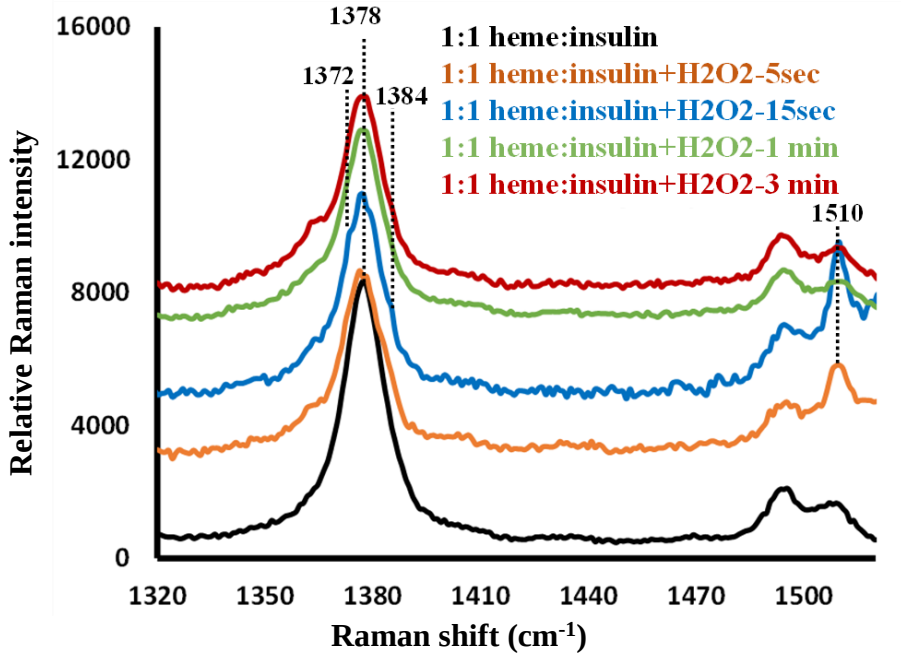

Figure 9. High frequency region of resonance Raman experimental spectrum of heme-insulin, black; with H_2O_2, at different time interval showing the changes of ν4 and ν3 marker bands, indicated by arrows.

5.3.5. Dityrosine cross-linking of insulin in presence of heme

It is now well-known that protein exposure to oxidative environments, both biologically and in dietary systems can harvest additional di-Tyr crosslinks that are not critical for native functions.[76,77] These linkages can be formed either inter- or intra-molecularly between two proteins, from two free Tyr, or between free Tyr and proteins, by radical–radical reactions involving two Tyr·.[78,79] Electron delocalization over the benzene ring and the phenolic oxygen results in the formation of two regio-isomers, one involving a C–O bond (C3–O, iso-dityrosine) and another with a C–C (C3–C3, o,o') bond, of which The latter is majorly preferred in thermodynamics.[80] The members of the peroxidase super-families like horseradish peroxidase, myeloperoxidase, laccase are known to generate crosslinks via enzyme-mediated oxidation of substrates to radicals which then undergo radical–radical coupling. One of the classic examples is oxidative coupling of Tyr and a range of other phenols via the phenoxyl generation of radical.

Experimentally, when heme-insulin complex is incubated with 10 eq of H_2O_2 and the resultant high valent species including compound I and compound II are subjected to mature

with free insulin, the result we get is quite interesting. The mixture of oxidant (ferryl oxo intermediates) and insulin sample are monitored using florescence spectroscopy where there is clear evidence of typical dityrosine formation and in longer times even tri-tyrosine is generated. A characteristic fluorescence spectrum (Iex =365, Iem= 400 nm) marking the presence of di-Tyr bond (Figure 10A) while the fluorescence ca. 310nm, seen in free insulin, is for mono tyrosine unit. Time-dependent changes in the fluorescence are observed where the 310 nm band gradually decreases and simultaneously the oligomeric bands rise. At 1 hour 30 min of the reaction, the amplitude of the fluorescence ca. 400 nm reached its maximum value and after that it decreased. A shoulder with emission maximum ca. 425 nm also rises in the spectrum which is expected for tri-Tyr and/or tetra-Tyr crosslinks (Figure 10B), so presumably at later times of the reaction, di-Tyr cross-links were converted to tri- or even tetra-Tyr. [81]

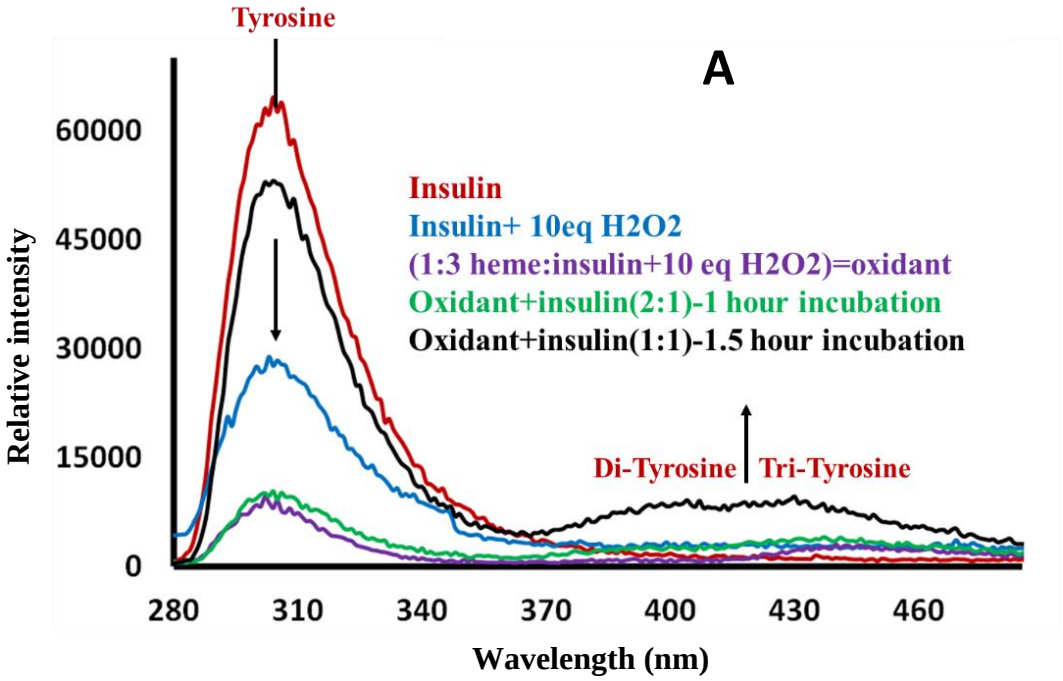

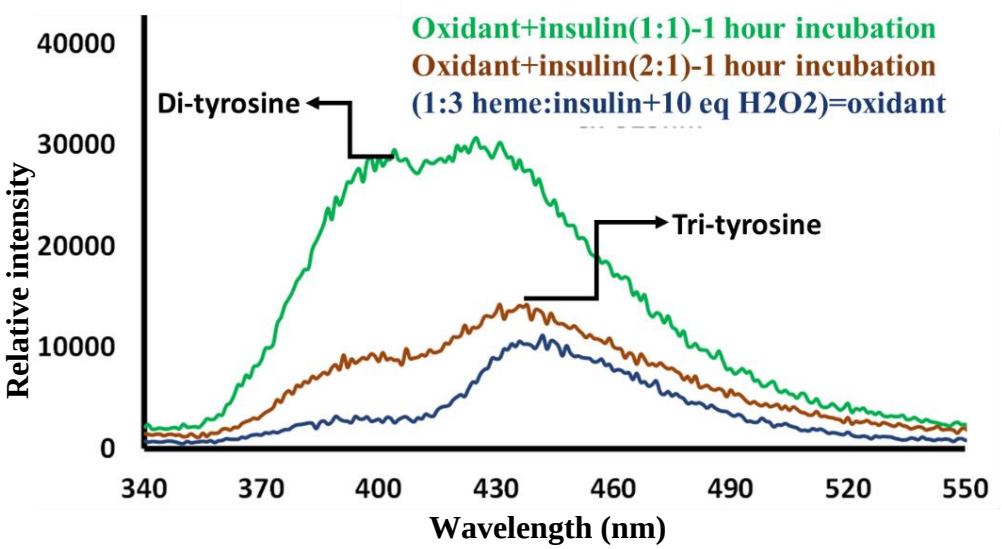

Figure 10. **(A)** Di-tyrosine fluorescence spectra; Fluorescence spectra collected at different times of incubation of insulin with H_2O_2 and heme-insulin (peroxidase), upon excitation at 265 nm. **(B)** The two bands at 400 nm and 425 nm correspond to di-Tyr and tri/tetra-Tyr, respectively, enhanced by exciting at 325nm.Arrows indicate the changes.

5.4. Discussion

When heme binds insulin, the absorption and resonance raman spectrum show that the active site consists of a mono-histidine bound high spin heme along with a trans axial weakly bound water derived ligand. On the other hand, another low spin ferric heme species with bis-His type coordination is also present as seen in case of cytochrome *b* and low spin heme-Aβ complex.[82,73] Thus, the heme-insulin complex consists of a mixture of a high spin mono-His and a low spin bis-His species. Till now, the reactivities associated with this complex and interaction with its counter-protein amylin have not been excavated in details. We have found that in terms of reactivity towards molecular oxygen, the reduced high spin 1:1 heme-insulin complex as well as the bis-His coordinated low spin 1:3 heme-insulin complex produce 8–12% partially reduced oxygen species (PROS) *i.e.* <50%, implying a one *e*- reduction of O_2 to $O_2^{\bullet-}$ which then disproportionate to form the H_2O_2. Thus, heme-insulin complexes in their reduced form generate PROS to a significantly lesser extent than heme-amylin (40 ± 2%, Figure 1).[45]

The co secreted amylin bound to heme to form the heme-amylin complex and when this is incubated with two equivalents of insulin, the absorption and rR features of the resultant

mixture is found to closely resemble those of the 1:2 heme-insulin complex (Figures 2, 3). Thus insulin can sequester heme from heme bound amylin complex. This is indeed obvious as insulin has a higher affinity (~106 M^{-1}) for heme compared to amylin (~103 M^{-1}).[58] The β cells in the pancreas secretes insulin along with the peptide hormone amylin, whose function is complementary to that of insulin.[45,83] The fact that heme can bind amylin and the resultant complex can generate significant oxidative stress in the pancreas can possibly account for the oxidative damage and dysfunction of the pancreatic β cells leading to Type 2 diabetes. Insulin, known to regulate the blood sugar level, can additionally implement its protective role by sequestering heme bound to amylin. The resultant heme-insulin complex produces much less oxidative damage (Scheme 3).

Scheme 3. **Insulin sequesters heme from heme-amylin complex to produce species identical to the heme-insulin complex having a low spin (major) component.**

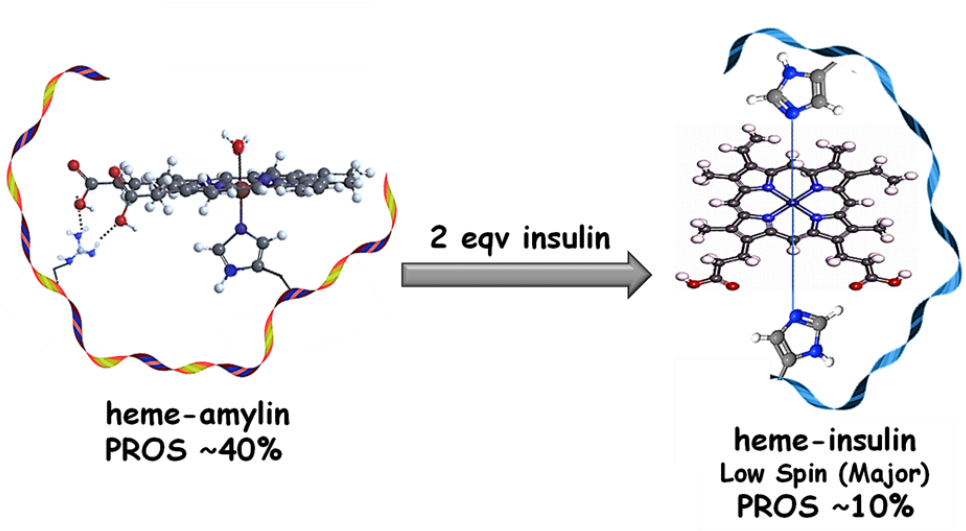

The peroxidase activity of heme-insulin complexes either in 1:1 complex or 1:3 complex is same but higher compared to that of free heme. Like other heme based protein/peptide complexes, it can similarly go through several high valent intermediates (Scheme 2). In fact, the absorption at 572 nm, 600 nm show the presence of a Fe(III)-OOH species at 40 sec. with time another broad band at 680 nm rises which is characteristic for compound I like species in the buffer medium (Figure 7). Although in absorption spectra, compound II could not be detected but the resonance Raman spectroscopy gives a probable proof for this. In rR spectrum n4 marker bands at 1372 cm^{-1} and 1384 cm^{-1} are characteristics for compound I and II (Figure 9). Literature survey suggest that partial homolysis of the peroxide bond of compound 0 can form compound II, but heterolysis has been suggested to be

the major process. The Arg at 22nd in the B-chain of insulin can probably exert the 'pull-effect' to ensure the heterolytic cleavage of O-O bond. In this peroxidase pathway tyrosine residue can act as a substrate and can get oxidised to form tyrosil radical which then undergo radical coupling to form oligomers (Scheme 4). Fluorescence spectroscopy supports the formation of di-tyrosine and tri-/tetra-tyrosine species in presence of peroxidase and H_2O_2 (Figure 10).

Scheme 4. **The schematic diagram of peroxides pathway of heme-insulin and oxidation of tyrosine residues by high-valent intermediates.**

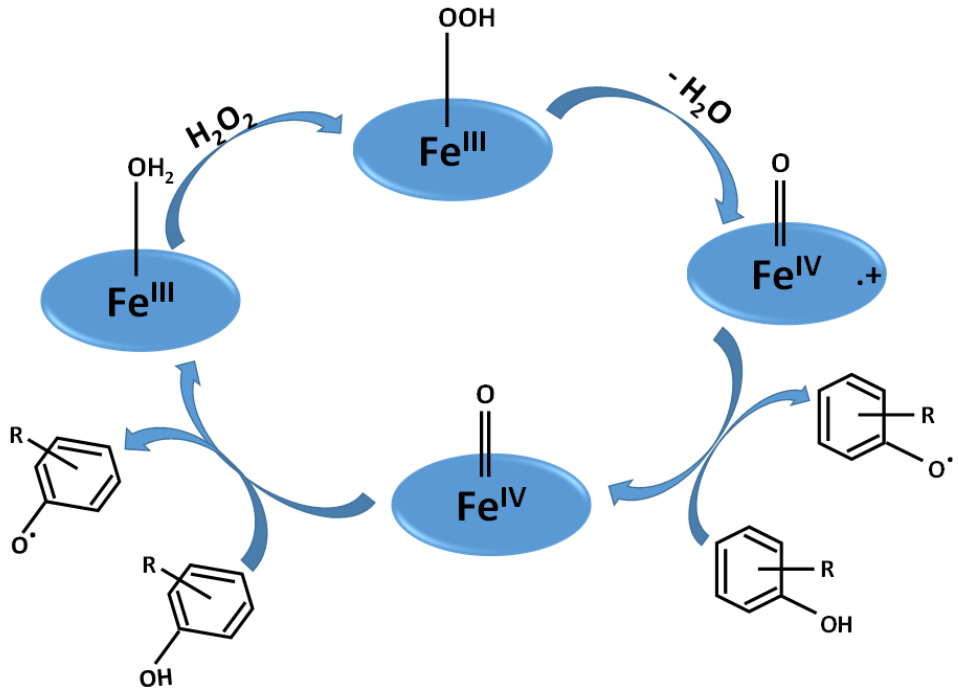

Biologically, several proteins are known to have dityrosine crosslinks as a post translational modification (PTM). Such covalent crosslinks within or in-between proteins are known to play a vital role in determining the structure and function of proteins. While some of them are formed intentionally by either natural enzymatic or molecular reactions and are essential for normal physiological function, others can be generated as a result of exposure to oxidants like toxic radicals, excited states or two-electron species which is formed in peroxidase pathway and other endogenous or external stimuli, or as a result of the actions of a number of enzymes including oxidases and peroxidases. Previous evidences indicate that the accumulation of unwanted crosslinks can be seen in ageing and multiple pathologies including amyloidogenic ones. These have either positive or negative effects on biological function as

well. In pathophysiological conditions, di-Tyr crosslinking have been reported in several diseases including in the tissues from a number of neurodegenerative situations e.g., amyloid-beta dimers in Alzheimer's disease and in α-synuclein, which contribute to Parkinson's disease; in lipofuscin pigments in the aged human brain; in plasma of patients with chronic renal failure; and higher levels of free dityrosine in urine of T2Dm patients, which can be associated with metabolic alterations including disrupted glucose metabolism.[84–88] Dityrosine has been identified as a biomarker of oxidative stress, aging, and different pathological conditions as well. The intermolecular cross-linking may result in protein aggregation. Aggregation of insulin leads to loss of activity and can trigger an unwanted immune response.[89] The formation of dityrosine cross-linked dimers may play an important role in oligomer toxicity. A role for metal catalyzed oxidation (MCO) in initiating the α-syn amyloid formation process in vitro has been observed which may implicate a metal catalyzed mechanism in vivo in PD. Such dityrosine cross-links may also stabilize the amyloid core resulting in accelerated assembly and thereby fibrils of longer contour length. It has been found that seeding α-syn with dityrosine cross-linked dimers accelerates α-syn fibril growth, suggesting that the essential rate-limiting step in the nucleation of α-syn fibrils is the formation of dityrosine cross-linked dimeric species. Similarly, insulin can also form aggregates via tyrosine cross-linking which would eventually hinder its monomeric form which is the functional and physiologically active unit of the peptide. The Insulin Receptor (IR) which belongs to tyrosine kinase receptor type, binds insulin and the binding site of insulin comprises of the tyrosine residues in its both A- and B- chains. Formation of Tyr covalent linkages indeed hamper the receptor's function, leading to the observed decline of insulin action in diabetic patient.

5.5. Conclusion

Type 2 diabetes mellitus, the prolonged metabolic disease, which is characterized by hyperglycemia and is instigated via hampered insulin secretion, making it unable to maintain glucose homeostasis over the progression of the disease. We have found a vital role of heme in the pathogenesis of this disease as heme can form peptide bound complexes and simultaneously alter the reactivities. Along with the interaction of heme with amylin peptide, which is involved in the amyloid deposits around the β-cells, heme is also found to bind another diabetes related peptide, insulin. Spectroscopy demonstrate that when heme is incubated with insulin in 1:1

stoichiometric ratio, heme binds insulin to form a mixture of six-coordinate high spin species as the major component with a possible mono-His coordination and a weakly bound water derived ligand in the distal site. All the heme(II)-insulin complexes produce only 8–12% PROS. Moreover, when the heme-amylin complex is treated with two equivalents of insulin, the latter sequesters heme from the former, forming heme-insulin (with the six-coordinate low spin species as major component) thereby bringing down the PROS from ~ 40% to ~ 10%. The peroxidase activity of heme-insulin is a little known property and as this is unregulated, such reactivity of heme-insulin can account for the abnormal glucose spike observed in T2Dm. Notably, the significant reduction of the insulin function and action leading to hyperglycemia is common phenomena in the pathology of T2Dm. In the absence of substrate, heme-insulin can oxidize the tyrosine residue to form dityrosine linkages between insulin peptides leading to their aggregation. Thus, the role of heme has been investigated in details here which suggest the oligomeric form of insulin due to its peroxidase activity can actually hamper the desired insulin action and the function of insulin receptor.

5.6. References

(1) Höppener, J. W.; Ahrén, B.; Lips, C. J. Islet Amyloid and Type 2 Diabetes Mellitus. *N. Engl. J. Med.* **2000**, *343* (6), 411–419. https://doi.org/10.1056/NEJM200008103430607.

(2) Marzban, L.; Park, K.; Verchere, C. B. Islet Amyloid Polypeptide and Type 2 Diabetes. *Exp. Gerontol.* **2003**, *38* (4), 347–351. https://doi.org/10.1016/S0531-5565(03)00004-4.

(3) Mukherjee, A.; Morales-Scheihing, D.; Butler, P. C.; Soto, C. Type 2 Diabetes as a Protein Misfolding Disease. *Trends Mol. Med.* **2015**, *21* (7), 439–449. https://doi.org/https://doi.org/10.1016/j.molmed.2015.04.005.

(4) Galicia-Garcia, U.; Benito-Vicente, A.; Jebari, S.; Larrea-Sebal, A.; Siddiqi, H.; Uribe, K. B.; Ostolaza, H.; Martín, C. Pathophysiology of Type 2 Diabetes Mellitus. *Int. J. Mol. Sci.* **2020**, *21* (17), 1–34. https://doi.org/10.3390/ijms21176275.

(5) Wu, Y.; Ding, Y.; Tanaka, Y.; Zhang, W. Risk Factors Contributing to Type 2 Diabetes and Recent Advances in the Treatment and Prevention. *Int. J. Med. Sci.* **2014**, *11* (11), 1185–1200. https://doi.org/10.7150/ijms.10001.

(6) Nagarathna, R.; Bali, P.; Anand, A.; Srivastava, V.; Patil, S.; Sharma, G.; Manasa, K.; Pannu, V.; Singh, A.; Nagendra, H. R. Prevalence of Diabetes and Its Determinants in the Young Adults Indian Population-Call for Yoga Intervention. *Front. Endocrinol. (Lausanne).* **2020**, *11* (December), 1–9. https://doi.org/10.3389/fendo.2020.507064.

(7) Reaven, G. M. Insulin-Independent Diabetes Mellitus: Metabolic Characteristics. *Metabolism* **1980**, *29* (5), 445–454. https://doi.org/https://doi.org/10.1016/0026-0495(80)90170-5.

(8) Abdul-Ghani, M.; DeFronzo, R. A.; Del Prato, S.; Chilton, R.; Singh, R.; Ryder, R. E. J. Cardiovascular Disease and Type 2 Diabetes: Has the Dawn of a New Era Arrived? *Diabetes Care* **2017**, *40* (7), 813 LP – 820. https://doi.org/10.2337/dc16-2736.

(9) Lee, M.-W.; Lim, H.-B.; Kim, M.-S.; Park, G.-S.; Nam, K.-Y.; Lee, Y.-H.; Kim, J.-Y. Effects of Prolonged Type 2 Diabetes on Changes in Peripapillary Retinal Nerve Fiber Layer Thickness in Diabetic Eyes without Clinical Diabetic Retinopathy. *Sci. Rep.* **2021**, *11* (1), 6813. https://doi.org/10.1038/s41598-021-86306-y.

(10) Dabla, P. K. Renal Function in Diabetic Nephropathy. *World J. Diabetes* **2010**, *1* (2), 48–56. https://doi.org/10.4239/wjd.v1.i2.48.

(11) Stroo, E.; Koopman, M.; Nollen, E. A. A.; Mata-cabana, A. Cellular Regulation of Amyloid Formation in Aging and Disease. *Front. Neurosci.* **2017**, *11* (February), 1–17. https://doi.org/10.3389/fnins.2017.00064.

(12) Woerle, H. J.; Szoke, E.; Meyer, C.; Dostou, J. M.; Wittlin, S. D.; Gosmanov, N. R.; Welle, S. L.; Gerich, J. E. Mechanisms for Abnormal Postprandial Glucose Metabolism in Type 2 Diabetes. *American Journal of Physiology - Endocrinology and Metabolism*. 2006. https://doi.org/10.1152/ajpendo.00529.2004.

(13) Cerf, M. E. Beta Cell Dysfunction and Insulin Resistance. *Front. Endocrinol. (Lausanne).* **2013**, *4*, 37. https://doi.org/10.3389/fendo.2013.00037.

(14) Wilcox, G. Insulin and Insulin Resistance. *Clin. Biochem. Rev.* **2005**, *26* (2), 19–39.

(15) Fazakerley, D. J.; Krycer, J. R.; Kearney, A. L.; Hocking, S. L.; James, D. E. Muscle and Adipose Tissue Insulin Resistance: Malady without Mechanism? *J. Lipid Res.* **2019**, *60* (10), 1720–1732. https://doi.org/https://doi.org/10.1194/jlr.R087510.

(16) Kahn, B. B. Type 2 Diabetes: When Insulin Secretion Fails to Compensate for Insulin Resistance. *Cell* **1998**, *92* (5), 593–596. https://doi.org/10.1016/s0092-8674(00)81125-3.

(17) Maedler, K.; Donath, M. Y. β-Cells in Type 2 Diabetes: A Loss of Function and Mass. *Horm. Res. Paediatr.* **2004**, *62(suppl 3* (Suppl. 3), 67–73. https://doi.org/10.1159/000080503.

(18) Laybutt, D. R.; Preston, A. M.; Åkerfeldt, M. C.; Kench, J. G.; Busch, A. K.; Biankin, A. V; Biden, T. J. Endoplasmic Reticulum Stress Contributes to Beta Cell Apoptosis in Type 2 Diabetes. *Diabetologia* **2007**, *50* (4), 752–763. https://doi.org/10.1007/s00125-006-0590-z.

(19) Kajimoto, Y.; Kaneto, H. Role of Oxidative Stress in Pancreatic Beta-Cell Dysfunction. *Ann. N. Y. Acad. Sci.* **2004**, *1011*, 168–176. https://doi.org/10.1007/978-3-662-41088-2_17.

(20) Kahn, S. E.; Hull, R. L.; Utzschneider, K. M. Mechanisms Linking Obesity to Insulin Resistance and Type 2 Diabetes. *Nature* **2006**, *444* (7121), 840–846. https://doi.org/10.1038/nature05482.

(21) Pinti, M. V; Fink, G. K.; Hathaway, Q. A.; Durr, A. J.; Kunovac, A.; Hollander, J. M. Mitochondrial Dysfunction in Type 2 Diabetes Mellitus: An Organ-Based Analysis. *Am. J. Physiol. Metab.* **2019**, *316* (2), E268–E285. https://doi.org/10.1152/ajpendo.00314.2018.

(22) Jeong-a Kim, Yongzhong Wei, and J. R. S. Role of Mitochondrial Dysfunction in Insulin Resistance. *Circ. Res.* **2008**, *102* (4), 401–414.

(23) Martin, B. C.; Warram, J. H.; Krolewski, A. S.; Soeldner, J. S.; Kahn, C. R.; Martin, B. C.; Bergman, R. N. Role of Glucose and Insulin Resistance in Development of Type 2 Diabetes Mellitus: Results of a 25-Year Follow-up Study. *Lancet* **1992**, *340* (8825), 925–929. https://doi.org/https://doi.org/10.1016/0140-6736(92)92814-V.

(24) Brange, J.; Langkjœr, L. Insulin Structure and Stability BT - Stability and Characterization of Protein and Peptide Drugs: Case Histories; Wang, Y. J., Pearlman, R., Eds.; Springer US: Boston, MA, 1993; pp 315–350. https://doi.org/10.1007/978-1-4899-1236-7_11.

(25) Blundell, T.; Dodson, G.; Hodgkin, D.; Mercola, D. Insulin: The Structure in the Crystal and Its Reflection in Chemistry and Biology By; Anfinsen, C. B., Edsall, J. T., Richards, F. M. B. T.-A. in P. C., Eds.; Academic Press, 1972; Vol. 26, pp 279–402. https://doi.org/https://doi.org/10.1016/S0065-3233(08)60143-6.

(26) Reaven, G. M.; Hollenbeck, C. B.; Chen, Y. D. I. Relationship between Glucose Tolerance, Insulin Secretion, and Insulin Action in Non-Obese Individuals with Varying Degrees of Glucose Tolerance. *Diabetologia* **1989**, *32* (1), 52–55. https://doi.org/10.1007/BF00265404.

(27) Guillausseau, P.-J.; Meas, T.; Virally, M.; Laloi-Michelin, M.; Médeau, V.; Kevorkian, J.-P. Abnormalities in Insulin Secretion in Type 2 Diabetes Mellitus. *Diabetes Metab.* **2008**, *34*, S43–S48. https://doi.org/https://doi.org/10.1016/S1262-3636(08)73394-9.

(28) Weyer, C.; Bogardus, C.; Mott, D. M.; Pratley, R. E. The Natural History of Insulin

Secretory Dysfunction and Insulin Resistance in the Pathogenesis of Type 2 Diabetes Mellitus. *J. Clin. Invest.* **1999**, *104* (6), 787–794. https://doi.org/10.1172/JCI7231.

(29) Mitrakou, A.; Kelley, D.; Mokan, M.; Veneman, T.; Pangburn, T.; Reilly, J.; Gerich, J. Role of Reduced Suppression of Glucose Production and Diminished Early Insulin Release in Impaired Glucose Tolerance. *N. Engl. J. Med.* **1992**, *326* (1), 22–29. https://doi.org/10.1056/NEJM199201023260104.

(30) Mitrakou, A.; Vuorinen-Markkola, H.; Raptis, G.; Toft, I.; Mokan, M.; Strumph, P.; Pimenta, W.; Veneman, T.; Jenssen, T.; Bolli, G. Simultaneous Assessment of Insulin Secretion and Insulin Sensitivity Using a Hyperglycemia Clamp. *J. Clin. Endocrinol. Metab.* **1992**, *75* (2), 379–382. https://doi.org/10.1210/jcem.75.2.1639939.

(31) Viles, J. H. Metal Ions and Amyloid Fiber Formation in Neurodegenerative Diseases . Copper, Zinc and Iron in Alzheimer ' s , Parkinson ' s and Prion Diseases. *Coord. Chem. Rev.* **2012**, *256* (May), 2271–2284.

(32) Rosas, H. D.; Chen, Y. I.; Doros, G.; Salat, D. H.; Chen, N.; Kwong, K. K.; Bush, A.; Fox, J.; Hersch, S. M. Alterations in Brain Transition Metals in Huntington Disease: An Evolving and Intricate Story. *Arch. Neurol.* **2012**, *69* (7), 887–893. https://doi.org/10.1001/archneurol.2011.2945.

(33) Alghrably, M.; Czaban, I.; Jaremko, Ł.; Jaremko, M. Interaction of Amylin Species with Transition Metals and Membranes. *J. Inorg. Biochem.* **2019**, *191* (November 2018), 69–76. https://doi.org/10.1016/j.jinorgbio.2018.11.004.

(34) Atari-hajipirloo, S.; Valizadeh, N.; Rasmi, Y.; Kheradmand, F. Altered Concentrations of Copper , Zinc , and Iron Are Associated With Increased Levels of Glycated Hemoglobin in Patients With Type 2 Diabetes Mellitus and Their First-Degree Relatives. *Int J Endocrinol Metab.* **2016**, *14* (2), 10–16. https://doi.org/10.5812/ijem.33273.Research.

(35) Taylor, C. G. Zinc, the Pancreas, and Diabetes: Insights from Rodent Studies and Future Directions. *Biometals an Int. J. role Met. ions Biol. Biochem. Med.* **2005**, *18* (4), 305–312. https://doi.org/10.1007/s10534-005-3686-x.

(36) Thomas, M. C.; MacIsaac, R. J.; Tsalamandris, C.; Jerums, G. Elevated Iron Indices in

Patients with Diabetes. *Diabet. Med.* **2004**, *21* (7), 798–802. https://doi.org/https://doi.org/10.1111/j.1464-5491.2004.01196.x.

(37) Yu, Y.-P.; Lei, P.; Hu, J.; Wu, W.-H.; Zhao, Y.-F.; Li, Y.-M. Copper-Induced Cytotoxicity: Reactive Oxygen Species or Islet Amyloid Polypeptide Oligomer Formation. *Chem. Commun.* **2010**, *46* (37), 6909–6911. https://doi.org/10.1039/C0CC02141E.

(38) Hang Li#†, Emmeline Ha#†, Robert P. Donaldson‡, Aleksandar M. Jeremic‡, and A. V. Rapid Assessment of Human Amylin Aggregation and Its Inhibition by Copper(II) Ions by Laser Ablation Electrospray Ionization Mass Spectrometry with Ion Mobility Separation. *Anal Chem.* **2015**, *87* (19), 9829–9837. https://doi.org/10.1021/acs.anal-chem.5b02217.The.

(39) Lee, S. J. C.; Choi, T. S.; Lee, J. W.; Lee, H. J.; Mun, D.-G.; Akashi, S.; Lee, S.-W.; Lim, M. H.; Kim, H. I. Structure and Assembly Mechanisms of Toxic Human Islet Amyloid Polypeptide Oligomers Associated with Copper. *Chem. Sci.* **2016**, *7* (8), 5398–5406. https://doi.org/10.1039/C6SC00153J.

(40) Gavrilova, J.; Tõugu, V.; Palumaa, P. Affinity of Zinc and Copper Ions for Insulin Monomers. *Metallomics* **2014**, *6* (7), 1296–1300. https://doi.org/10.1039/c4mt00059e.

(41) Xu, Y.; Yan, Y.; Seeman, D.; Sun, L.; Dubin, P. L. Multimerization and Aggregation of Native-State Insulin: Effect of Zinc. *Langmuir* **2012**, *28* (1), 579–586. https://doi.org/10.1021/la202902a.

(42) Chausmer, A. B. Zinc, Insulin and Diabetes. *J. Am. Coll. Nutr.* **1998**, *17* (2), 109–115. https://doi.org/10.1080/07315724.1998.10718735.

(43) Dunn, M. F. Zinc–Ligand Interactions Modulate Assembly and Stability of the Insulin Hexamer – A Review. *Biometals* **2005**, *18* (4), 295–303. https://doi.org/10.1007/s10534-005-3685-y.

(44) Khan, A. R.; Awan, F. R. Metals in the Pathogenesis of Type 2 Diabetes. *J. Diabetes Metab. Disord.* **2014**, *13* (1), 16. https://doi.org/10.1186/2251-6581-13-16.

(45) Poudel, R.; Bhusal, Y.; Tharu, B.; Kafle, N. Role of Zinc in Insulin Regulation and Diabetes. *J. Soc. Heal. Diabetes* **2017**, *5*, 83.

(46) Huang, Q.; Du, J.; Merriman, C.; Gong, Z. Genetic, Functional, and Immunological Study of ZnT8 in Diabetes. *Int. J. Endocrinol.* **2019**, *2019*, 1524905. https://doi.org/10.1155/2019/1524905.

(47) Li, L.; Hölscher, C. Common Pathological Processes in Alzheimer Disease and Type 2 Diabetes: A Review. *Brain Res. Rev.* **2007**, *56* (2), 384–402. https://doi.org/10.1016/j.brainresrev.2007.09.001.

(48) Ott, A.; Stolk, R. P.; Hofman, A.; van Harskamp, F.; Grobbee, D. E.; Breteler, M. M. Association of Diabetes Mellitus and Dementia: The Rotterdam Study. *Diabetologia* **1996**, *39* (11), 1392–1397. https://doi.org/10.1007/s001250050588.

(49) Janson, J.; Laedtke, T.; Parisi, J. E.; O'Brien, P.; Petersen, R. C.; Butler, P. C. Increased Risk of Type 2 Diabetes in Alzheimer Disease. *Diabetes* **2004**, *53* (2), 474 LP – 481. https://doi.org/10.2337/diabetes.53.2.474.

(50) Smith, M. A.; Harris, P. L.; Sayre, L. M.; Perry, G. Iron Accumulation in Alzheimer Disease Is a Source of Redox-Generated Free Radicals. *Proc. Natl. Acad. Sci. U. S. A.* **1997**, *94* (18), 9866–9868. https://doi.org/10.1073/pnas.94.18.9866.

(51) Ghosh, C.; Seal, M.; Mukherjee, S.; Dey, S. G. Alzheimer ' s Disease : A Heme − Aβ Perspective. *J. Alzheimer's Dis.* **2015**, *48*, 2556–2564. https://doi.org/10.1021/acs.accounts.5b00102.

(52) Pramanik, D.; Dey, S. G. Active Site Environment of Heme-Bound Amyloid Associated with Alzheimer ' s Disease. *J. AM. CHEM. SOC.* **2011**, *133* (15), 81–87.

(53) Huth, C.; Beuerle, S.; Zierer, A.; Heier, M.; Herder, C.; Kaiser, T.; Koenig, W.; Kronenberg, F.; Oexle, K.; Rathmann, W.; Roden, M.; Schwab, S.; Seissler, J.; Stöckl, D.; Meisinger, C.; Peters, A.; Thorand, B. Biomarkers of Iron Metabolism Are Independently Associated with Impaired Glucose Metabolism and Type 2 Diabetes: The KORA F4 Study. *Eur. J. Endocrinol.* **2015**, *173* (5), 643–653. https://doi.org/10.1530/eje-15-0631.

(54) Roy, M.; Pal, I.; Nath, A. K.; Dey, S. G. Peroxidase Activity of Heme Bound Amyloid b Peptides Associated with Alzheimer ' s Disease. *Chem. Comm.* **2020**, *56*, 4505–4518. https://doi.org/10.1039/c9cc09758a.

(55) Desai, G.; Zheng, C.; Geetha, T.; Mathews, S. T.; White, B. D.; Huggins, K. W.; Zizza, C. A.; Broderick, T. L.; Babu, J. R. The Pancreas-Brain Axis : Insight into Disrupted Mechanisms Associating Type 2 Diabetes and Alzheimer's Disease. *J. Alzheimer's Dis.* **2014**. https://doi.org/10.3233/JAD-140018.

(56) Madhuparna Roy†, Ishita Pal†, Chinmay Dey, A. D.; Dey*, and S. G. Electronic Structure and Reactivity of Heme Bound Insulin. *J. Porphyrins Phthalocyanines* **2021**, *1088424621* (Scheme 1), A-K. https://doi.org/10.1142/S1088424621500346.

(57) Mayer, J. P.; Zhang, F.; DiMarchi, R. D. Insulin Structure and Function. *Biopolymers* **2007**, *88* (5), 687–713. https://doi.org/10.1002/bip.20734.

(58) Huang, Y.; Yang, Z.; Xu, H.; Zhang, P.; Gao, Z.; Li, H. Insulin Enhances the Peroxidase Activity of Heme by Forming Heme-Insulin Complex : Relevance to Type 2 Diabetes Mellitus. *Int. J. Biol. Macromol.* **2017**, *102*, 1009–1015.

(59) Correia, M.; Neves-Petersen, M. T.; Jeppesen, P. B.; Gregersen, S.; Petersen, S. B. UV-Light Exposure of Insulin: Pharmaceutical Implications upon Covalent Insulin Dityrosine Dimerization and Disulphide Bond Photolysis. *PLoS One* **2012**, *7* (12), e50733. https://doi.org/10.1371/journal.pone.0050733.

(60) Kahn, S. E.; D'Alessio, D. A.; Schwartz, M. W.; Fujimoto, W. Y.; Ensinck, J. W.; Taborsky, G. J. J.; Porte, D. J. Evidence of Cosecretion of Islet Amyloid Polypeptide and Insulin by Beta-Cells. *Diabetes* **1990**, *39* (5), 634–638. https://doi.org/10.2337/diab.39.5.634.

(61) Lorenzo, A.; Razzaboni, B.; Weir, G. C.; Yankner, B. A. Pancreatic Islet Cell Toxicity of Amylin Associated with Type-2 Diabetes Mellitus. *Nature* **1994**, *368* (6473), 756–760. https://doi.org/10.1038/368756a0.

(62) Rittle, J.; Green, M. T. Cytochrome P450 Compound I: Capture, Characterization, and C-H Bond Activation Kinetics. *Science (80-.).* **2010**, *330* (6006), 933 LP – 937. https://doi.org/10.1126/science.1193478.

(63) Holland, V. R.; Saunders, B. C.; Rose, F. L.; Walpole, A. L. A Safer Substitute for Benzidine in the Detection of Blood. *Tetrahedron* **1974**, *30* (18), 3299–3302. https://doi.org/https://doi.org/10.1016/S0040-4020(01)97504-0.

(64) Pal, I.; Roy, M.; Dey, S. G. Interaction of ApoMyoglobin with Heme-HIAPP Complex. *J. Inorg. Biochem.* **2021**, *216* (December 2020), 111348. https://doi.org/10.1016/j.jinorgbio.2020.111348.

(65) Rodriguez-Lopez, J. N.; Smith, A. T.; Thorneley, R. N. Effect of Distal Cavity Mutations on the Binding and Activation of Oxygen by Ferrous Horseradish Peroxidase. *J. Biol. Chem.* **1997**, *272* (1), 389–395. https://doi.org/10.1074/jbc.272.1.389.

(66) Denisov, I. G.; Makris, T. M.; Sligar, S. G. Formation and Decay of Hydroperoxo-Ferric Heme Complex in Horseradish Peroxidase Studied by Cryoradiolysis. *J. Biol. Chem.* **2002**, *277* (45), 42706–42710. https://doi.org/10.1074/jbc.M207949200.

(67) Egawa, T.; Shimada, H.; Ishimura, Y. Formation of Compound I in the Reaction of Native Myoglobins with Hydrogen Peroxide. *J. Biol. Chem.* **2000**, *275* (45), 34858–34866. https://doi.org/10.1074/jbc.M004026200.

(68) Hewson, W. D.; Hager, L. P. Oxidation of Horseradish Peroxidase Compound II to Compound I. *J. Biol. Chem.* **1979**, *254* (9), 3182–3186.

(69) Yokota, S.; Fujii, H. Critical Factors in Determining the Heterolytic versus Homolytic Bond Cleavage of Terminal Oxidants by Iron(III) Porphyrin Complexes. *J. Am. Chem. Soc.* **2018**, *140* (15), 5127–5137. https://doi.org/10.1021/jacs.7b13037.

(70) Fujii, H.; Ichikawa, K. Preparation and Characterization of an A1u (Oxo) Iron(IV) Porphyrin .Pi.-Cation-Radical Complex. *Inorg. Chem.* **1992**, *31* (6), 1110–1112. https://doi.org/10.1021/ic00032a039.

(71) Schulz, C. E.; Rutter, R.; Sage, J. T.; Debrunner, P. G.; Hager, L. P. Moessbauer and Electron Paramagnetic Resonance Studies of Horseradish Peroxidase and Its Catalytic Intermediates. *Biochemistry* **1984**, *23* (20), 4743–4754. https://doi.org/10.1021/bi00315a033.

(72) Hu, S.; Smith, K. M.; Spiro, T. G. Assignment of Protoheme Resonance Raman Spectrum by Heme Labeling in Myoglobin. *J. Am. Chem. Soc.* **1996**, *118* (50), 12638–12646. https://doi.org/10.1021/ja962239e.

(73) Spiro, T. G.; Strekas, T. C. Resonance Raman Spectra of Heme Proteins. Effects of Oxidation and Spin State. *J. Am. Chem. Soc.* **1974**, *96* (2), 338–345.

https://doi.org/10.1021/ja00809a004.

(74) Paeng, K. J.; Kincaid, J. R. The Resonance Raman Spectrum of Horseradish Peroxidase Compound I. *J. Am. Chem. Soc.* **1988**, *110* (23), 7913–7915. https://doi.org/10.1021/ja00231a073.

(75) Sengupta, K.; Chatterjee, S.; Dey, A. Catalytic H 2 O 2 Disproportionation and Electrocatalytic O 2 Reduction by a Functional Mimic of Heme Catalase: Direct Observation of Compound 0 and Compound I in Situ. **2016**. https://doi.org/10.1021/acscatal.5b02668.

(76) Sies, H. Oxidative Stress: Concept and Some Practical Aspects. *Antioxidants (Basel, Switzerland)* **2020**, *9* (9). https://doi.org/10.3390/antiox9090852.

(77) Hellwig, M. The Chemistry of Protein Oxidation in Food. *Angew. Chemie Int. Ed.* **2019**, *58* (47), 16742–16763. https://doi.org/https://doi.org/10.1002/anie.201814144.

(78) GROSS, A. J.; SIZER, I. W. The Oxidation of Tyramine, Tyrosine, and Related Compounds by Peroxidase. *J. Biol. Chem.* **1959**, *234* (6), 1611–1614.

(79) Heinecke, J. W.; Li, W.; Francis, G. A.; Goldstein, J. A. Tyrosyl Radical Generated by Myeloperoxidase Catalyzes the Oxidative Cross-Linking of Proteins. *J. Clin. Invest.* **1993**, *91* (6), 2866–2872. https://doi.org/10.1172/JCI116531.

(80) Giulivi, C.; Traaseth, N. J.; Davies, K. J. A. Tyrosine Oxidation Products: Analysis and Biological Relevance. *Amino Acids* **2003**, *25* (3–4), 227–232. https://doi.org/10.1007/s00726-003-0013-0.

(81) Nomura, K.; Suzuki, N.; Matsumoto, S. Pulcherosine, a Novel Tyrosine-Derived, Trivalent Cross-Linking Amino Acid from the Fertilization Envelope of Sea Urchin Embryo. *Biochemistry* **1990**, *29* (19), 4525–4534. https://doi.org/10.1021/bi00471a004.

(82) Ghosh, C.; Mukherjee, S.; Seal, M.; Ghosh, S. Peroxidase to Cytochrome b Type Transition in the Active Site of Heme-Bound Amyloid β Peptides Relevant to Alzheimer's Disease. *Inorg. Chem.* **2016**, *55*. https://doi.org/10.1021/acs.inorgchem.5b02683.

(83) Leighton, B.; Cooper, G. J. S. Pancreatic Amylin and Calcitonin Gene-Related Peptide Cause Resistance to Insulin in Skeletal Muscle in Vitro. *Nature* **1988**, *335* (6191), 632–635. https://doi.org/10.1038/335632a0.

(84) Al-Hilaly, Y. K.; Williams, T. L.; Stewart-Parker, M.; Ford, L.; Skaria, E.; Cole, M.; Bucher, W. G.; Morris, K. L.; Sada, A. A.; Thorpe, J. R.; Serpell, L. C. A Central Role for Dityrosine Crosslinking of Amyloid-β in Alzheimer's Disease. *Acta Neuropathol. Commun.* **2013**, *1* (1), 83. https://doi.org/10.1186/2051-5960-1-83.

(85) Pennathur, S.; Jackson-Lewis, V.; Przedborski, S.; Heinecke, J. W. Mass Spectrometric Quantification of 3-Nitrotyrosine, Ortho-Tyrosine, and o,o'-Dityrosine in Brain Tissue of 1-Methyl-4-Phenyl-1,2,3, 6-Tetrahydropyridine-Treated Mice, a Model of Oxidative Stress in Parkinson's Disease. *J. Biol. Chem.* **1999**, *274* (49), 34621–34628. https://doi.org/10.1074/jbc.274.49.34621.

(86) Kato, Y.; Maruyama, W.; Naoi, M.; Hashizume, Y.; Osawa, T. Immunohistochemical Detection of Dityrosine in Lipofuscin Pigments in the Aged Human Brain. *FEBS Lett.* **1998**, *439* (3), 231–234. https://doi.org/https://doi.org/10.1016/S0014-5793(98)01372-6.

(87) Kato, Y.; Dozaki, N.; Nakamura, T.; Kitamoto, N.; Yoshida, A.; Naito, M.; Kitamura, M.; Osawa, T. Quantification of Modified Tyrosines in Healthy and Diabetic Human Urine Using Liquid Chromatography/Tandem Mass Spectrometry. *J. Clin. Biochem. Nutr.* **2009**, *44* (1), 67–78. https://doi.org/10.3164/jcbn.08-185.

(88) Yang, Y.; Zhang, H.; Yan, B.; Zhang, T.; Gao, Y.; Shi, Y.; Le, G. Health Effects of Dietary Oxidized Tyrosine and Dityrosine Administration in Mice with Nutrimetabolomic Strategies. *J. Agric. Food Chem.* **2017**, *65* (32), 6957–6971. https://doi.org/10.1021/acs.jafc.7b02003.

(89) Gibson, T. J.; Murphy, R. M. Inhibition of Insulin Fibrillogenesis with Targeted Peptides. *Protein Sci.* **2006**, *15* (5), 1133–1141. https://doi.org/10.1110/ps.051879606.

Chapter 6

The Effect of Second Sphere on the Reactivity of Synthetic Heme with Peroxides

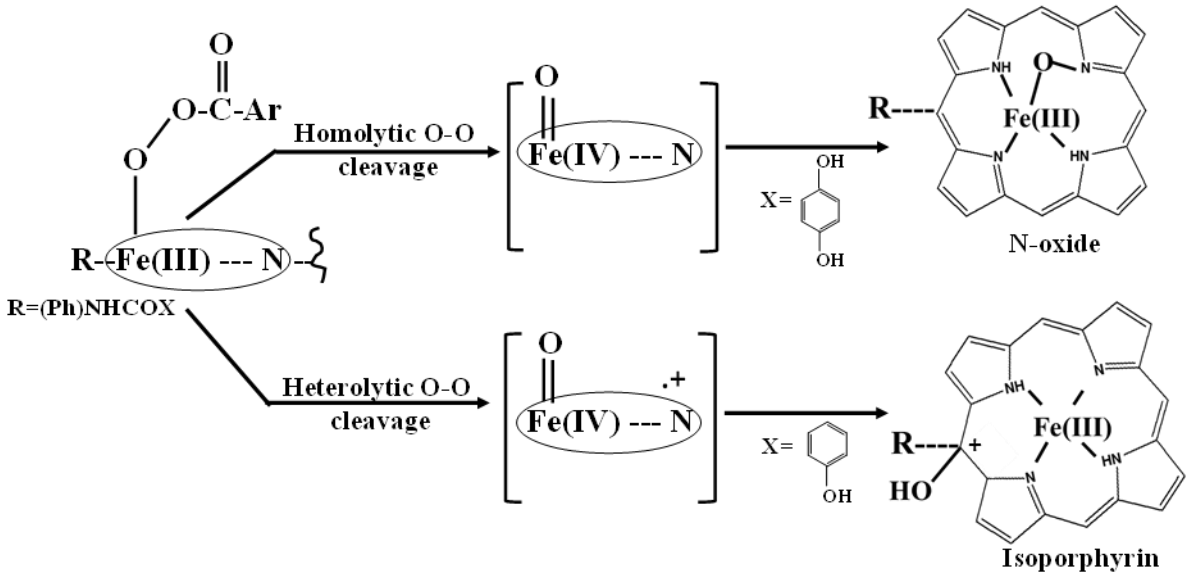

To address the role of second sphere groups, two iron porphyrin complexes are synthesized which includes a pendant quinol ($FeQH_2$) and a phenol group (FePh) respectively. Upon reacting with mCPBA, they show different products which essentially come via different pathways. For $FeQH_2$, the formation of Fe(III)-N-oxide as the major product might be a result of homolytic O-O bond cleavage of compound 0 while the FePh might have a heterolytic O-O bond cleavage leading to isoporphyrin like species formation as can be seen in bare Fe-tetra phenyl porphryrins. Thus, the mechanisms of heterolytic versus homolytic O-O bond cleavage by engeenering the attached group in modified synthetic porphyrins have been examined in this chapter to observe the effect of second spheres.

6.1. Introduction

The dioxygen activation mechanism by cytochrome P450 and related high valent metal oxo species have drawn a large attention of the bioinorganic community as most of the oxygen activating heme and non heme enzymes employ high valent metal oxo intermediates to perform C-H bond activation, mono-oxygenase activity, halogenation, desaturations, epoxidation, hydroxylation etc.[1-6] In the catalytic cycle of cytochrome P450 O-O bond heterolysis results in formation of Fe^{IV}-oxo porphyrin cation radical (compound I) which performs C-H bond activation, halogenation, desaturation etc.[2,3] In the catalytic cycle of heme dioxyginases compound I is formed which performs H atom transfer reaction. Similarly in the catalytic cycle of non heme enzymes like Escherichis coli taurine: α ketogluarate dioxygenases (TauD), prolyl-4-hydroxylase, haloginase Cyt C3 etc. high valent Fe^{IV}-oxo intermediate is formed which are well known to perform substrate oxidation.[4,6-11]

A number of synthetic Fe porphyrins have been reported, which form high valent metal oxo species including Fe^{IV}-oxo π cation radical (compound I) or Fe^{IV}-oxo (compound II) upon reaction with H_2O_2 or mCPBA.[12] The heterolytic cleavage of O-O bond of ferric peroxo intermediate leads to formation of compound I as observed in cytochrome P450 and other heme based peroxidases while homolytic cleavage results in formation of compound II as observed in cytochrome C oxidase or myoglobin like proteins.[2,3] An alternative bridged intermediate, N-bridged iron porphyrin (Fe-P) N-oxide has been suggested back in time.[13] This suggestion was on the basis of the crystal structures of N-bridged Fe porphyrin carbenes and the existence of some metalloporphyrin N-oxides along with an N-bridged nitrene.[13,14] Such species are shown to be chemically distinct from the formally isomeric oxoiron (IV) porphyrin cation radical (compound I) complexes, reported for many well-known heme proteins and synthetic porphyrins. Literature suggests that mainly in nonpolar solvents and in the absence of acids, O−O bond homolysis occurs to afford this relatively unusual Fe (III) porphyrin N-oxide species, and a diacylperoxide as products, whereas a ferryl species, is formed for alkyl acylperoxy-Fe (III) complexes due to more rapid decarboxylation of the alkyl acyl radicals.[13] The biological significance of N-oxide compounds is derived from the presumed involvement of these Fe (III) complexes as intermediated in heme degradation pathway and during the P-450 suicide reaction, while Groves and Watanabe first pointed out that this complex has no monooxygenase activity.[15] MO calculations also have predicted that Fe-Porphyrin N-oxide is more stable than

the isomeric Fe (IV)=0 porphyrin cation radical. Tsurumaki et al. has demonstrated that the N-oxide has a high-spin ferric-iron centre with a large rhombicity, shown in EPR.[16]

Another intermediate which is found during the heme degradation by heme oxygenase enzyme, is, Isoporphyrin, a unique tautomer of porphyrin. It is formed due to one proton migration from pyrrole nitrogen atoms of the ring to its meso position, converting that meso-C to a sp^3 C atom and thus disrupting the ring current flow. Isoporphyrins are characteristic due to their strong absorption at the near-IR region and have incredible redox behaviour.[17] The enzyme heme oxygenase catalyzes the degradation of heme to biliverdin, the ring opening product with the release of CO and free Fe in the presence of O_2, reducing agent NADPH, and cytochrome P450 reductase. Heme oxygenase can regiospecifically catalyse the oxidation of heme at the α-meso position of the porphyrin ring. Such heme degradation leading to final product, verdoheme via an isoporphyrin intermediate can form from an Fe (IV) oxo porphyrin π-cation radical i.e. compound I.[18] Through the heterolytic cleavage of an Fe (III)-hydroperoxo intermediate (compound 0) known to form a transient compound-I type species, is followed by the H_2O/OH attack at the meso position of ring to yield an isoporphyrin intermediate. Fuji and co-workers reported the conversion of a Fe (IV)-oxo porphyrin radical to Fe (III) mesochloro-isoporphyrin in the presence of trifluoroacetic acid and chloride ion.[19]

In model system the nature of O-O bond scission of alkyl or acyl peroxo intermediate depends on several factors.[13] In dichloromethane-methanol solvent heterolytic cleavsge of O-O bond of ^tBu-O-O-H or H_2O_2 adduct of Fe porphyrins have been reported by Traylor and coworkers, while in aqueous and nonpolar medium the O-O bond is cleaved homolytically.[20-22] The nature of O-O bond scission is also depend on nature of axial ligand.[23] With stronger electron donating ligand like hydroxide, chloride, fluoride, acetate O-O bond cleaves homolytically while heterolytic cleavage is observed with weaker electron donating ligands such as triflate, nitrate, perchlorate etc.along with the nature of axial ligands, solvents, pH etc., the nature of attached group to the phenyl substituent at meso position of porphyrin can also control the O-O bond cleavage. Various Fe (III) porphyrin complexes containing electron withdrawing and -donating substituents on phenyl groups at the meso position of the porphyrin ring were employed to study the electronic effect of porphyrin ligands on the heterolytic versus homolytic O-O bond cleavage of the hydroperoxides.[24]

In this manuscript a Fe(III) porphyrin with hydroquinone ring ($FeQH_2$) and another with a phenol group (FePh), attached covalently with poprhyrin macrocycle (Figure 1) along with the standard Fe(III)Tetra Phenyl Porphyrin (FeTPP) are used to investigate the reaction mechanism of this reaction with mCPBA at room temperature. In a recent report hydroquinone ring has been observed to transfer H atom to metal bound superoxide complex of $FeQH_2$ intramolecularly.[25] Absorption experiments were performed for the reaction of resting Fe^{III} porphyrin with mCPBA, which show strikingly different results for the above mention porphyrins.

6.2. Materials and methods

6.2.1. Materials

All reagents and solvents were purchased from commercial sources. m-chloro perbenzoic acid (m-CPBA), CD_3OD, Na_2S, 2,5-Dimethoxy benzoic acid, 2-hydroxy benzoic acid, FeBr2, 2,4,6-collidine, KPF_6 were purchased from Sigma Aldrich. Electron Paramagnetic Resonance (EPR) spectra were recorded on a JEOL instrument. Resonance Raman data were collected using 413.1 nm excitation from a Kr+ ion source (Sabre Coherent Inc) and a Trivista 555 triple spectrophotometer (gratings used in the three stages were 900, 900 and 1800/2400 grooves/mm) fitted with an electronically cooled Pixis CCD camera (Princeton Instruments). UV absorption data and kinetic data were collected using stopped flow instrument.

6.2.2. Synthesis of Fe porphyrin complexes

All the Fe(III)-porphyrins were synthesized starting from o-aminophenyltris(phenyl)-porphyrin (monoamine, 1a in Scheme S1A), which, successively, was prepared by the condensation of 1 equivalent of o-nitrobenzaldehyde, 3 equivalent of benzaldehyde, and 4 equivalent of pyrrole, followed by a reduction of the nitro group by adding $SnCl_2$ in dilute HCl followed by purification via a silica gel column.

6.2.2.1. FePh

One equivalent of 2-methoxy benzoic acid is dissolved in dry tetrahydrofuran (THF) solvent. It is then reacted with 4 equivalent of oxalyl chloride added drop-wise under refluxing condition and kept under argon atmosphere overnight. Excess oxalyl chloride is evaporated to get the acid chloride (quantitative yield) as a yellowish oil. It is then treated with o-aminophenyl-tris(phenyl)-porphyrin dissolved in dry THF in the presence of 4 equiv of dry triethylamine and kept overnight at RT. The reaction mixture is then evaporated, dissolved in dichloromethane (DCM) solvent, and washed with water in a separatory funnel. The organic part is extracted, dried over anhydrous Na_2SO_4, and evaporated via a rotary evaporator. The solid crude product is then purified with column chromatography with silica gel (60−120 mesh) and an 80% DCM-hexane solvent mixture as the eluent. The final product is a violet powder. Yield: (>90%). The resulting porphyrin is dissolved in dry DCM and allowed to react with 50 equiv of BBr_3 for 20 h at 0 °C. It is then neutralized with a saturated aqueous solution of sodium bicarbonate. The reaction mixture is then evaporated, dissolved in DCM, and washed with waterin a separatory funnel. The organic part is extracted and then dried over anhydrous Na_2SO_4 and evaporated via a rotary evaporator. The crude reaction mixture is then purified using column chromatography with silica gel (60−120 mesh) and a 60% DCM-hexane mixture. The final product is a reddish-brown powder. Yield: (80%). 1H NMR (400mHz, CDCl3) δ ppm = 11.51 (s, 1H), 8.90 (m, 8H), 8.27 (m, 7H), 8.15 (m, 8H), 7.82 (m, 4H), 7.81(m,1H), 7.78 (m,1H), 7.61 (d, 1H), 7.26 (s,1H), 6.5 (d, 1H), −2.61 (s, 2H) (Figure S1). Electrospray ionization mass spectrometry (ESI-MS) (positive ion mode in acetonitrile (ACN)): m/z (%) = 749 (100) (Figure S2).

The porphyrin ligand is then metalated using $FeBr_2$ in dry THF in the presence of 2 equiv of 2,4,6-collidine under Ar atmosphere. The excess $FeBr_2$ is removed by working up the reaction mixture with dilute HCl, and the complex is extracted using DCM. The organic part is then dried over anhydrous Na_2SO_4 and evaporated using a rotary evaporator. The crude product is then purified using column chromatography with silica gel (60−120 mesh) and a 1% methanol-DCM solvent mixture as the eluent. The final product FePh is a deep purple powder (Scheme 1B). Yield: (70−75%) ESI-MS (positive ion mode in ACN): m/z (%) = 804 (100) (Figure S3). It exhibits paramagnetic shifts of the meso-phenyl protons in its 1H NMR consistent with a high-spin (HS) ferric porphyrin (Figure S4).[26]

***Scheme 1*. Molecular structures of iron–porphyrin complexes used in this study: (A) $Fe^{III}QH_2$ (B) $Fe^{III}Ph$ (C) $Fe^{III}TPP$.**

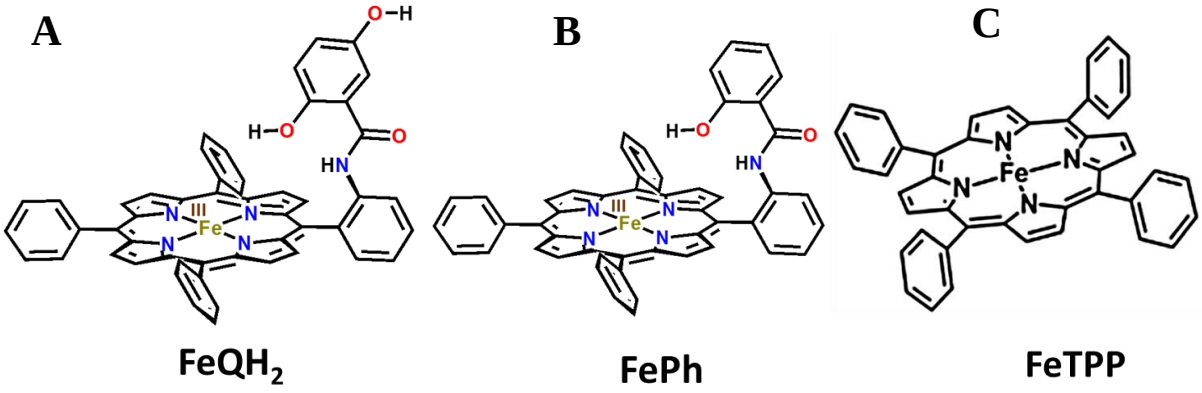

6.2.2.2. $FeQH_2$

The iron porphyrin complex ($FeQH_2$ in Scheme 1A) is synthesized as reported previously.[27,32] First o-amino tetraphenyl porphyrin was synthesized following reported procedure. The hydroxyl groups of 2,5-dihydroxy benzoic acid were blocked by performing acetylation of hydroxyl groups using acetic anhydride and pyridine. It is now reacted with thionyl chloride under argon atmosphere in THF followed by addition of o-amino tetraphenyl porphyrin, which leads to formation of porphyrin macrocycle with a tethered acetylated hydroquinone ring through an amide linkage. Hydrolysis of acetyl group by stirring the porphyrin with 4% HCl-MeOH mixture for 3-4 hours generates porphyrin ring with a hydroquinone moiety attached to it. It was characterised by recording mass spectra (Figure S5). It was then metalated with FeBr2 in dry degassed THF under argon atmosphere. An acidic work-up with HCl-H2O followed by column chromatography in 60-120 silica gel were performed to obtain pure Fe^{III}QH2 (Scheme S1B). The final product was then characterised using mass spectroscopy (Figure S6). Anal Calcd for C63H61ClFeN5O3: C, 73.64; H, 6.98; N, 6.82. Found C, 74.34; H, 5.54; N, 6.47.

6.2.3. Experimental procedure

UV-Vis sample preparation

Fe(III)-porphyrin is dissolved in DCM to make a solution having strength of 1mM. It is then diluted with to get a final solution having strength of 30µM. A 20mM solution of m-chloro perbenzoic acid (m-CPBA) in acetonitrile was prepared separately. It is then diluted to get a solution of mCPBA having strength of 300µM and mixed with porphyrin solution at room temperature under stirring condition. The change of the absorption feature is recorded after every 0.5 Sec for a definite period of time. To get the kinetic isotope effect 3% by volume MeOH was added to the solution of 1mM $FeQH_2$ and kept overnight. Similarly $FeQD_2$ was generated using CH_3OD instead of CH_3OH and stirred for overnight.

Resonance Raman sample preparation

Fe (III) porphyrin is dissolved in DCM to make a solution having strength of 1mM. The sample tubes are then prepared by transferring 200 µl solution from the aliquote in each NMR tube. A 20mM solution of m-chloro perbenzoic (m-CPBA) acid in acetonitrile was prepared separately. 5 equvalent of mCPBA was then added to each tube and kept the tubes at room temperature for different time to get different incubation period. The samples are then frozen in liq N_2 bath. For collecting resonance Raman data these sample tubes are aligned in the finger dewar containg liq. N_2. The samples are then excited using a laser light having wavelength at 413.1 nm.

6.3. Results and Analysis

6.3.1. $FeQH_2$

Absorption spectroscopy

Fe porphyrin with a hydroquinone ring attached in the distal site of the porphyrin in DCM is allowed to react with acetonitrile solution of mCPBA and the kinetics of the reaction is monitored under constant stirring condition. The data shows a dramatical red-shift in the soret band region from 418 nm to 446 nm and in the Q-band region, band at 660 nm grows

gradually along with the decay of 510 nm band (Figure 1A and 1B).These bands are characteristics for typical Fe(III)-P N-oxide.[13,14]

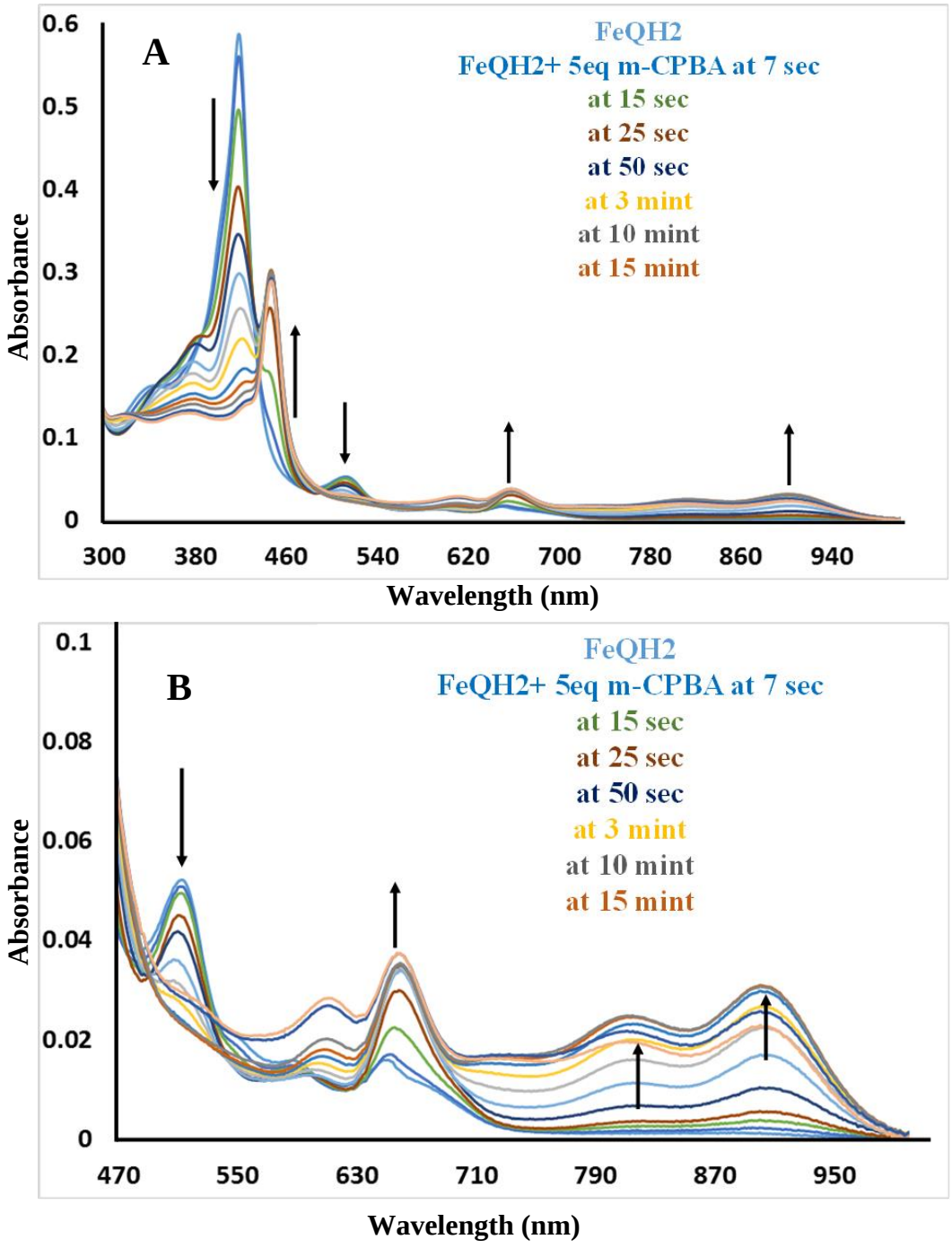

Figure 1. **(A)** Absorption spectra of Fe (III)-N-oxide, formed in the reaction of Fe^{III} porphyrin with mCPBA at room temperature, in different time interval. **(B)** The Q-band region of the same. Arrows indicated the spectral changes with time.

Along with the formation of N-oxide, there is also some minor changes reflected in the Q-region i.e. a growth in 810 nm and 904 nm bands, which is typical of the isoporphyrin species formation (Figure 1B).[20] thus, from the absortion feature a mixture of species formation has been indicated at room temperature.

Kinetics

The decay kinetics of the soret 418 nm band and the growth of newly formed species at 446 nm band are monitered in kinetics setup (Figure 2A). Using CH_3OD instead of CH_3OH, the kinetic data of 446 nm band waas monitored. Formation of N-oxide becomes slower for $FeQD_2$ than that of $FeQH_2$ and Kh/Kd shows that the formation of the N-oxide species is associated with a kinetic isotope effect of 2.71 (Figure 2B). This KIE value is consistent with the previously repoted KIE for H atom transfer process observed in $FeQH_2$ system.[25] Thus the formation of the intermediate involves H atom transfer reaction.

.

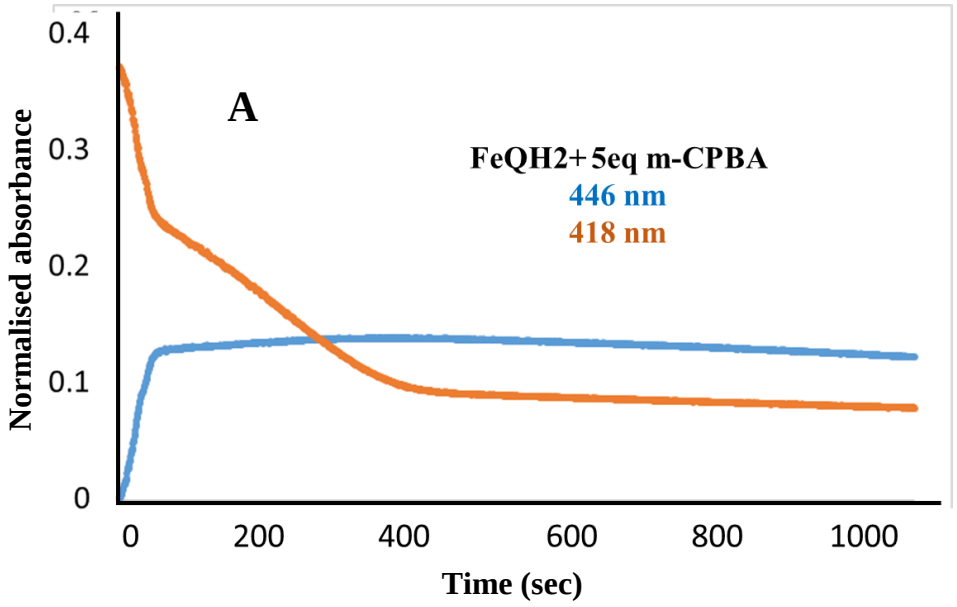

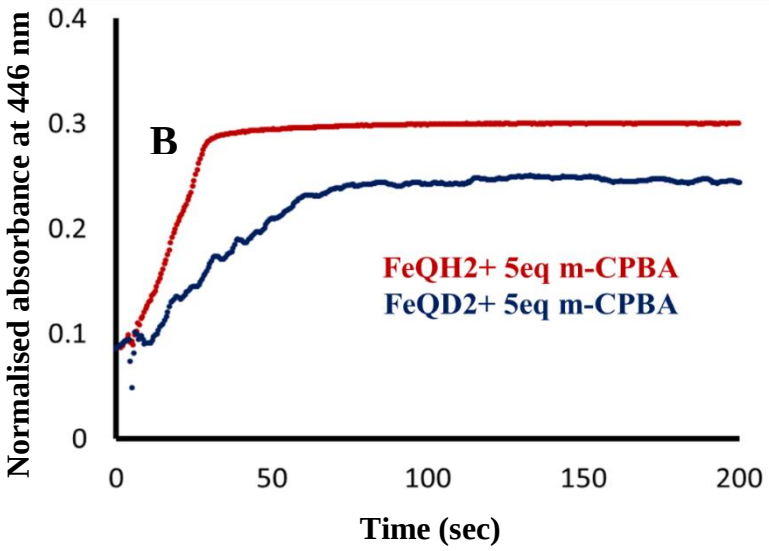

Figure 2. **(A)** The kinetic traces of the bands at 418 nm and 446 nm in the reaction of $FeQH_2$ with m-CPBA. **(B)** Formation of N-oxide (446 nm); $FeQH_2$ with m-CPBA in both CH_3OH (in red) and CH_3OD (in blue).

Resonance Raman spectroscopy

The rR spectra of iron tetraphenylporphyrins have multiple modes which are sensitive to the oxidation, ligand coordination and spin state of the iron center. For example the marker bands ν_4 (pyrrole half ring symmetric stretch involving N, C_2 and C_5 atoms of four pyrroles) and ν_2 (pyrrole C_3-C_4 symmetric stretch involving all four pyrroles) of vibrations high spin Fe^{III} occur at 1360-1363 cm^{-1} and 1555 cm^{-1}, 1365-1366 cm^{-1} and 1563-1566 cm^{-1} for LS Fe^{III} and 1369-1372 cm^{-1} and 1568-1570 cm^{-1} for Fe^{IV}=O species etc. In tetraphenylporphyrins both the ν_4 and ν_2 bands shift with oxidation and spin state and can be used to unambiguously assign the oxidation and spin state of the iron. Observation of an intense ν_3 is generally associated with a 5C species. In resonance Raman spectra it has been observed that after the addition of 5 equivalent of mCPBA to the concentrated solution of $FeQH_2$ oxidation and spin state marker bands appear at 1332 cm^{-1},1358 cm^{-1} and 1533,1547 cm^{-1}, respectively. This corresponds to the Fe(III)-N-oxide along with the remaining Fe^{III} HS species having the ν_4 and ν_2 at 1363 cm^{-1} and 1553 cm^{-1} (Figure 3).[28] Thus the decay of Fe^{III} high spin species is associated with the growth of marker bands corresponding to N-oxide high spin species at room temperature.

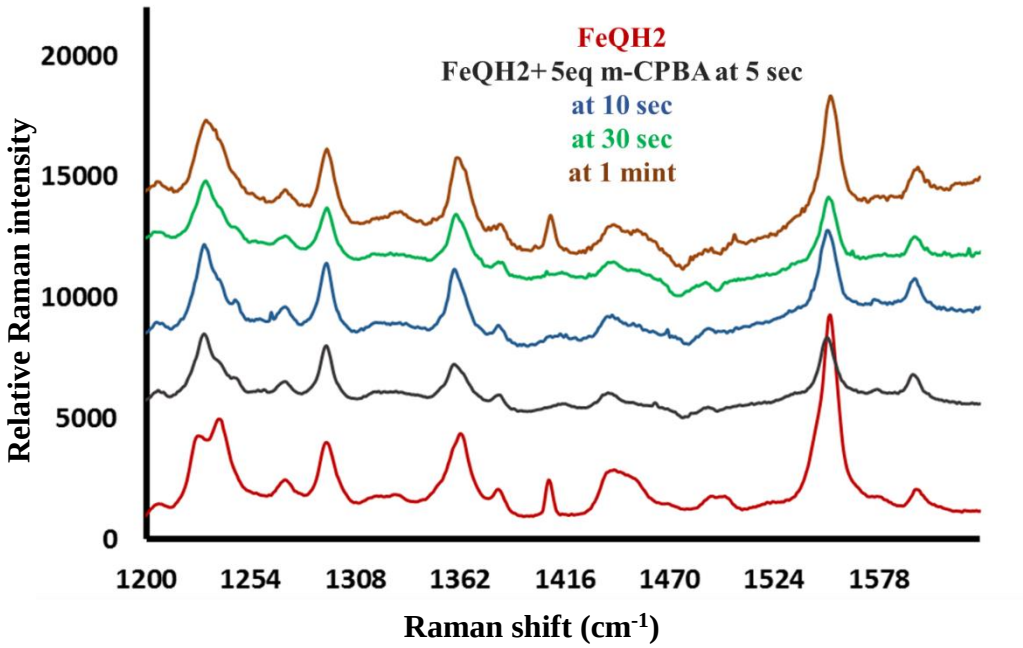

Figure 3. Resonance Raman spectra at different time intervals in the reaction of 1mM FeQH2 with 5 eqv of m-CPBA.

6.3.2. FePh

Absorption spectroscopy

Fe porphyrin with a phenol ring attached in the distal site of the porphyrin in DCM is allowed to react with acetonitrile solution of mCPBA and the kinetics of the reaction is monitored under constant stirring condition. The data shows a rapid decay of the Fe(III)-porphyrin soret at 413 nm with a broadening of soret at 440-450 nm region (Figure 4A). The Q-region shows prominent bands at 820nm and 910 nm which is characteristic of the isoporphyrin-type intermediate (Figure 4B). Unlike FeQH2, there is no evidence of N-oxide formation in this case. FePh behaves similar like the bare Fe(III)TPP in presence of peracid where FeTPP also converts to isoporphyrin in DCM medium (Figure S7).[29]

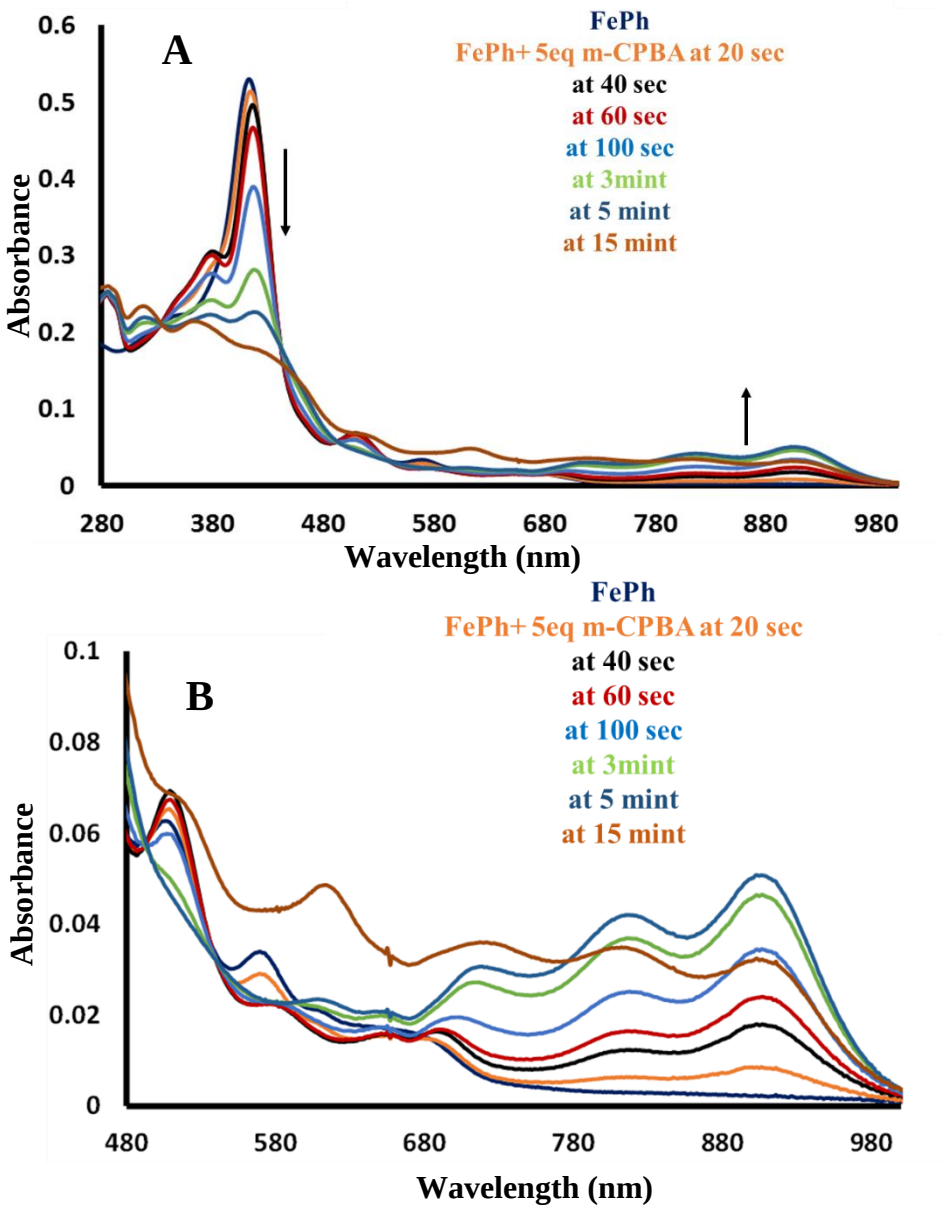

Figure 4. **(A)** Absorption spectra of isoporphyrin, formed in the reaction of Fe(III)Ph with mCPBA at room temperature, in different time interval. **(B)** The Q-band region of the same. Arrows indicated the spectral changes with time.

Kinetics

The decay kinetics of the soret 413 nm band is monitered in kinetics setup (Figure 5A). Additionally, the formation kinetics of isoporphyrin species in each of the Fe-porphyrins has been compared and the result shows that isoporphyrin formation fastest in the FeTPP and in $FeQH_2$, it is slowest (Figure 5B).

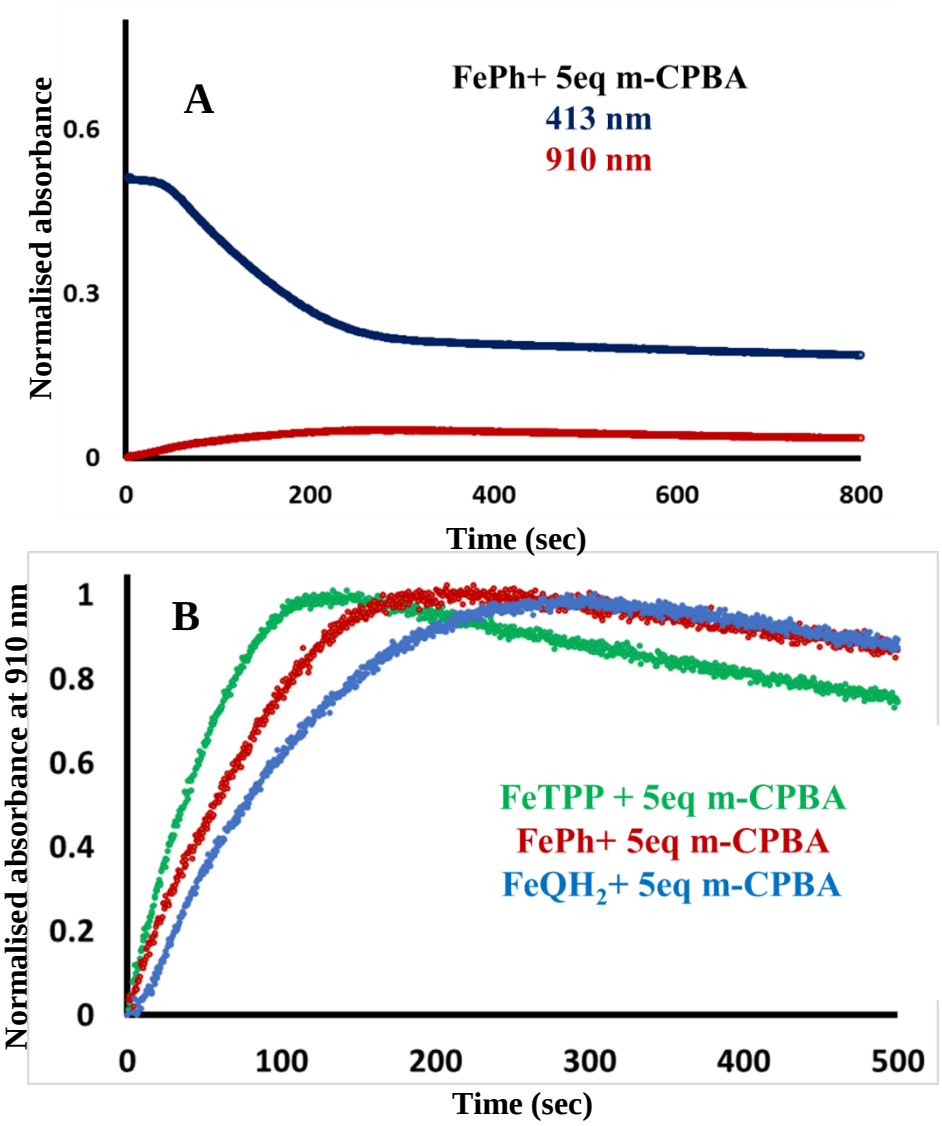

Figure 5. **(A)** The kinetic traces of the bands at 413 nm and 910 nm in the reaction of FePh with m-CPBA. **(B)** Comparison of formation kinetics of isoporphyrin (910 nm) of $FeQH_2$; blue, FePh; red, FeTPP; green with 5 eqv of m-CPBA in DCM.

6.4. Discussion

Absorption and resonance Raman data suggest that upon addition of mCPBA to Fe(III)-porphyrins, having different pendent groups, show different degradation products. Figure 1 shows the drastic change in the absorption feature when $FeQH_2$ is reacted with mCPBA. rR spectra also supports the formation of N-oxide like in absorption (Figure 3). Along with this, a small amount of minor isoporphyrin product is also seen. Unlike $FeQH_2$, FePh does not show the N-oxide generation, rather, it converts to isoporphyrin solely (Figure 4). When, FeTPP

which is a porphyrin having no pendant group attached to it, is subjected to react with peracid, similar isoporphyrin forms which confirms that FePh is also going through the same pathway as FeTPP. Interestingly, it has been seen that the rate of isoporphyrin formation is maximum in FeTPP probably owing to its bare second sphere. FePh, having a phenol group, is somehow retarding the isoporphyrin formation, making its rate slower than FeTPP (Figure 5B). $FeQH_2$, with its quinol group shows slowest rate for the generation of isoporphyrin while it has its major pathway leading to the N-oxide formation. Overall, they are going through different pathways to produce different final products, probably via different intermediates (Scheme 2).

Scheme 2. **Schematic representation of probable pathways of reaction of Fe-porphyrin with mCPBA, leading to different products.**

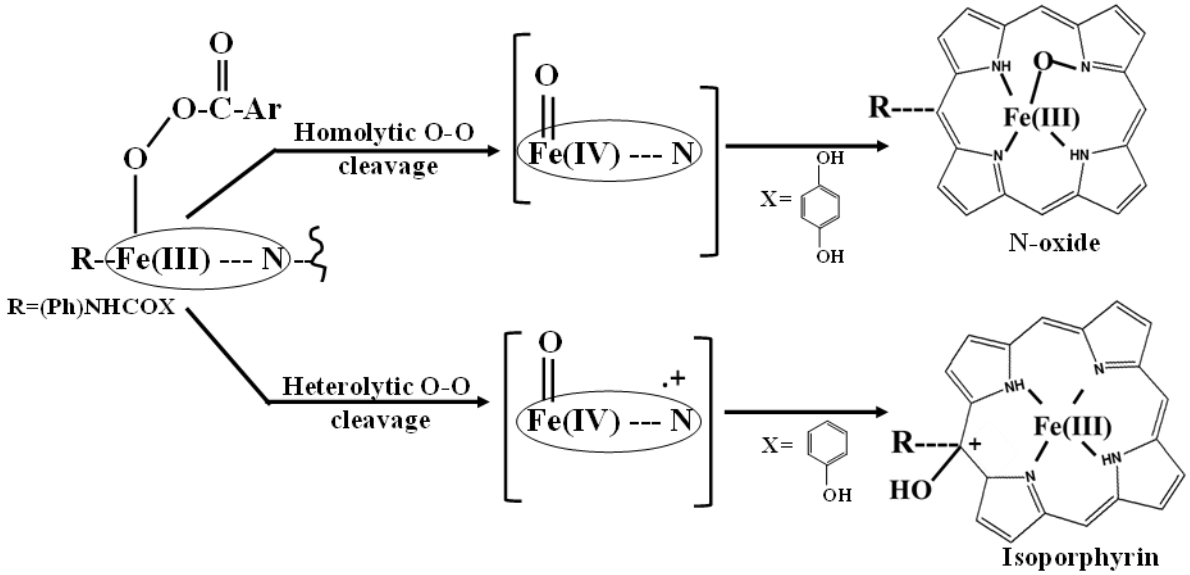

Initially an acyl peroxo (compound 0) complex of ferric porphyrin has to be formed which can then have its O-O bond cleaved in different manner, either homolytically or heterolytically or even in a concerted way.[30,31] The formation of N-oxide type species goes via the homolytic cleavage of O-O bond of Fe(III)-OOR complex while the isoporphyrin is proposed to be formed via the transient Compound I type intermediate which requires a heterolytic cleavage of O-O bond. Thus, the second spheres around the porphyrin centre can actually tune the O-O bond cleavage. Quinol might favours the homolytic cleavage or it can stabilise the compound II via H-bonding to promote N-oxide as the final product. The

associated KIE of 2.7 also indicates the involvement of a proton in the reaction pathway (Figure 2B). While, there might be no such H-bond donation for the phenol owing to a higher BDE (90Kcal/mol) than that of quinol (BDE=80Kcal/mol) which ultimately leads to a heterolytic cleavage to have compound I which then can hydroxilate the meso position of porphyrin to generate isoporphyrin. This needs further experimental proof to be able to get the holistic mechanism.

6.5. Conclusion

In summary, we have spectroscopically demonstrated that the second spheres can tune the reactivity of porphyrins (Scheme 2). It can control the O-O bond cleavage of Fe(III)-acyl peroxo, i.e. compound 0 which will eventually decide the formation of different intermediates and the final products. The quinol group in $FeQH_2$ helps in homolytic cleavage while the phenol favours a heterolytic cleavage which can be seen from their respective product formation. Hence, modifying the pendant groups we can control the reactivities of synthetic porphyrin.

6.6. References

(1) Krebs, C.; Galonić Fujimori, D.; Walsh, C. T.; Bollinger, J. M. Non-Heme Fe(IV)–Oxo Intermediates. *Accounts of Chemical Research* **2007**, *40*, 484-492.

(2) Meunier, B.; de Visser, S. P.; Shaik, S. Mechanism of Oxidation Reactions Catalyzed by Cytochrome P450 Enzymes. *Chemical Reviews* **2004**, *104*, 3947-3980.

(3) Denisov, I. G.; Makris, T. M.; Sligar, S. G.; Schlichting, I. Structure and Chemistry of Cytochrome P450. *Chemical Reviews* **2005**, *105*, 2253-2278.

(4) Abu-Omar, M. M.; Loaiza, A.; Hontzeas, N. Reaction Mechanisms of Mononuclear Non-Heme Iron Oxygenases. *Chemical Reviews* **2005**, *105*, 2227-2252.

(5) Ortiz de Montellano, P. R. Hydrocarbon Hydroxylation by Cytochrome P450 Enzymes. *Chemical Reviews* **2010**, *110*, 932-948.

(6) Kryatov, S. V.; Rybak-Akimova, E. V.; Schindler, S. Kinetics and Mechanisms of Formation and Reactivity of Non-heme Iron Oxygen Intermediates. *Chemical Reviews* **2005**, *105*, 2175-2226.

(7) Hoffart, L. M.; Barr, E. W.; Guyer, R. B.; Bollinger, J. M.; Krebs, C. Direct spectroscopic detection of a C-H-cleaving high-spin Fe(IV) complex in a prolyl-4-hydroxylase. *Proceedings of the National Academy of Sciences* **2006**, *103*, 14738.

(8) Krebs, C.; Price, J. C.; Baldwin, J.; Saleh, L.; Green, M. T.; Bollinger, J. M. Rapid Freeze-Quench 57Fe Mössbauer Spectroscopy: Monitoring Changes of an Iron-Containing Active Site during a Biochemical Reaction. *Inorganic Chemistry* **2005**, *44*, 742-757.

(9) Galonić, D. P.; Barr, E. W.; Walsh, C. T.; Bollinger Jr, J. M.; Krebs, C. Two interconverting Fe(IV) intermediates in aliphatic chlorination by the halogenase CytC3. *Nature Chemical Biology* **2007**, *3*, 113.

(10) Bollinger Jr, J. M.; Price, J. C.; Hoffart, L. M.; Barr, E. W.; Krebs, C. Mechanism of Taurine: α-Ketoglutarate Dioxygenase (TauD) from Escherichia coli. *European Journal of Inorganic Chemistry* **2005**, *2005*, 4245-4254.

(11) Shan, X.; Que, L. High-valent nonheme iron-oxo species in biomimetic oxidations. *Journal of Inorganic Biochemistry* **2006**, *100*, 421-433.

(12) Nam, W.; Han, H. J.; Oh, S.-Y.; Lee, Y. J.; Choi, M.-H.; Han, S.-Y.; Kim, C.; Woo, S. K.; Shin, W. New Insights into the Mechanisms of O−O Bond Cleavage of Hydrogen Peroxide and tert-Alkyl Hydroperoxides by Iron(III) Porphyrin Complexes. *Journal of the American Chemical Society* **2000**, *122*, 8677-8684.

(13) Groves J. T., Watanabe Y. Preparation and Characterization of an Iron(III) Porphyrin N-Oxide: J. Am. Chem. Soc. **1986**, 108, 7837-7839.

(14) Bennett R.; Ridge R.; Appelman E. Porphyrin N-Oxides. J.C.S. CHEM. COMM., **1978**, 310-311.

(15) Choe S. J. Comparison of Different Theory Models and Basis Sets in Calculations of. TPOP24N-Oxide Geometry and Geometries of meso-Tetraphenyl Chlorin N-Oxide Regioisomers. Bull. Korean Chem. Soc. **2012**, Vol. 33, No. 9.

(16) Tsurumaki H.; Watanabe Y.; Morishima I. Preparation, Characterization, and Reactions of Novel Iron(III) Porphyrin Dication Complexes. J. Am. Chem. Soc. **1993**, 115, 11784-11788.

(17) Bhuyan J. Metalloisoporphyrins: from synthesis to applications. Dalton Trans., **2015**, 44, 15742.

(18) I. Garcia-Bosch, S. K. Sharma and K. D. Karlin, A Selective Stepwise Heme Oxygenase Model System: An Iron(IV)-Oxo Porphyrin π^{-}Cation Radical Leads to a Verdoheme-Type Compound via an Isoporphyrin Intermediate J. Am. Chem. Soc., **2013**, 135, 16248.

(19) J. P. Evans, F. Niemevz, G. Buldain, and P. O. Montellano; Isoporphyrin Intermediate in Heme Oxygenase Catalysis oxidation of meso-phenylheme. The journal of biological chemistry, vol. 283, **2008,** NO. 28, pp. 19530–19539.

(20) Traylor, T. G.; Tsuchiya, S.; Byun, Y. S.; Kim, C. High-yield epoxidations with hydrogen peroxide and tert-butyl hydroperoxide catalyzed by iron(III) porphyrins: heterolytic cleavage of hydroperoxides. *Journal of the American Chemical Society* **1993**, *115*, 2775-2781.

(21) Traylor, T. G.; Kim, C.; Richards, J. L.; Xu, F.; Perrin, C. L. Reactions of Iron(III) Porphyrins with Oxidants. Structure-Reactivity Studies. *Journal of the American Chemical Society* **1995**, *117*, 3468-3474.

(22) Almarsson, O.; Bruice, T. C. A Homolytic Mechanism of O-O Bond Scission Prevails in the Reactions of Alkyl Hydroperoxides with an Octacationic Tetraphenylporphinato-Iron(III) Complex in Aqueous Solution. *Journal of the American Chemical Society* **1995**, *117*, 4533-4544.

(23) Nam, W.; Lim, M. H.; Oh, S.-Y. Effect of Anionic Axial Ligands on the Formation of Oxoiron(IV) Porphyrin Intermediates. *Inorganic Chemistry* **2000**, *39*, 5572-5575.

(24) W. Nam; H. J. Han; S. Oh; Y. J. Lee; M. Choi; S. Han; C. Kim; S. K. Woo; and W. Shin. New Insights into the Mechanisms of O-O Bond Cleavage of Hydrogen Peroxide and *tert*-Alkyl Hydroperoxides by Iron(III) Porphyrin Complexes. *J. Am. Chem. Soc.* **2000,** *122*, 8677-8684.

(25) Singha, A.; Dey, A. Hydrogen atom abstraction by synthetic heme ferric superoxide and hydroperoxide species. *Chemical Communications* **2019**, *55*, 5591-5594.

(26) A. Singha, A. Mondal, A. Nayek, S. G. Dey, and A. Dey. Oxygen Reduction by Iron Porphyrins with Covalently Attached Pendent Phenol and Quinol. J. Am. Chem. Soc. **2020**, 142, 21810−21828.

(27) Singha, A.; Dey, A. Hydrogen atom abstraction by synthetic heme ferric superoxide and hydroperoxide species. Chem. Commun. **2019**, 55, 5591−5594.

(28) Y. Mizutani; Y. Watanabe; and T. Kitagawa. Resonance Raman Characterization of Iron(III) Porphyrin N-Oxide: Evidence for an Fe-O-N Bridged Structure1. J. Am. Chem. Soc. **1994**, 116. 3439-3441.

(29) S. Bhunia; A. Rana; S. G. Dey; A. Ivancich; A. Dey. A designed second-sphere

hydrogen-bond interaction that critically influences the O–O bond activation for heterolytic cleavage in ferric iron–porphyrin complexes. Chem. Sci., **2020**, 11, 2681.

(30) X. Huang; and J. T. Groves. Oxygen Activation and Radical Transformations in Heme Proteins and Metalloporphyrins. Chem. Rev., **2010**.

(31) Krest, C. M.; Onderko, E. L.; Yosca, T. H.; Calixto, J. C.; Karp, R. F.; Livada, J.; Rittle, J.; Green, M. T. Reactive Intermediates in Cytochrome P450 Catalysis. J. Biol. Chem. **2013**, 288, 17074−17081.

(32) I. Tabushi, N. Koga and M. Yanagita, Tetrahedron Letters, **1979**, 20, 257-26.

6.7. Supporting Information

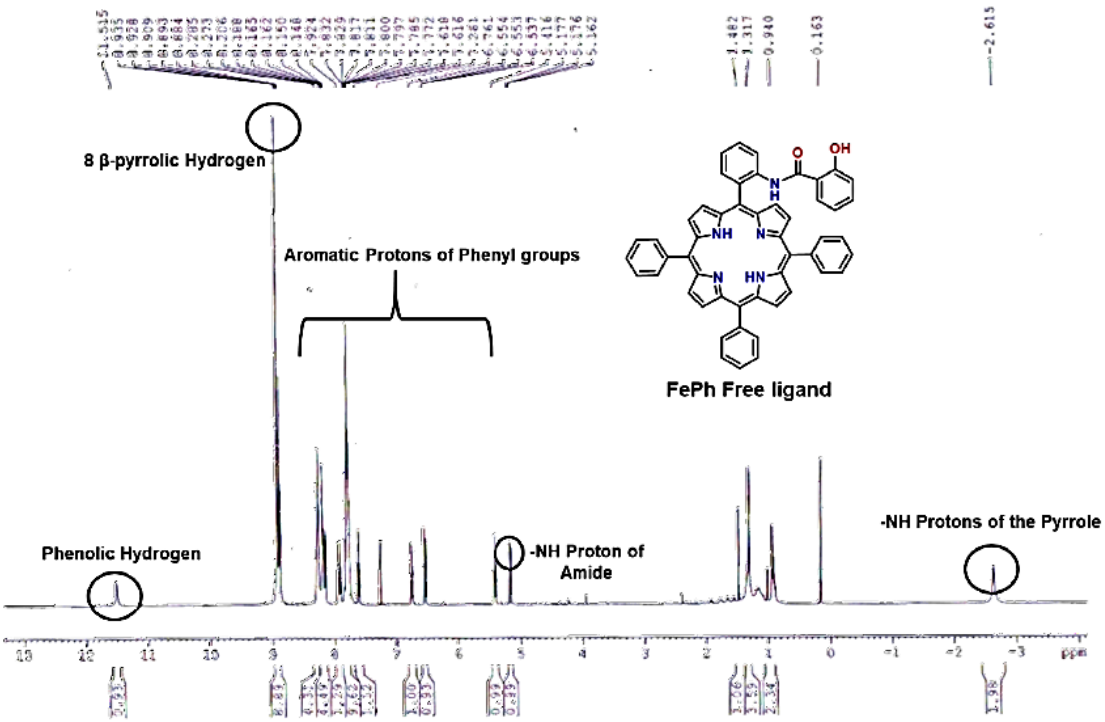

Figure S1. 1H NMR spectra of free ligand of FePh.

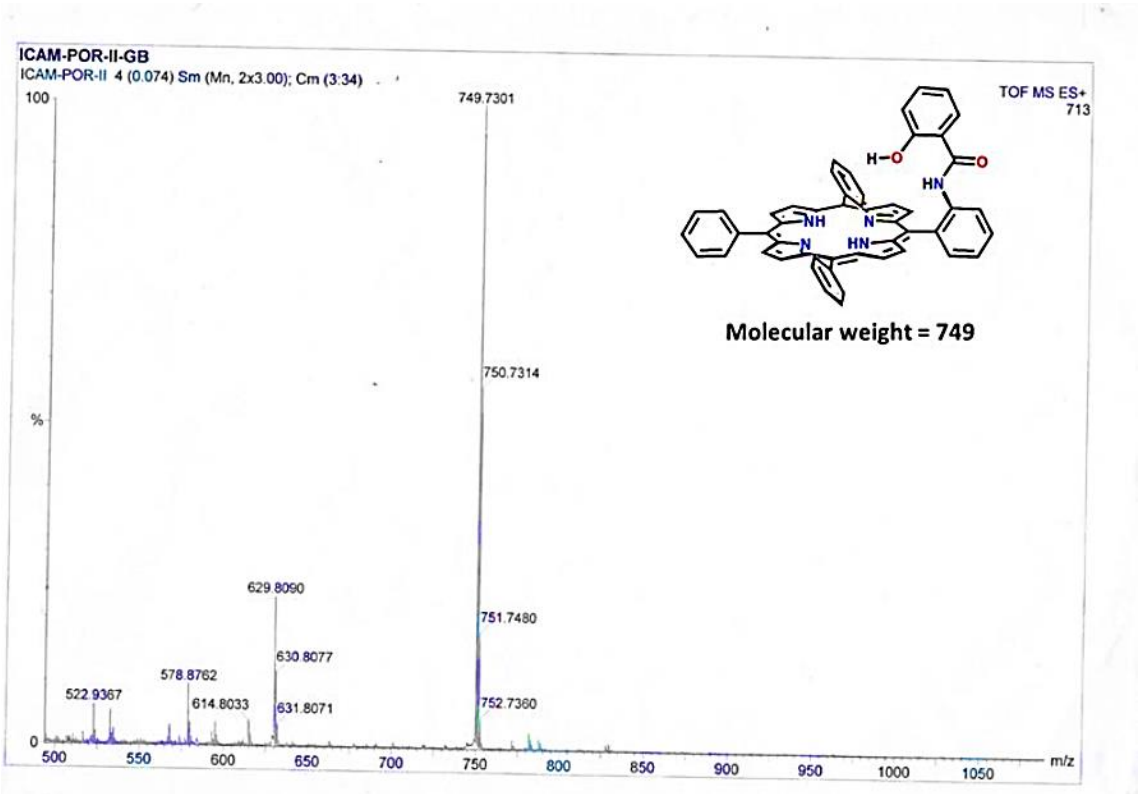

Figure S2. ESI-MS spectra of free ligand of FePh.

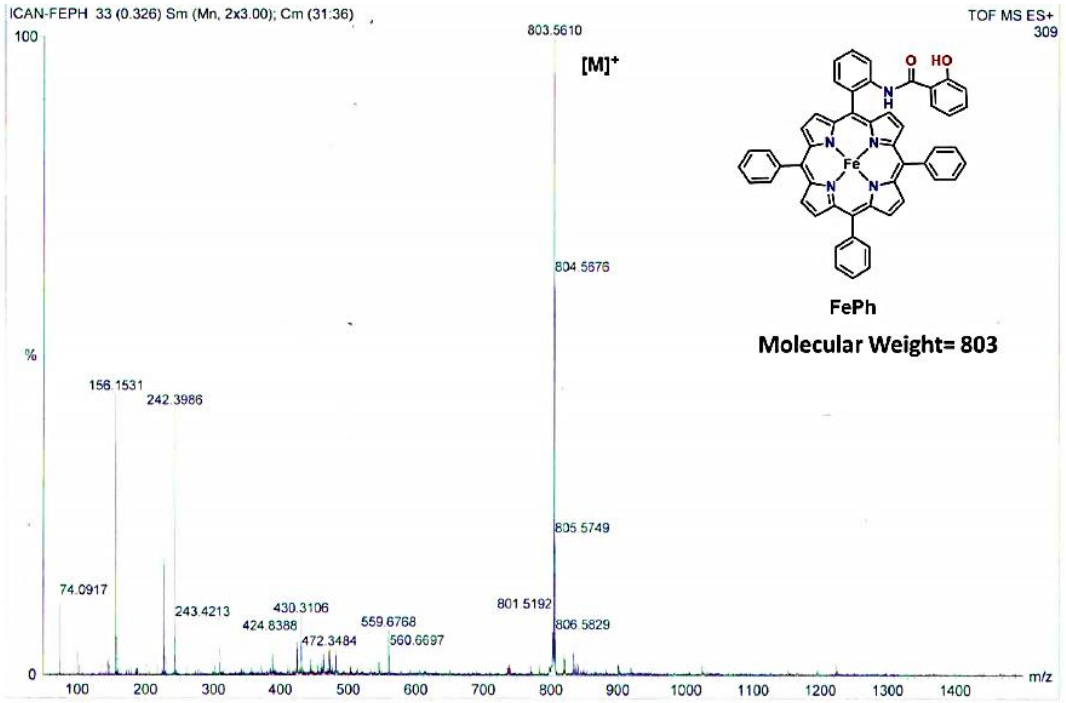

Figure S3. ESI-MS spectra of metallated FePh.

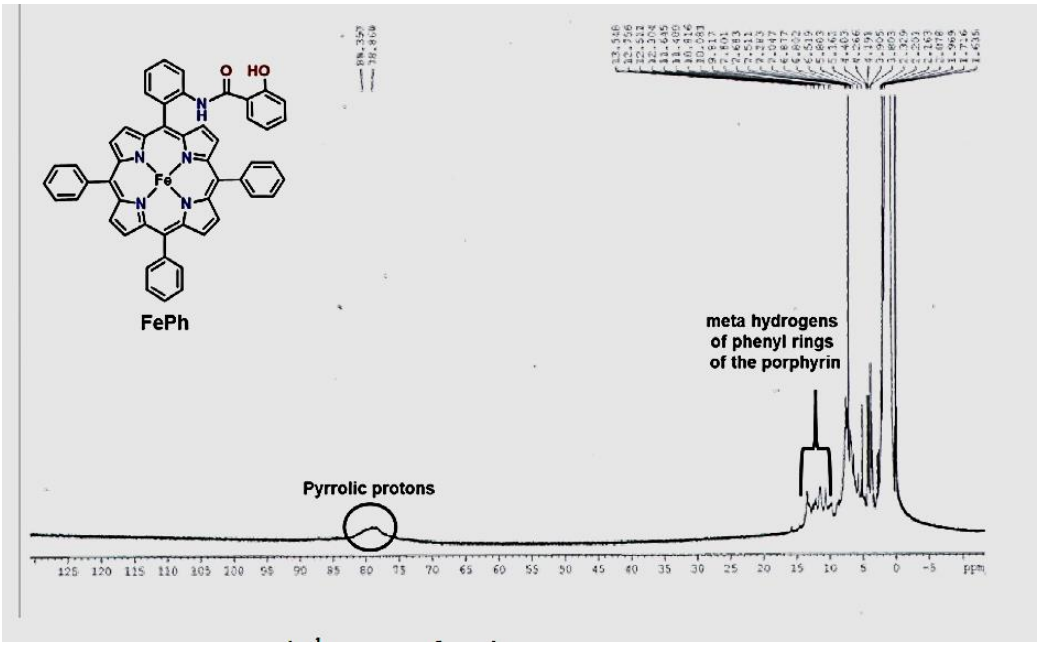

Figure S4. Paramagnetic 1HNMR of FePh.

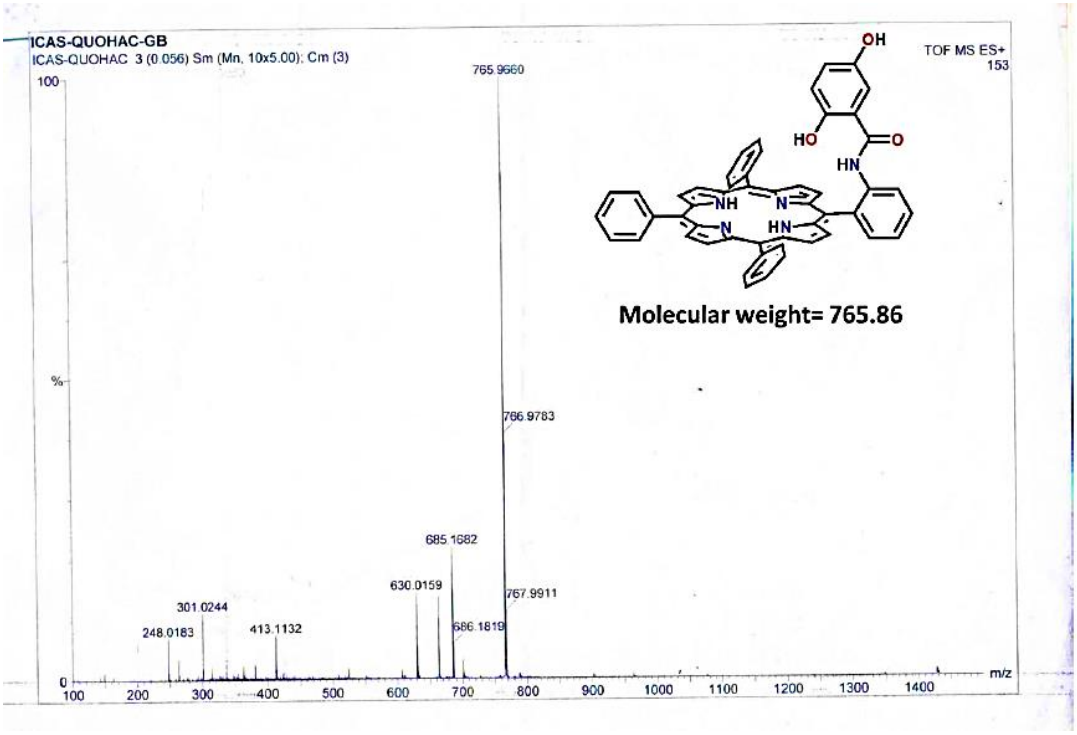

Figure S5. Mass spectra of metal free porphyrin macrocycle with a hydroquinone ring attached to it.

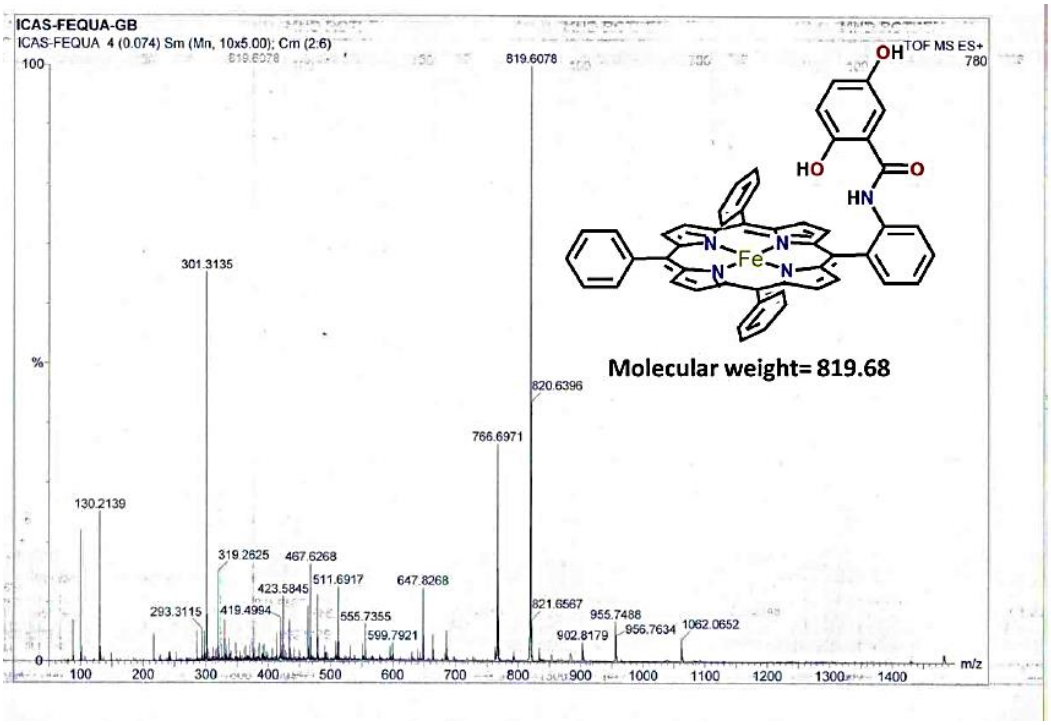

Figure S6. Mass spectra of metallated porphyrin $FeQH_2$.

***Scheme S1*. Synthetic Scheme of Preparation of (A) FePh (1c) and (B) $FeQH_2$.**

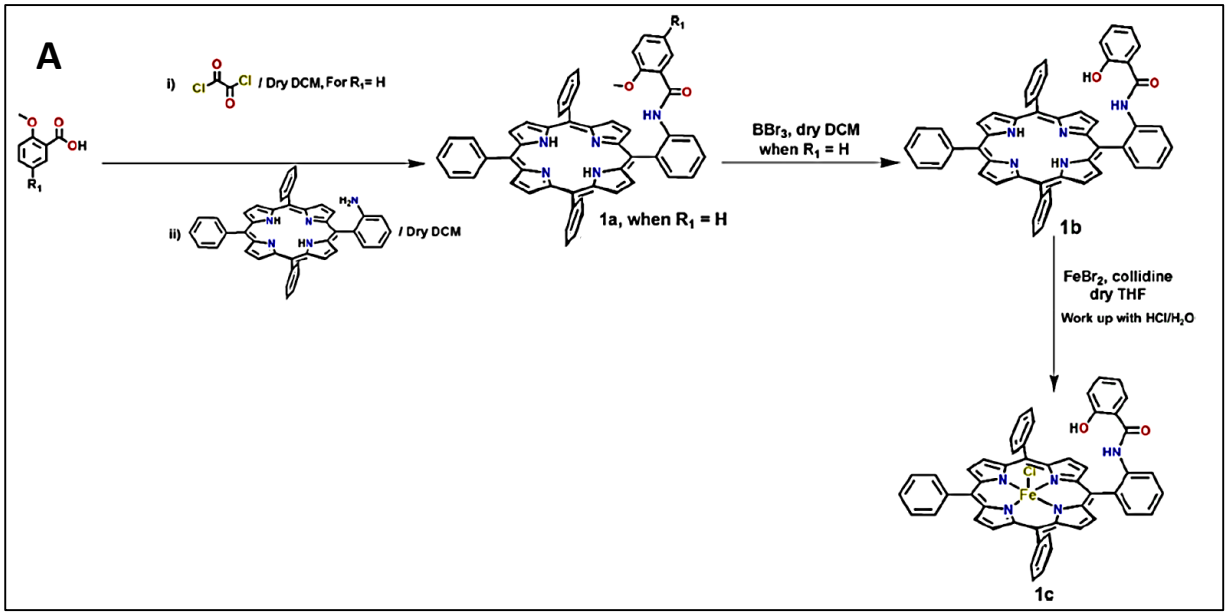

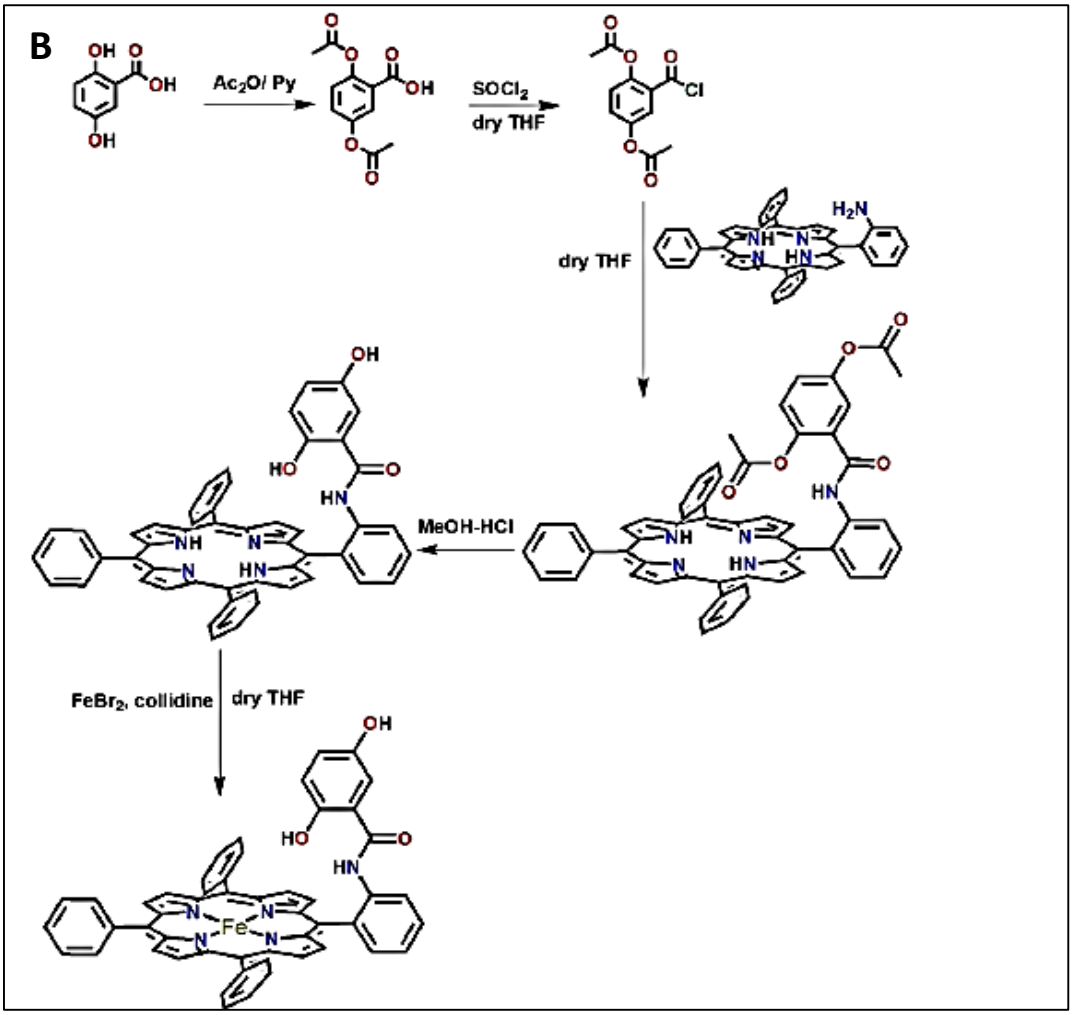

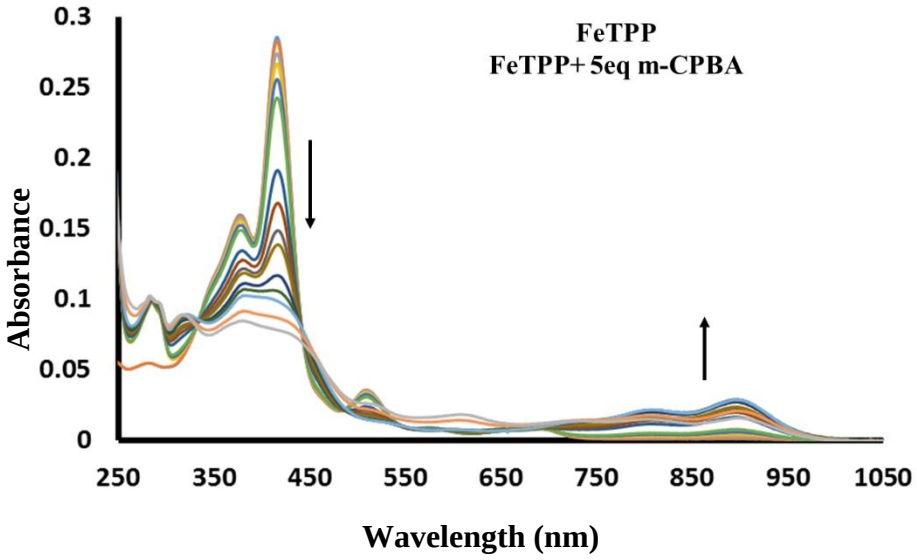

Figure S7. Reaction of $Fe^{III}TPP$ with 5 equivalent of mCPBA, resulting in the isoporphyrin formation in DCM medium. Arrows indicate the spectral changes with time.

Chapter 7

Interaction of ApoMyoglobin with Heme-hIAPP Complex

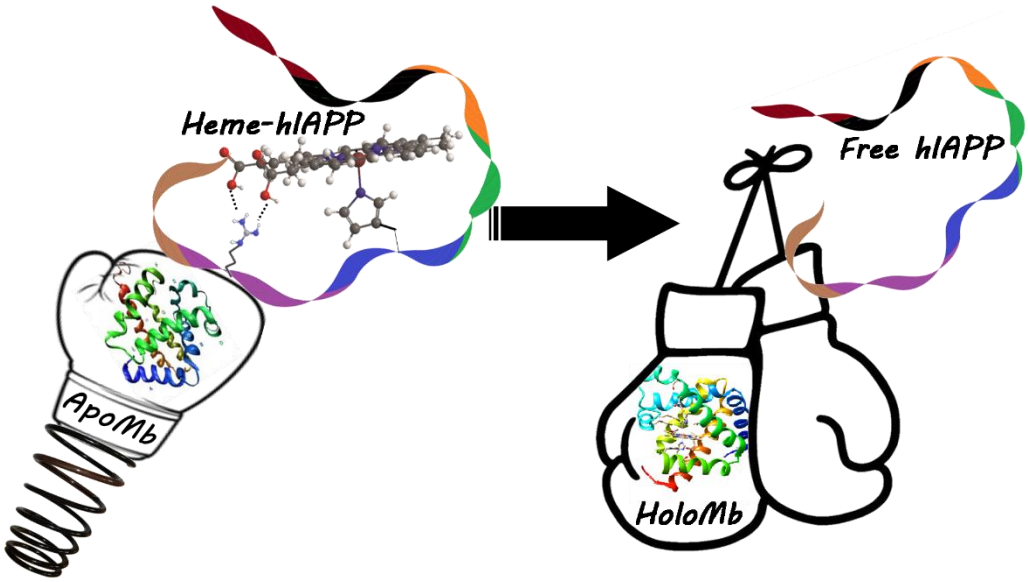

Human Islet Amyloid Polypeptide (hIAPP)/amylin, can bind heme and the resultant complexes are prone to generate partially reduced oxygen species (PROS). The formation of PROS and the related oxidative stress highlight the importance of Heme-hIAPP in the onset and development of Type 2 Diabetes mellitus (T2Dm) in humans. In this study, the interaction of Heme-hIAPP with apomyoglobin (ApoMb) has been investigated using a combination of spectroscopic and electrophoresis techniques and the results confirm that ApoMb can uptake heme from Heme-hIAPP and constitute a six-coordinate high-spin ferric heme active site identical to that of myoglobin (Mb). The heme transfer reaction has two distinct kinetic steps with a possible mechanism of heme transfer to the apoprotein in the first step followed by a reorganisation of the protein chain to form the active site of native Mb. Increase in the pH of the reaction medium enhances the rate of the second step of heme transfer, corresponding to the deprotonation of a propionate side chain of the heme moiety at high pH which facilitates secondary interactions with the conserved distal Lys45 residue of horse heart Mb. Additionally, ApoMb sequesters ligand bound heme from Heme-hIAPP. After the heme transfer reaction, the amount of PROS diminishes significantly. This not only potentially diminishes heme-induced toxicity in the pancreatic β-cells but also produces Mb which has well-documented functions throughout the respiratory system and can thereby likely reduce the risks associated with T2Dm.

7.1. Introduction

Diabetes mellitus is a chronic metabolic disorder, characterized by hyperglycemia, insulin resistance, and relative insulin deficiency.[1–3] The most common form of this disease is Type 2 Diabetes mellitus (T2Dm), which results from the interaction between various genetic, environmental and behavioural risk factors.[4,5] T2Dm is mainly characterized by insulin insensitivity arising due to insulin resistance, combined with a decline in insulin production and eventually pancreatic β-cell failure which ultimately leads to a decrease in glucose transport into the liver, muscle cells, and fat cells.[6–8] Human Islet Amyloid Polypeptide (hIAPP), commonly known as amylin, is another small hormonal peptide which is co-produced and co-secreted along with insulin from the β-cells of the islets of Langerhans in pancreas.[9–12] It functions as a synergistic partner to insulin and contributes to the glycemic control in our blood.[13] This small peptide consisting of 37 amino acid residues, is extremely amyloidogenic with the 20-29th segment constituting its amyloidogenic core.[14,15] Under normal physiological conditions, hIAPP exists as a soluble monomer. However, in T2Dm, hIAPP undergoes a stepwise conformational change from normally soluble monomers to oligomers, protofibrils and eventually to insoluble fibrils that are deposited in pancreatic islets.[16,17] This deposition and aggregation of human amylin within the β-cells of pancreatic islets of Langerhans is implicated in the pathology of T2Dm.[16] More importantly, these amylin aggregates can produce reactive oxygen species (ROS) which are known to be cytotoxic and the resultant oxidative stress might be one of the possible reasons for the apoptosis of pancreatic β-cells in T2Dm patients.[18–21] Consequently, it creates a dysfunction in both insulin action on glucose and insulin secretion from these cells. The protein aggregation seen in T2Dm is also the central event in many other diseases such as Alzheimer's disease (AD), Parkinson's disease etc.[22,23] The impaired metabolism of several metals such as Fe, Cu and Zn is another common feature that connects these diseases.[24–26] In fact, high levels of Cu have been found in the blood serum of diabetic patients.[27] Cu has also been reported to bind amylin via the terminal amine, His18 and amidates to form a 1:1 Cu-hIAPP complex.[28] This complex can generate H_2O_2 at physiological pH which in turn may contribute towards the oxidative stress in the pancreatic β cells.[28] Cu can increase the apoptosis induced by amylin from 45% to 70% in cultured β cells.[29] Some studies suggest that interaction of Cu with amylin can delay the aggregation.[30–32] However, recent studies indicate that Cu binding to monomeric amylin obstructs β sheet formation while it possibly favours the generation of oligomers which are potentially more

toxic to the β cells of the pancreas than the fibrillar form.[33,34] In case of Zn, elevated concentration in the β cells along with an overall deficiency of the metal has been observed in the histopathology of T2Dm.[35,36] In vitro studies have shown that Zn^{2+} ions play a vital role in stimulating amylin aggregation and it was proposed that Zn^{2+} ions bind to His18 in the amylin monomer.[37,38] According to recent scientific evidences, serum ferritin, which is an indicator of the amount of iron the body stores, is found to be significantly high in diabetic patients and this level increases considerably with the increase in duration of the disease. Hence ferritin level can be a useful marker of the risk of developing Diabetes mellitus and the associated spike in body iron stores may be linked to the iron influenced glucose metabolism seen in T2Dm. The ferritin level reported in normal healthy men is <287 μg/L whereas in T2Dm patient, it is ~520 μg/L.[39–41] According to one report the mean free iron concentration is 105.34 ± 3.5, 107.33 ± 3.45, and 125.58 ± 3.45 μg/dL in healthy individual, T2Dm patients with optimal glycaemic control and T2Dm patients with suboptimal glycaemic control respectively.[42] Such elevated level of iron in β cells of pancreas can lead to ROS like H_2O_2, $HO_2^{\cdot+}$, ·OH formation (via Fenton's mechanism) which can cause β cell death and hence insulin deficiency.[43] Excess iron deposition can also induce insulin resistance by inhibiting glucose uptake by skeletal muscles and adipose tissues along with reduction in insulin extraction capacity of liver.[24,44] Some research also confirmed that iron enhances the amylin beta pleated sheet formation.[36]

Heme, which is distributed all over the human body as the co-cofactor of several proteins, contributes significantly towards the iron content of the body when ingestion of heme-iron by meal is quite high. Recent studies have positively associated the increased heme iron intake with a risk of developing T2Dm.[45–47] Incidentally several consequences of heme deficiency such as high iron intake, altered heme homeostasis, dysfunction of mitochondrial complex IV, high levels of heme oxygenase I and transferrin, elevated bilirubin concentration, oxidative stress etc. are the symptoms of AD where heme has been implicated to play an important role.[47–49] These are also the pathological features of T2Dm which points towards a possible involvement of heme.[50] The interaction between heme and hIAPP has not been widely investigated till date, and the survey of the few existing literature indicates that heme dramatically inhibits the hIAPP aggregation by preventing its conformational changes leading to partial dismantled hIAPP aggregates.[51,52] In addition to this, using several spectroscopic techniques, it has been experimentally demonstrated that hIAPP peptide has the heme binding domain in its non-amyloidogenic 1–19 segment and it binds to heme in 1:1 concentration ratio

forming a Heme-hIAPP complex. Histidine at the 18th position binds heme along with Arginine at 11th position which hydrogen bonds with the propionate side chain of heme. There is an exchangeable water derived ligand (pKa ~ 7.3) at the distal pocket of this species.[19] This heme-peptide complex reduces O_2 by 1 e^- pathway forming superoxide which disproportionates to yield ~ 40% H_2O_2. Thus, heme binding to amylin may account for the ROS induced oxidative stress in pancreatic β cells of T2Dm patients. The dioxygen adduct of heme which is the intermediate involved during this ROS formation has been trapped and characterized.[53]

Myoglobin (Mb), a globular monomeric protein consisting of 153–154 amino acids, is a mobile carrier of oxygen, and is developed in the red muscles in response to mitochondrial demand for O_2.[54–56] It transports oxygen from the sarcolemma to the mitochondria of vertebrate heart and red muscle cells. Other than diffusion of O_2, Mb also influences oxidative phosphorylation, defence against oxidative damage, enhancement of NO concentration gradients, and inactivation of enzymes.[57–61] In the active site of Mb a single protoheme IX prosthetic group is bound through the coordination of heme iron by a histidyl residue and a variety of non-covalent interactions between the protein and the heme.[62] Apomyoglobin (ApoMb) which is the Mb without the heme prosthetic group, is known to have high affinity towards heme and readily binds it akin to other apoglobins.[63] Recently, it has been shown that ApoMb as well as Aponeuroglobin (ApoNgb) can sequester heme from neurotoxic Heme-Amyloid β complex to form Mb and neuroglobin (Ngb) respectively and thus reduce the ROS-induced neurotoxicity which is relevant to AD.[64,65] Here, we demonstrate sequestration of toxic heme from the Heme-hIAPP complex by incorporating ApoMb. In this study, we investigate the effect of ApoMb on Heme-hIAPP complex using UV-VIS, resonance Raman spectroscopy, gel electrophoresis and kinetics which may possibly help in mitigating the ill-effects of the said metal-peptide complex in the context of T2Dm.

7.2. Materials and methods

7.2.1. Materials

All reagents were of the highest grade commercially available and were used without further purification. hIAPP (amylin) peptide (1–19) (sequence:Lys1-Cys2-Asn-Thr-Ala-Thr-Cys7-Ala-Thr-Gln-Arg11-Leu-Ala- Asn-Phe-Leu-Val-His18-Ser19) was purchased from Ontores (China) Ltd. with >95% purity. Hemin, myoglobin (Mb) from equine heart and buffers and NaN3 were purchased from Sigma. Phosphate buffer (for pH 6–8) and CHES buffer (for pH 9) were used in the experiment.

7.2.2. Preparation of ApoMb by heme extraction

Apomyoglobin (ApoMb) was prepared from Myoglobin (Mb) using Teale's method.[66] In brief, pH of the sample protein was lowered to 2.0 using ice-chilled 0.1 M HCl followed by mixing with equal volume of cold butanone to separate the phases. The colourless aqueous layer containing ApoMb was separated carefully from the heme containing red organic layer and dialyzed against 20 mM phosphate buffer, pH 7.0. The apoprotein was then centrifuged at 4 ◦C to a concentrated solution. The concentration of the Mb and ApoMb solutions were determined using the molar extinction coefficients (ϵ =179 mM^{-1} cm^{-1} at 408 nm for Mb and ϵ =13.5 mM^{-1} cm^{-1} at 280 nm for ApoMb).

7.2.3. Sample preparation

Amylin peptide stock solutions were prepared in 100 mM phosphate buffer at pH 7, and hemin solution was prepared by dissolving hemin chloride in 1 M NaOH and the concentration of the heme solution was determined spectrophotometrically (ε385 = 58.44 mM^{-1} cm^{-1}). Peptide stock solutions were 0.5 mM, and heme stock solution was 5 mM. Heme–hIAPP complexes were prepared by incubating 1 equivalent of hIAPP with 0.8 equivalent of heme solution for ~ 6 h. The pH of the Heme-hIAPP complex was calibrated to pH 7 using 1 M H_3PO_4. For pH variation studies, pH of the Heme-hIAPP complexes were adjusted accordingly in suitable buffers.

Azide solution (2 mM) was prepared by dissolving NaN_3 salt in mili- Q water. This solution was added gradually in the Heme-hIAPP(1–19) complex (0.2 mM). At ~300 eq of Azide, the

saturation point arrived. To confirm the complete binding this ligand-metal-peptide mixture was kept for ~1 h.

To obtain the ferrous and ferrous-CO absorption spectra, all Heme–hIAPP(1–19) and Mb samples were degassed by purging with argon in anaerobic vials for ~30 min. Reduction of Heme-hIAPP sample was carried out in anaerobic cuvettes by adding an anaerobically prepared stock solution of 20 mM sodium dithionite. CO adducts were prepared by purging CO(g) through the headspace of septum-sealed cuvette with gentle agitation of the samples, until no further change was noticed in absorption spectra. CO (g) was generated by adding concentrated H_2SO_4 to ammonium formate and then passing the generated gas through 4 M KOH.

7.2.4. Absorption spectra and kinetics

All the spectral data were obtained by an UV–vis diode array spectrophotometer (Agilent 8453). For all absorption spectroscopy experiments, final concentration of solution was 2 μM and the spectra were recorded by adding 20 μL of the Heme-hIAPP complex solution in 1 mL of 100 mM of the required buffer needed for the particular pH range. The Heme-hIAPP sample was incubated with 1 equivalent of ApoMb for ~1 h to ensure complete transfer of heme. Kinetics of this reaction at different pH were studied using absorption spectroscopy in the before-said instrument. Kinetics data were obtained at 0.5 s intervals, which is the fastest time resolution of Agilent 8453. The second step of kinetic data have been fitted using first order kinetics.

7.2.5. Calculation of percentage of heme transfer

The percentage of heme transfer at a particular pH was calculated by adding the spectra of Heme-hIAPP and pure Mb at that pH in such proportions that the resultant spectrum resembled the one obtained after reaction of Heme-hIAPP with 1 equivalent ApoMb. Further, the final concentration of newly formed Mb was measured from its ϵ value at 408 nm using Lambert-Beer's law $A(\lambda) = \varepsilon(\lambda)\, l\, c$ (ϵ =179 mM^{-1} cm^{-1} at 408 nm).

7.2.6. Resonance Raman

Resonance Raman data were obtained at room temperature using a Trivista 555 spectrograph (Princeton Instruments) using 413.1 nm excitation from a diode laser (MDL-E-415-50 mW).

The optics (plano-convex lens, mirror etc.), used for the collection of rR data were purchased from Sigma-Koki Japan. The power on the samples was ~5 mW. rR samples were 0.2 mM in concentration (concentration of ApoMb and hIAPP were 0.4 mM).

7.2.7. Partially reduced oxygen species (PROS) calculation

Xylenol orange assay was applied for partially reduced oxygen species (PROS) calculation. A total of 4.9 mg of Mohr's salt and 3.9 mg of xylenol orange were dissolved in 5 mL of 250 mM H_2SO_4 and stirred for 10 min. A 200 µL portion of this solution was taken in 1.8 mL of nanopure water, and a calibration curve for the quantitative estimation of H_2O_2 was obtained for 0.05, 0.1, 0.5, 1, 2.5, 5, and 10 µM concentrations of H_2O_2 by recording their absorbance at 560 nm as a function of H_2O_2 concentrations in micromolar units for a 2 mL volume.[67] A blank was obtained in the UV–vis spectrophotometer with 1.8 mL nanopure water in a cuvette. A total of 200 µL xylenol orange solution was added to the above cuvette and absorbance was measured. This served as the control. The Heme-hIAPP complex and Heme-hIAPP-ApoMb mixture and all the buffer and reagent solutions were degassed first and then were purged with argon in anaerobic vials for ~ 30 min. Thereafter, the samples were reduced using a minimal amount of dithionite under anaerobic conditions, followed by their reoxidation by O_2 (monitored by absorption). A total of 200 µL of 0.025 mM of reoxidized solutions were separately added to the cuvette containing the control, and their absorbance were recorded. The value of absorbance of the above solutions (after deducting the control) at 560 nm when plotted on the calibration curve yielded the corresponding H_2O_2 concentration.

7.2.8. Gel electrophoresis

In the SDS-PAGE, 10% - 15% gradient polyacrylamide gel was used as the resolving gel. The samples were prepared by mixing 20 µL of each sample (containing 20 µg samples) with equal volume of Laemmli buffer. Laemmli buffer was prepared following the standard protocol.[68] 4% stacking gel was prepared on top of the resolving gel, and the comb was inserted carefully. After formation of the defined wells the gel was loaded in the electrophoresis setup. It was then filled with 1× tank buffer (conc. SDS etc), and the samples were loaded into the wells. It was then allowed to run for 1 h at 150 V. After the run time was over, the gel was removed carefully from the setup. Finally it was stained overnight with Coomassie blue (G-250) dye to obtain the

protein bands, and after complete staining, it was de-stained several times with a solution of 25% methanol, 7% acetic acid, and water.

7.3. Results and Analysis

7.3.1. Absorption spectroscopy

The absorption spectrum of heme bound hIAPP (1–19) is characterized by a split Soret band at 365 and 392 nm and a Q-band at 605 nm (Figure 1, Figure S1). As the heme binding domain resides in the 1–19 part of the peptide, the short fragment has been used in this study. Mb has a sharp Soret band at 408 nm and Q bands at 500, 540, and 630 nm (Figure 1). ApoMb (without the heme cofactor) lacks any absorption bands in the visible region of the spectrum. When Heme-hIAPP(1–19) and ApoMb are incubated in 1:1 stoichiometric ratio, the resultant absorption spectrum resembles that of native Mb (Figure 1), implying that heme has transferred from Heme-hIAPP(1–19) to ApoMb forming native Mb. The absorption data indicate that ApoMb can quantitatively uptake heme from oxidized Heme-hIAPP and produce native Mb (Materials and methods section).

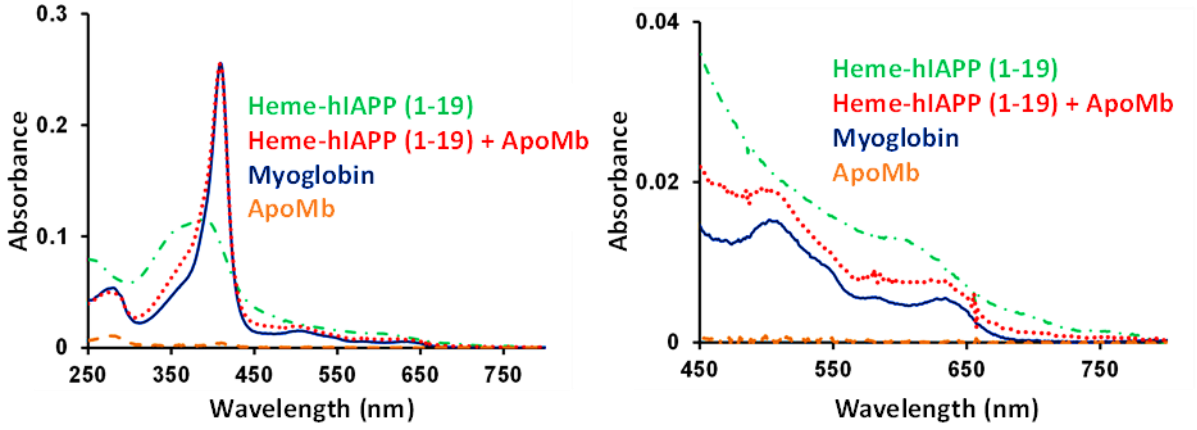

Figure 1. **(A)** Absorption spectra of Heme-hIAPP (1–19), green (dash-dotted line); Heme-hIAPP(1–19) incubated with 1 equivalent of ApoMb, red (dotted line); pure myoglobin, blue (solid line) and ApoMb, orange (dashed line). **(B)** Higher wavelength region of the same in 100 mM phosphate buffer; pH 7.

7.3.2. Resonance Raman spectroscopy

In the resonance Raman spectroscopy, the oxidation state (ν4), coordination number (ν3), and spin state (ν2) marker bands are observed at 1374, 1491, and 1569 cm^{-1} respectively for Heme-hIAPP(1–19) while, ν10, the depolarized spin state marker band arises at 1628 cm^{-1} indicating the presence of a six coordinate high-spin Fe^{3+} centre (Figure 2, Figure S2).[19] Mb displays the marker bands at 1371 (ν4), 1482 (ν3), 1563 (ν2) cm^{-1} along with the νca=cb band at 1621 cm^{-1} (Figure 2) representing the presence of a six coordinate high-spin Fe^{3+} active site.[69,70] Figure 2 shows that when Heme-hIAPP(1–19) and ApoMb are incubated in 1:1 stoichiometric ratio, the resultant rR spectrum resembles that of the native Mb, implying that heme has been transferred from the metal-peptide complex to the apoglobin.

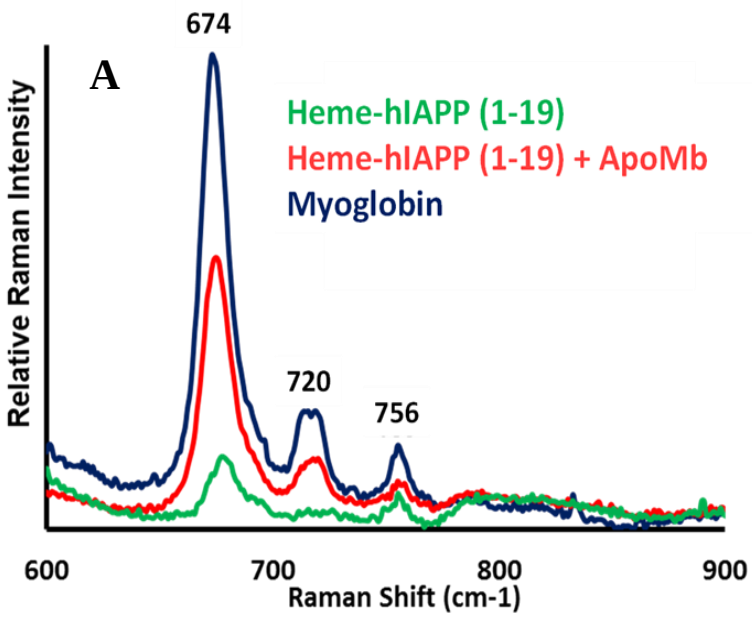

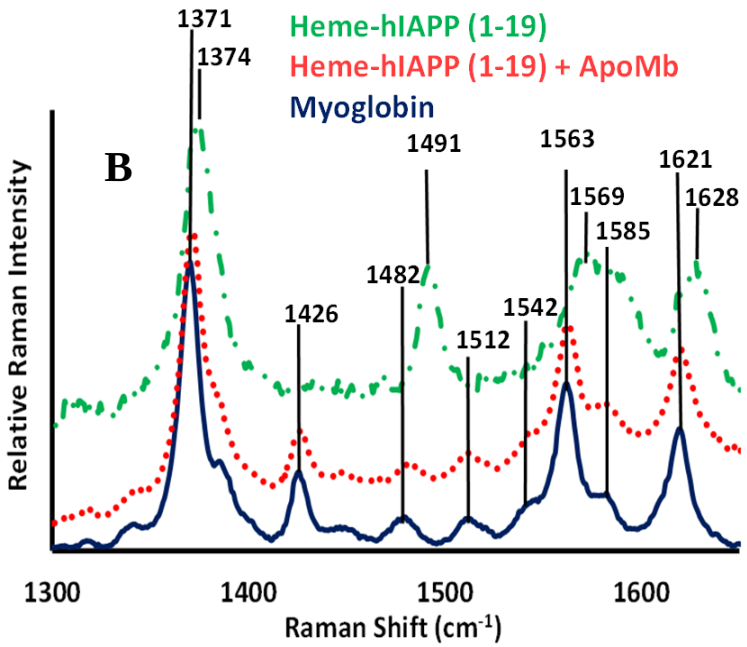

Figure 2. **(A)** Lower frequency range of rR spectra of Heme-hIAPP(1−19), green; Heme-hIAPP(1−19) incubated with ApoMb, red; and Mb, blue. **(B)** High frequency rR spectra of Heme-hIAPP(1–19), green (dash-dotted line); Heme-hIAPP(1–19) incubated with ApoMb, red (dotted line); and Myoglobin, blue (solid line) in 100 mM phosphate buffer at pH 7. Data were obtained with an excitation wavelength of 413.1 nm (~5 mW) at room temperature.

7.3.3. SDS–PAGE analysis

Heme transfer from Heme-hIAPP(1–19) to ApoMb is also confirmed by gel electrophoresis, where the proteins get denatured by SDS (sodium dodecyl sulphate) so that they can move based on their molecular weight only. Five lanes are loaded with different protein samples of same *w*/*v*. After staining with Coomassie blue (G-250), the position of protein bands confirm Mb formation after incubating Heme-hIAPP with ApoMb (Figure 3).

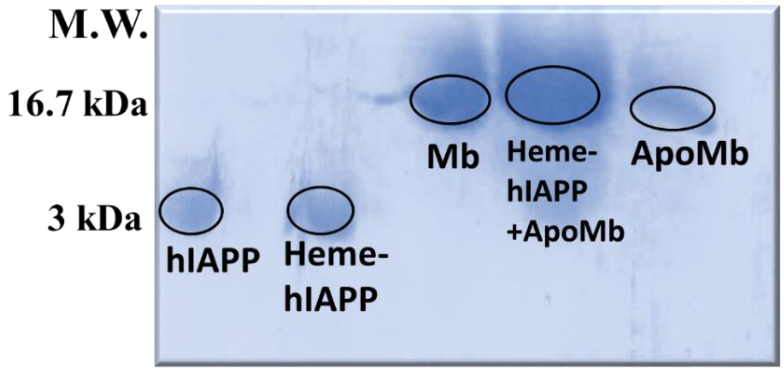

Figure 3. SDS gel electrophoresis run in gradient polyacrylamide gel shows heme transfer from Heme- hIAPP (1–19) to ApoMb (with Coomassie blue staining).

7.3.4. Kinetics

The kinetic traces show that there is fast first step, followed by a relatively slower second step (Figure 4, green trace, Figure S3). The first step is dependent of the concentration of the ApoMb (Figure S4), indicating that it follows a second order kinetics. The slower second step is independent of ApoMb concentration, following a first order kinetics (k_2= (2.7±0.1) $\times 10^{-2}$ s^{-1} at pH 7). The two steps likely indicates a fast heme transfer step, followed by a slower reorganisation of the protein chain around the active site. The percentage of heme transfer from Heme-hIAPP (1–19) to ApoMb is ~95±3%.

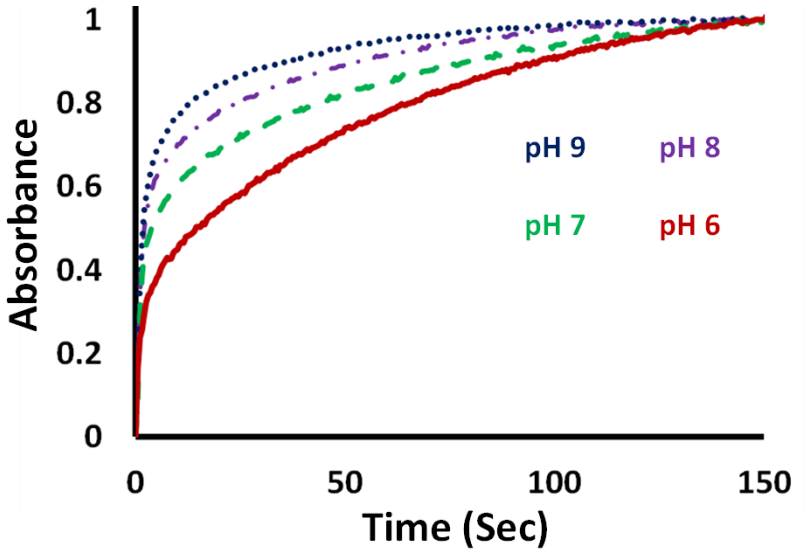

Figure 4. Heme sequestration by ApoMb at different pH. Trace at pH 6, red (solid line); pH 7, green (dashed line); pH 8, violet (dash-dotted line); pH 9, blue (dotted line).

All kinetic traces are monitored by the increase in absorption intensity at 408 nm (Abs vs time plot).

7.3.5. Effect of pH

Kinetics of heme sequestration by ApoMb is monitored at different pH (pH 6, 7, 8 and 9). The initial rates are found to be unchanged with changing pH (Figure S5) while the rate of the slower step increases with increasing pH (Figure 4, Table 1). When the second rate constant, k is plotted against pH, we get the pKa at around 6.8±0.2 (Figure 5).

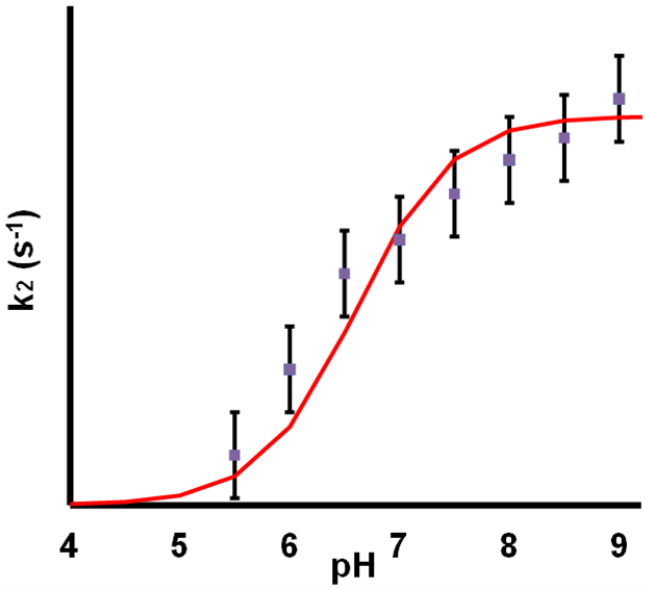

Figure 5. Rate constant (k2) vs. pH plot.

7.3.6. Partially reduced oxygen species (PROS) detection assay

To detect the amount of H_2O_2 produced after heme sequestration from Heme-hIAPP, xylenol orange assay (Materials and Methods Section, Figure S6) is performed. This assay indicates that Heme(Fe^{2+})-hIAPP(1–19) generates 38 ± 5% H_2O_2. After sequestering heme using ApoMb, ~ 10 ± 5% H_2O_2 is produced (Figure 6). PROS generation by free heme in solution is ~ 24 ± 2%.

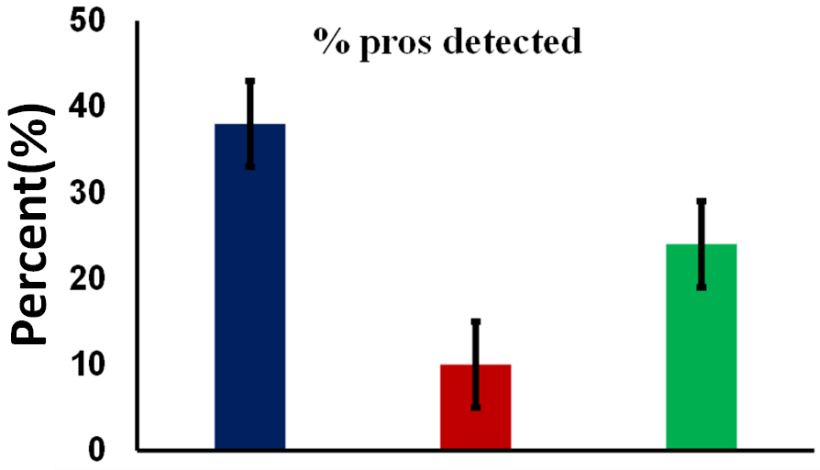

Figure 6. Percentage of PROS detected using Xylenol orange assay for **(A)** Heme-hIAPP (1–19), blue; **(B)** Heme-hIAPP with ApoMb, red; and **(C)** free heme, green.

7.3.7. Sequestration of ligand bound Heme by ApoMb

When azide ligand is added to Heme-hIAPP(1–19) in its oxidized state, it forms a six-coordinated azide bound complex having a blue shifted Soret at 370 nm with Q-bands at 516, 550 and 650 nm (Figure 7). When ApoMb is incubated with azide bound Heme-hIAPP complex (Heme-hIAPP-Azide), the characteristic bands of Heme-hIAPP-Azide disappear and a sharp soret at 421 nm appears along with bands at 545 and 580 in the Q-region. These newly formed bands are identical to that of Mb–Azide complex (Figure 7). This indicates that ApoMb can also extract azide-bound heme from Heme-hIAPP-Azide resulting in the formation of Mb–Azide complex. The small diatomic CO ligand binds to Heme-hIAPP (1–19) in its reduced state showing a characteristic Soret band at 422 nm and bands at 539 and 570 nm in the Q-region. After reaction with ApoMb, a sharp and more intense Soret band grows at 423 nm, together with bands at 541 and 580 nm in the Q-band region. CO bound Mb also shows similar absorption features which demonstrates that CO bound heme has also been sequestered by ApoMb to form the Mb-CO complex (Figure 8).

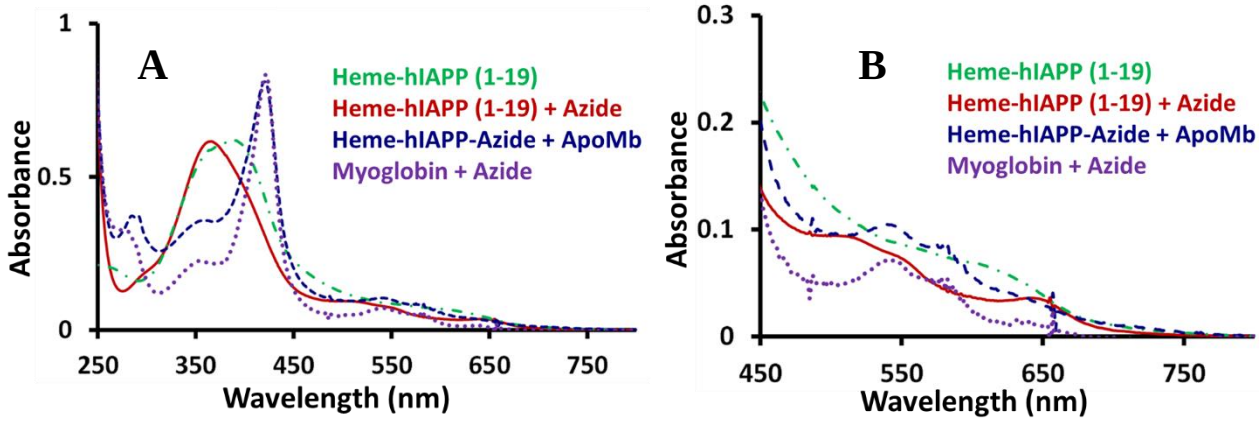

Figure 7. **(A)** Absorption spectra of Heme–hIAPP (1–19), green (dash-dotted line); azide complex of Heme–hIAPP (1–19), red (solid line); Heme-hIAPP (1–19)–Azide incubated with ApoMb, blue (dashed line); and Mb–Azide, violate (dotted line) **(B)** Q-band region of the corresponding absorption spectra; in 100 mM phosphate buffer at pH 7.

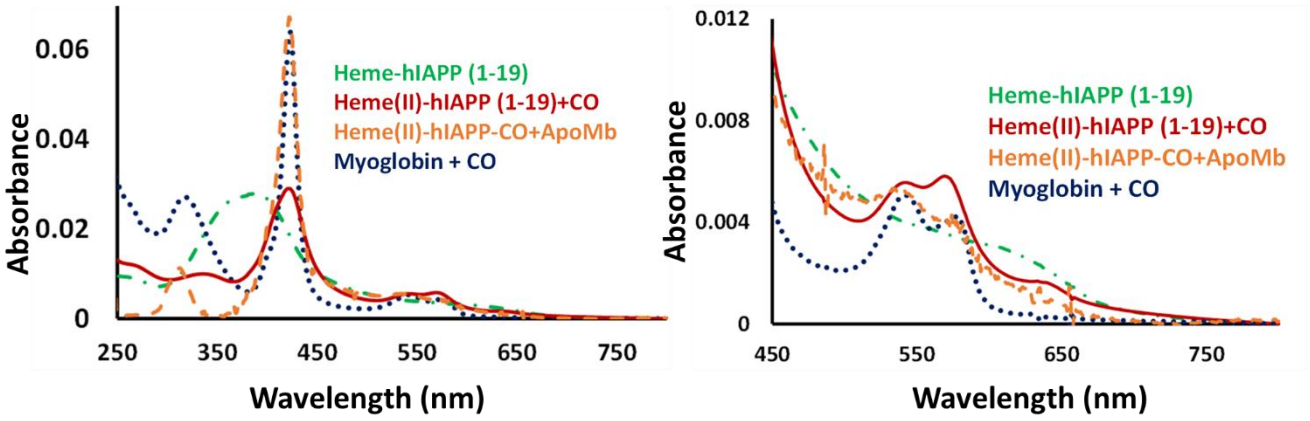

Figure 8. Absorption spectra of Heme–hIAPP (1–19), green (dash-dotted line); CO complex of Heme–hIAPP (1–19), red (solid line); Heme-hIAPP (1–19)–CO incubated with ApoMb, orange (dashed line); and Mb–CO, blue (dotted line) **(A)** Soret band region **(B)** Q-band region of the corresponding absorption spectra; in 100 mM phosphate buffer at pH 7.

7.4. Discussion

In the reduced state, Heme-hIAPP can react with molecular O_2 to produce significant amounts of partially reduced oxygen species (PROS) (~40%, implying one electron reduction to superoxide). This is why the complex has been proposed to play a potential role behind the apoptosis of pancreatic β-cells, which are in general extremely susceptible towards oxidative

stress. This may contribute to the reduction of β-cell mass and its dysfunction as observed in T2Dm. So, the removal of this toxic heme prosthetic group from the metal-peptide complex by some easily available biomolecule which leads to a non-toxic product, could be a possible remedy. ApoMb can uptake heme from the Heme-hIAPP complex forming native Mb i.e., when Heme-hIAPP is incubated with ApoMb in 1:1 ratio, there is a (95 ± 3) % heme transfer (which is perceived from the characteristic absorption changes (Figure 1, materials and methods section)). This is further corroborated by the rR data (Figure 2) for Heme-hIAPP, Mb and Heme-hIAPP incubated with ApoMb in 1:1 ratio, where a six-coordinate high-spin heme appears for Mb which is different from that of the metal-peptide complex. SDS-PAGE also confirms this heme transfer reaction (Figure 3). Thus, experimental evidences indicate heme sequestration from toxic Heme-hIAPP complex by available biomolecule, ApoMb which renders the complex less harmful as after the heme transfer, almost negligible amount of PROS (10 ± 5) % has been detected (Figure 6). Moreover, the generated Mb being an important O_2 carrier protein, can supply oxygen to the muscle tissues. The heme transfer has two distinct kinetic steps. There is an initial fast second order kinetic step followed by a slower second step having a first order rate constant, $k_2 = (2.7 \pm 0.1)\times10\text{-}2\ s^{-1}$ at pH 7 (Table 1).

Table 1. Rate constant values of the second step (k_2) of heme sequestration at different pH.

pH	$k_2\ (s^{-1})$
6	$(1.4\pm0.2)\times10^{-2}$
7	$(2.7\pm0.1)\times10^{-2}$
8	$(3.5\pm0.1)\times10^{-2}$
9	$(4.1\pm0.2)\times10^{-2}$

Spectroscopic data indicate (95 ± 3) % heme transfer from Heme-hIAPP to ApoMb at all pH. Note that the formation of an Mb-hIAPP complex cannot be ruled out. A possible mechanism of this reaction involves heme transfer to the apoprotein in the first step followed by a reorganisation of the protein chain to form the active site of native Mb (Scheme 1).[63,71] The first rate constant k_1, corresponding to the heme transfer step remains almost unperturbed

because of the high affinity of ApoMb for heme (1×10^{14} M^{-1}) irrespective of the pH of the medium between 4 and 9 (Figure 4, Table 1), while that of small hIAPP peptide is 1.5×10^{3} M^{-1}.[63,72] On the other hand, the rate constant k_2, likely corresponding to the refolding of the protein chain, increases with increasing pH having a pKa 6.8 ± 0.2 (Figure 5, Table 1). This possibly corresponds to the deprotonation of a propionate side chain of the heme moiety at high pH which facilitates H-bonding and electrostatic interactions (salt bridge) with the distal Lys45 residue of horse heart Mb or Arg45 residue of sperm whale Mb.[73–77] Lys/Arg residues are conserved at 45th position in all mammalian myoglobins and function as a 'gate' to control the ligand binding kinetics to the Fe-centre.[76,78] The positively charged Lys/ Arg residues act as a donor while propionate side chains act as the acceptor in the H-bond. The formation of the native holoprotein is consequent to the protein reorganisation which requires ion pairs to form between the Lys45 (or Arg 45) residue and the heme cofactor propionate chain (Scheme 1). The Lys/Arg45-heme-6-propionate salt bridge and H-bond breaks between a pH range of 7–5 which matches well with the pKa of the second slow step and suggests that this reorganisation is possibly the 2nd step of heme transfer.[73,75,79] Additionally, ApoMb can also sequester ligand bound heme from the Heme-hIAPP complex. This has been demonstrated by the sequestration of azide bound heme and CO-bound heme from the Heme-hIAPP-azide and Heme-hIAPP-CO complexes, respectively (Figure 7, Figure 8). Early reports suggests that apoglobins are capable of binding heme–CO to form CO-bound holoproteins.[63] Overall, ApoMb may likely inhibit the PROS-induced toxicity and damages caused by Heme-hIAPP. Additionally the newly formed Mb can function as the typical O_2 storage and carrier. Its rapid release after muscle damage can act as a potential biomarker in the early phases of injury. Thus, ApoMb or the apo forms of structurally similar proteins like hemoglobin and neuroglobin might exhibit a protective role against the possible damages of Heme-hIAPP by taking up heme.

Scheme 1. **Schematic representation of two step mechanism of heme transfer from Heme-hIAPP by ApoMb.**

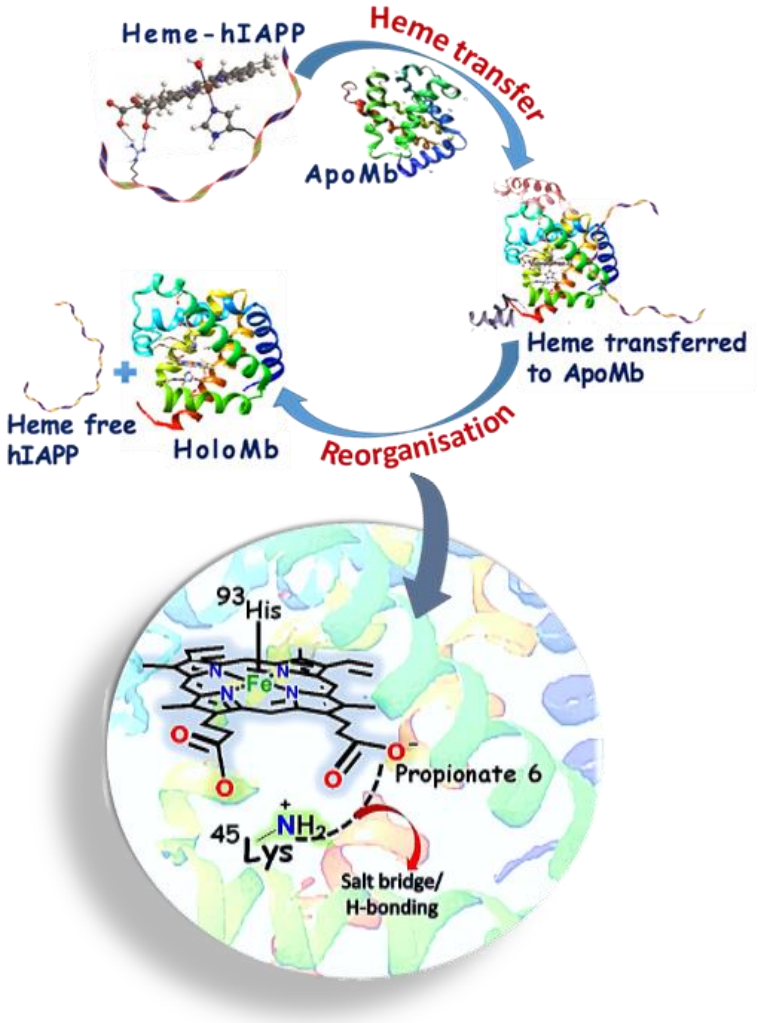

7.5. Conclusion

In summary, we have spectroscopically demonstrated that heme bound human hIAPP(1−19) peptides can transfer heme to ApoMb in both ligand bound and in free state, resulting in the formation of Mb. Kinetic analysis has been performed to determine the rate of heme uptake by ApoMb form Heme-hIAPP(1-19). The reaction has a fast heme-transfer step followed by a slower reorganisation of holomyoglobin. The rate of heme uptake is faster in higher pH medium owing to the Lys/Arg45-heme-6-propionate salt bridge and H-bonding which breaks between a pH ranges of 7–5. Importantly, the amount of partially reduced oxygen species generated is significantly reduced after heme sequestration. These results might implicate that ApoMb can play a protective role against the cytotoxicity that Heme-hIAPP can induce during diseased condition.

7.6. References

(1) Chen, L.; J., M. D.; Zimmet, P. Z. The worldwide epidemiology of type 2 diabetes mellitus--present and future perspectives. *Nat Rev Endocrinol.* **2011**, *8*, 228-236.

(2) Weyer, C.; Bogardus, C.; Mott, D. M.; Pratley, R. E. The natural history of insulin secretory dysfunction and insulin resistance in the pathogenesis of type 2 diabetes mellitus. *The Journal of Clinical Investigation* **1999**, *104*, 787-794.

(3) Kahn, C. R. Banting Lecture. Insulin action, diabetogenes, and the cause of type II diabetes. *Diabetes.* **1994**, *43*, 1066-1084.

(4) Wang, C. H.; Wang, C. C.; Wei, Y. H. Mitochondrial dysfunction in insulin insensitivity: implication of mitochondrial role in type 2 diabetes. *Ann N Y Acad Sci.* **2010**, *1201*, 157-165.

(5) O'Rahilly, S. P.; Rudenski, A. S.; Burnett, M. A.; Nugent, Z.; Hosker, J. P.; Darling, P.; Turner, R. C. Beta-cell dysfunction, rather than insulin insensitivity, is the primary defect in familial type 2 diabetes. *The Lancet* **1986**, *328*, 360-364.

(6) Pillay, K.; Govender, P. Amylin uncovered: a review on the polypeptide responsible for type II diabetes. *Biomed. Res. Int.* **2013**, *2013*, 1-17.

(7) Lorenzo, A.; Razzaboni, B.; Weir, G. C.; Yankner, B. A. Pancreatic islet cell toxicity of amylin associated with type-2 diabetes mellitus. *Nature* **1994**, *368*, 756-760.

(8) Moore, C. X.; Cooper, G. J. S. Co-secretion of amylin and insulin from cultured islet β-cells: Modulation by nutrient secretagogues, islet hormones and hypoglycemic agents. *Biochemical and Biophysical Research Communications* **1991**, *179*, 1-9.

(9) Kahn, S. E.; Alessio, D. A.; Schwartz, M. W.; Fujimoto, W. Y.; Ensinck, J. W.; Taborsky, G. J.; Porte, D. Evidence of Cosecretion of Islet Amyloid Polypeptide and Insulin by β-Cells. *Diabetes* **1990**, *39*, 634.

(10) Roberts, A. N.; Leighton, B.; Todd, J. A.; Cockburn, D.; Schofield, P. N.; Sutton, R.; Holt, S.; Boyd, Y.; Day, A. J.; Foot, E. A. Molecular and functional characterization of

amylin, a peptide associated with type 2 diabetes mellitus. *Proceedings of the National Academy of Sciences* **1989**, *86*, 9662.

(11) Hayden, M. R.; Tyagi, S. C. "A" is for amylin and amyloid in type 2 diabetes mellitus. *JOP*. **2001**, *2*, 124-139.

(12) Madine, J.; Jack, E.; Stockley, P. G.; Radford, S. E.; Serpell, L. C.; Middleton, D. A. Structural Insights into the Polymorphism of Amyloid-Like Fibrils Formed by Region 20−29 of Amylin Revealed by Solid-State NMR and X-ray Fiber Diffraction. *Journal of the American Chemical Society* **2008**, *130*, 14990-15001.

(13) Jaikaran, E. T.; Clark, A. Islet amyloid and type 2 diabetes: from molecular misfolding to islet pathophysiology. *Biochim Biophys Acta.* **2001**, *1537*, 179-203.

(14) Green, J. D.; Goldsbury, C.; Kistler, J.; Cooper, G. J. S.; Aebi, U. Human Amylin Oligomer Growth and Fibril Elongation Define Two Distinct Phases in Amyloid Formation. *J. Biol. Chem.* **2004**, *279*, 12206-12212.

(15) Kodali, R.; Wetzel, R. Polymorphism in the intermediates and products of amyloid assembly. *Curr Opin Struct Biol.* **2007**, *17*, 48-57.

(16) Mukherjee, S.; Dey, G. S. Heme Bound Amylin: Spectroscopic Characterization, Reactivity, and Relevance to Type 2 Diabetes. *Inorg. Chem.* **2013**, *52*, 5226-5235.

(17) Zraika, S.; Hull, R. L.; Udayasankar, J.; Aston-Mourney, K.; Subramanian, S. L.; Kisilevsky, R.; Szarek, W. A.; Kahn, S. E. Oxidative stress is induced by islet amyloid formation and time-dependently mediates amyloid-induced beta cell apoptosis. *Diabetologia* **2009**, *52*, 626-635.

(18) Haataja, L.; Gurlo, T.; Huang, C. J.; Butler, P. C. Islet Amyloid in Type 2 Diabetes, and the Toxic Oligomer Hypothesis. *Endocrine Reviews* **2008**, *29*, 303-316.

(19) Irvine, G. B.; El-Agnaf, O. M.; Shankar, G. M.; Walsh, D. M. Protein Aggregation in the Brain: The Molecular Basis for Alzheimer's and Parkinson's Diseases. *Molecular Medicine* **2008**, *14*, 451-464.

(20) M. Ashraf, G.; H. Greig, N.; A. Khan, T.; Hassan, I.; Tabrez, S.; Shakil, S.; A. Sheikh, I.; K. Zaidi, S.; Akram, M.; R. Jabir, N.; K. Firoz, C.; Naeem, A.; M. Alhazza, I.; A. Damanhouri, G.; A. Kamal, M. Protein Misfolding and Aggregation in Alzheimer's Disease and Type 2 Diabetes Mellitus. *CNS & Neurological Disorders - Drug Targets-CNS & Neurological Disorders* **2014**, *13*, 1280-1293.

(21) Jiang, R.; Manson, J. E.; Meigs, J. B.; Ma, J.; Rifai, N.; Hu, F. B. Body Iron Stores in Relation to Risk of Type 2 Diabetes in Apparently Healthy Women. *J. Am. Med. Assoc. (JAMA)* **2004**, *291*, 711-717.

(22) Kazi, T. G.; Afridi, H. I.; Kazi, N.; Jamali, M. K.; Arain, M. B.; Jalbani, N.; Kandhro, G. A. Copper, chromium, manganese, iron, nickel, and zinc levels in biological samples of diabetes mellitus patients. *Biol Trace Elem Res.* **2008**, *122*, 1-18.

(23) Rungby, J. Zinc, zinc transporters and diabetes. *Diabetologia* **2010**, *53*, 1549-1551.

(24) Naka, T.; Kaneto, H.; Katakami, N.; Matsuoka, T. A.; Harada, A.; Yamasaki, Y.; Matsuhisa, M.; Shimomura, I. Association of serum copper levels and glycemic control in patients with type 2 diabetes. *Endocr J.* **2013**, *60*, 393-396.

(25) Seal, M.; Dey, S. G. Active-Site Environment of Copper-Bound Human Amylin Relevant to Type 2 Diabetes. *Inorg. Chem.* **2018**, *57*, 129-138.

(26) Ma, L.; Li, X.; Wang, Y.; Zheng, W.; Chen, T. Cu(II) inhibits hIAPP fibrillation and promotes hIAPP-induced beta cell apoptosis through induction of ROS-mediated mitochondrial dysfunction. *J Inorg Biochem* **2014**, *140*, 143-152.

(27) Ward, B.; Walker, K.; Exley, C. Copper(II) inhibits the formation of amylin amyloid in vitro. *J Inorg Biochem* **2008**, *102*, 371-375.

(28) Alghrably, M.; Dudek, D.; Emwas, A.-H.; Jaremko, Ł.; Jaremko, M.; Rowińska-Żyrek, M. Copper(II) and Amylin Analogues: A Complicated Relationship. *Inorganic Chemistry* **2020**, *59*, 2527-2535.

(29) Rivillas-Acevedo, L.; Sánchez-López, C.; Amero, C.; Quintanar, L. Structural Basis for the Inhibition of Truncated Islet Amyloid Polypeptide Aggregation by Cu(II): Insights

into the Bioinorganic Chemistry of Type II Diabetes. *Inorganic Chemistry* **2015**, *54*, 3788-3796.

(30) Lee, S. J. C.; Choi, T. S.; Lee, J. W.; Lee, H. J.; Mun, D. G.; Akashi, S.; Lee, S. W.; Lim, M. H.; Kim, H. I. Structure and assembly mechanisms of toxic human islet amyloid polypeptide oligomers associated with copper.

(31) Sinopoli, A.; Magrì, A.; Milardi, D.; Pappalardo, M.; Pucci, P.; Flagiello, A.; Titman, J. J.; Nicoletti, V. G.; Caruso, G.; Pappalardo, G.; Grasso, G. The role of copper(ii) in the aggregation of human amylin. *Metallomics* **2014**, *6*, 1841-1852.

(32) Khan, F. A.; Al Jameil, N.; Arjumand, S.; Khan, M. F.; Tabassum, H.; Alenzi, N.; Hijazy, S.; Alenzi, S.; Subaie, S.; Fatima, S. Comparative Study of Serum Copper, Iron, Magnesium, and Zinc in Type 2 Diabetes-Associated Proteinuria. *Biological Trace Element Research* **2015**, *168*, 321-329.

(33) Alghrably, M.; Czaban, I.; Jaremko, Ł.; Jaremko, M. Interaction of amylin species with transition metals and membranes. *J. Inorg. Biochem.* **2019**, *191*, 69-76.

(34) Brender, J. R.; Hartman, K.; Nanga, R. P. R.; Popovych, N.; de la Salud Bea, R.; Vivekanandan, S.; Marsh, E. N. G.; Ramamoorthy, A. Role of zinc in human islet amyloid polypeptide aggregation. *Journal of the American Chemical Society* **2010**, *132*, 8973-8983.

(35) Wei, L.; Jiang P Fau - Xu, W.; Xu W Fau - Li, H.; Li H Fau - Zhang, H.; Zhang H Fau - Yan, L.; Yan L Fau - Chan-Park, M. B.; Chan-Park Mb Fau - Liu, X.-W.; Liu Xw Fau - Tang, K.; Tang K Fau - Mu, Y.; Mu Y Fau - Pervushin, K.; Pervushin, K. The molecular basis of distinct aggregation pathways of islet amyloid polypeptide.

(36) Jiang, R.; Manson, J. E.; Meigs, J. B.; Ma, J.; Rifai, N.; Hu, F. B. Body iron stores in relation to risk of type 2 diabetes in apparently healthy women. *J. Am. Med. Assoc. (JAMA)* **2004**, *291*, 711-717.

(37) Raj, S.; Rajan, G. V. Correlation between elevated serum ferritin and HbA1c in type 2 diabetes mellitus. *Int. J. Res. Med. Sci.* **2017**, *1*, 12-15.

(38) Kaye, T. B.; Guay At Fau - Simonson, D. C.; Simonson, D. C. Non-insulin-dependent diabetes mellitus and elevated serum ferritin level.

(39) Misra, G.; Bhatter, S. K.; Kumar, A.; Gupta, V.; Khan, M. Y. Iron Profile and Glycaemic Control in Patients with Type 2 Diabetes Mellitus. *Med Sci (Basel)* **2016**, *4*, 22.

(40) Fenton, H. J. H. LXXIII.—Oxidation of tartaric acid in presence of iron. *J. Chem. Soc. Trans.* **1894**, *65*, 899-910.

(41) Papanikolaou, G.; Pantopoulos, K. Iron metabolism and toxicity. *Toxicol Appl Pharmacol.* **2005**, *2002*, 199-211.

(42) Rajpathak, S.; Ma, J.; Manson, J.; Willett, W. C.; Hu, F. B. Iron intake and the risk of type 2 diabetes in women: a prospective cohort study. *Diabetes. Care.* **2006**, *29*, 1370-1376.

(43) Zhao, Z.; Li, S.; Liu, G.; Yan, F.; Ma, X.; Huang, Z.; Tian, H. Body iron stores and heme-iron intake in relation to risk of type 2 diabetes: a systematic review and meta-analysis. *PLoS One.* **2012**.

(44) Bao, W.; Rong, Y.; Rong, S.; Liu, L. Dietary iron intake, body iron stores, and the risk of type 2 diabetes: a systematic review and meta-analysis. *BMC Medicine* **2012**, *10*, 119.

(45) Ndisang, J. F. Role of Heme Oxygenase in Inflammation, Insulin-Signalling, Diabetes and Obesity. *Mediators of Inflammation* **2010**, *2010*, 359732.

(46) Gerbitz, K. D.; Gempel, K.; Brdiczka, D. Mitochondria and Diabetes: Genetic, Biochemical, and Clinical Implications of the Cellular Energy Circuit. *Diabetes* **1996**, *45*, 113.

(47) de la Monte, S. M.; Wands, J. R. Alzheimer's disease is type 3 diabetes-evidence reviewed. *J Diabetes Sci Technol.* **2008** *2*.

(48) Wu, J.; Zhao, J.; Yang, Z.; Li, H.; Gao, Z. A.-O. Strong Inhibitory Effect of Heme on hIAPP Fibrillation.

(49) Sengupta, K.; Chatterjee, S.; Mukherjee, S.; Dey, S. G.; Dey, A. Heme bound amylin self-assembled monolayers on an Au electrode: an efficient bio-electrode for O2 reduction to H2O. *Chemical Communications* **2014**, *50*, 3806-3809.

(50) Seal, M.; Mukherjee, S.; Dey, S. G. Fe–oxy adducts of heme–Aβ and heme–hIAPP complexes: intermediates in ROS generation. *Metallomics* **2016**, *8*, 1266-1272.

(51) Millikan, G. A. MUSCLE HEMOGLOBIN. *Physiological Reviews* **1939**, *19*, 503-523.

(52) Wittenberg, J. B. Myoglobin-facilitated oxygen diffusion: role of myoglobin in oxygen entry into muscle. *Physiol Rev.* **1970**, *50*, 559-636.

(53) Ordway, G. A.; Garry, D. J. Myoglobin: an essential hemoprotein in striated muscle. *J Exp Biol.* **2004**, *207*.

(54) Wittenberg, J. B.; Wittenberg, B. A. Mechanisms of cytoplasmic hemoglobin and myoglobin function. *Annu Rev Biophys Biophys Chem.* **1990**, *19*, 217-241.

(55) Galaris, D.; Cadenas, E.; Hochstein, P. Redox cycling of myoglobin and ascorbate: a potential protective mechanism against oxidative reperfusion injury in muscle. *Arch Biochem Biophys.* **1989** *273*, 497-504.

(56) Lancaster, J. R., Jr. Simulation of the diffusion and reaction of endogenously produced nitric oxide. *Proc Natl Acad Sci U S A.* **1994** *91*, 8137-8141.

(57) Liu, X.; Miller, M. J.; Joshi, M. S.; Thomas, D. D.; Lancaster, J. R., Jr. Accelerated reaction of nitric oxide with O2 within the hydrophobic interior of biological membranes. *Proc Natl Acad Sci U S A.* **1998** *95*, 2175-2179.

(58) Miura, T.; Muraoka, S.; Fujimoto, Y. Inactivation of creatine kinase induced by dopa and dopamine in the presence of ferrylmyoglobin. *Chem Biol Interact.* **1999**, *123*, 51-61.

(59) Braunitzer, G.; Hilse, K.; Rudloff, V.; Hilschmann, N.: The Hemoglobins. In *Advances in Protein Chemistry*; Anfinsen, C. B., Anson, M. L., Edsall, J. T., Richards, F. M., Eds.; Academic Press, 1964; Vol. 19; pp 1-71.

(60) Hargrove, M. S.; Barrick, D.; Olson, J. S. The association rate constant for heme binding to globin is independent of protein structure. *Biochemistry* **1996**, *35*, 11293-11299.

(61) Seal, M.; Uppal, S.; Kundu, S.; Dey, S. G. Interaction of apoNeuroglobin with heme–Aβ complexes relevant to Alzheimer's disease. *J. Biol. Inorg. Chem.* **2015**, *20*, 563-574.

(62) Pramanik, D.; Mukherjee, S.; Dey, S. G. Apomyoglobin Sequesters Heme from Heme Bound Aβ Peptides. *Inorganic Chemistry* **2013**, *52*, 10929-10935.

(63) Teale, F. W. J. Cleavage of the haem-protein link by acid methylethylketone. *Biochimica et Biophysica Acta* **1959**, *35*, 543.

(64) Pramanik, D.; Dey, S. G. Active Site Environment of Heme-Bound Amyloid β Peptide Associated with Alzheimer's Disease. *J. Am. Chem.l Soc.* **2011**, *133*, 81-87.

(65) Laemmli, U. K. Cleavage of Structural Proteins during the Assembly of the Head of Bacteriophage T4. *Nature* **1970**, *227*, 680-685.

(66) Hu, S.; Smith, K. M.; Spiro, T. G. Assignment of Protoheme Resonance Raman Spectrum by Heme Labeling in Myoglobin. *J. Am. Chem. Soc.* **1996**, *118*, 12638-12646.

(67) Spiro, T. G.; Strekas, T. C. Resonance Raman spectra of heme proteins. Effects of oxidation and spin state. *J. Am. Chem. Soc.* **1974**, *96*, 338-345.

(68) Bhakta, M. N.; Wilks, A. The Mechanism of Heme Transfer from the Cytoplasmic Heme Binding Protein PhuS to the δ-Regioselective Heme Oxygenase of Pseudomonas aeruginosa. *Biochemistry* **2006**, *45*, 11642-11649.

(69) Hargrove, M. S.; Wilkinson, A. J.; Olson, J. S. Structural factors governing hemin dissociation from metmyoglobin. *Biochemistry* **1996**, *35*, 11300-11309.

(70) Mukherjee, S.; Mukherjee, M.; Bandyopadhyay, S.; Dey, A. Three phases in pH dependent heme abstraction from myoglobin. *J. inorg. biochem.* **2017**, *172*, 80-87.

(71) Kanai, Y.; Harada, A.; Shibata, T.; Nishimura, R.; Namiki, K.; Watanabe, M.; Nakamura, S.; Yumoto, F.; Senda, T.; Suzuki, A.; Neya, S.; Yamamoto, Y. Characterization of Heme Orientational Disorder in a Myoglobin Reconstituted with a Trifluoromethyl-Group-Substituted Heme Cofactor. *Biochemistry* **2017**, *56*, 4500-4508.

(72) Carver, T. E.; Olson, J. S.; Smerdon, S. J.; Krzywda, S.; Wilkinson, A. J.; Gibson, Q. H.; Blackmore, R. S.; Ropp, J. D.; Sligar, S. G. Contributions of residue 45(CD3) and heme-6-propionate to the bimolecular and geminate recombination reactions of myoglobin. *Biochemistry* **1991**, *30*, 4697-4705.

(73) Schulze, B. G.; Evanseck, J. D. Cooperative Role of Arg45 and His64 in the Spectroscopic A3 State of Carbonmonoxy Myoglobin: Molecular Dynamics Simulations, Multivariate Analysis, and Quantum Mechanical Computations. *Journal of the American Chemical Society* **1999**, *121*, 6444-6454.

(74) Evans, S. V.; Brayer, G. D. Horse heart metmyoglobin. A 2.8-A resolution three-dimensional structure determination.

(75) Oldfield, T. J.; Smerdon, S. J.; Dauter, Z.; Petratos, K.; Wilson, K. S.; Wilkinson, A. J. High-resolution x-ray structures of pig metmyoglobin and two CD3 mutants: Mb(Lys45 .fwdarw. Arg) and Mb(Lys45 .fwdarw. Ser). *Biochemistry* **1992**, *31*, 8732-8739.

(76) Yang, F.; Phillips Jr, G. N. Crystal Structures of CO−, Deoxy- and Met-myoglobins at Various pH Values. *Journal of Molecular Biology* **1996**, *256*, 762-774.

7.7. Supporting Information

7.7.1. UV–VIS of free heme and Heme–hIAPP

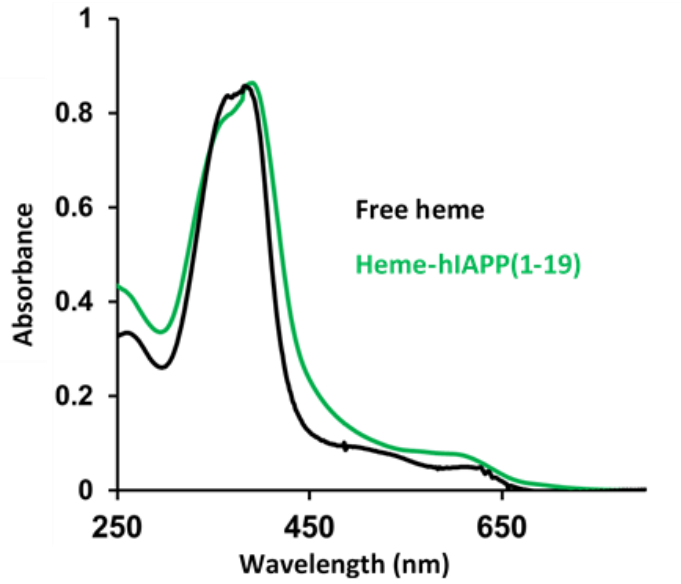

Figure S1. Absorption spectra of Heme-hIAPP (1-19), green and free heme, black at pH 7.

7.7.2. Resonance Raman spectra of free heme and Heme–hIAPP

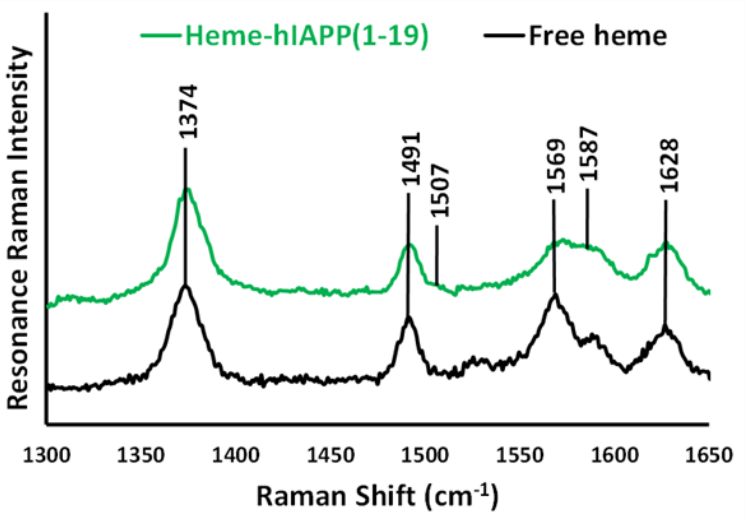

Figure S2. High frequency resonance Raman spectra of Heme-hIAPP(1-19), green and free heme, black at pH 7.

7.7.3. Heme transfer reaction at different time interval at pH 7.

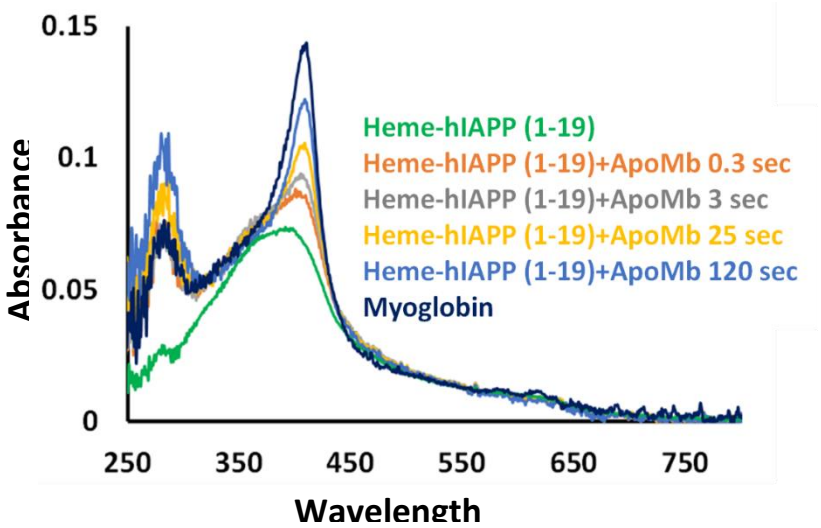

Figure S3. Heme-hIAPP(1-19) with ApoMb at different time interval, in pH 7 100mM phosphate buffer.

7.7.4. Dependence of Heme transfer reaction on concentration of ApoMb

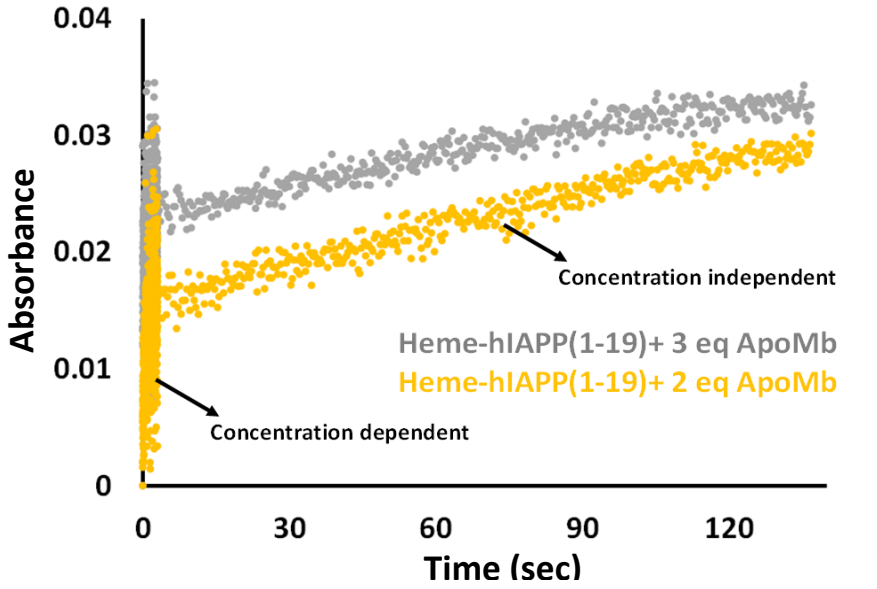

Figure S4. Heme-hIAPP(1-19) with varying concentration of ApoMb, in pH 8 100mM phosphate buffer.

7.7.5. pH variation effect on the rate constant k_1 of heme transfer reaction

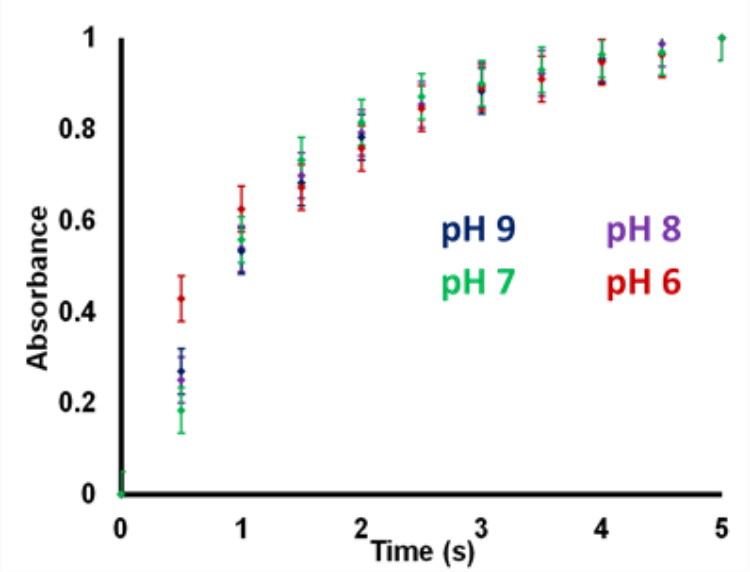

Figure S5. pH variation of initial rate (with rate constant k_1) of heme transfer.

7.7.6. Xylenol orange assay

When 1 equiv of dithionite is added to the Heme-hIAPP peptide solutions, the resting Fe^{3+} site of heme is reduced to Fe^{2+}. Addition of O_2 to the fully reduced Heme(Fe^{2+})-hIAPP(1−19) complexes, can reoxidise the Fe^{2+} to the Fe^{3+} form as indicated by absorption spectroscopy. In this process the O_2 gets reduced by $1e^-$ pathway which produce reactive oxygen species (ROS) like superoxide ($O_2^{\bullet-}$), peroxide (H_2O_2) etc. Any H_2O_2 formed during the O_2 reduction process has been detected by using the xylenol orange assay.

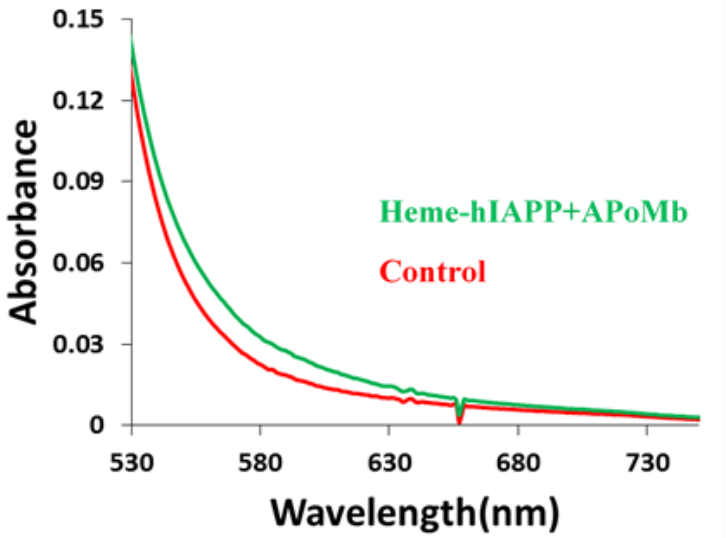

Figure S6. Xylenol orange incubated sample, green; control sample, red.

List of Publications

1. *Formation of compound I in heme bound Aβ-peptides relevant to Alzheimer's disease.*
   I. Pal[§], A. K. Nath[§], M. Roy, M. Seal, C. Ghosh, A. Dey*, S. G. Dey*.
   Chemical science; 10 (36), 8405-8410, **2019.**
   [§]Both of the authors contributed equally to the work.

2. *Active-site environment of Cu bound amyloid β and amylin peptides*.
   I. Pal, M. Roy, S. G. Dey*.
   Journal of Biological Inorganic Chemistry*;* 24 (8), 1245-1259, 3, **2019.**

3. *Interaction of ApoMyoglobin with Heme-hIAPP complex.*
   I. Pal, M. Roy, S. G. Dey*.
   Journal of Inorganic Biochemistry*;* 216, 111348, **2021.**

4. *Electronic structure and reactivity of heme bound insulin.*
   M. Roy[§], **I. Pal**[§], C. Dey, A. Dey and S. G. Dey*.
   Journal of Porphyrins and Phthalocyanines*;* 25:05n06, 511-521, **2021.**
   [§]Both of the authors contributed equally to the work.

5. *Peroxidase activity of heme bound amyloid β peptides associated with Alzheimer's disease.*
   M. Roy, **I. Pal**, A. K. Nath, S. G. Dey*.
   Chemical Communications*;* 56 (33), 4505-4518, 4, **2020.**

6. *Second Sphere Interactions in Amyloidogenic Diseases.*
   M. Roy, A. K. Nath, **I. Pal**, S. G. Dey*.
   Chemical Reviews*; manuscript under revision.*

7. *Characterization of the Intermediates in the Oxygen Reduction Pathway of Heme-Aβ relevant to Alzheimer's disease.*

M. Roy, **I. Pal,** S. G. Dey*.

Chemical Communications*; manuscript under preparation.*

8. *Effect of second sphere on the reaction pathway of synthetic porphyrins with peroxides.*

I. Pal, A. Sinha, S. G. Dey*, A. Dey*; *manuscript under preparation.*

9. *Role of High-valent Reactive Intermediates of heme bound Insulin complexes in Type 2 Diabetes Mellitus Pathology.*

I. Pal, S. G. Dey*; *manuscript under preparation.*